VAN DEN BERG, WILLEMIEN

BASE METAL MINERALISATION IN THE ROOIBERG GROUP NEAR RUST DE WINTER: SOME CHARACTERISTICS OF THE HYDROTHERMAL SYSTEM

MSc   UP   1996

BASE METAL MINERALISATION IN

THE ROOIBERG GROUP NEAR

RUST DE WINTER:

SOME CHARACTERISTICS OF THE

HYDROTHERMAL SYSTEM

by
Willemien van den Berg
Submitted in partial fulfilment of
the requirements for
the degree Magister Scientia
in the
Faculty of Science
University of Pretoria
Pretoria
April 1996

ACKNOWLEDGEMENTS

Abstract

The studied hydrothermal system operated in an agglomerate layer which forms part of the "Union Tuff member" that occurs in the uppermost part of the Rooiberg Felsites. In contrast to the Sn and F deposits characteristic of this part of the Rooiberg Group, this hydrothermal system in the Rust de Winter area contains predominately base metals and a small amount of gold. It is believed that this hydrothermal system was possibly the product of a granitic intrusion, but represents a later, cooler mineralisation stage further away from the body.

The mineralised areas in the agglomerate layer can be divided into three types, based on differences in the host rock, mineralisation style and mineral associations. The first type occurs in quartz + chlorite veins in the agglomerate and carries mainly arsenopyrite (with inclusions of native bismuth and gold), pyrite, chalcopyrite, sulphosalts and Cu-sulphides. The second type is disseminated in the agglomerate and consists predominately of sphalerite and chalcopyrite. The third type is found at the contact between the agglomerate and underlying massive rhyolite and consists of quartz + chlorite + siderite veins with lesser pyrite and chalcopyrite.

The sulphide minerals of the quartz + chlorite veins suggest a history of precipitation in at least three stages. The first stage includes the precipitation of the arsenopyrite, pyrite and chalcopyrite. The sulphide minerals of the second stage (Bi-Pb-Cu-sulphosalt, galena and chalcopyrite) precipitated interstitially with respect to the first generation sulphides. The third stage includes minerals that formed due to supergene alteration by a Cu-rich fluid, for example a variety of Cu-sulphides and the Bi-Cu-sulphosalt. Chamosite (Fe-rich chlorite) and quartz are the dominant silicate minerals associated with the sulphides. Away from the vein system a zone in the agglomerate is encountered where areas dominated by sphalerite alternate with areas dominated by chalcopyrite; no alteration by a Cu-rich fluid was detected here.

The chlorite geothermometer indicates temperatures of formation (of the chlorite) in the range 315° - 360°C. Chlorites overprinted by a Fe-rich fluid must have formed at higher temperatures along with some of the primary sulphides (arsenopyrite, pyrite, and chalcopyrite). A second stage of sulphide precipitation followed at slightly lower temperatures resulting in the formation of the Bi-Pb-Cu-sulphosalt and small amounts of galena and a second generation chalcopyrite. These two stages were succeeded by a period of "alteration" by a Cu-rich fluid, that represents the last stage of sulphide mineral precipitation.

The microthermometric investigation gives pressure corrected temperatures in the range 150° - 380°C. It is unsure which sulphide phases precipitated at what temperature interval. The salinity of the fluid(s) falls into three groups (i.e. a very high salinity, an intermediate salinity and a very low salinity), which can be explained by fluid mixing (resulting in lowering the salinity) and fluid boiling (increasing the salinity). Base metals will be preferentially transported by a higher salinity fluid (5.5 eq. wt% NaCl), whereas gold complexes prefer low salinities (0 - 5 eq. wt. NaCl).

TABLE OF CONTENTS

vii

List of Figures

List of Tables

Introduction

This thesis is based on the mineralogical investigation of base metal mineralisation intersected in boreholes near Rust de Winter in the Rooiberg Felsites (**Fig. 1.1**). The borehole core was kindly made available by GENMIN. However, the exact location of the boreholes is confidential.

1.1 AIMS OF THIS STUDY

The main aims of this study were as follows:
- to investigate the degree of alteration in the host rock
- to describe and interpret the mineralogy of the gangue minerals associated with the ore minerals
- to describe and interpret the mineralogy of the opaque minerals
- to deduce the relevant characteristics of the ore-forming fluids.

1.2 GENERAL CHARACTERISTICS OF THE ROOIBERG GROUP

1.3.1 Lithostratigraphy:

The Rooiberg Group is regarded by SACS (1980) as part of the upper portion of the Transvaal Supergroup and forms the roof of the Bushveld Complex (whereas the lower parts of the Transvaal Supergroup forms its floor). The distribution of the Rooiberg Group, related to that of the Bushveld Complex and lower portion of the Transvaal Supergroup, is given in **Figure 1.1**. The age of the Rooiberg Group is estimated at ~ 2150 Ma (SACS, 1980).

The upper portion of the Rooiberg Group consists of: flow-banded rhyolites with occasional quartz xenocrysts, and discontinuous sediments and pyroclastic flows. Twist (1985) expanded on Clubley-Armstrong's (1977) subdivision of the Rooiberg succession, and distinguished 9 units, based on geochemical characteristics. The stratigraphic subdivisions of the Rooiberg Felsite Group are discussed in detail by Clubley-Armstrong (1977; 1980), De Bruiyn (1980), Rhodes and Du Plessis (1976), Stear (1977), Twist (1985), Eriksson et al. (1993). More recently, Schweitzer et al. (1995a) proposed a new subdivision (not yet approved) in which the Dullstroom Formation (formerly part of the Pretoria Group) is regarded as the base of the Rooiberg Group (**Table 1.1**).

Table 1.1 : Newly proposed Rooiberg Group subdivision compared to the one currently used (SACS, 1980).

SACS, 1980   Schweitzer et al., 1995a

Group	Formation	Member	Group	Formation	Member
Rooiberg	Selons River	Klipnek	Rooiberg	Schrikkloof	
		Doornkloof		Kwaggasnek	Union Tin
	Damwal			Damwal	
				Dullstroom	
Pretoria	Dullstroom				

1.3.2 <u>Economic potential:</u>

Twist (1983) evaluated the economic potential of the Rooiberg Felsites and concluded that the most likely ore-types to be expected in this acid volcanic environment are:
(1) Base metal (Zn-Pb-Cu) volcanogenic exhalative sulphide deposits.
(2) Precious metal (Ag-Au) epithermal ores (usually associated with regional alteration in the vicinity of volcanic vents).
(3) Tin ores.
(4) Fluorspar deposits, produced by metasomatic replacement.

According to Schweitzer et al. (1995b), four major ore-types can be identified in the Rooiberg Group: (1) Hydrothermal copper mineralisation in the lowermost portion of the Rooiberg Group, overlying the Rustenburg Layered Suite and linked to the intrusion of the Bushveld Complex (SACS, 1980); (2) Stratabound arsenic mineralisation that took place after extrusion of the

3

Damwal Formation in response to contact metamorphism; (3) Pb-Zn mineralisation concentrated towards the contact with the Rustenburg Layered Suite (also in response to contact metamorphism); and (4) Sn and F mineralisation in the uppermost portion of the rhyolite succession, linked to the intrusion of the Lebowa Granite Suite. Schweitzer et al. (1995b) concluded that the mineralisation in the Rooiberg Felsite is largely controlled by the associated Bushveld Complex (that comprises of, from bottom to top: Rustenburg Layered Suite, Lebowa Granites, Rooiberg Felsites, and Granophyres). Therefore, exploration models have to consider the complex inter-relationship of the various extrusive and intrusive events of the Bushveld Complex.

Schweitzer et al. (1995b) linked their stratigraphic subdivision to mines (and commodities mined) in the Rooiberg Felsites (**Fig. 1.2**). The lower portions of the Rooiberg Group (i.e. Dullstroom and Damwal Formations, as well as the bottom portion of the Kwaggasnek Formation) are typified generally by base metal deposits, whereas the upper Kwaggasnek and Schrikkloof Formations have tin and fluorspar deposits.

1.3 GEOLOGICAL SETTING OF THE STUDY AREA

The hydrothermal mineralisation which forms the basis of this study is hosted by an agglomerate layer overlying barren rhyolite in the upper part of the Rooiberg Group, in the Rust de Winter area, north of Pretoria.

Figure 1.3 shows the distribution of the various formations in the Rooiberg Group as well as that of the granites of the Bushveld Complex. From this geological map it is clear that the Rust de Winter area (near the Vergenoeg fluorspar mine) falls close to the contact between the Kwaggasnek and Schrikkloof Formations. In **Fig. 1.2** (from Schweitzer and co-workers, 1995b) an agglomerate and tuff layer is shown between the Schrikkloof and Kwaggasnek Formations. According to stratigraphic indicators and evidence in the investigated drill cores, the agglomerate in which the hydrothermal mineralisation at Rust de Winter occurs, seems to agree with the agglomerate layer between the Kwaggasnek and Schrikkloof formations and seems to underlie the Union Tin Tuff Member. According to the subdivision of Twist (1985) the underlying rhyolite belongs to unit 8 and the overlying rhyolite is unit 9 (Smith, 1993).

4

Because the studied agglomerate layer forms the marker horizon between the Kwaggasnek and Schrikkloof Formations, it could be expected that the most common type of mineralisation would be tin and/or fluorspar. However, the hydrothermal mineralisation studied and reported on here, contains the base metals, Cu, Fe and Zn in varying amounts, and none of the expected F- or Sn-containing minerals. A schematic summary of the mineralisation encountered in the drill cores, GD1, GD2 and GD3, is given in **Fig. 1.4** and described in more detail in **Chapter 2**. The main mineralised zone or vein system (i.e. chlorite + quartz + sulphide veins), in which the majority of base metals are found, is present exclusively in the agglomerate unit. For economic reasons, the bulk of the study centred around this mineralisation encountered only in GD1 and GD2.

Figure 1.2: Stratigraphic subdivision of the Rooiberg Group based on regional lithological and chemical features. Mines and mineral occurrences related to the specific commodity, are listed according to their stratigraphic position (from Schweitzer et al., 1995b).
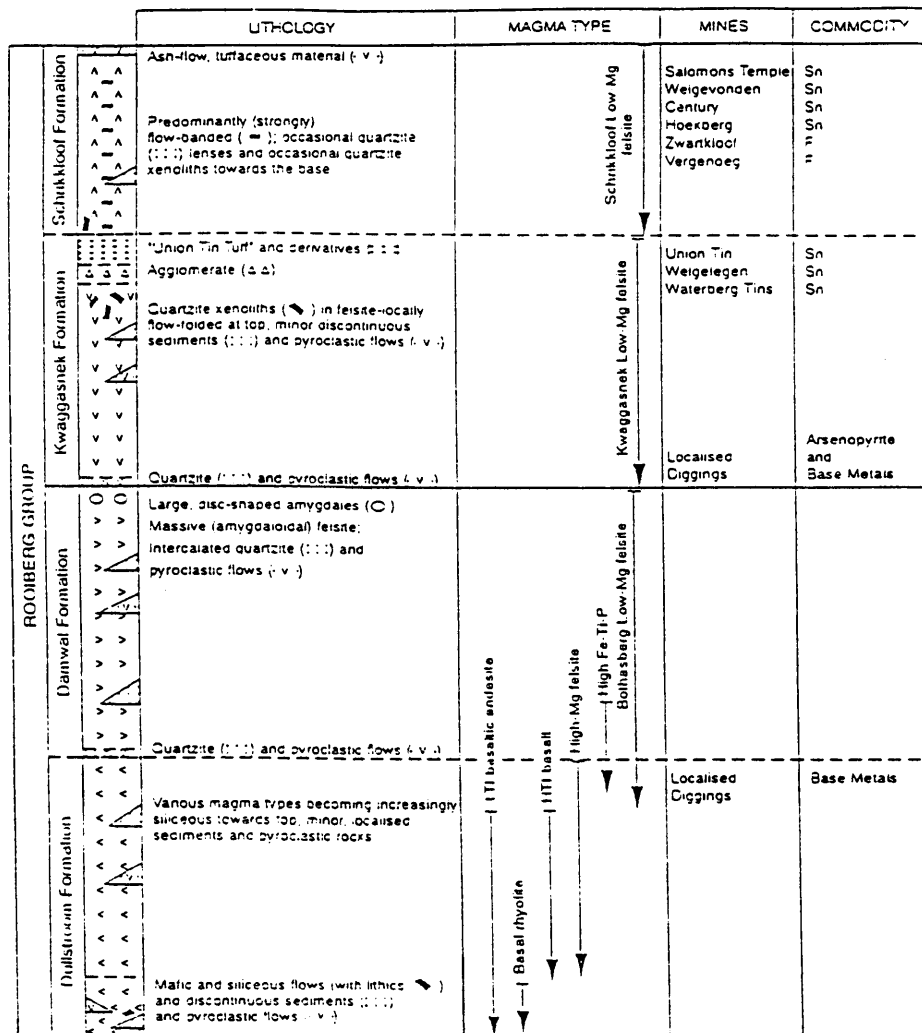
Figure 1.3: Geographic distribution of the various Rooiberg Group formations. Also shown are the positions of mines within the Rooiberg Group rocks. The Stavoren and Rooiberg Fragments are comprised of sedimentary rocks and Rooiberg Group volcanic rocks, and are situated within Bushveld Granite (from Schweitzer et al., 1995a).
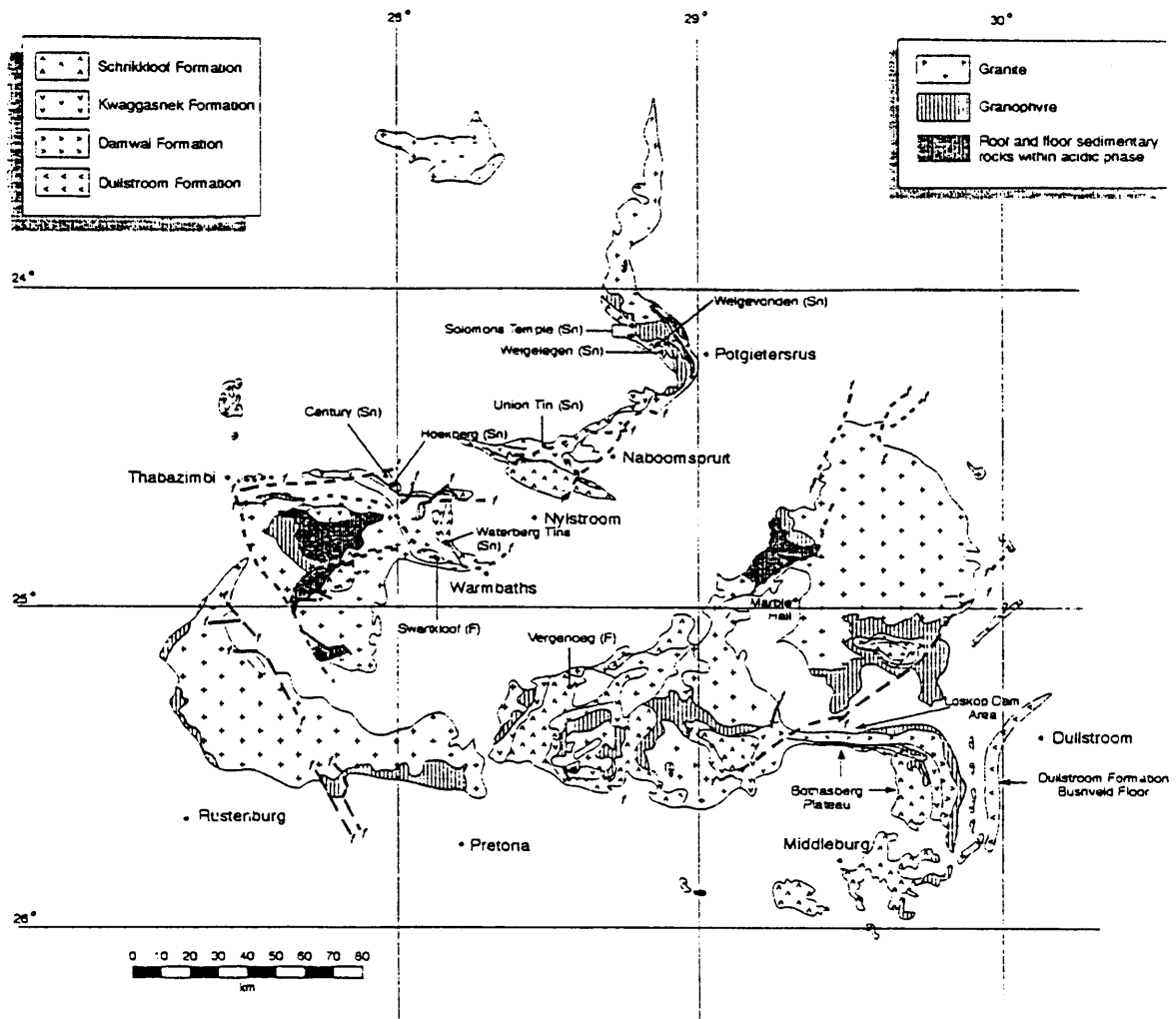
Figure 1.4 : Schematic profile of boreholes GD1, GD2 and GD3 in the Rust de Winter area, showing the different mineralisation styles, and the surrounding host rocks. The right corner box is a plan layout and the arrows indicate the inclination of the boreholes.

CHLORITE-QUARTZ-SULPHIDE VEINS

ALTERNATING SPHALERITE AND YELLOW SULPHIDES

DISSEMINATED SPHALERITE

QUARTZ-SULPHIDE-(SIDERITE) VEINS IN RED FELSITE

MASSIVE AGGLOMERATE

BRECCIATION ZONE AT CONTACT BETWEEN AGGLOMERATE AND FELSITE

MASSIVE GREY FELSITE
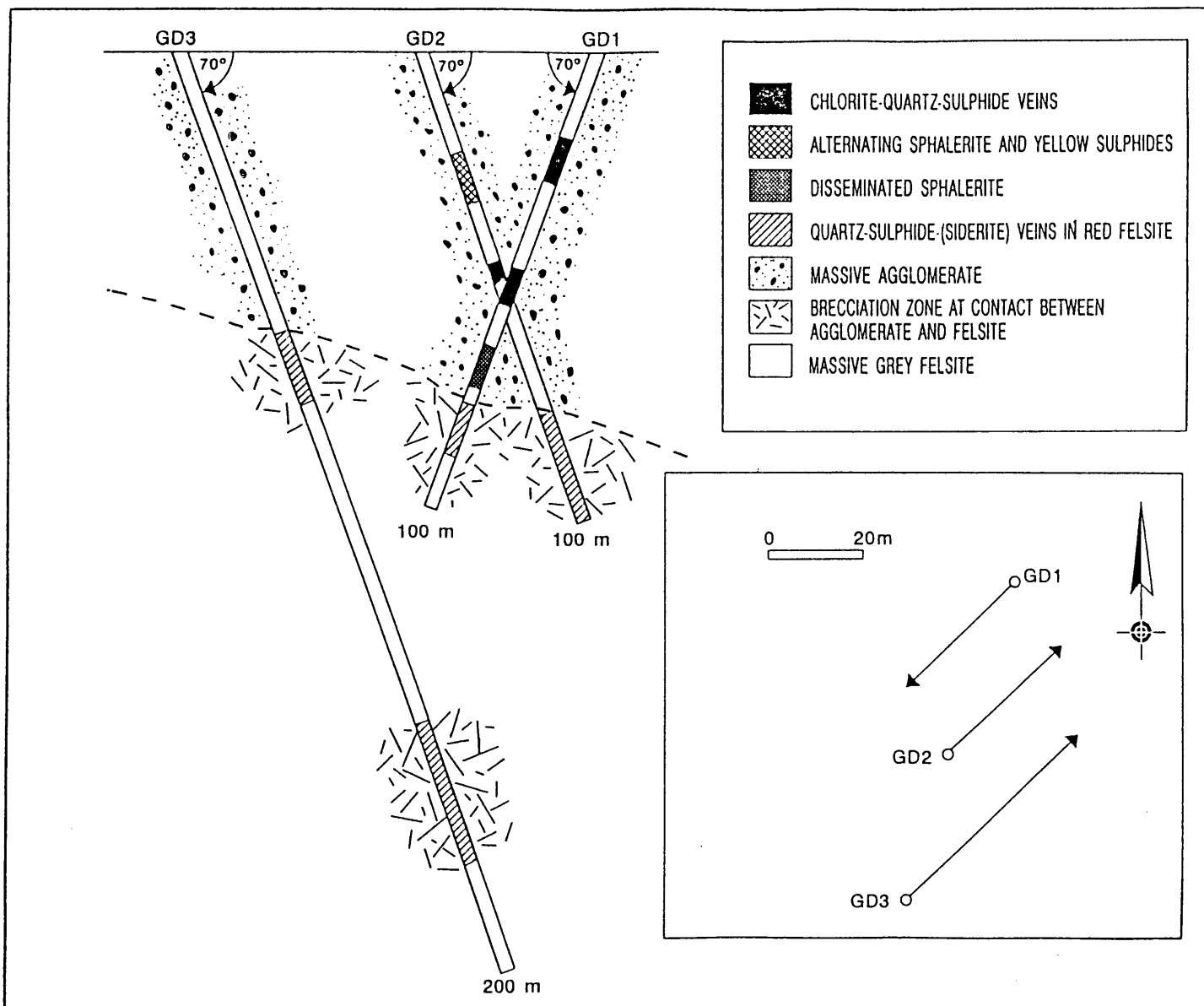
Macroscopic description of drill core

2.1 GENERAL

The sequence of rock types found in the drill cores is a minimum of 120m massive (i.e. unaltered) Rooiberg felsites (from here on called rhyolite), overlain by a 15-20m thick zone of "brecciated" rhyolite, covered by 60-70m of agglomerate (**Fig. 1.4**).

The massive rhyolite is usually grey in colour and fairly homogeneous. The rhyolite in GD3 is occasionally red with associated quartz and quartz + siderite vein systems (**Fig. 2.1**). The only sulphides present in these veins are pyrite and chalcopyrite (**Fig. 2.2**).

The brecciated zone is characterised by large fragments of rhyolite, separated by quartz and quartz + siderite veins with pyrite and chalcopyrite as the major sulphide phases (**Fig. 2.3**).

The agglomerate layer above the rhyolite contains significant amounts of sulphides. This layer consists of clasts, which differ in size, shape, and composition, within an usually green-grey matrix. Typical clasts in the agglomerate are: red-green flow-banded rhyolitic clasts (**Fig. 2.4**) up to 10 x 10cm, the green being chlorite, replacing part of the clast; smaller red, fairly homogeneous, rhyolitic clasts (**Fig. 2.5**) with dimensions up to 8 x 5cm; approximately 1 x 1cm red rhyolitic clasts (**Fig. 2.6**); small chlorite clasts (**Fig. 2.7**) (0.5 x 0.5cm), and rounded quartz clasts (**Fig. 2.8**) (1 x 0.5cm).

The matrix of the agglomerate consists of very small grains of a variety of minerals (e.g. quartz, feldspar, chlorite). It often changes gradually from green to reddish, and is red even in the vicinity of unmineralised/open fractures. The sulphide distribution in these different areas does not change with colour. Occasionally, narrow veins of chlorite (up to 10cm in thickness) perpendicular to the drill core (which has an inclination of 70°),

with these veins. This type of agglomerate will be referred to as "massive" agglomerate.
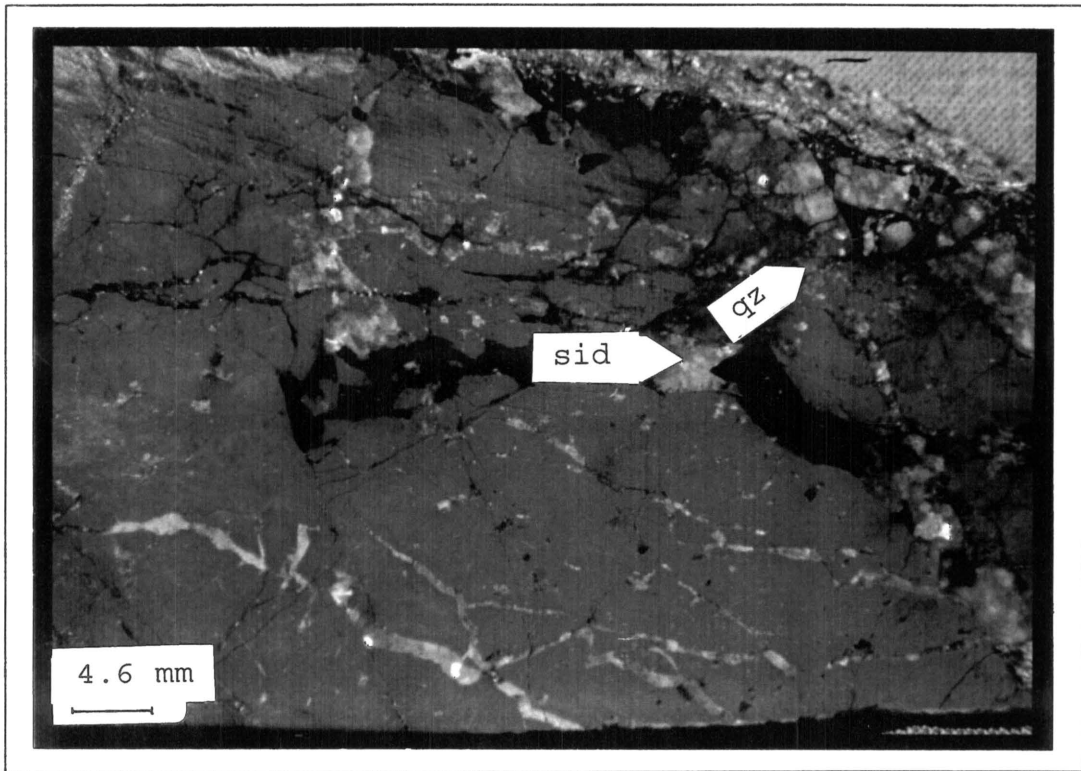
Fig. 2.1: Quartz(qz)-siderite(sid) veins in red rhyolite (GD3 at 158.33m).
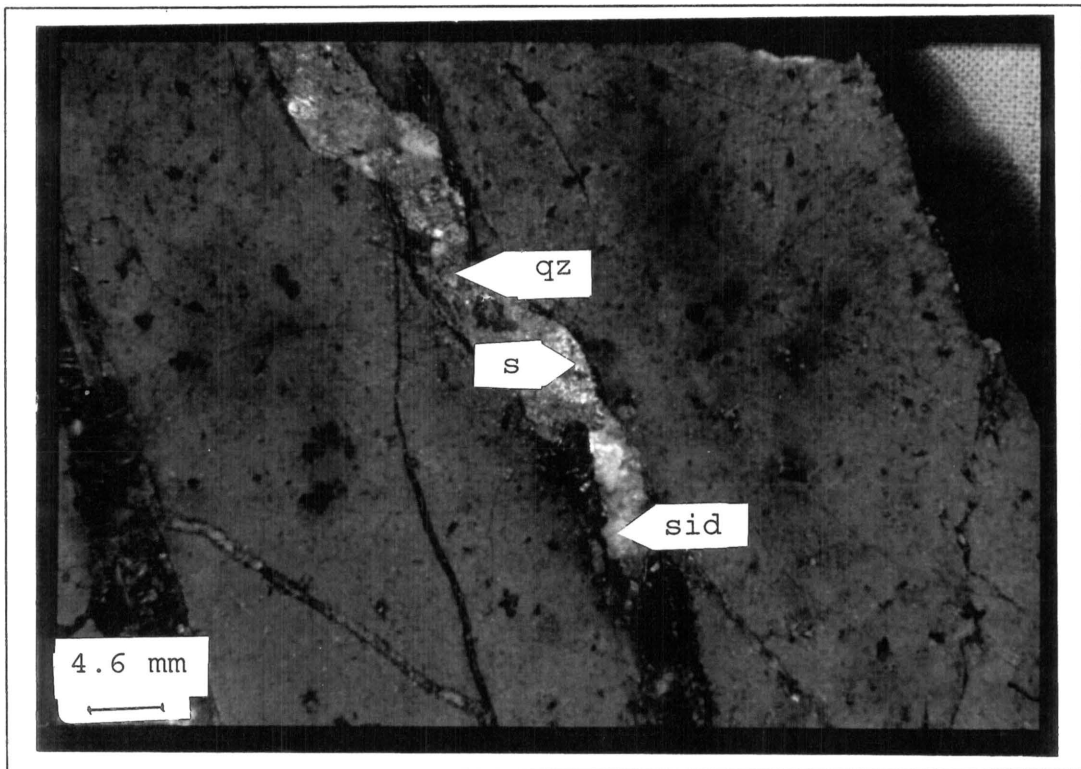
Fig. 2.2: Quartz(qz)-siderite(sid) vein with sulphides(s) (pyrite and chalcopyrite) in rhyolite (GD3 at 154.90m).

9
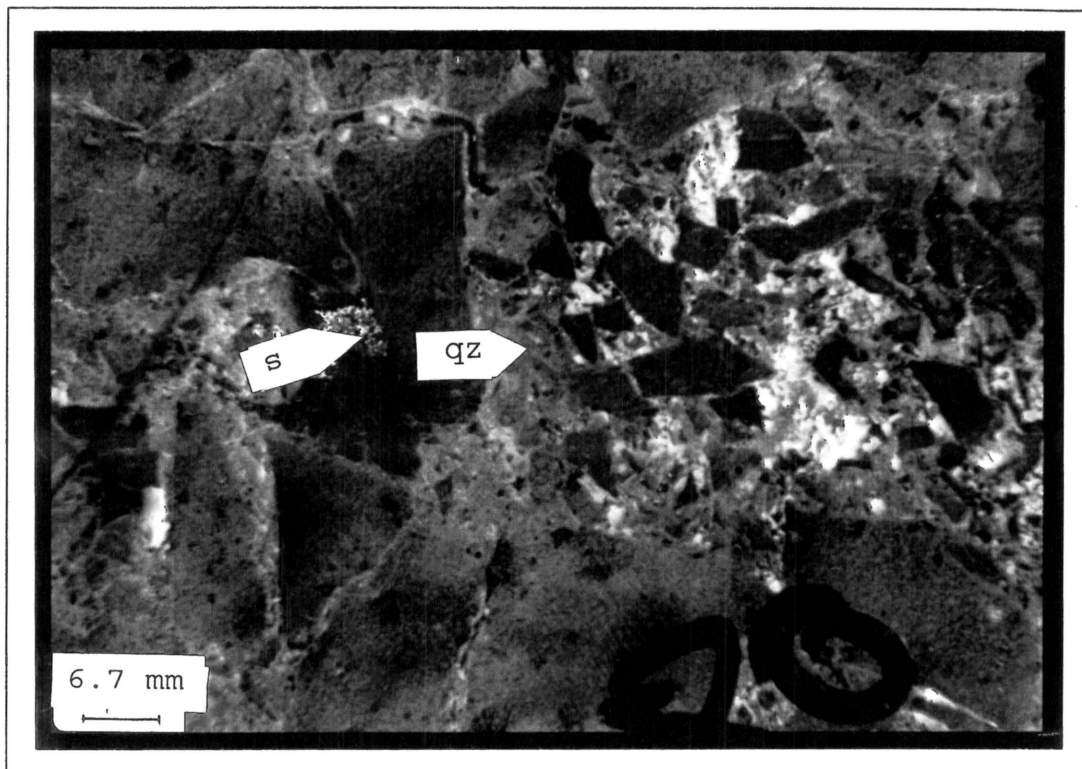
Fig. 2.3: Brecciated zone at contact between the agglomerate and rhyolite layer, filled with quartz(qz) and occasional sulphides(s) (GD1 at 80.0m).
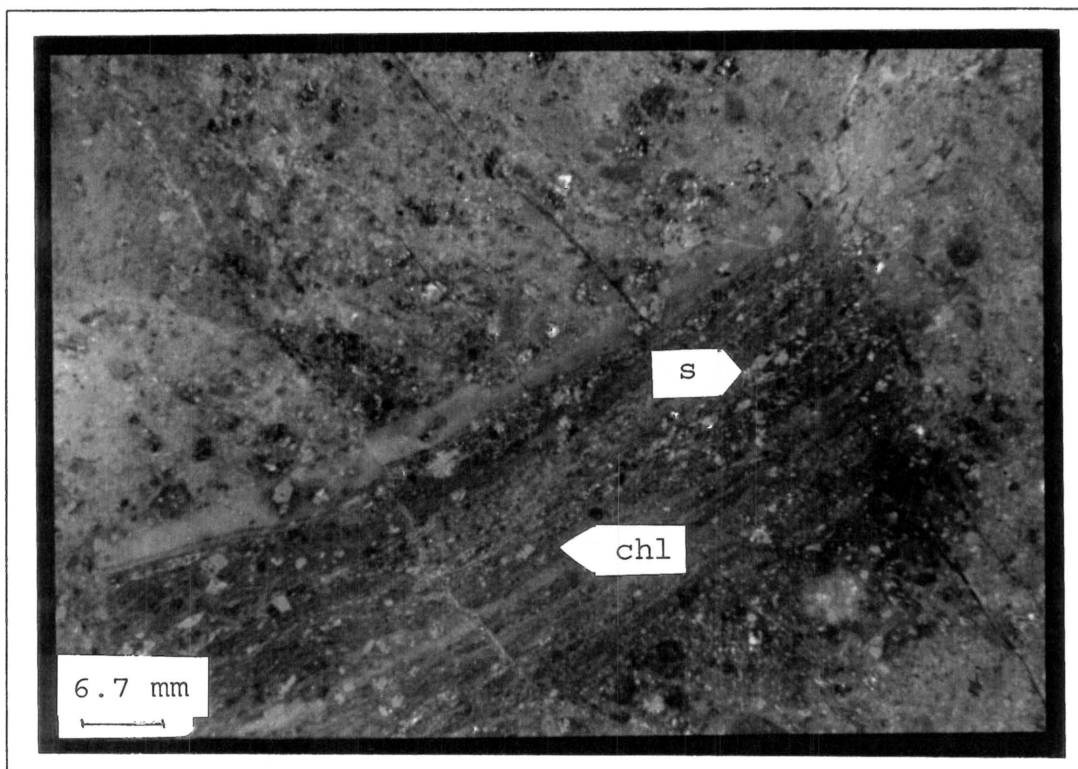
Fig. 2.4: Flow-banded clast, with sulphides(s) associated with chlorite(chl), in red agglomerate in GD2 at 19.60m.
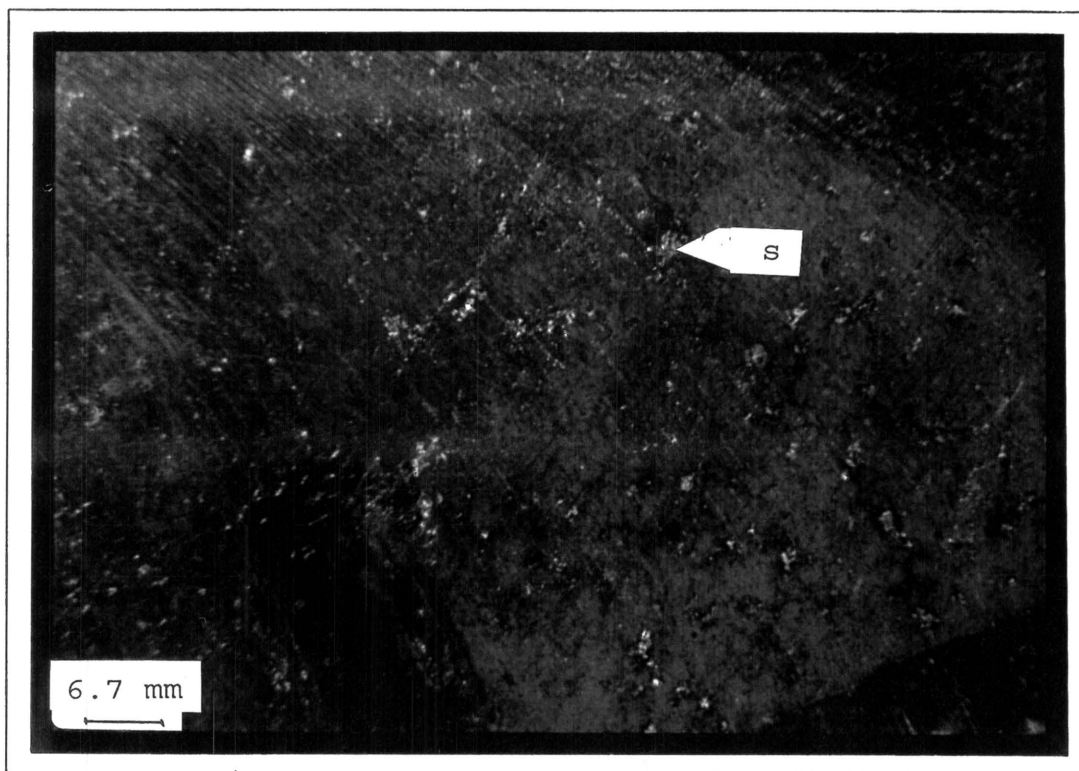
Fig. 2.5: Red, homogeneous rhyolitic clast with sulphides(s) in green agglomerate (GD1 at 22.60m).
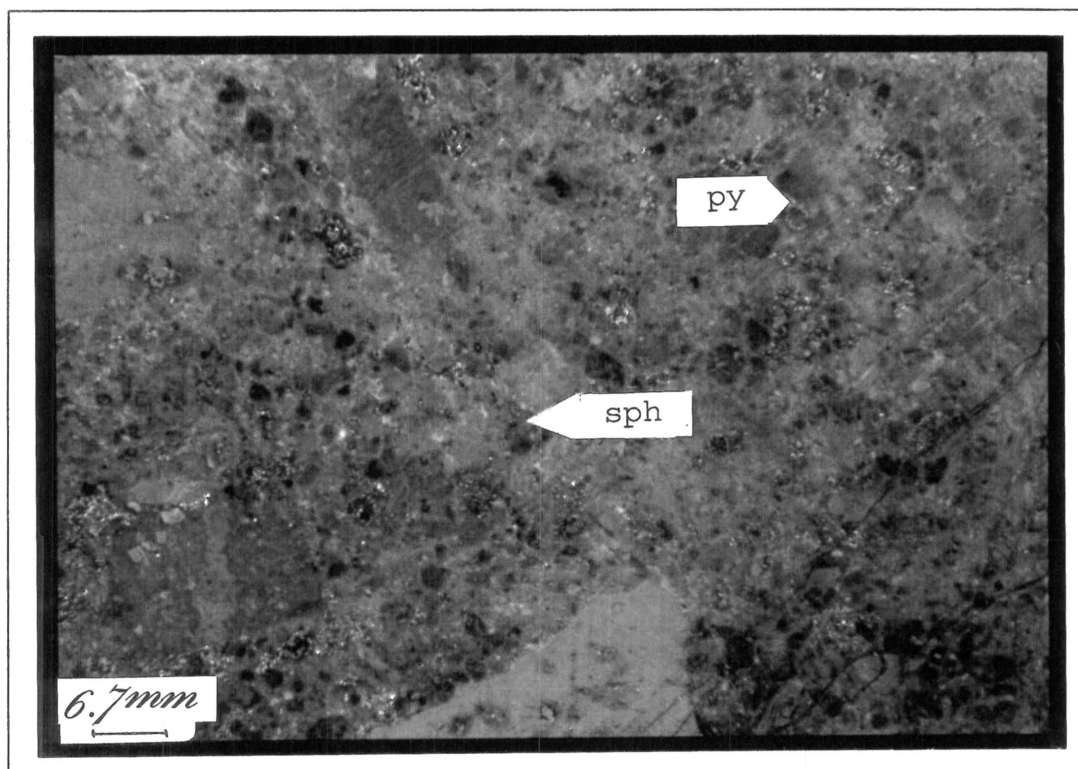
Fig. 2.6: Small red rhyolitic clasts and sphalerite(sph) and pyrite(py) in red agglomerate (GD2 at 27.20m).

11
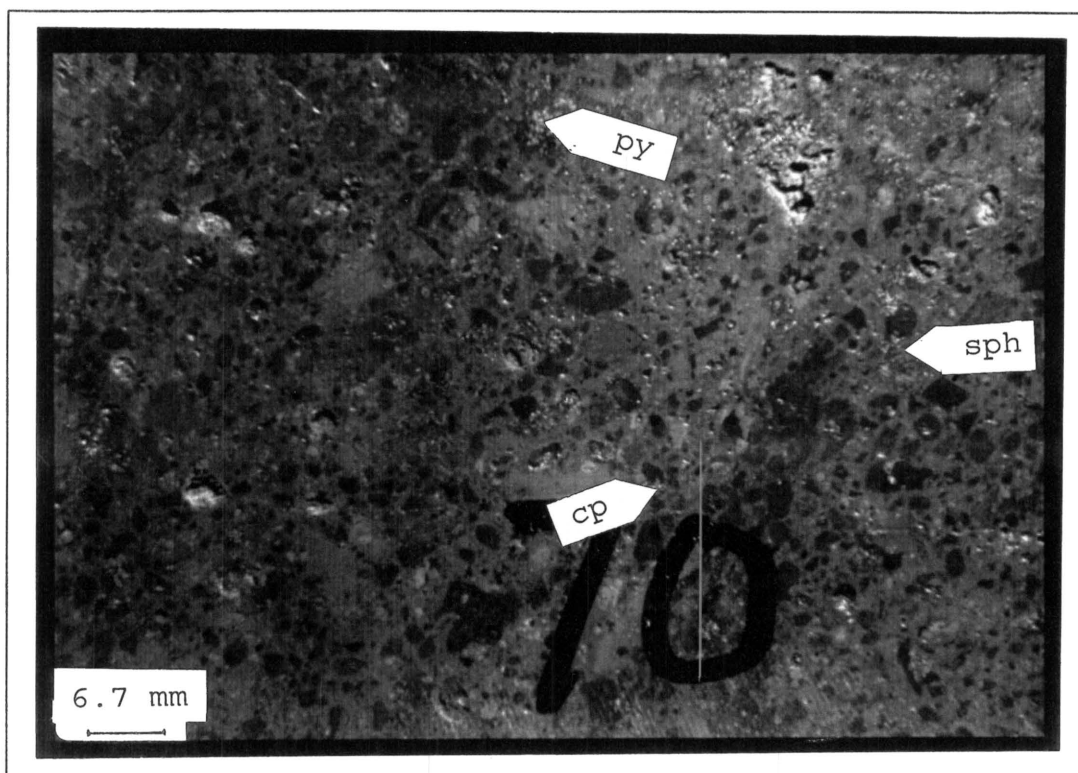
Fig. 2.7: Small chloritic clasts, some associated pyrite(py), chalcopyrite(cp) and sphalerite(sph), in green agglomerate (GD2 at 70.0m).
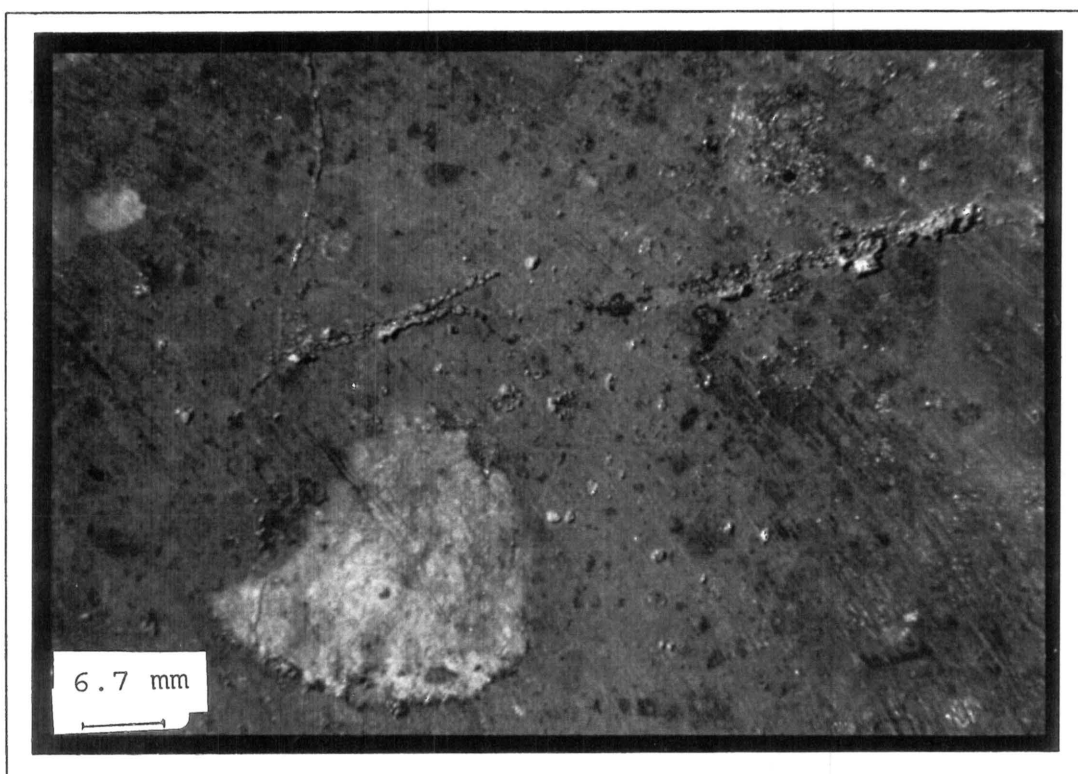
Fig. 2.8: Rounded quartz clasts in red agglomerate (GD1 at 27.35m).

Apart from narrow chlorite veins in the agglomerate, a prominent vein system, containing chlorite, quartz, and sulphides was intersected. This sulphide bearing "vein" is much wider (5-10m thick) and affected by supergene alteration in GD2. The dominant sulphide mineral is arsenopyrite with smaller amounts of visible pyrite and chalcopyrite (**Fig. 2.9**).

GD4 and GD5 look very similar to GD1, GD2 and GD3 but are unmineralised with respect to ore minerals, and were only used as stratigraphic correlation and possible geochemical references. Other core (GD6 - GD11) intersecting the same formations of the Rooiberg Group in the Rust de Winter area was only briefly looked at. The agglomerate in these core was generally fine grained and together with the rhyolite, highly oxidised.

2.2 DRILL CORE DESCRIPTION

2.2.1 GD1:

The first 5m of GD1 are weathered agglomerate, followed by 12m of an alternating change in colour of the matrix (green and red). However, no change in the sulphide assemblages is associated with this change in colour. Occasionally minor disseminated grains of pyrite and chalcopyrite were observed in the matrix, associated with chlorite clasts, quartz clasts, and flow-banded red rhyolitic clasts (similar to **Fig. 2.10**).

Open fractures are occasionally present. Directly adjacent to these fractures the matrix is stained dark red. Another characteristic feature of the areas next to the fractures is the occurrence of small chlorite veins, perpendicular to the core axis. These veins do not contain any ore minerals.

In the interval from 17-26m, the first major sulphide concentration appears, associated with massive chlorite(-quartz) mineralisation. The most dominant ore mineral is arsenopyrite, which occurs in massive "clusters" within the chlorite (**Fig. 2.9**). No distinct orientation of the chlorite (+ quartz) + arsenopyrite vein could be established.
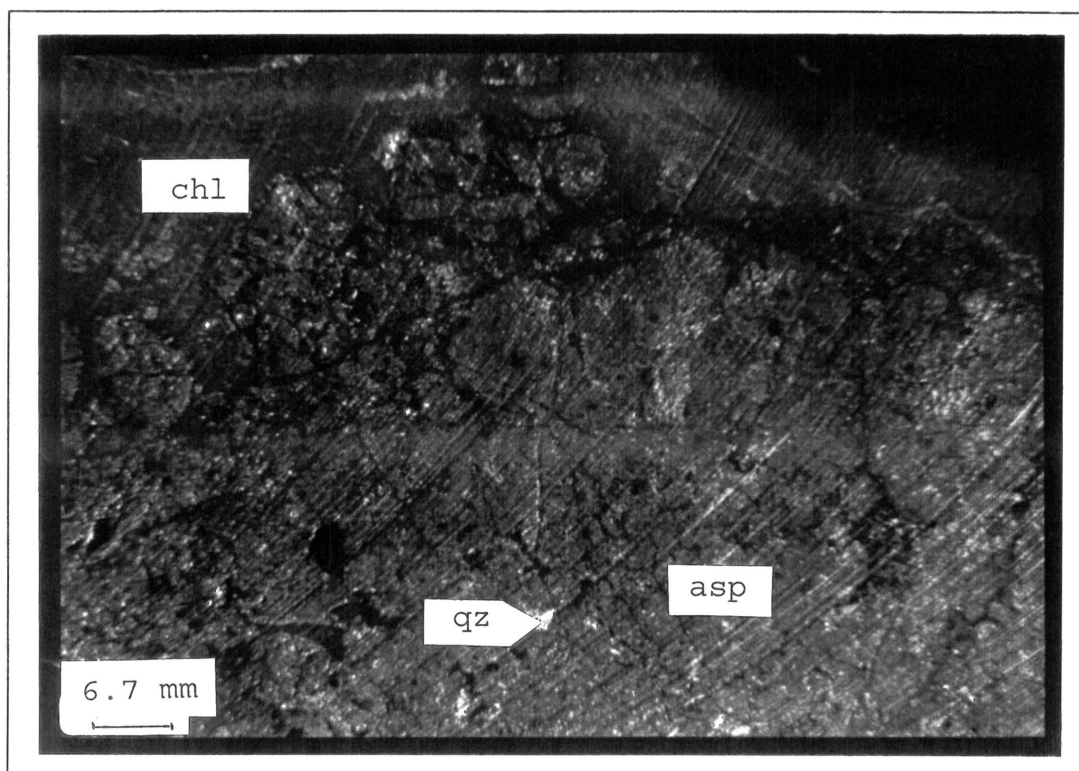
Fig. 2.9: Massive arsenopyrite(asp) in a matrix of chlorite(chl)-quartz(qz) (GD1 at 22.40m).
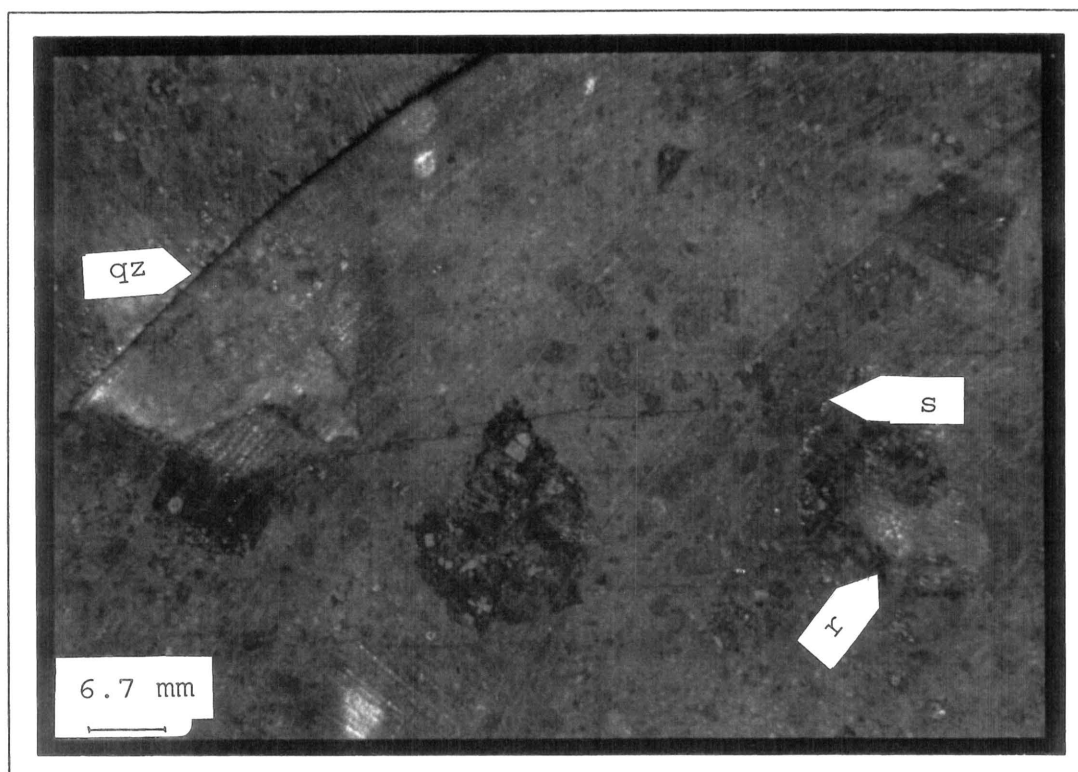
Fig. 2.10: Sulphides(s) along the rim of rhyolitic(r) and quartz(qz) clasts in red agglomerate (GD1 at 29.20m).

14

The 20-44m level has the same appearance as the previously described massive agglomerate zone (5-17m level), characterised by green and red areas. This interval is fairly unaltered with only minor fracturing. The fractures are in places filled with sulphides, quartz, and chlorite. The small green chloritic clasts often contain sulphides present in the middle of the clast. Sulphides also occur in the vicinity of larger rhyolitic clasts (**Fig. 2.10**), or within and/or in the vicinity of large flow-banded rhyolitic clasts. In general, the sulphide mineralisation seems to be preferentially associated with chlorite mineralisation, either in veins, in chloritic clasts or as chlorite replacements in flow-banded rhyolitic clasts.

At a depth of 45-53m, the same type of altered chlorite vein as described above (17-26m level) occurs, also with predominantly arsenopyrite as ore mineral. The main difference between this vein and the similar one to the top, is that here supergene alteration resulted in the replacement of sulphides by copper-sulphides (**Fig. 2.11**).

This chlorite + quartz + arsenopyrite vein is followed by massive agglomerate, in which disseminated sulphides were observed. Between 62-70m sphalerite appears in the agglomerate matrix, together with pyrite and chalcopyrite (**Fig. 2.12**). Arsenopyrite occurs in small amounts, in the form of individual grains, in small quartz + chlorite veins.

The amount of sulphides decreases sharply as the brecciated contact (at 74m) between the rhyolite and the agglomerate is approached. Sulphides in the quartz veins, between the rhyolite fragments, are primarily pyrite and chalcopyrite. Beneath this brecciated zone, the rhyolite is grey, fairly massive, and unaltered. Sulphides were observed only as rarities.

2.2.2 <u>GD2:</u>

In GD2, a transition from a narrow zone (5m) of weathering to the unweathered massive agglomerate occurs over the first 20m. From 20-32m, a characteristic alternation of the yellow sulphides (i.e. pyrite and chalcopyrite) with sphalerite occurs. The contacts of the alternating sulphide zones are gradual on a centimetre scale (**Fig. 2.13**).

15
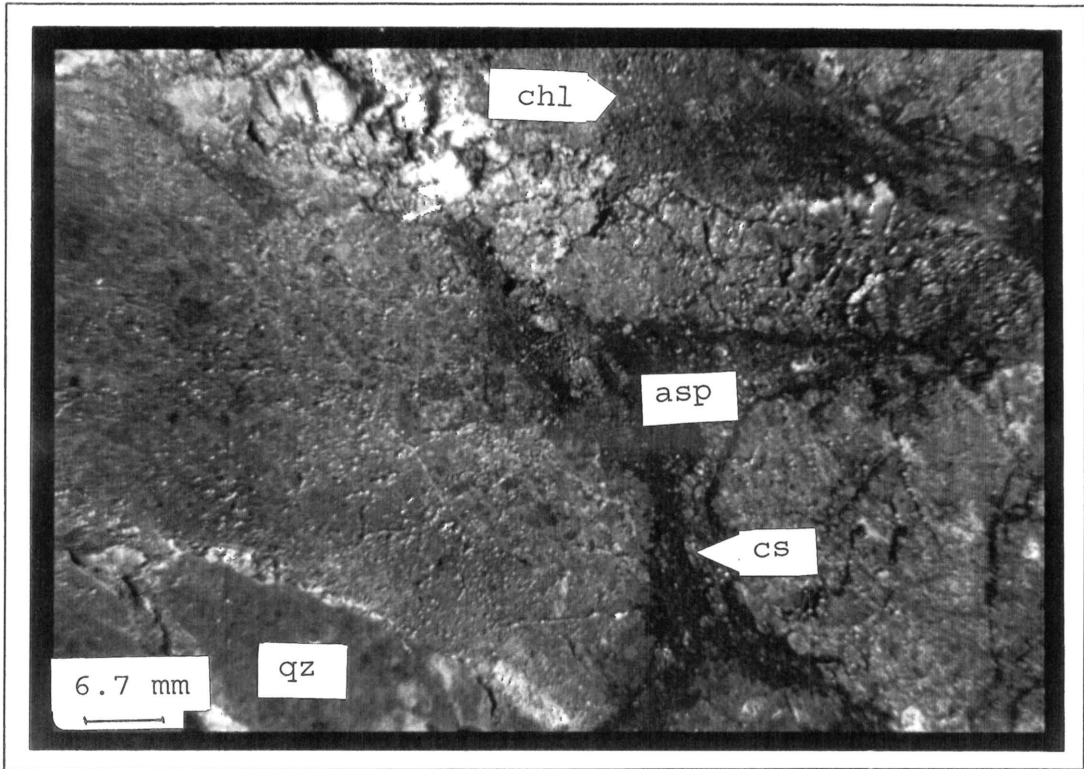
Fig. 2.11: Chlorite(chl) + quartz(qz) + arsenopyrite(asp) vein with copper sulphides(cs)(GD1 at 47.20m).
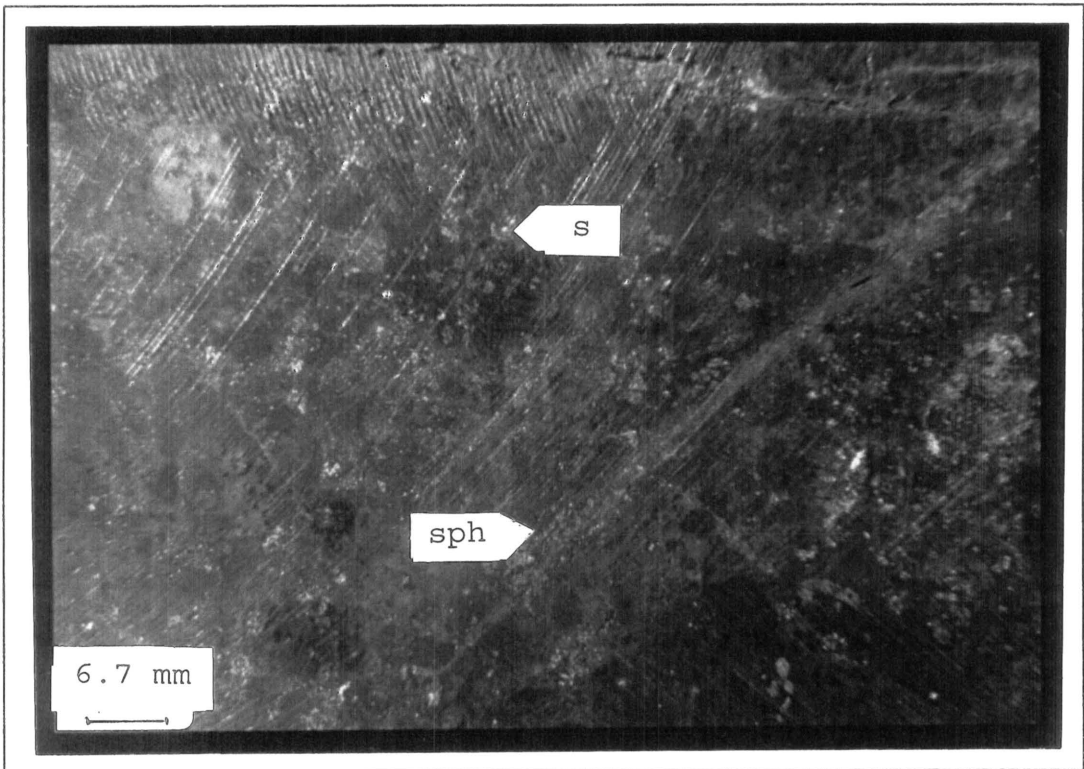
Fig. 2.12: Disseminated sphalerite(sph) together with other sulphides(s) in green agglomerate (GD1 at 70.50m).

16
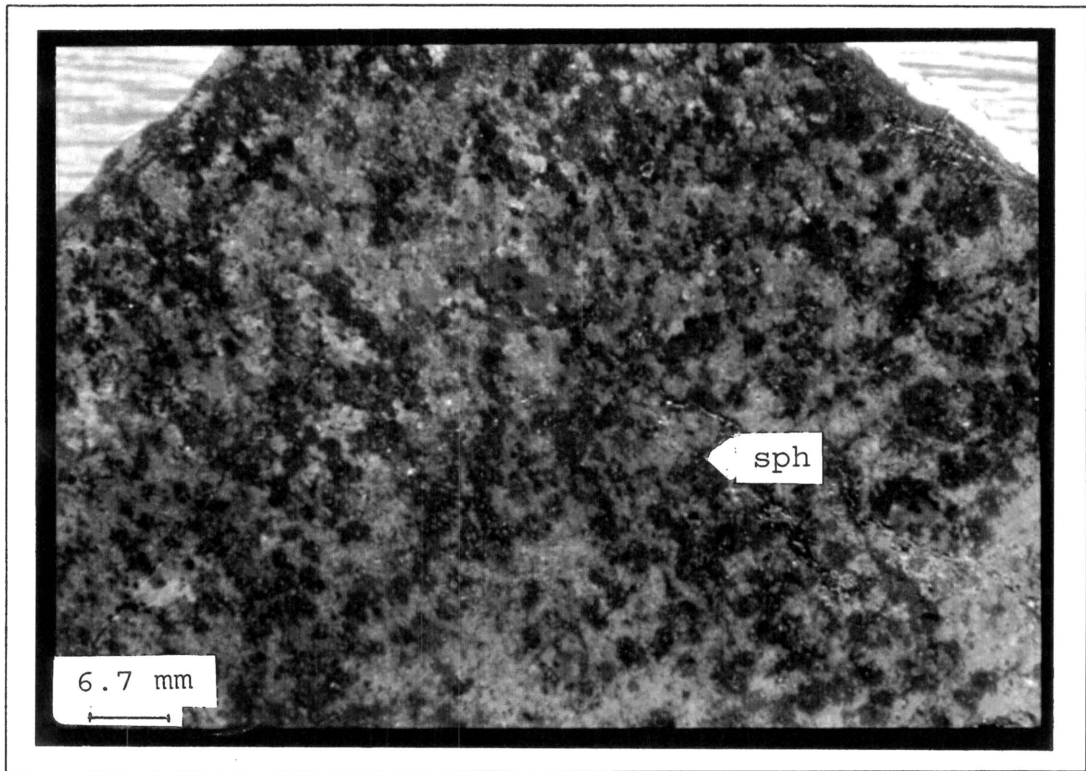
Fig. 2.13: Disseminated sphalerite(sph) in the matrix of red
agglomerated (GD2 at 20.20)m.
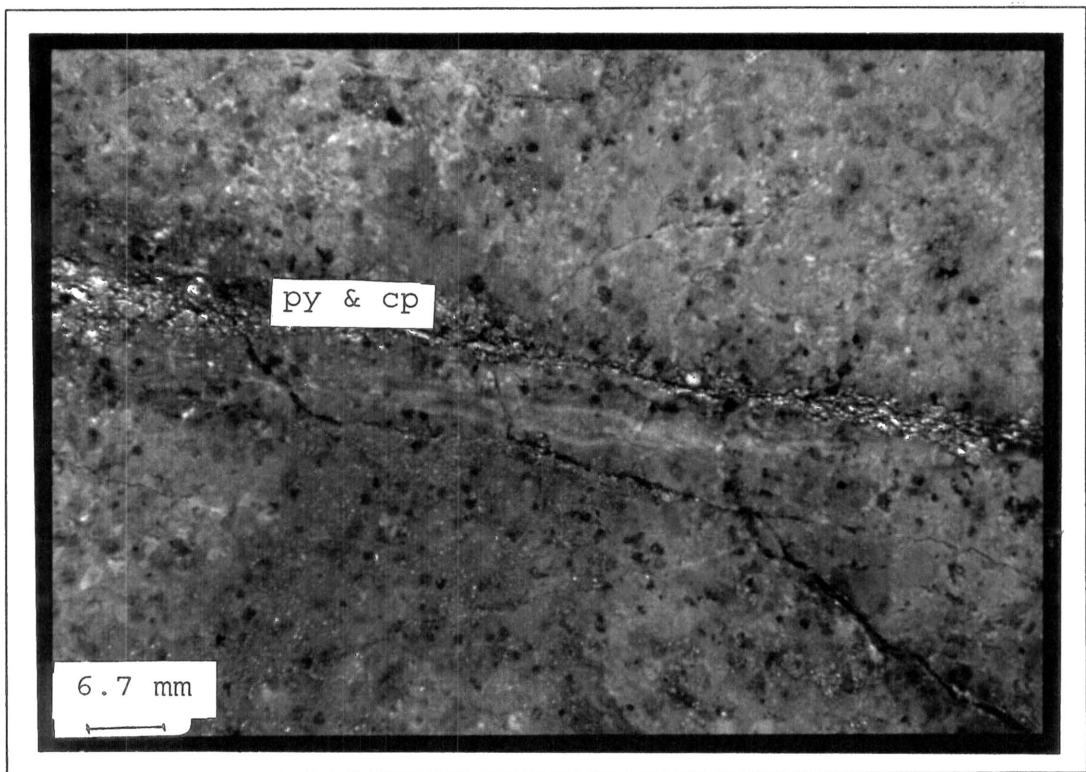
Fig. 2.14: Pyrite(py) and chalcopyrite(cp) in a vein and also
disseminated in the red agglomerated matrix adjacent to the vein
(GD2 at 24.60m).

A massive agglomerate zone (13m thick) occurs between the zone of base metal sulphide alteration and the first chlorite + quartz + arsenopyrite vein. This vein is 3m in thickness, characterised by massive arsenopyrite clusters within the chlorite, and shattered quartz vein fragments occasionally associated with pyrite and chalcopyrite. This occurrence of arsenopyrite is mineralogically linked to the two areas in GD1 that contain the same mineral assemblages, and it is concluded that these areas belong to the same mineralising vein system.

This arsenopyrite concentration is followed by massive agglomerate. Directly above the brecciated rhyolite zone, an area (at 70m) of sphalerite mineralisation occurs, 1 meter in thickness. The brecciated lavas in this core have a similar appearance to those within GD1.

2.2.3 GD3:

GD3 is characterised by very small amounts of sulphide in the massive agglomerate (except that of the common disseminated sulphides in the matrix and occasionally in fine chlorite veins). Thus, the first 60m are fairly constant in regard to clast, matrix, and sulphide distribution. At a depth of 60m, the brecciated zone in the rhyolite (18m in thickness) is reached and the same picture emerges as described for GD1 and GD2.

As a distinct difference, two major zones, in which the colour of the rhyolite changes from grey to red, are intersected in GD3 (at 60m and 150m). Red coloured rhyolite contains quartz- and quartz-siderite veins, carrying pyrite and chalcopyrite. The brecciated zone is followed by a zone of grey massive rhyolite. At 146m, a second brecciated red rhyolite with veins appears with the same features as that of the first red brecciated zone. Beneath 172m, the lava changes its colour back to grey with the disappearance of veins and associated sulphides.

2.3 SUMMARY

2.3.1 Stratigraphic succession:

In the investigated study area the stratigraphic succession comprises 60 to 75 meters of agglomerate, overlying massive rhyolite. The agglomerate layer belongs to the Union Tuff

18

Member and the rhyolite layer is part of the Kwaggasnek Formation, according to Schweitzer et al. (1995a) or unit 8 of the Rooiberg Felsites according to Twist (1985). The agglomerate layer is the host for a disseminated Zn-Cu mineralisation as well as a hydrothermal mineralisation comprising arsenopyrite, base metals (e.g. Fe, Cu, Bi, and Pb) and gold. The rhyolite layer is virtually barren except for localised siderite + quartz veins with small amounts of pyrite and chalcopyrite. A more complete description of GD1, GD2 and GD3 is given in **Appendix A.**

2.3.2 <u>Styles of mineralisation:</u>

Six styles of mineralisation can be distinguished (**Table 3.1**).

Table 2.1: The styles of sulphide mineralisation:

Rock Type	Characteristics of mineralisation	Main sulphide minerals	Figures
1. Agglomerate	Surrounding quartz clasts	pyrite and chalcopyrite	Fig. 2.10
2. Agglomerate	Within chlorite clasts	pyrite and chalcopyrite	Fig. 2.7
3. Agglomerate	Rhyolite clasts, surrounded by sulphides; flow-banded rhyolite clasts with chlorite bands	pyrite and chalcopyrite	Fig. 2.4 Fig. 2.5
4. Agglomerate	Disseminated in matrix and surrounding other sulphides	Sphalerite, pyrite and chalcopyrite	Fig. 2.13
5. Agglomerate *	Chlorite + quartz veins	Arsenopyrite, pyrite, chalcopyrite, copper-sulphides, Bi-containing sulphosalts**	Fig. 2.9 Fig. 2.14
6. Breccia zone between agglomerate and rhyolite	Quartz + siderite veins	pyrite and chalcopyrite	Fig. 2.2

* The dominant mineralisation style

** Based on microscopic examination (**Chapter 6**)

19

Methods of investigation

3.1 Drill core sampling

Core samples from GD1, GD2, GD3 and GD5 were selected to represent the different mineralisation styles (**Table 2.1**) and unmineralised samples were also selected for geochemical analysis. The samples of the mineralisation styles were taken for the mineralogical investigation of the ore and gangue minerals. Samples for geochemical analyses were taken of both the agglomerate and the underlying rhyolite. Sampling the already heterogeneous agglomerate from core required caution, because large clasts will bias the geochemical data. Therefore, samples were on average 30 cm long (with a diameter of 6 cm), 2 - 6 kg and relatively homogeneous, with visible clasts not bigger than approximately 1 x 2 cm.

3.2 THIN SECTION MICROSCOPY

Uncovered thin sections were prepared to study the gangue minerals (chlorite, quartz, mica and siderite) in the veins. Sections of these were used to analyse chlorite and siderite with the electron microprobe. Polished thin sections were also made to investigate the relationship of the gangue minerals and the ore minerals in the veins.

3.3 XRF - ANALYSES OF WHOLE ROCK SAMPLES

Whole rock geochemical analysis was performed on 29 core samples from all the boreholes (GD1 - GD11). Samples were first crushed and then milled in a tungsten mill to 63 micron and analysed for major and trace elements on fused discs and powder briquettes respectively. Geochemical analyses of the red and green agglomerate are summarised in **Appendix B**.

3.4 ORE MICROSCOPY

Polished sections and polished thin sections were made to study the opaque minerals in the veins as well as that in the matrix of the agglomerate. Microscopy was done in air and in oil immersion. Some of these sections were selected to determine the chemical composition of some of the ore minerals (arsenopyrite, sulphosalts, and sphalerite).

3.5 X-RAY DIFFRACTION

3.5.1 Chlorite:

An XRD investigation was carried out to study the chlorites in clasts and veins in the study area, and the minerals intimately associated with it. The interlayering of other sheet silicates (e.g. muscovite, smectite, and illite) will increase the basal spacing of the chlorite and this will be displayed in the XRD pattern. Under oxidising conditions, the alteration of a tri-octahedral chlorite may lead to the formation of smectite (Nieto et al. 1994). The position of the characteristic 14 Å peak will then shift to the left of the XRD pattern (i.e. higher d-values) after treatment with a ethylene glycol solution (**Appendix C**). It was found that the chlorites of the study area contain no interlayered swelling clay, but that varying amounts of muscovite and quartz are occasionally present in chlorite in veins.

3.5.2 Copper sulphides:

Samples from an area in GD2 that contains large amounts of copper sulphides have been analysed to identify the various copper sulphide phases associated with supergene alteration. Optically these phases look very similar and are sometimes finely intergrown. The XRD pattern and d-values are given in **Appendix D** and results are discussed in **Chapter 6**.

3.6 ELECTRON MICROPROBE ANALYSIS

Analysis of the sulphide minerals and siderite was carried out using the energy despersive method on a JEOL 733 electron

microprobe, connected to a Linkam eXL II software programme. For chlorite the wavelength despersive method was used. Analytical conditions are summarised in **Appendix E**.

3.6.1 <u>Chlorite:</u>

Chlorite in 40 thin sections were analysed quantitatively. During the measurements different problems were encountered: (1) the poor polish of chlorite, due to its layered nature, led to an uneven surface that influenced the counting statistics; (2) the very small grains of chlorite in the clasts created the same problem, and consequently the result was low totals of 76 - 85 wt%, compared to 88 - 90 wt% for an average H_2O content of 10 - 12 wt%; (3) semi-quantitative microprobe analyses indicated higher amounts of K_2O than allowed in the chlorite structure. This implies that chlorite and mica are intimately intergrown in some clasts, although the white mica is not always visible under the optical microscope. The microprobe cannot distinguish interlayering, as the spacial resolution of microprobe analyses for chlorite, under the chosen analytical conditions, is in the order of 10μm. But on the basis of the XRD pattern the possibility of such an interlayering is ruled out; mica is thus present as very small grains. This problem is restricted to the chloritic clasts; where mica appears in the veins it normally occurs as large, well defined grains. **Appendix F** shows the microprobe analysis of some of the chlorites analysed.

3.6.2 <u>Sulphide minerals:</u>

Arsenopyrite and sphalerite were analysed quantitatively; the quantitative analysis of the Bi-containing sulphosalts was problematic, due to the lack of appropriate reference materials. For the semi-quantitative analyses, bismuthinite (Bi_2S_3) and galena (PbS) were used as standards for Bi and Pb, but because of the lack of a Cu_2S standard, cuprite (CuO) was used as a standard for Cu. Bismuthinite (Bi_2S_3) and PbS were used as a sulphide standard for this sulphosalt. Alternative standards for sulphur, that were tried to improve the analyses were: pyrite (Fe_2S), chalcopyrite ($FeCuS_2$), and stibnite (Sb_2S_3).

3.7 FLUID INCLUSION STUDIES

3.7.1 Sample preparation:

The intergrown nature of quartz and chlorite in the main mineralised veins caused problems in preparing double-polished sections. The alternative was to make sections from veins which contain a larger proportion of quartz. The risk is, however, that these veins may not (and normally do not) contain the same mineral assemblages found in the main mineralised zone (i.e. chlorite + quartz + sulphides; the latter being mainly arsenopyrite, pyrite, Bi-sulphosalts and chalcopyrite). The implication is that the physico-chemical properties of fluids in these veins can be expected to differ from those in the main mineralised zone. However, results may still be meaningful because these veins are close enough (a few meters) to the main mineralised zone, although multi-stage mineralisation may imply different temperatures. Only the most consistent results are given and interpreted together with other geothermometric data (e.g. chlorite geothermometery).

A total of 22 double-polished thin sections were studied optically to identify the areas of fluid inclusions suitable for investigation. A large proportion of the fluid inclusions is very small and vapour bubbles cannot be (clearly) seen. These inclusions are not suitable for fluid inclusion analyses. Inclusions denoted as secondary occur as strings on grain boundaries and those reported as primary are normally single inclusions inside a quartz grain or do not form part of a string. All inclusions analysed consist of a (single) liquid and vapour phase (L + V); no inclusions with daughter minerals were observed.

A total of 44 inclusions were measured on a Linkam LNP2 gas heating-freezing system, that gives reproducible results to $\pm 1°C$ for heating runs and $\pm$ 0.1°C for freezing runs. Data were read into the "PVTX Software Modelling for Fluid Inclusions Version 1" software package, and all consequent calculations were done with this program.

3.7.2 Microthermometry:

To prevent decrepitation of inclusions at high temperatures, the inclusions were first cooled down to measure the melting temperature (T_m). Due to the often unclear phase transformation from liquid to solid (ice), inclusions were usually supercooled to a temperature below -60°. This process was then succeeded by heating the section to a temperature at which the vapour bubble will dissappear (T_h). Some inclusions were cooled and heated twice to ensure that the temperatures T_m and T_h are correct.

Characteristics of the host-rock

4.1 PETROGRAPHY

4.1.1 Rhyolite:

Due to the fine texture of the rhyolite it was not possible to optically identify different minerals in the rock. At the contact with the agglomerate layer and further down in GD3 (150m) the colour of the rhyolite changes to red. This red colour is possibly the result of oxidation, that is not clearly displayed in the mineralogy.

4.1.2 Agglomerate:

During the logging of the core it was found that the agglomerate in which the mineralization occurs contains green and red patches. Based on a microscopic study it was concluded that the green appearance of the agglomerate was an effect of chloritisation while the red agglomerate was oxidised to varying degrees possibly during a different stage of fluid activity. Thus, the colour of the agglomerate is considered to be an indication of the alteration style.

4.2 GEOCHEMISTRY

4.2.1 Introduction:

Geochemical data of whole rock samples can be used as an aid in exploration, and up to date it has been used mainly to subdivide the Rooiberg Felsite Group (e.g. Clubley-Armstrong, 1977; De Bruiyn, 1980; Twist, 1985; Schweitzer et al., 1995a).

Alteration zones are attractive targets for precious and base metal exploration (Clarke and Govett, 1990), and anomalies of the more mobile elements (e.g. K, Na, Ca and Mg) will be the first indicators of mineralisation. Hydrothermal activity that is not part of an ore-forming system may also lead to propylitic alteration, but would lack additional indicators like anomalous concentrations of characteristic pathfinder elements such as Sb, As, Hg, Tl, Mo, W, and Mn. The upper levels of a gold-containing epithermal system normally contain higher contents of some or all of As, Sb, Ba, F, Hg, B, and Tl, whereas at greater depths elevated contents of any of the following elements are characteristic: Cu, Pb, Zn, Mo, Ag, Bi, Te and Co (Clarke and Govett, 1988).

Lesher et al. (1986) considered high-level subvolcanic magma chambers (e.g., rhyolitic volcanic centres) to be essential components of ore-forming hydrothermal systems. The trace-element geochemistry of such rhyolitic metavolcanic rocks may aid in selecting targets for base metal exploration.

In the Iktinah paleovolcano (Roobol and Hackett, 1987) the central and adjacent parts of the proximal volcanic facies contain disseminated pyrite in argillised host rocks. This indicates an extensive original hydrothermal core, surrounded by halos of base metal occurrences. It may be possible that a similar system exists in the Rooiberg Felsite, and that the studied base metal occurrences may be part of such a halo. A geophysical feature (personal communication by geophysical staff of Genmin) in the area of the investigated system could be an indication of such a centre. Generally, if no metallic deposits are known in the area of eruptive centres, this may be the function of a shallow erosion level rather than the absence of mineralization (Watts and Hassemer, 1989). If the centre can be located, target areas may be identified more accurately with the aid of geochemistry and geophysics.

Geochemical data can also be used to fingerprint a specific stratigraphic unit. Immobile trace elements proved to be valuable tools in stratigraphic correlation (with regard to geochemistry,

26

age, alteration etc.), regardless of the extend of alteration (Davies et al., 1979; Davies and Whitehead, 1980). A stratigraphic correlation of the studied sequences at Rust de Winter based on the geochemical information have been identified by Smith (1993). However, by correlating the geochemical data of the Rust de Winter area with that of published geochemical data on the same unit, the type of alteration present in the agglomerate layer at Rust de Winter can be identified.

In search of a close reference, material from boreholes GD6, GD8 and GD9 (that became available later in the study and intersect the same unit at a distance from the hydrothermally altered agglomerate) were considered. However, this agglomerate could not be used as reference for the unaltered agglomerate, because it was strongly oxidised as is evidenced by the higher Fe-content and the obvious red colour. Because it can be assumed that the bulk of the material that constitutes the agglomerate layer originates from the underlying rhyolite (unit 8), the geochemical data of this layer in the Loskop Dam (Twist, 1985) and in the Rust de Winter area (De Bruiyn, 1980), were considered to be good references for the studied agglomerate layer.

4.2.2 The immobile elements:

Before a decision can be made as to what the composition of the precursor rock of the hydrothermally altered agglomerate has been, the reliability of "immobile" elements as indicators of mass transfer (as described by Gresens (1967), Grant (1986) and MacLean (1990)) have to be considered. The elements most commonly used for this purpose are Zr and Ti since they normally stay immobile during hydrothermal alteration. Yttrium, Sc and Nb, are also frequently considered immobile, but they can be extremely mobile during alteration of volcanic rocks, due to metamorphism, hydrothermal events, and weathering (e.g., Finlow-Bates and Stumpfl, 1981).

It has, however, been found that the geochemical data of two vein samples which consist mainly of chlorite show a significantly higher Zr content (>500 ppm) relatively to that of the altered

27

agglomerate and underlaying rhyolite (which are in the order of 200 - 400 ppm). Chlorite can contain Zr as a trace element, but concentrations are usually very low (~43 ppm, Albee et al., 1965).

Based on this observation it is necessary to look into the conditions under which so-called immobile elements like Zr and Ti can become mobile. This specific aspect has been investigated by several researchers. In the metabasalts of the Ascot Formation, SE Quebec, Hynes (1980) found a strong correlation between Ti, Zr and Y concentrations and the degree of carbonatisation, i.e., high CO_2 levels in the fluid phase during metamorphism. Low carbonate rocks are severly depleted in Ti, Y, and Zr whereas high carbonate rocks are depleted in Y and Zr and enriched in Ti. Based on two contact aureoles in Italy, Gieré (1986, 1989) concluded that F^- and PO_4^{3-} could also act as ligands for complexing with high valence cations, such as Ti^{4+} , Zr^{4+} and Y^{3+} in K-rich metasomatic fluids. Rubin and co-workers (1989;1993) also found that Zr can be highly mobile in most F-rich systems related to alkalic, F-rich igneous suites, but may also be promoted by sulphate complexing as in the case of Ertsberg, Indonesia. The availability of Zr, however, depends strongly on the Zr mineralogy of igneous source rocks, i.e. hydrothermal solutions could easily break down aegirine and arfvedsonite to release trace amounts of Zr, but zircon is only moderately attacked (Rubin et al., 1993).

Therefore, although Zr and Ti are normally immobile in hydrothermal systems, they can be mobilised in a fluid rich in any of the following ions and compounds: F^- , PO_4^{3-} , CO_2 and SO_4^{2-} .

Scattergrams show that there exist well defined linear relationships between both TiO_2 - Zr and Al_2O_3 - Zr. The positive correlation between TiO_2 and Zr (**Fig. 4.1**) as well as Al_2O_3 and Zr (**Fig. 4.2**) are an indication that these elements behaved similarly during hydrothermal alteration. If Zr was mobilised during chloritization, by implication, so were TiO_2 and Al_2O_3.

The immobile element data from the agglomerates are compared with those of the Schrikkloof and Kwaggasnek successions (Schweitzer et al. 1995b) in a TiO_2 - Zr plot (**Fig. 4.3**). From

this it is clear that the trend in the study area corresponds well with data for the Schrikkloof and Kwaggasnek Formations.

— (Linear Fit)
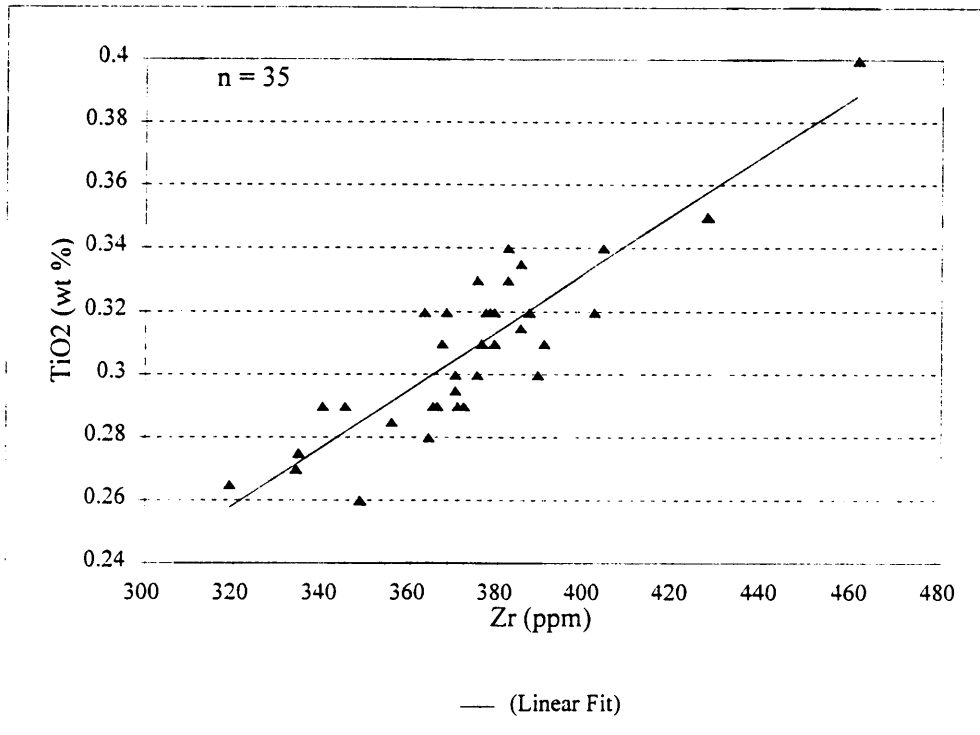
Figure 4.1: The linear relationship between TiO_2 and Zr (Spearman rank correlation coefficient, r = 0.7984)

— (Linear Fit)
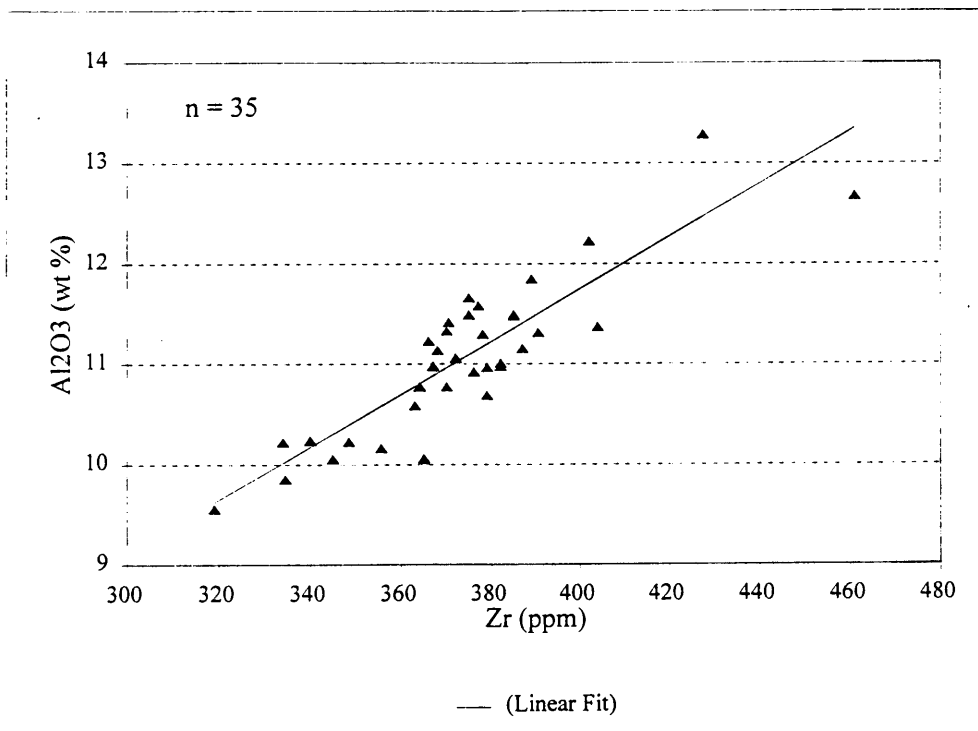
Figure 4.2: The linear relationship between Al_2O_3 and Zr (Spearman rank correlation coefficient, r = 0.7929)

29
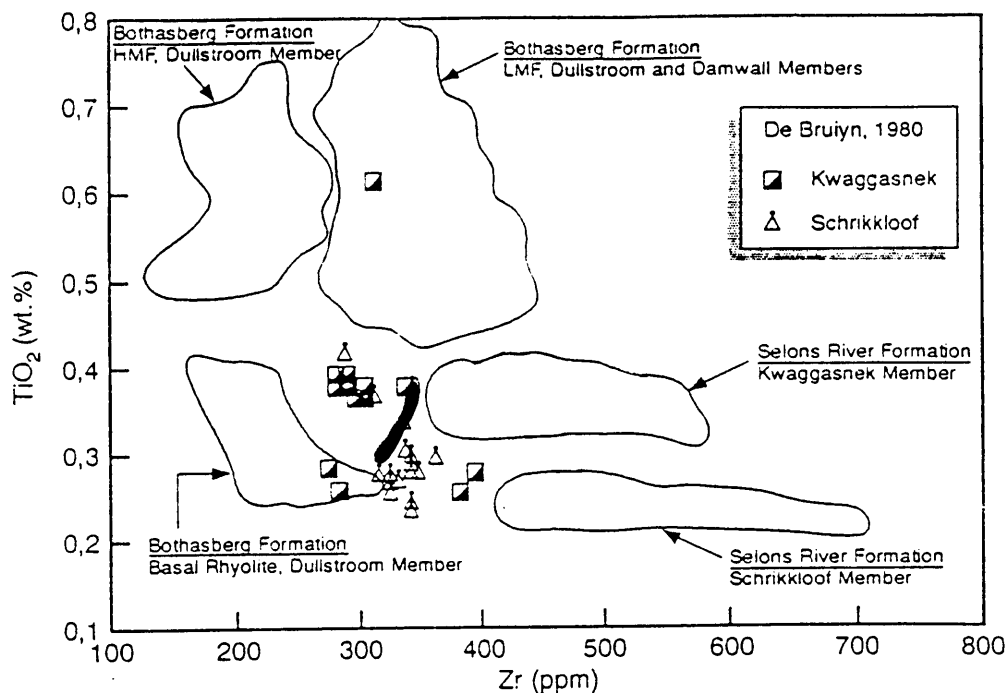
Figure 4.3: Data from the agglomerate in Rust de Winter (dark coloured area) correlated with published TiO₂/Zr patterns in the Rooiberg Group. The TiO₂/Zr ratio of the Rust de Winter agglomerate plots in the expected vicinity of the TiO₂/Zr ratio of the Schrikkloof and Kwaggasnek Formations in the same area (De Bruiyn, 1980). The other areas indicated on the diagram show the distribution of TiO₂/Zr ratios in other Formations of the Rooiberg Group (Schweitzer et al., 1995a). (HMF and LMF are respectively a high Mg felsite and a low Mg felsite).

4.2.3 Geochemical alteration of the agglomerate:

When normalised to an average Rooiberg Felsite of unit 8 (Twist, 1985) (Fig. 4.4a) and an average rhyolite in the Rust de Winter area (De Bruiyn, 1980) (Fig. 4.4b), the following observations were made regarding the major elements of the red (oxidised) agglomerate: little movement of SiO_2, TiO_2 and Al_2O_3. With the exception of 2 samples, FeO(total) shows a slight increase, which is probably the effect of oxidation. MnO and MgO show large deviation from the reference data, and no relationship with the variation of FeO(total). Enrichment or depletion of MnO may be

the result of variable redox conditions, and is expected to show the same trend as that of FeO(total). An interesting aspect is the enrichment of MgO, since the underlying (and overlying) rhyolite is denoted to be generally low in Mg. CaO, Na_2O and P_2O_5 appeared to be depleted, but K_2O is enriched relative to the reference values.

Likewise, the major elements of the green agglomerate relative to the two references were studied (**Fig. 4.5a** and **Fig. 4.5b**). The trend of the SiO_2, TiO_2 and Al_2O_3 contents in the green agglomerate is the same as that in the red agglomerate. The FeO(total) and MgO are invariably enriched in the green agglomerate, whereas the behaviour of the MnO is variable. Scattergrams showed that there exist no relationship between the FeO(total) and the MnO, but that there is a positive relationship between FeO(total) and MgO (**Fig. 4.6**). The CaO and Na_2O contents in this agglomerate are generally low and seem to stay low; this implies a depletion in these oxides (however, it is difficult to evaluate any movement because of the very low concentrations). K_2O is depleted, and P_2O_5 shows no definite trend.

The trace element distribution in both the green and red agglomerate follows very much the same pattern (**Fig. 4.7** and **Fig. 4.8**). Copper is highly enriched, whereas other chalcophile elements are depleted or enriched. Amongst the lithophile elements U seems to be slightly enriched, Rb slightly enriched in the red agglomerate only, whereas Sr and Ba tend to be depleted. Zirconium, Nb and Y seem to have been immobile relative to the Unit 8 rhyolites (no trace element data from the Rust de Winter (De Bruiyn, 1980) area were available). Zinc and Pb show large variations in both the green and red agglomerate.
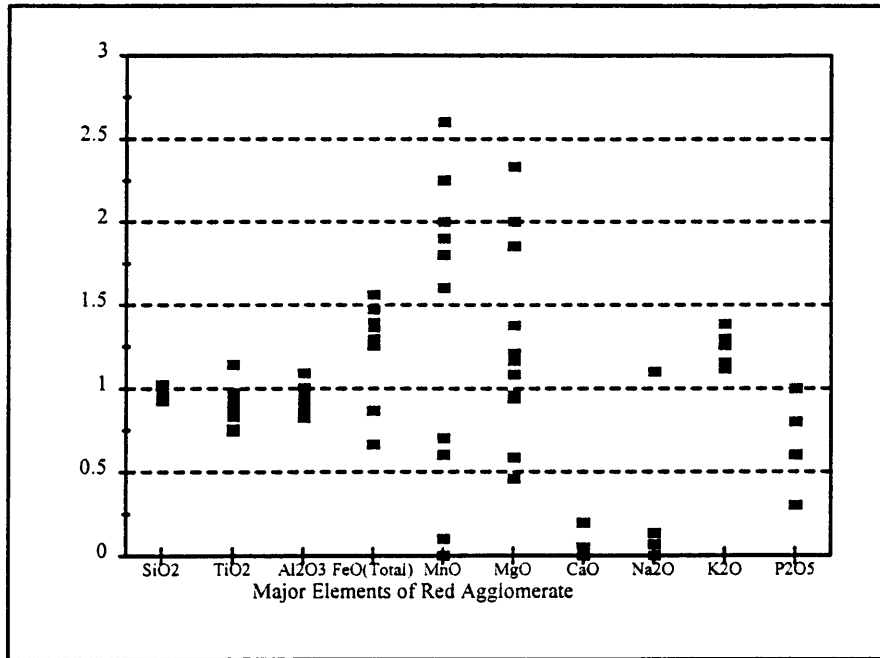
Figure 4.4a: The major element concentrations in the red agglomerate, normalised to an average value for rhyolite in unit 8 of the Loskop Dam area (Twist, 1985).
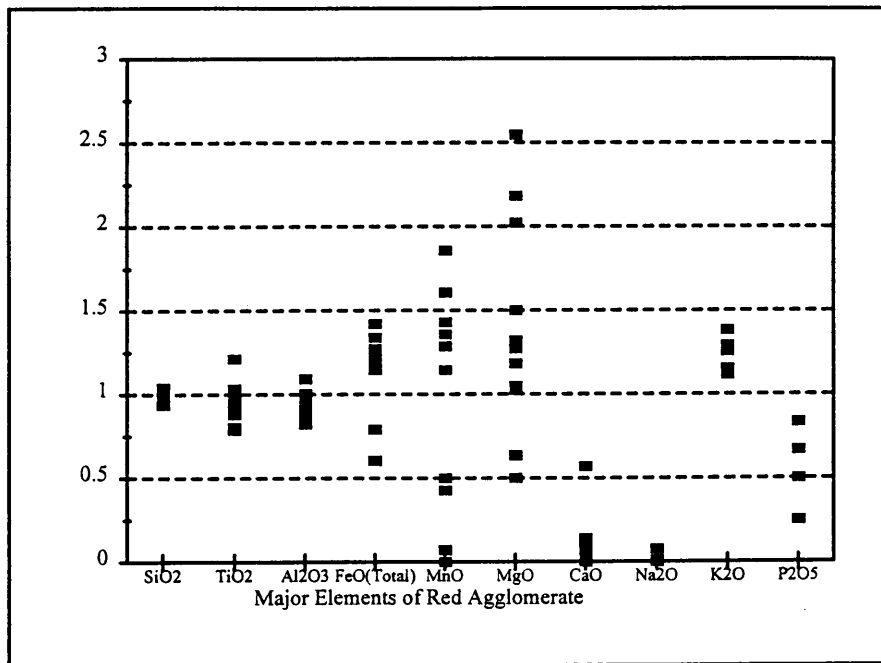
Figure 4.4b: The major element concentrations in the red agglomerate, normalised to an average value for rhyolite in the Rust de Winter area (De Bruiyn, 1980).

32
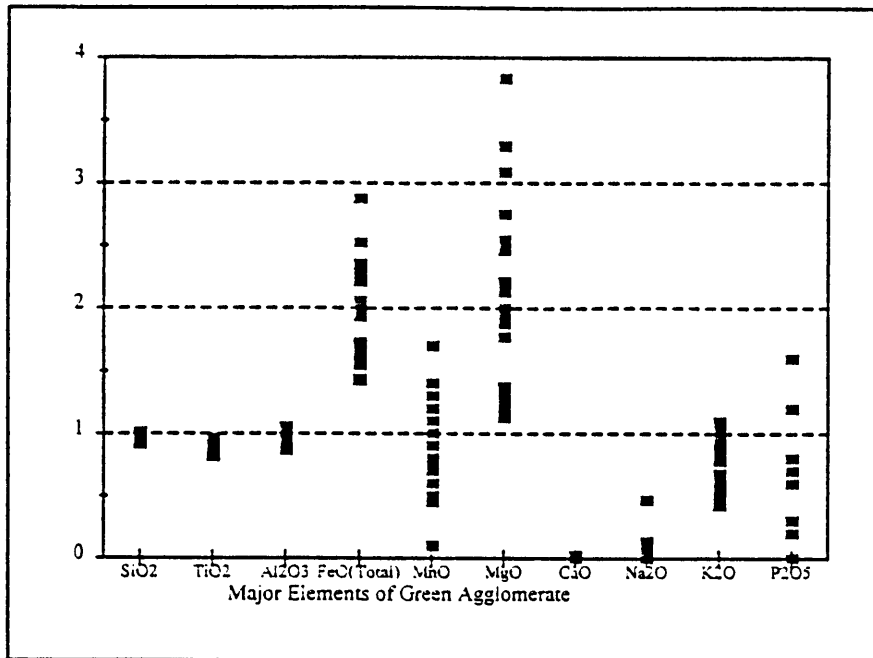
Figure 4.5a: The major element concentrations in the green agglomerate, normalised to an average value for rhyolite in unit 8 of the Loskop Dam area (Twist, 1985).
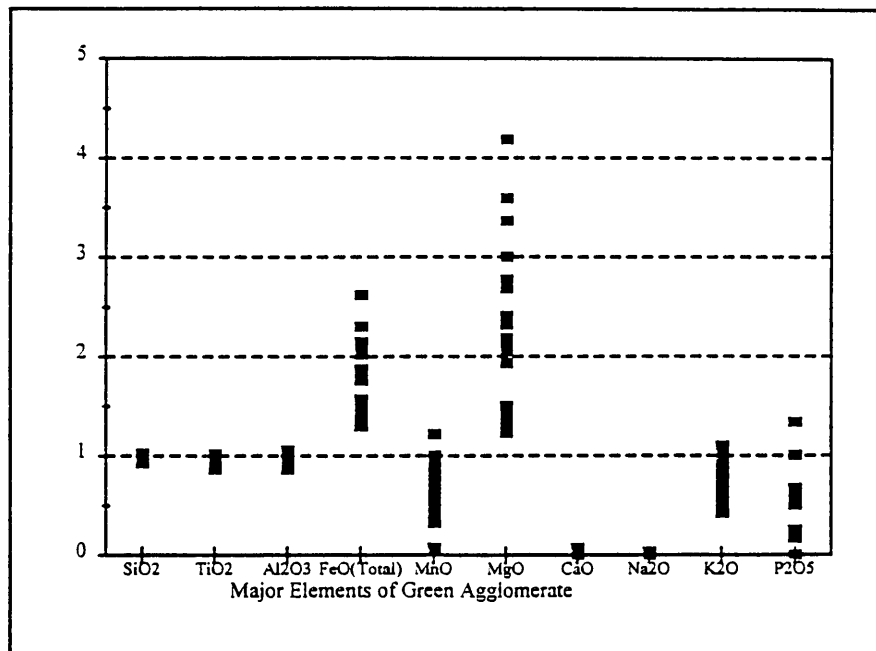
Figure 4.5b: The major element concentrations in the green agglomerate, normalised to an average value for rhyolite in the Rust de Winter area (De Bruiyn, 1980).

33
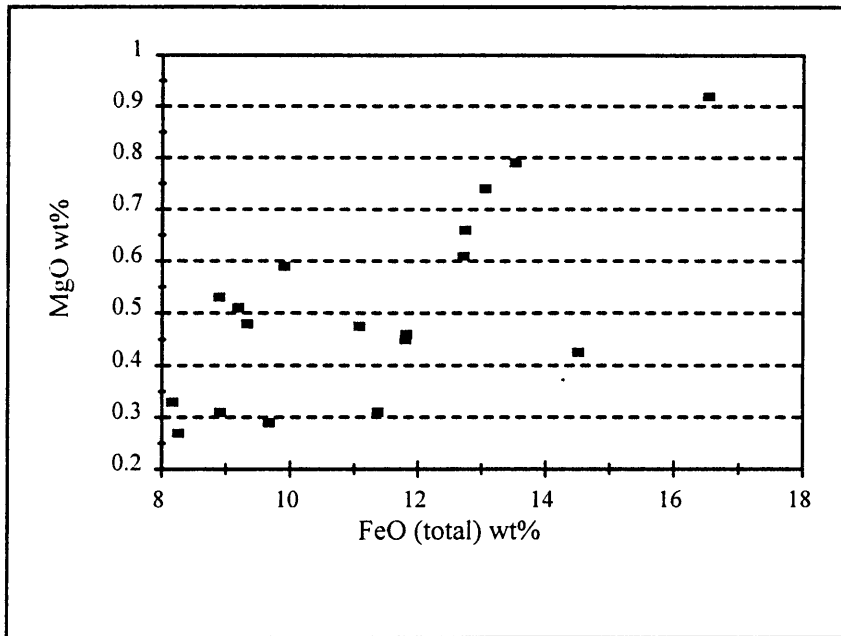
Figure 4.6: Scattergram showing the positive relationship between FeO(total) and MgO in the green agglomerate.
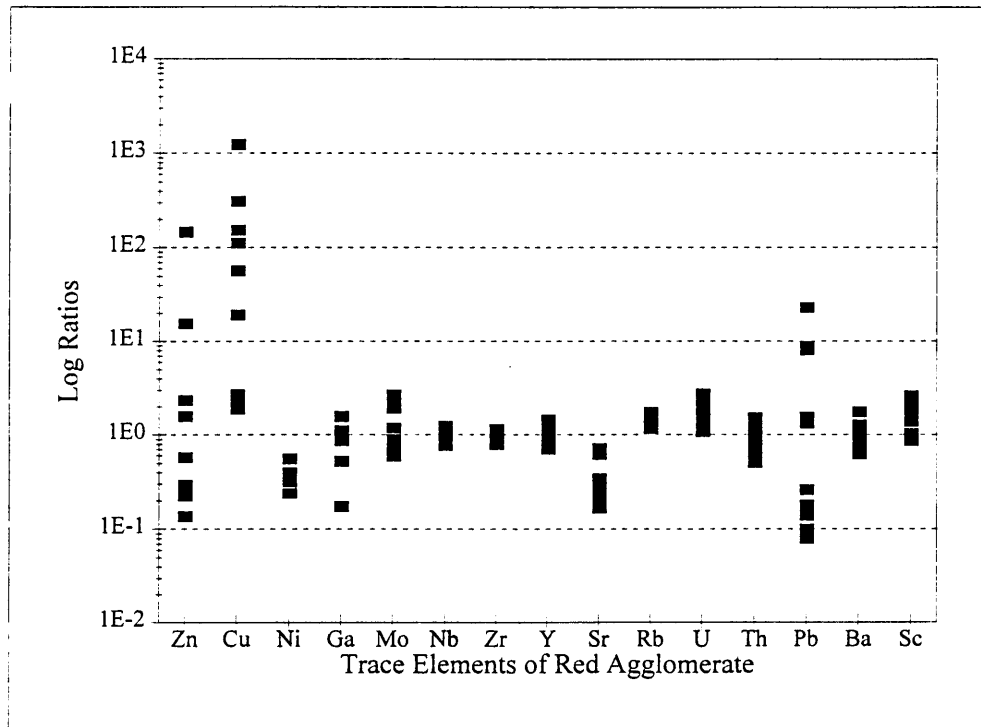
Figure 4.7: The trace element concentrations in the red agglomerate, normalised to an average value for rhyolite in unit 8 of the Loskop Dam area (Twist, 1985).
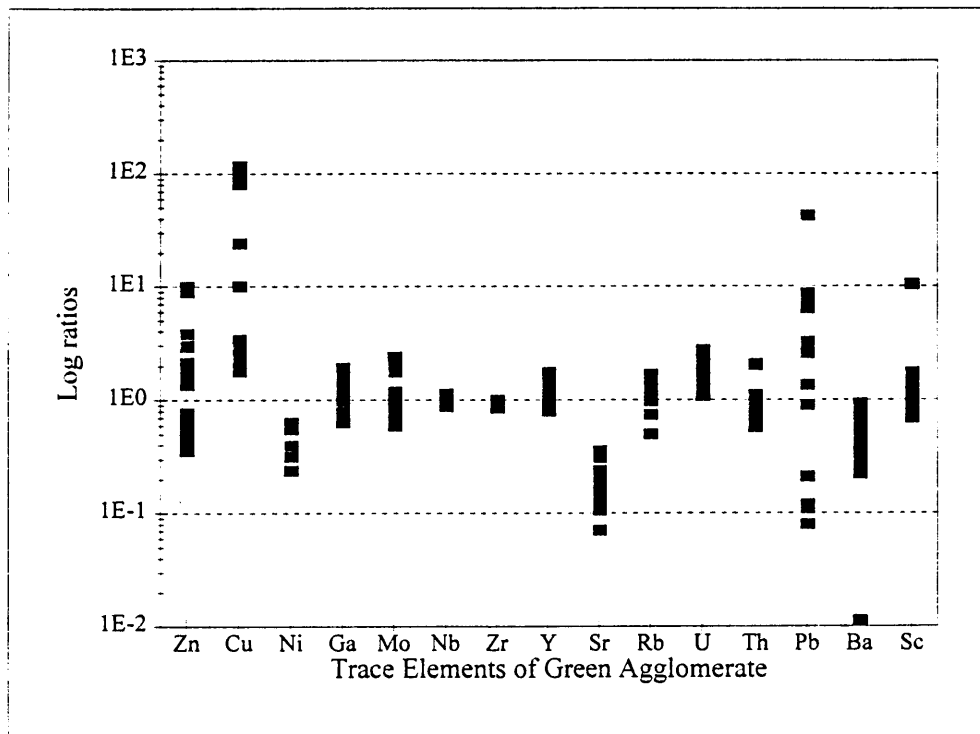
Figure 4.8: The trace element concentrations in the green agglomerate, normalised to an average value for rhyolite in unit 8 of the Loskop Dam area (Twist, 1985).

4.2.4 Discussion:

The major element geochemistry of the green and red agglomerate is compared with each other (**Fig. 4.9**), in order to determine the type of alteration that took place in the green agglomerate, and to examine the relative movement of elements and oxides during this alteration. The only significant differences between the red and green agglomerate are the FeO(total), MgO and K_2O contents. The higher K_2O content in the red agglomerate may be the result of K-feldspar or sericite forming during oxidation.

The chloritisation process in the green agglomerate might account for the high Fe content (the chlorite in these rocks is very high in Fe; **Chapter 5**). There is no mineralogical evidence that the MgO is largely captured in one specific phase; however, the positive relationship with FeO(total) may indicate that these two elements are present in the same mineral phase (possibly chlorite). However, iron-containing sulphides co-existing with

35

quartz and chlorite in veins will also be important hosts for Fe, while Cu and Zn are the components of sulphides like chalcopyrite or low temperature copper sulphides, and sphalerite respectively. The samples selected for geochemical analyses were, however, virtually free of visible sulphides.

The antipathetic behaviour of FeO(total) and MnO (**Fig. 4.5a & 4.5b**) in the green agglomerate probably reflects the specific redox state of the fluid. Under naturally occurring Eh-pH conditions, Fe^{2+} is more easily oxidised to insoluble Fe^{3+}, than is the case with Mn^{2+} (Boctor, 1985); consequently the Mn^{2+} ion will stay in solution much longer than the Fe^{2+} ion. Boctor (1985) further mentioned that Mn solubility in a supercritical fluid increases slightly with increasing pH, iron solubility on the other hand decreases with increasing pH. For a given temperature and pressure, Fe^{2+} will be oxidised to Fe^{3+} with an increase of pH, and be removed from the fluid.

Other factors influencing Fe-solubility in supercritical fluids are salinity, temperature, pressure, pH/aHClº, fO_2 and fS_2. Of these, reduced pressure and/or elevated temperatures and salinities are considered to enhance Fe-solubility (Williams, 1994). With alkali-chloride solutions reacting with micas to form feldspars, the Cl^- concentration in the fluid is likely to increase. This increased Cl^- content will enhance Fe solubility in that a high-order chlorine complex (e.g. $FeCl_4^{2-}$) becomes stable at higher temperatures (>400ºC), and thus Fe becomes more soluble in the fluid. According to McPhail (1993), with a decrease in temperature (<400ºC), the lower-order $FeCl_2$(aq) complex becomes stable and this results in the precipitation of Fe-bearing minerals. McPhail (1993) concluded that the temperature and salinity (a_{Cl}) rather that the acidity (pH), fluid mixing, wall rock interaction or boiling, are the predominant factors that influence the precipitation of Fe in the temperature interval 500 - 300ºC. This temperature interval represents typical conditions prevailing in hydrothermal systems. Therefore, the salinity of the fluid at these temperatures strongly affected the solubility of Fe in this system.

36
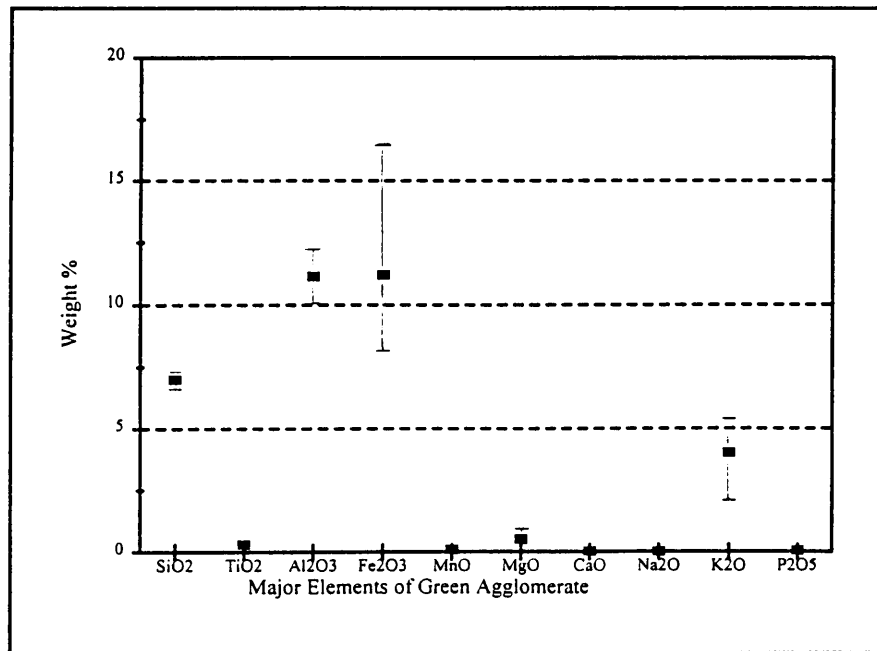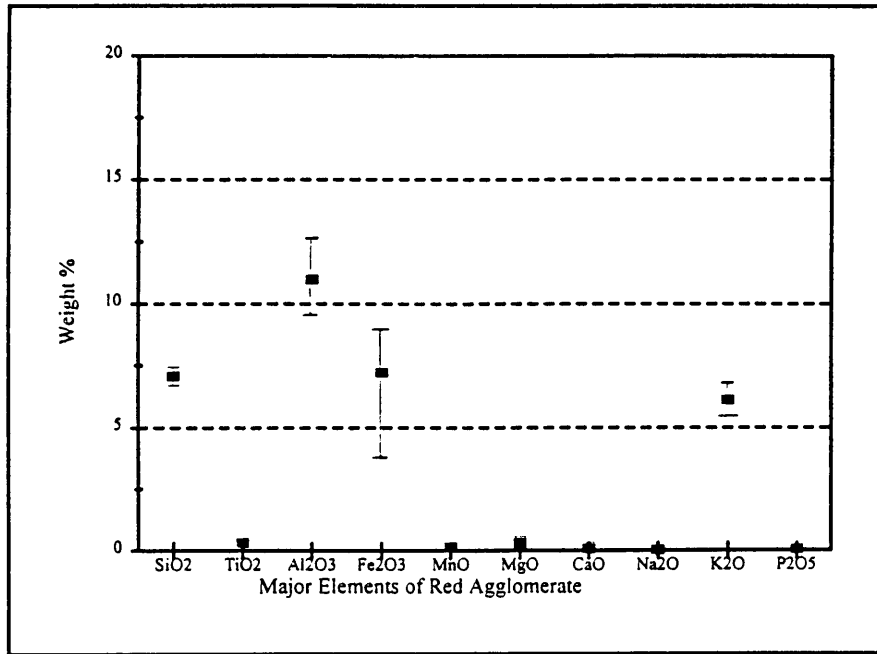
Figure 4.9: Comparison of the average and range of the major elements of the green and red agglomerate (note that the value of SiO_2 was divided by 10 to fit on the diagram).

37

Gangue mineralogy

5.1 INTRODUCTION

The optical study, supported by the XRD investigation of the different chlorite occurrences (i.e. veins and clasts) showed that there are also varying amounts of quartz, K-containing mica, hematite, siderite, microcline, and minor amphibole and plagioclase associated with the chlorite. The amounts of hematite, amphibole and plagioclase are very small and these minerals could not be optically identified. Quartz is a common component of both the chloritised clasts and the veins (**Fig. 5.1**). A white (K-containing) mica is often clearly visible in the veins (**Fig. 5.2a &b**) but less obvious in clasts.

In this investigation the emphasis will be placed on the translucent minerals of the veins only.
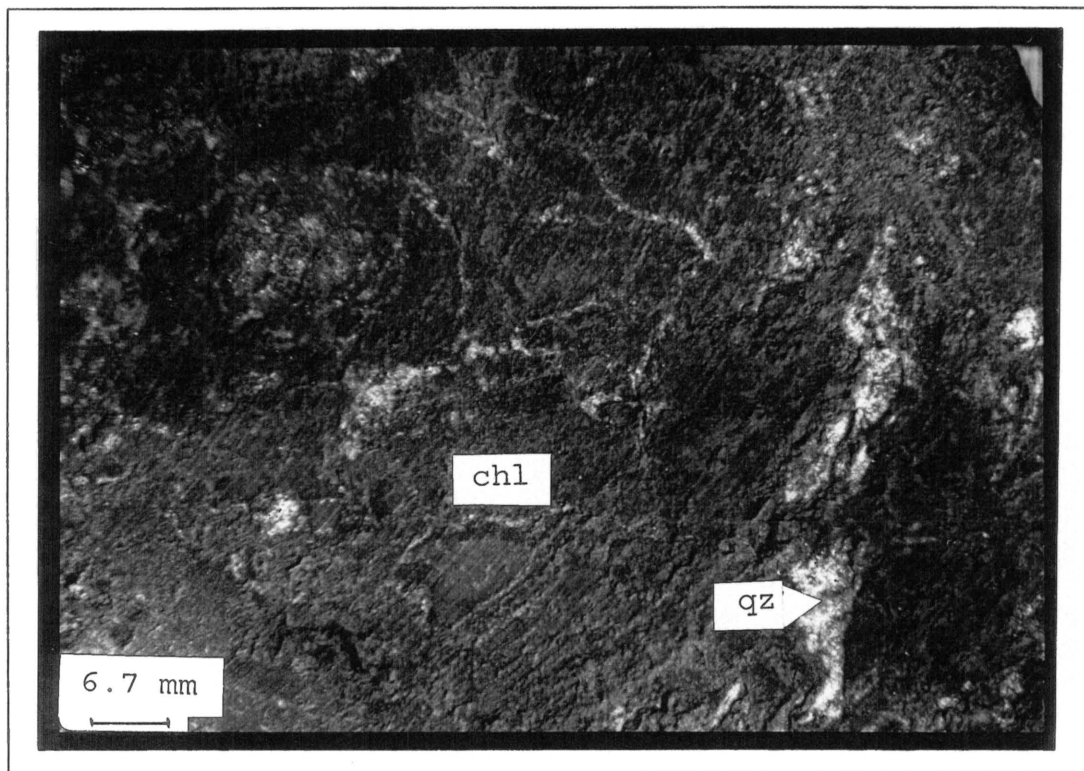
Fig. 5.1: A typical chlorite(chl)-quartz(qz) intergrowth from a vein in agglomerate (GD1 at 21.80m).
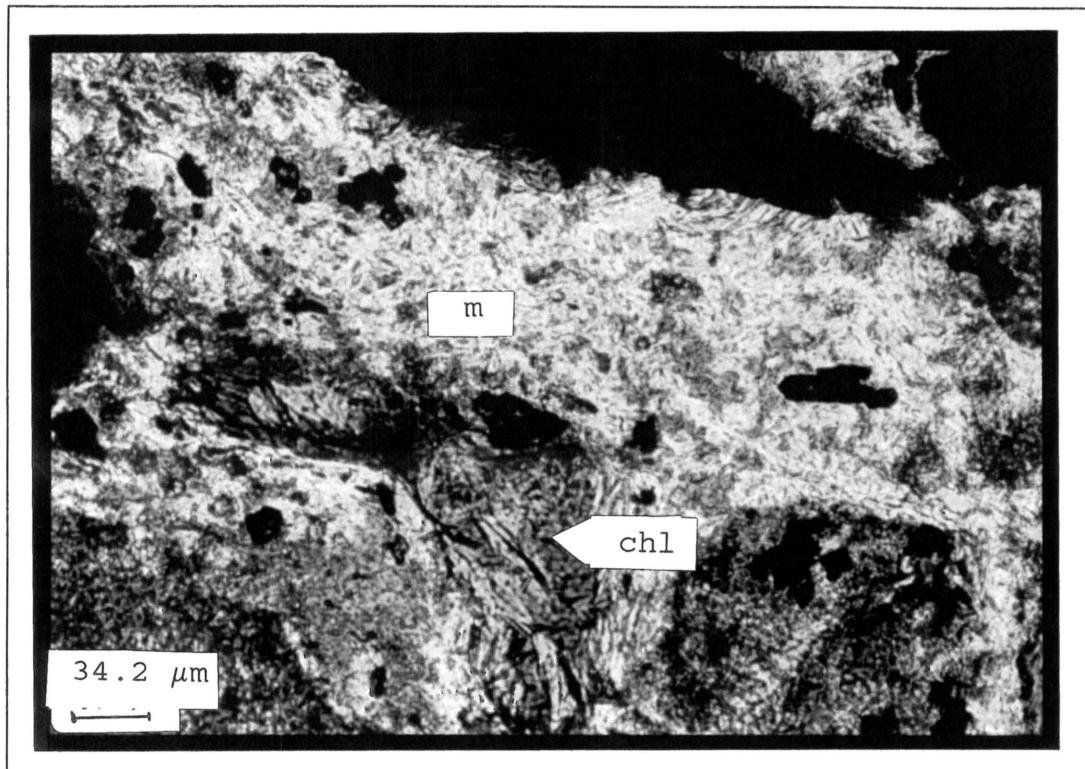
Fig. 5.2a: A chlorite(chl)-mica(m) vein in agglomerate; the
black grains are sulphides. (GD1 at 25.90m).
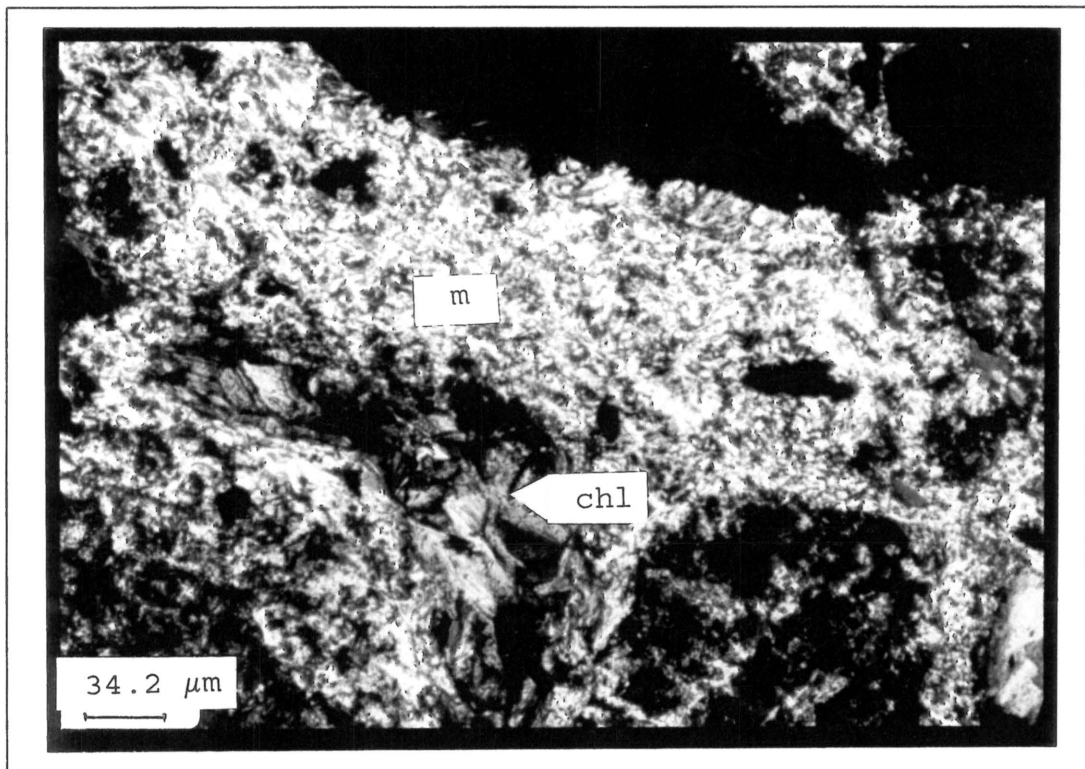
Fig. 5.2b: The same vein as in Fig. 5.2a under crossed Nicols,
showing the presence of a large amount of mica(m) intergrown
with chlorite(chl) in a vein.

5.2 SIDERITE

Siderite is a sporadic constituent of veins and is in textural equilibrium with quartz and chlorite as well as sulphides (usually chalcopyrite and pyrite). Not much emphasis was placed on the quartz + chlorite + siderite veins (**Fig. 2.1 and 5.3**) in the brecciated zone, but microprobe analyses (**Appendix G**) showed that the siderite is very high in iron. On a FeO-MnO-CaO ternary diagram (**Fig.5.4**), the data points plot on the CaO-poor side of the diagram.
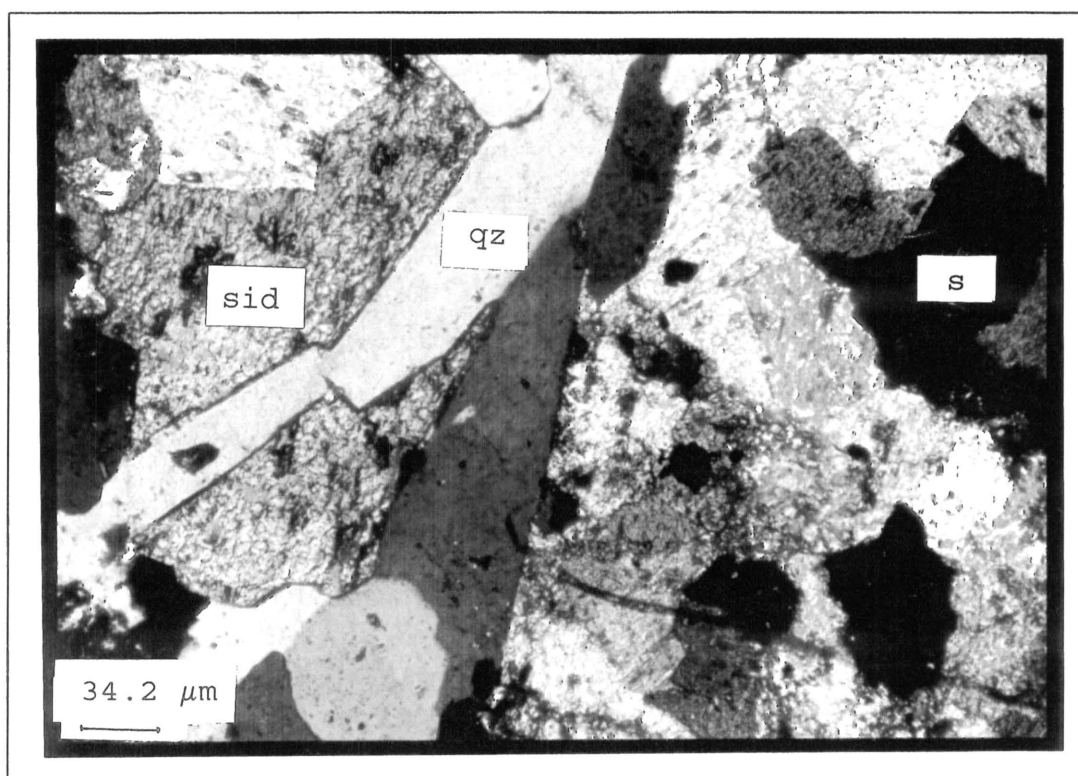
Fig. 5.3: Siderite(sid) with quartz(qz) and sulphides(s) in a vein in rhyolite (GD3 at 185.33m).

5.3 CHLORITE

5.3.1 Microscopical:

Representative samples for a microscopic investigation were taken from the different chlorite occurrences, i.e. chloritic clasts and chlorite- filled veins. An optical study showed that chlorite occurs either as fine grained, dark green grains (typical of

40

chloritic clasts) (**Fig. 5.5**), or coarse grained, light green grains (typically in veins) (**Fig. 5.6**).
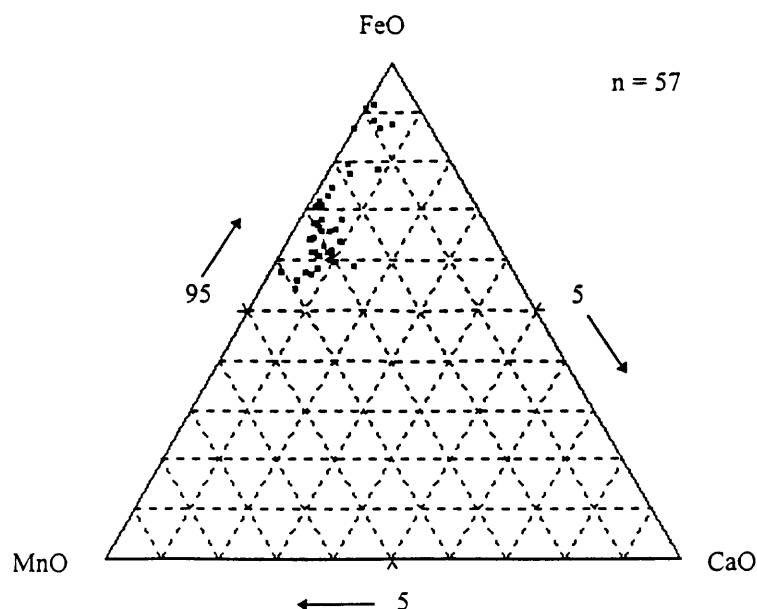
Figure 5.4: Siderite compositions plotted on a FeO-MnO-CaO ternary diagram.

The fine-grained chlorites of the clasts are occasionally intergrown with a white mica and quartz, which increases the mechanical hardness of the chloritic clasts in contrast to the much softer chlorite in veins. The vein chlorites are associated with quartz (**Fig. 5.7a & b**) and sulphides such as arsenopyrite, sphalerite, pyrite and chalcopyrite. Chlorite-filled veins cut through chloritic clasts and based on textural evidence the original chloritic clast seems to have been subjected to a second stage of chloritisation with concomitant precipitation of sulphides. These areas of replacement appear lighter in colour than the rest of the clast. The optical study also proved that sulphides (mainly chalcopyrite and pyrite) do occur occasionally in clasts, but they are either associated with chlorite-filled veins that cut through the clasts, or with areas of lighter colour in the clasts.
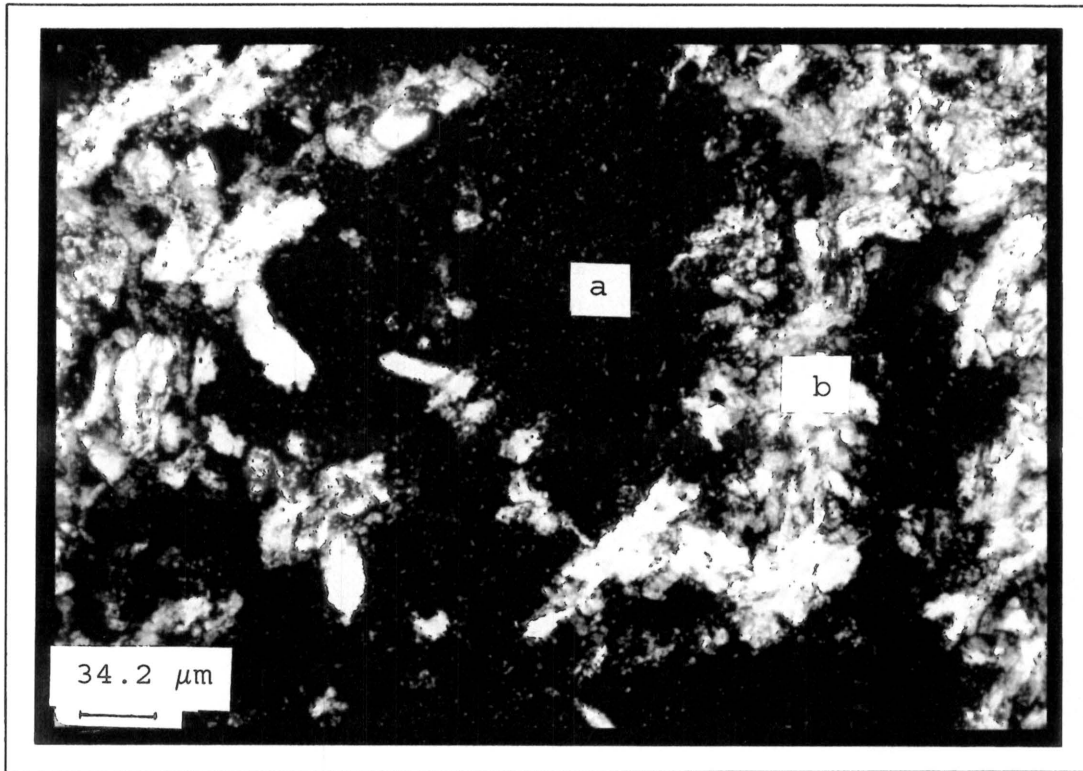
Fig. 5.5: Fine grained chlorite(a) in a clast, with adjacent larger chlorite grains(b) of a vein under crossed Nicols (GD5 at 154.50m).
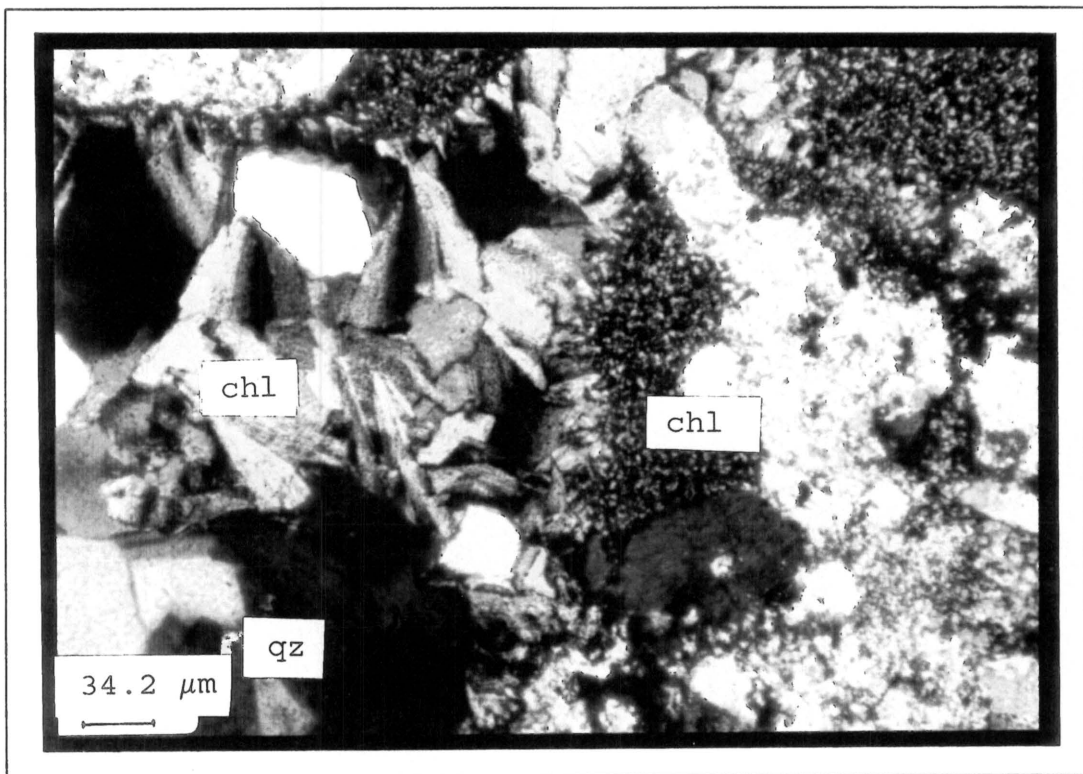
Fig. 5.6: Coarse and fine grained chlorite(chl) and quartz(qz) grains in a vein in agglomerate under crossed Nicols (GD3 at 154.30m).
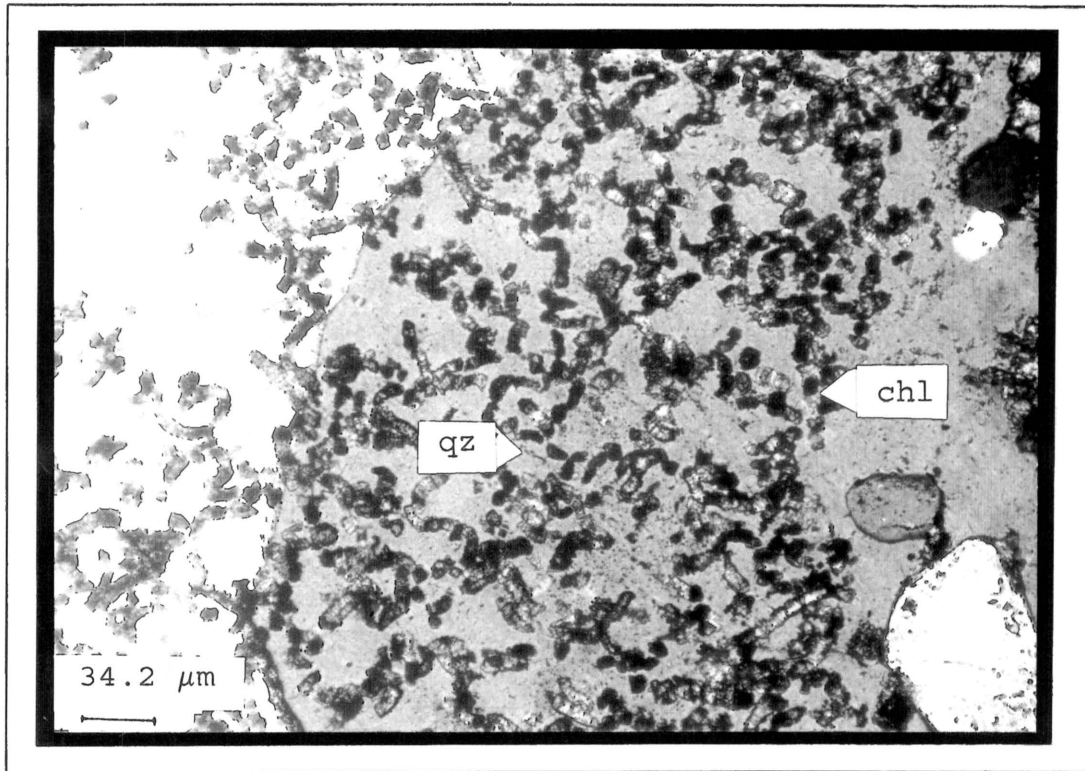
Fig. 5.7a: An interesting intergrowth of chlorite(chl) and quartz(qz). The chlorite grains are elongated in the c-direction and create a "worm-like" texture, under crossed Nicols (GD1 at 61.90m).
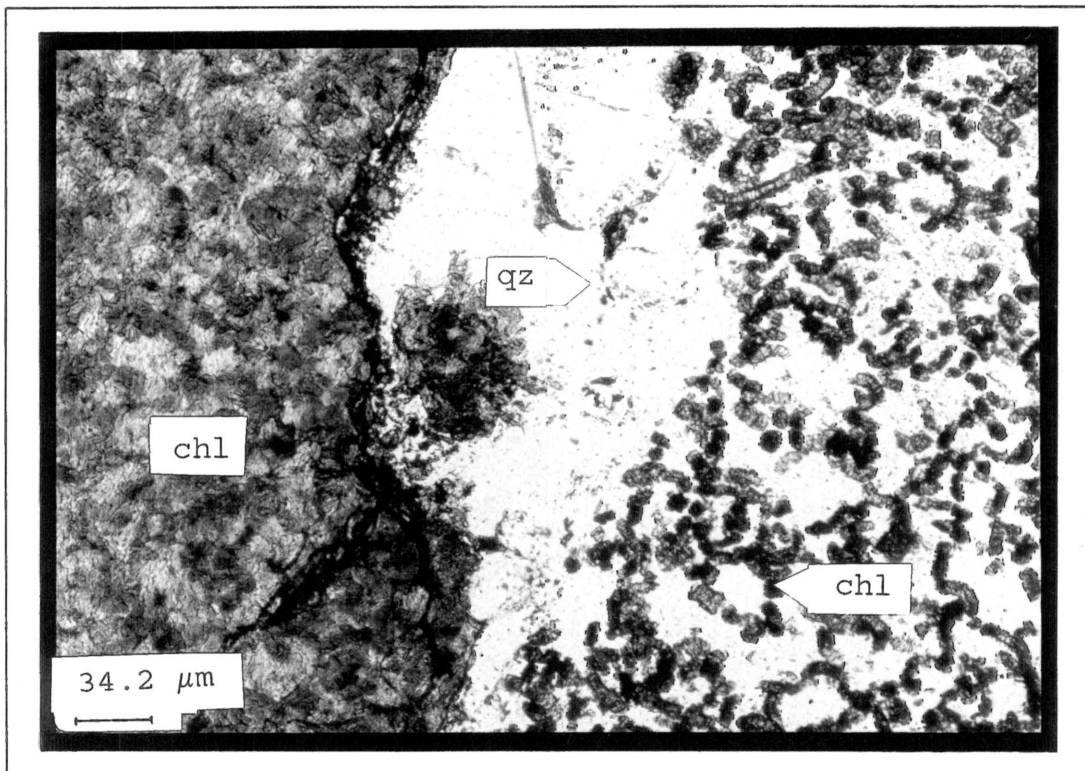
Fig. 5.7b: The same worm-like texture of chlorite(chl) in quartz(qz). To the left of the quartz grain is the typical chlorite texture of a vein, under crossed Nicols (GD1 at 61.90m).

5.3.2 Crystal structure:

To understand the compositional changes of chlorite and their dependence on the conditions of formation, it is necessary to consider the structural properties of chlorite. The chlorite structure consists of alternating talc - like ($Y_6Z_8O_{20}[OH]_4$) and brucite - like ($Y_6[OH]_{12}$) layers, where Y represent octahedral and Z tetrahedral sites (Fig. 5.8).
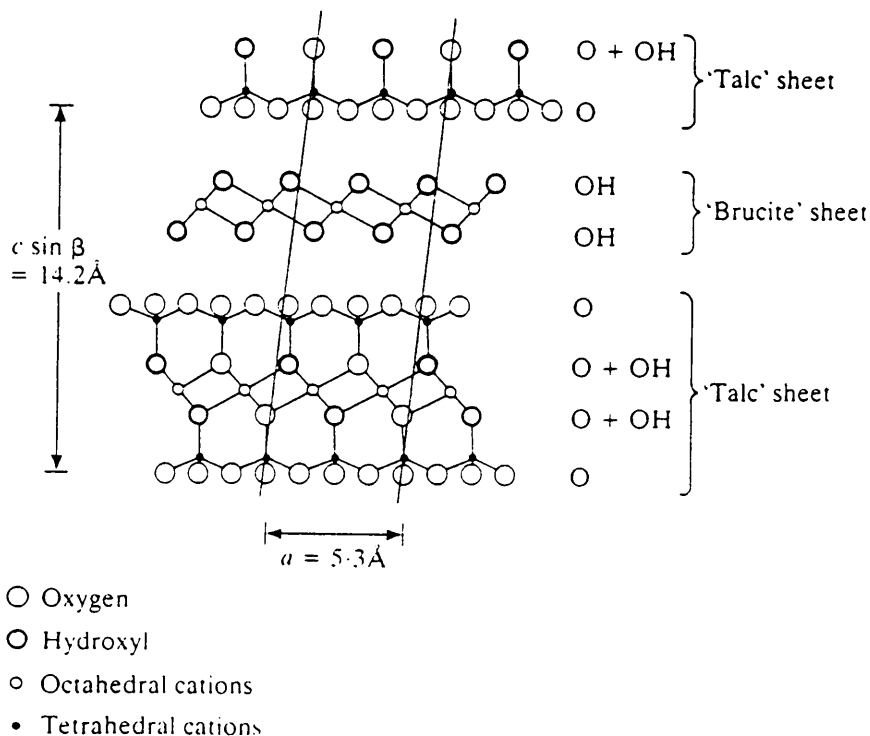
Figure 5.8: Idealised chlorite structure; projection on (010) (from Brown and Bailey, 1962)

Chlorites are divided into two groups based on the number of octahedral cations. If the number of octahedral cations per $O_{20}(OH)_{16}$ is 12.0, and approximately equivalent amounts of Al^{3+} are present in the tetrahedral and octahedral sites, it is referred to as tri-octahedral chlorite. Sometimes the number of octahedral cations is less than 10, and these chlorites are then described as di-octahedral chlorites (Deer et al., 1992).

In order for *a* and *b* axis parameters to be similar and the structure to be stable, it is essential that Al^{3+} is present in both the octahedral and tetrahedral layers. An Al content of 20 - 35 cation per cent is required for the best structural fit. The basal spacing d_{001} will reduce with a substitution of Al^{3+} for (Mg^{2+}, Fe^{2+}) and Al^{3+} for Si^{4+}. The substitution of Mg^{2+} by (Fe^{2+}, Mn^{2+}) will increase the *a* and *b* axis parameters (Deer et al., 1992). In addition, substitution of Fe^{3+} or Cr^{3+} ions for Mg^{2+} in the octahedral layers, accompanied by substitution of Al^{3+} for Si^{4+} in the tetrahedral layers, results in contraction of the octahedral, and expansion of the tetrahedral layers (Phillips, 1964). Expansions or contractions like these may be displayed in the powder XRD-pattern, where deviations of peak positions from the ideal *d* values occur.

In re-calculating the microprobe analysis of chlorites into a structural formula, the different site allocations of elements like Al^{3+}, Fe^{2+} and Fe^{3+} play an important role. A Mössbauer spectroscopy investigation by Townsend et al. (1986) on Mg-chamosite, Mn-Mg-chamosite and Fe-clinochlore, proved that Fe ions are not uniformly distributed in octahedral sites of the brucite-layer and talc-layer. The octahedral sites in the talc-layer of Mn-Mg-chamosite and Mg-chamosite contained 64 and 68 at%, respectively, of the total Fe content (Kodama et al., 1982; Townsend et al., 1986). Of the total Fe, at least 65 at% is in the ferrous state (Kodama et al., 1982), which occurs in the two different octahedral positions (i.e. in the brucite or talc layer).

The Fe^{3+} is usually also octahedrally co-ordinated, but under certain conditions and with an Al^{3+} deficiency, Fe^{3+} can be tetrahedrally co-ordinated (Goodman and Bain, 1979, 1978). However, according to Deer et al. (1992) this does not necessary indicate oxidation of the ferrous iron. If oxidation of the specimens did take place, so that the oxidation of Fe^{2+} to Fe^{3+} produces more than the normal amount of Fe^{3+} and was accompanied by hydrogen loss, the effect could be seen in a lower H_2O content and less than 12 octahedral cations (Deer et al., 1992). In the samples of chamosite studied by Kodama et al. (1982), the

Mössbauer spectra indicated no tetrahedral iron. A possible explanation may be found in the hypothesis of Kodama and co-workers (1982), that structurally strained Fe^{2+} ions are relatively easily oxidised because reduction in ionic radius from 0.74 (Fe^{2+}) to 0.64 Å (Fe^{3+}) with oxidation should relax the structural stress.

Stoessell (1984) experimentally investigated the effects of a change in the Al^{3+} content in a four end-member solid solution (amesite, chamosite, Fe^{3+}-chamosite and talc-3 brucite) of authigenic chlorite, while holding the molar Mg^{2+}/Fe^{2+} ratio constant. Trends in molar ratios of Mg^{2+}/Fe^{2+} should therefore be independent of trends in Al content. $Fe^{3+}/(Fe^{3+} + Fe^{2+})$ ratios are much more sensitive to changes in the conditions of formation (Mather, 1970). According to Stoessell (1984) even small changes in parameters like pressure, pH, and activities of HS^- and CO_3^{2-} seem to have a large effect on the aMg^{2+}/aFe^{2+} molar ratio in the process of precipitating chlorite. If equilibrium is not reached due to reaction kinetics, these molar ratios may be preserved in some chlorites (Stoessell, 1984). Therefore, the vein chlorites could be expected to have a wide compositional range, due to the constantly changing conditions of hydrothermal fluids.

5.3.3 X-ray diffraction:

The intergrowth of chlorite with other layered silicates like biotite (Mellini et al., 1991), smectite (Nieto et al., 1994), or illite and muscovite (Lee et al., 1984), is fairly common in diagenetic chlorites. In hydrothermal chlorites, however, it is a less frequent phenomenon, but still worthwhile to consider since in some veins and clasts muscovite occurs together with chlorite.

With the use of X-ray powder diffraction, microprobe analysis and transmission electron microscopy (TEM), Mellini et al. (1991) discovered that a chlorite-like, hydrated mineral produced 16 - 16.5 Å spacings in the XRD pattern and low oxide sums (in the order of 79 - 85 wt%) in microprobe analysis. It was concluded that this 16 Å hydrated chlorite is a retrograde alteration product that formed from the grains consisting of a chlorite-mica

association. Interleaved with this 16 Å material were also lamellae of hematite.

The presence of mica-chlorite interlayering may be detected in the XRD pattern as a 16 Å chlorite (Mellini et al., 1991). The chlorites studied show peaks only in the range of 14.127 - 14.593 Å. Although microscopic intergrowths between chlorite and mica occur, these two sheet silicates do not seem to be interlayered.

The chlorites in the veins fall into two groups: chlorites with a peak between 14.45 - 14.59 Å and those with a peak between 14.12 - 14.24 Å (**Fig. 5.9**). Chlorite of veins with associated arsenopyrite falls mainly into the first group and chlorite of veins further away from this zone, with less or no sulphides, into the second group. The chlorite in the chloritic clasts is not characteristic with regard to the d_{001} peak and their values vary from 14.12 - 14.83 Å.

5.3.4 Chemical analysis:

By determining the composition of the chlorites in the veins, it was hoped to understand the nature of fluids causing the sulphide mineralization. The movements and mixing, pH, and temperature of this fluid phase(s) may be reflected in the Fe^{2+}/Mg^{2+} ratio of the vein chlorites (Shikazono and Kawahata, 1987), although the Fe^{2+}/Mg^{2+} ratio of chlorite precipitating from ascending fluids also depends on the extent of deviation from equilibrium between fluids and surrounding rocks (Shikazono and Kawahata, 1987). Thus, the Fe^{2+}/Mg^{2+} value of the host rock will have a direct effect on the Fe^{2+}/Mg^{2+} ratio of the chlorites forming in veins. Cathelineau and Nieva (1985) postulated that the Fe/(Fe + Mg) ratio is poorly correlated with temperature, but rather dependent on the composition of the host rock. Giggenbach (1984) concluded that a number of processes such as adiabatic and conductive cooling and mixing of fluids can cause deviation from equilibrium between fluids and surrounding rocks.
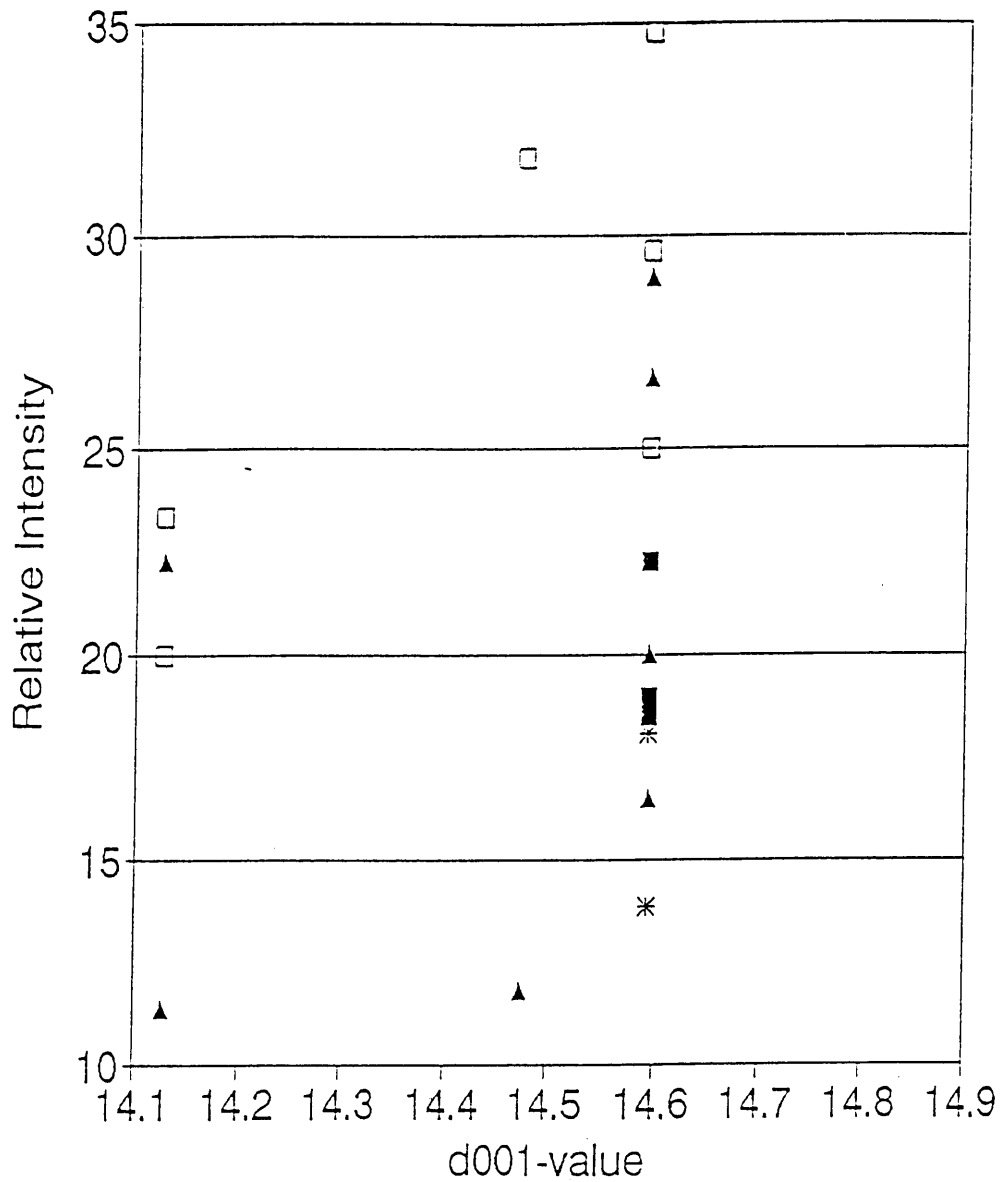
Figure 5.9: Relationship between the relative intensity and the d_{001} value in different chlorites. (■ : chlorite in veins associated with arsenopyrite; ▲: chlorite in barren veins in agglomerate; * : chlorite in veins in rhyolite; □ : chlorite clasts)

The redox state of the wall rocks had an influence on the exchange of Fe and Mn between metamorphic fluids and vein chlorites from Harlech Dome, north Wales. Bottrell and Yardley (1991) found that while their predictions of Fe/Mn partitioning between fluid and chlorite are good for veins from relatively oxidised rocks, vein fluids from reduced hosts are enriched in iron. The reason for Fe-enrichment could be additional Fe^{2+} dissolving in the fluid. The same process may have had an influence on the Fe/Mg ratio of chlorites in the studied system, causing a fractionation of Fe and Mg between oxidising and reducing environments, because Fe^{2+} is more soluble that Fe^{3+}, which will precipitate immediately if conditions change to a more oxidising environment.

Differences in colour, textures and age of chlorites imply different conditions of formation. Therefore, both the chlorite clasts and the chlorite in veins were analysed and compared with regard to composition, mineral associations and, where possible, also temperature of formation. Analysing the chlorite in clasts was difficult because of its finely intergrown nature with quartz, the chlorite in veins was normally large grains and gave good analyses.

One of the problems with the microprobe analyses was to explain the low totals. Apart from interlayering with other sheet silicates and oxides, Ferrow and Roots (1989) found with a special TEM technique that chlorites which deviate from the ideal chlorite composition sometimes have missing talc-like and brucite-like layers. Missing brucite-layers give a Si^{4+} excess relative to the ideal chlorite composition, and missing talc-layers give a Si^{4+} deficiency, both displayed in microprobe analysis (Veblen, 1983; Ferrow and Roots, 1989). However, the microprobe analyses of chlorites measured during this study did not show any major deviation from the normal Si^{4+} contents for chlorites. Because the number of octahedral cations per $O_{20}(OH)_{16}$ is in the order of 12, these chlorites are classified as tri-octahedral chlorites.

Since the vein chlorites in the study area show very little variation in their Fe/(Fe + Mg) ratios of 0.91 to 1, they can be classified as the iron rich member of the solid solution series

49

amesite $(Mg_4Al_4Si_2O_{10}[OH]_8)$ - chamosite $(Fe^{2+}_4Al_4Si_2O_{10}[OH]_8)$. **Figure 5.10** shows the classification of chlorite according to its Si content and Fe/(Fe + Mg + Mn) ratio. The chlorites of the study area plot in the chamosite field in the upper left corner. This composition is indeed very unusual for chlorites in a hydrothermal vein system.
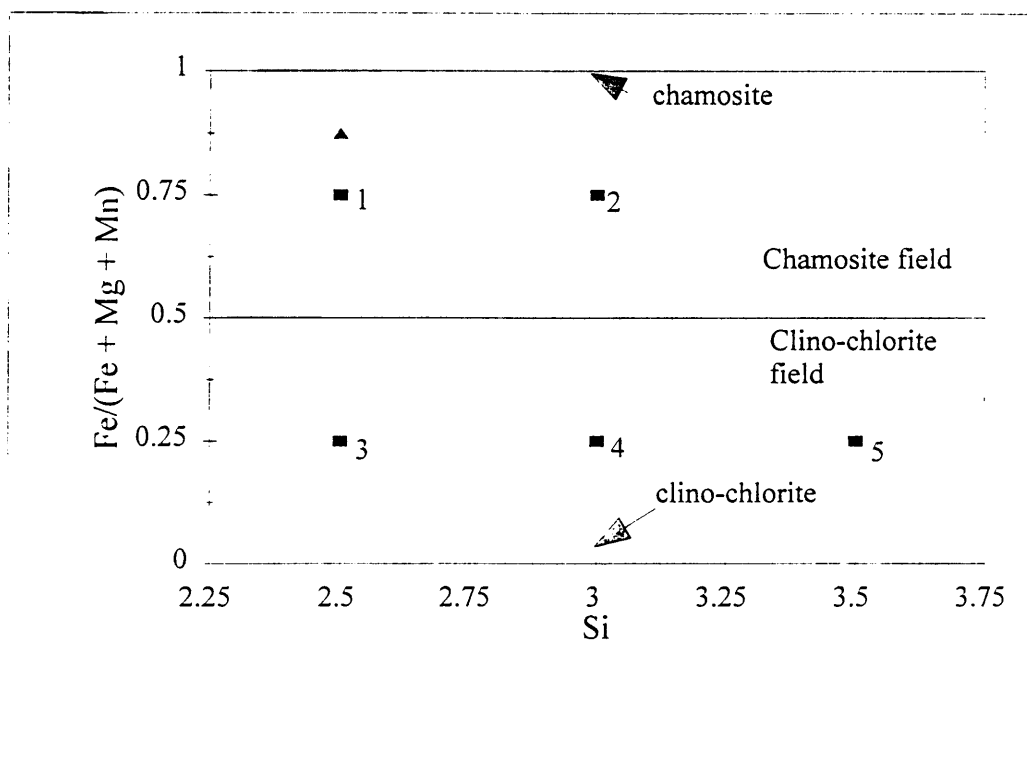
Figure 5.10: Classification of chlorites (1) Mg-Al-chamosite (2) Mg-chamosite (3) Fe-Al-clino-chlorite (4) Fe-clino-chlorite (5) Fe-Si-clino-chlorite (after Bayliss, 1975). The chlorites from the study area are indicated with a ▲.

5.3.5 Chlorite geothermometry:

"The non-stoichiometric behaviour of chlorite makes it a potentially attractive geothermometer, as chlorite composition records invaluable information about the physico-chemical conditions prevailing during its formation. The condition for this compositional geothermometer to perform satisfactory is that it should directly relate chlorite composition to temperature of formation" - De Caritat et al. (1993).

50

The earliest chlorite geothermometer was based on the polytypism of chlorite. The manner in which brucite- and talc-layers are stacked in the z-direction defines the polytype of chlorite, and four natural chlorite polytypes were distinguished by various scientists (Bailey and Brown, 1962; Hayes, 1970): IIb, Ib (ß=90°), Ib (ß=97°) and Ia. Chlorite polytype geothermometery is presently largely qualitative and lacks in-depth investigation of the processes controlling polytype transition (De Caritat et al., 1993). Therefore, this investigation will concentrate on the geothermometers based on the composition of chlorite.

Compositional chlorite geothermometry can be grouped into two categories, an empirical approach (Cathelineau and Nieva, 1985; Cathelineau, 1988) and an approach whereby the thermodynamic properties of chlorite components are considered (Walshe, 1986).

5.3.5.1 Empirical Approach:

The empirical approach has two advantages: firstly it takes into account the compositional effects of a multitude of thermodynamic variables that do not need to be measured, and secondly it is simple to apply since it has the form of a linear function (De Caritat et al., 1993).

Cathelineau and Nieva (1985) found a positive correlation between Al^{IV} and temperature in the Los Azufres geothermal system, Mexico, where chlorite constitutes a major hydrothermal alteration product of an andesitic host rock. Temperatures range between 130° and 310°C and they suggested that Al^{IV} could be used as a geothermometer on the condition that no other parameters like bulk rock composition, nature of geothermal fluids, and pressure, vary significantly. The derived equation is (Cathelineau and Nieva, 1985; Fig. 10):

$$T = 212.31Al^{IV} + 7.54 \dots\dots\dots\dots\dots\dots\dots\dots (5.1)$$

where T is in °C and Al^{IV} is the at% Al in the tetrahedral position.

Based on new data from Los Azufres (Cathelineau, 1988) and recalculated data from the Salton Sea (McDowell and Elders, 1980), Cathelineau (1988) derived at a more reliable relationship between temperature and Al^{IV}:

$$T = 321.98Al^{IV} - 61.92 \dots\dots\dots\dots\dots\dots\dots\dots (5.2)$$

The Al^{IV} appears to be independent of rock composition and fluid composition (De Caritat et al., 1993).

Several workers have suggested modifications to this approach. Kranidiotis and MacLean (1987) calculated a corrected Al^{IV}, to adapt this function to situations where chlorite grows in an Al-saturated environment:

$$T = 106Al^{IV}_{C} + 18 \dots\dots\dots\dots\dots\dots\dots\dots\dots\dots (5.3)$$
$$\text{where } Al^{IV}_{C} = Al^{IV}_{M} + 0.7[Fe/(Fe+Mg)]$$
$$Al^{IV}_{M} = \text{measured } Al^{IV}$$
$$Al^{IV}_{C} = \text{calculated } Al^{IV}$$

Jowett (1991) suggested a similar type of correction, derived form an isothermal $Fe/(Fe+Mg)$ normalisation, based on Salton Sea and Los Azufres chlorite compositions. He claimed that this Fe-Mg-modified geothermometer is applicable to a variety of systems in the range 150°-325°C for chlorites with $Fe/(Fe+Mg) < 0.6$:

$$T = 319Al^{IV}_{C} - 69 \dots\dots\dots\dots\dots\dots\dots\dots\dots\dots (5.4)$$
$$\text{where } Al^{IV}_{C} = Al^{IV}_{M} + 0.1[Fe/(Fe+Mg)]$$

These empirical geothermometers rely on the variation in Al^{IV} with temperature and may be sensitive to changes in the activity of Al^{3+} imposed by coexisting minerals via changes in activity of species dissolved in the fluid phase (De Caritat et al., 1993). De Caritat et al. (1993) evaluated the different chlorite geothermometers and concluded that the empirical thermometers either overestimate or underestimate the temperature by roughly 75° - 215°C! **Table 5.1** gives a summary of the four different empirical geothermometers and their advantages and disadvantages.

Table 5.1: Summary of the four empirical geothermometers

	Cathelineau and Nieva (1985)	Cathelineau (1988)	Kranidiotis and MacLean (1987)	Jowett (1991)
Equation	5.1	5.2	5.3	5.4
Study Area	Los Azufres, Mexico	Los Azufres and Salton Sea	Phelps Dodge, Quebec	Los Azufres and Salton Sea
System	Geothermal	Geothermal	Geothermal	Geothermal
Host Rocks	Andesite	Feldspathic sandstone	Rhyodacite and Rhyolite	Andesite and Sandstone
Limitations		* Al-chlorite mol proportion > 0.24	Work best for: * Low Al-chlorite mol proportions * Low Fe/(Fe+Mg)	* Al-chlorite mol proportion > 0.24 * Fe/(Fe+Mg) < 0.6
Disadvantage	* Based on one system only	* Over-estimate T by 75°-215°C	* Over/Under-estimate T by 20°-150°C * Under-estimate T when high Al-chlorite mol proportions and high Fe/(Fe+Mg)	* Over-estimate T more than Cathelineau (1988) * Fe/(Fe+Mg) < 0.6
Advantages		* Based on two different geothermal systems	* Al^{IV} corrected for changes in Fe/(Fe+Mg) * Applicable to Al-saturated environment	* Al^{IV} corrected for changes in Fe/(Fe+Mg) * T ranges between 50°-325°C (variety of systems)

5.3.5.2 Thermodynamic Approach:

Walshe (1986) developed a six-component chlorite solid solution model to determine the conditions of chlorite formation in hydrothermal systems. The activities of the six chlorite components are calculated from chlorite composition. Assuming the presence of quartz, these activities are then used to derive six unknowns about the physico-chemical conditions of chlorite formation: temperature, $a(H_4SiO_4)$, $a(Al^{3+})/a(H^+)^3$, $a(R^{2+})/a(H^+)^2$, $a(H_2O)$ and fO_2 (Walshe, 1986). Kavaliers et al. (1990) used this model very successfully in resolving the temperature and redox state of the hydrothermal fluids that caused gold mineralization in the Pani Volcanic Complex, Indonesia.

With an iron sulphide in equilibrium with chlorite and quartz it is possible to determine the fS_2 of the fluid at the time of precipitation. This gives a means of confirming the temperature calculated by the thermometer, by looking at the temperature at which a certain sulphide assemblage will coexist at a given fS_2. Together with the Eh of the environment, the availability of sulphur to extract Fe from chlorite may be an important controlling mechanisms for the Fe/Mg ratio of the chlorites. A high activity of reduced sulphur results in the formation of abundant pyrite and low Fe contents of coexisting chlorite and sphalerite. In contrast, a lower sulphur activity in the depositional environment produces lower Mg contents in chlorite, Fe-rich sphalerite and possibly pyrrhotite (FeS_{1-x}). Siderite may precipitate if the amount of available dissolved carbonate is sufficiently high (McLeod and Stanton, 1984).

The absence of either magnetite + pyrite or pyrrhotite + pyrite assemblages means that the fS_2 and/or fO_2 cannot easily be determined. Therefore, veins with pyrite, quartz and chlorite in equilibrium were identified, in order to at least estimate the fS_2. The quartz + chlorite assemblage is rather common but assemblages of quartz + chlorite + pyrite or chlorite + pyrite are very rare. Chalcopyrite, and occasionally sphalerite and arsenopyrite, occur with chlorite and quartz in the veins. These

54

sulphides could be used as indicators of the fS_2 instead of pyrite.

All five thermometers (the four empirical and one thermodynamic thermometer) were applied to calculate the formation temperature of the chlorite in the veins. In evaluating the use of a thermometer it is necessary to take all the advantages and disadvantages into account, and then select a thermometer which would reflect the formation conditions the best and fits the mineralogical observations.

The first geothermometer (Cathelineau and Nieva, 1985) must be treated with care since it is based on data from only one geothermal system. Furthermore, Cathelineau and Nieva warned that this thermometer can only be applied if thermo-chemical conditions during chlorite formation stay fairly constant. This limitation can disqualify this thermometer because conditions in a hydrothermal system can be expected to change constantly. An interesting aspect, however, is that of all the empirical thermometers, this one gives temperatures closest to that of Walshe's thermodynamic thermometer **(Fig. 5.11)**.

The second thermometer (Cathelineau, 1988) was derived from data from two different geothermal fields and the relationship between Al^{IV} and T should theoretical be more reliable. However, temperatures estimated are in the order of 50° - 80°C higher than that of Walshe's geothermometer.

The two thermometers (Kranidiotis and MacLean, 1987; and Jowett, 1991) that make use of a calculated AI^{IV} value, give temperatures that deviate even more from the thermodynamic thermometer of Walshe. Kranidiotis and MacLean's thermometer derived temperatures 70° - 100°C lower than Walshe's, and Jowett's thermometer calculated temperatures in the order of 80° - 100°C higher. Kranidiotis and MacLean (1987) did state, however, that this thermometer may underestimate the formation temperature of chlorites with a high Fe/(Fe+Mg) ratio. Likewise, Jowett (1991) puts a limitation of less than 0.6 on the Fe/(Fe+Mg) ratio of chlorites. Based on the high Fe content of chlorites in the

studied area, it is unlikely that these two geothermometers could give realistic temperature estimates.
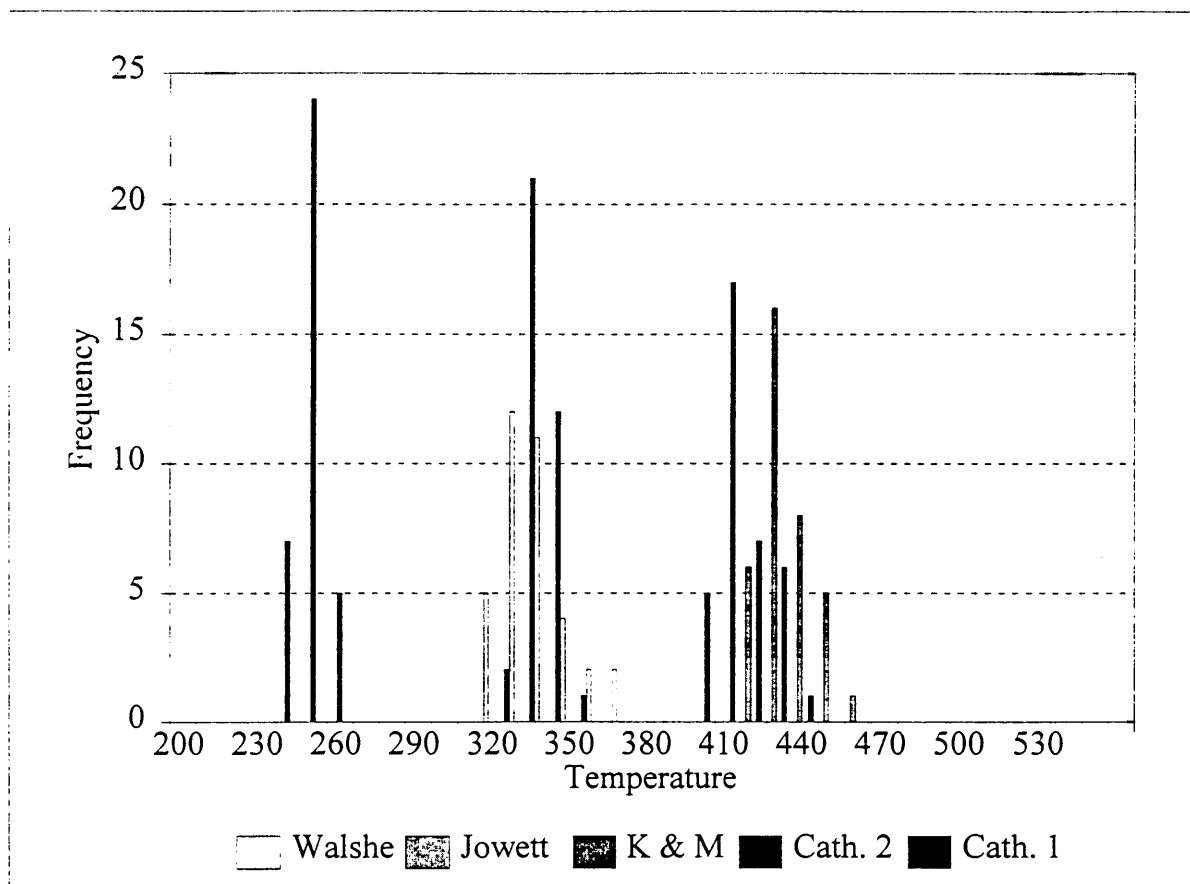
Figure 5.11: Histograms showing the result from the chlorite geothermometers (Walshe = Walshe, 1986; Jowett = Jowett, 1991; K & M = Kranidiotis and MacLean, 1987; Cath 1 = Cathelineau and Nieva, 1985; Cath 2 = Cathelineau, 1988).

If Walshe's thermodynamic geothermometer is agreed on as the most accurate one, the conclusion is that the temperature at which the vein chlorites in the studied hydrothermal system precipitated is between 315° and 360°C, the average of 33 analyses being 332°C (σ = 12°C).

It is, however, dangerous to expect only one geothermometer to give reliable estimates of the temperature range prevailing in this hydrothermal system. Furthermore conditions in a hydrothermal system are constantly changing, so that data from only one or two minerals in such a system cannot be taken as representative of the system as a whole. This investigation should therefore, be supported by a microthermometric study on fluid inclusions in hydrothermal quartz (**Chapter 7**).

Sulphide mineralogy

6.1 ARSENOPYRITE

6.1.1 Mode of occurrence:

Arsenopyrite occurs in large quantities in chlorite + quartz veins in the agglomerate (**Fig. 6.1**), together with other first stage sulphides, mainly pyrite and chalcopyrite. Arsenopyrite seems to be the sole host for gold, native bismuth, and two Bi-containing sulphosalts (**Fig. 6.2**). Native bismuth and gold occur as microscopic inclusions in arsenopyrite whereas the Bi-containing sulphosalts and galena (together with chalcopyrite) occur interstitially or as fracture fillings in the arsenopyrite (**Fig. 6.3**). Where supergene alteration is more pronounced, the arsenopyrite is replaced along fractures by blue Cu-sulphides (**Fig. 6.4**).

6.1.2 Chemical composition:

A total of 682 microprobe analyses (**Appendix H**) show that arsenopyrite contains an average of 4.0 ($\sigma = 1.97$) at% Co, resulting in a slightly lower Fe content (29.4 ($\sigma = 2$) at%) than usual (33 ($\sigma = 1$) at%, Kretschmar and Scott, 1976). The average atomic ratio As/S = 1.2, indicating As-rich arsenopyrite possibly of high-temperature (Kretschmar and Scott, 1976). **Figure 6.5** shows the negative correlation between Fe and Co. Other trace elements sometimes present in arsenopyrite (e.g. Ni, Sb, Bi and Cu) are all below the lower limit of detection.

Native gold is also present in the arsenopyrite. Surface adsorption is a mechanism to concentrate gold on arsenopyrite (Renders and Seward, 1989). Bancroft and Jean (1982) suggested that Au^{3+} is adsorbed on the sulphide as a hydrated or hydrolysed species, and then reduced by the sulphide according to the reaction (6.1):

$$8Au^{3+} + 3S^{2-} + 12H_2O \rightarrow 8Au^\circ + 3SO_4^{2-} + 24H^+ \ldots \ldots (6.1)$$
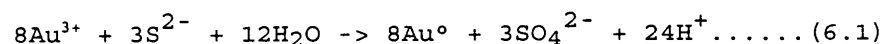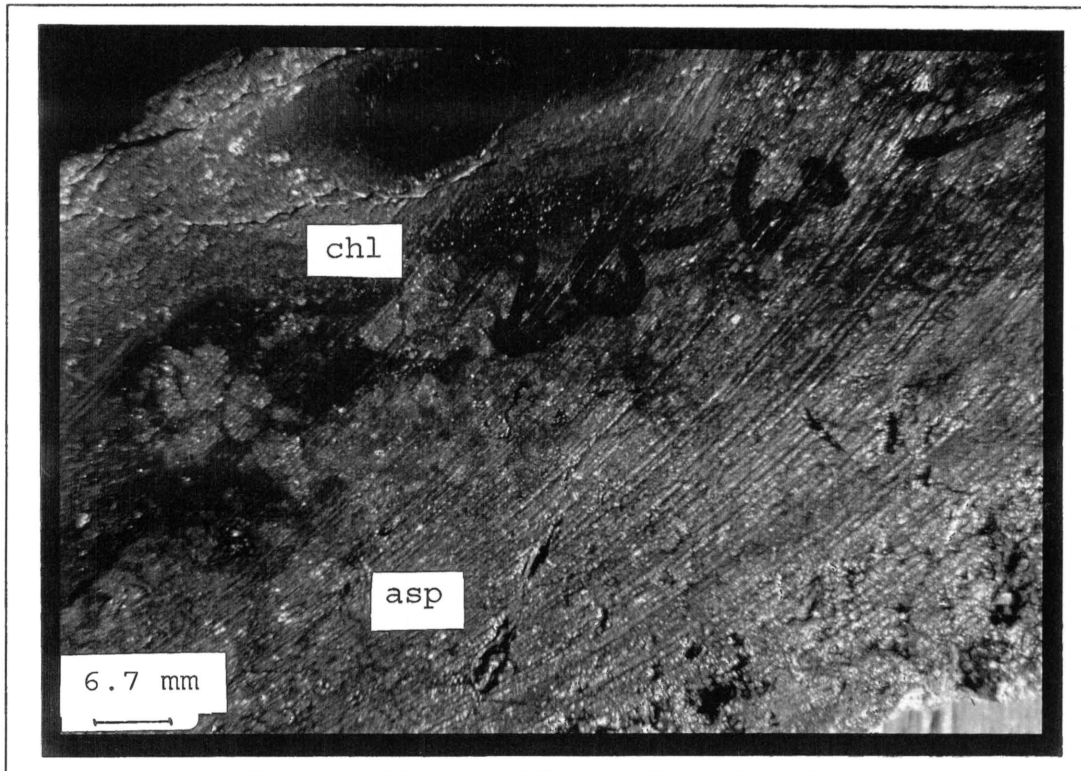
Fig. 6.1: Massive arsenopyrite(asp) in a matrix of chlorite(chl) in a vein in agglomerate (GD1 at 20.60m).
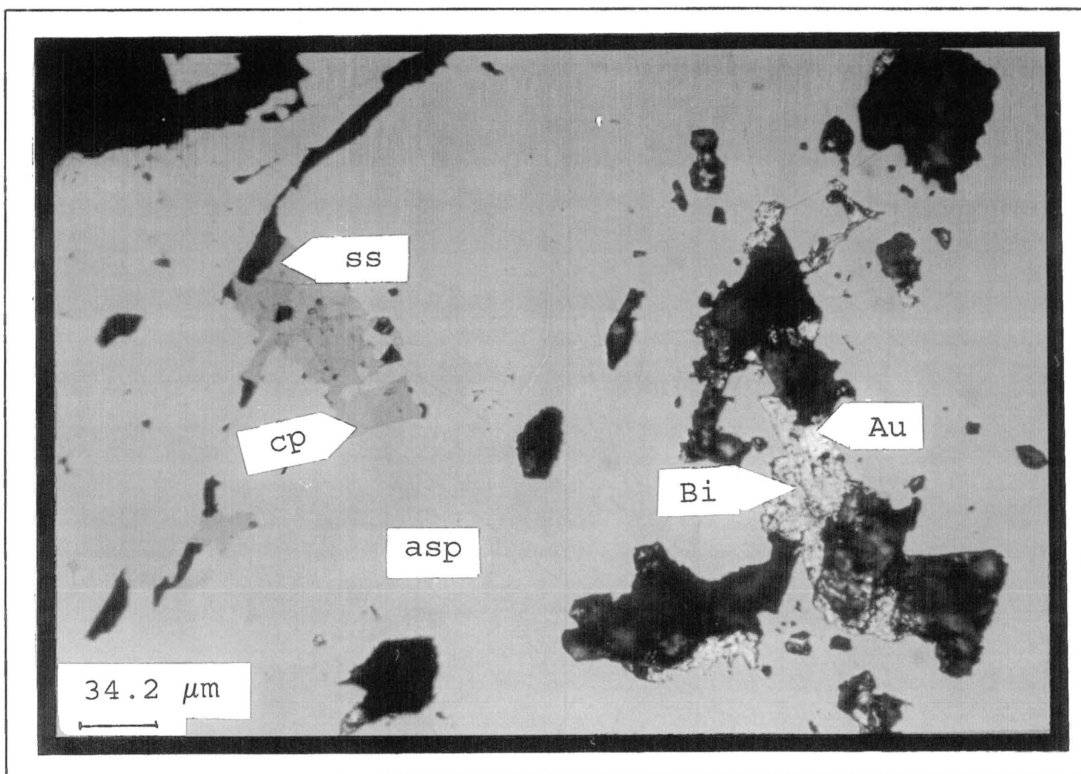
Fig. 6.2: Arsenopyrite(asp) with inclusions of native bismuth(Bi) and gold(Au), chalcopyrite(cp), and a Bi-sulphosalt(ss) (GD1 at 25.30m).

59
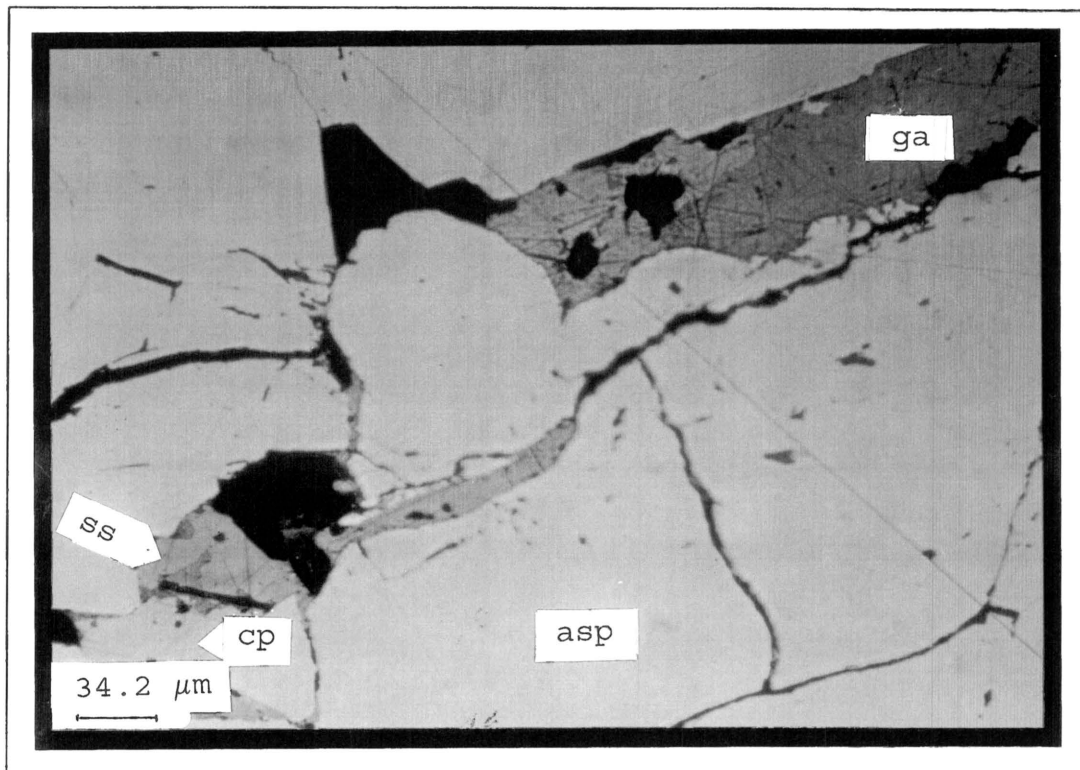
Fig. 6.3: Arsenopyrite(asp) with fracture fillings of galena(ga), chalcopyrite(cp), and the Bi-sulphosalt(ss) (GD1 at 25.30m).
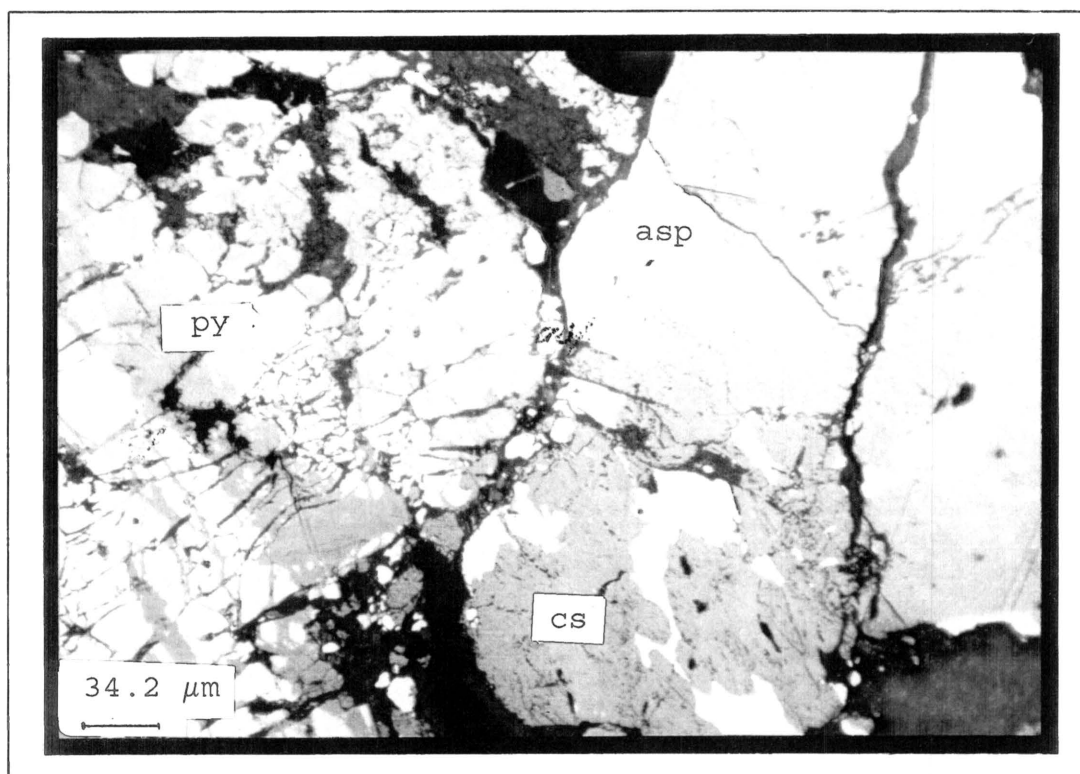
Fig. 6.4: Arsenopyrite(asp) and pyrite(py) being replaced along cracks by a copper sulphide(cs) (GD2 at 45.75m).

60
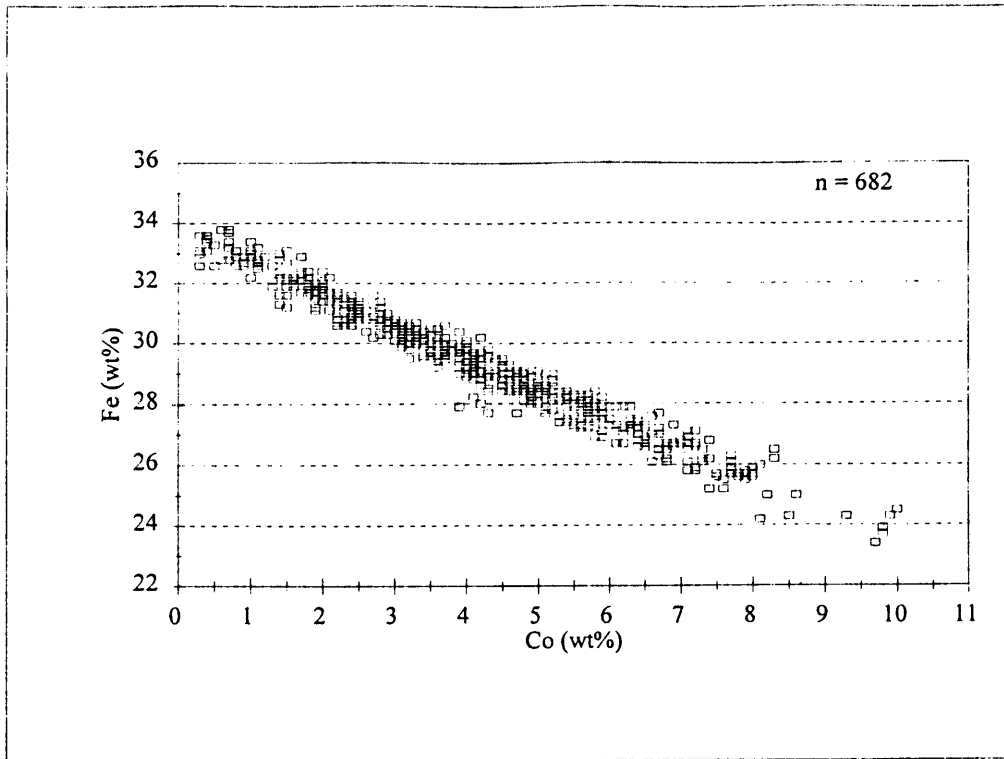
Figure 6.5: The negative correlation between Fe and Co in arsenopyrite (Spearman rank correlation coefficient = -0.9697)

6.1.3 Arsenopyrite geothermometery:

Cathelineau and co-workers (1989) found that Au-rich arsenopyrites normally crystallise at low temperature (200° ± 50°C), whereas Au-poor arsenopyrites crystallise together with native gold at temperatures ranging from 300° to 500°C. A more reliable method of estimating the temperature of formation of the arsenopyrite is by using the arsenopyrite geothermometer described by Kretschmar and Scott (1976). However, they advised the following precautions: (1) arsenopyrite should be chosen with care from equilibrium, $a(S_2)$-buffered assemblages. In vein deposits, arsenopyrite can be assumed to be in equilibrium with other simultaneously deposited minerals. It is, however, known that high-temperature As-rich arsenopyrites can be overgrown by low-temperature S-rich arsenopyrites. (2) The combined minor-element content of the arsenopyrite should be < 1 wt%. (3) If arsenopyrite is analysed by a powder-XRD technique, the d_{131} value should be determined with a CaF_2 as a standard, using a_o = 5.4626Å for the fluorite (this is to be consistent with the determinative curve in Fig. 3 by Kretschmar and Scott, 1976).

61

(4) If arsenopyrite is analysed by electron microprobe, a standard of proven homogeneity should be used but not with $FeAs_2$ or As as standards, as the As is not bonded in the same way as in arsenopyrite. The effect of pressure on the arsenopyrite composition and the phase equilibria in the system Fe-As-S has been discussed by Sharp et al. (1985) and Ayora et al. (1993). They found that pressure has no influence on the composition of arsenopyrite coexisting with pyrite; hence pressure also does not effect the determined temperature.

In the studied mineralised hydrothermal system, arsenopyrite only coexists with pyrite and therefore falls in the field arsenopyrite + pyrite + liquid (asp + py + L) on a T/at% As diagram (**Fig. 6.6**). The indicated temperature will therefore, be between 363° - 491°C. However, the average at% As in arsenopyrite is 36, which does not agree with the supposed stability field of asp + py + L. The reason for this discrepancy is the high atomic As/S ratio, although the amount of Co ($\approx$ 4 at%) replacing the Fe may also be important (**Fig. 6.7**). Kretschmar and Scott (1976) were uncertain about the effect of Co on the As/S ratio in arsenopyrite, other than that it would increase the d_{131} value. A plot of Co against the As/S ratio (**Fig. 6.8**) shows a weak positive correlation between these two variables.
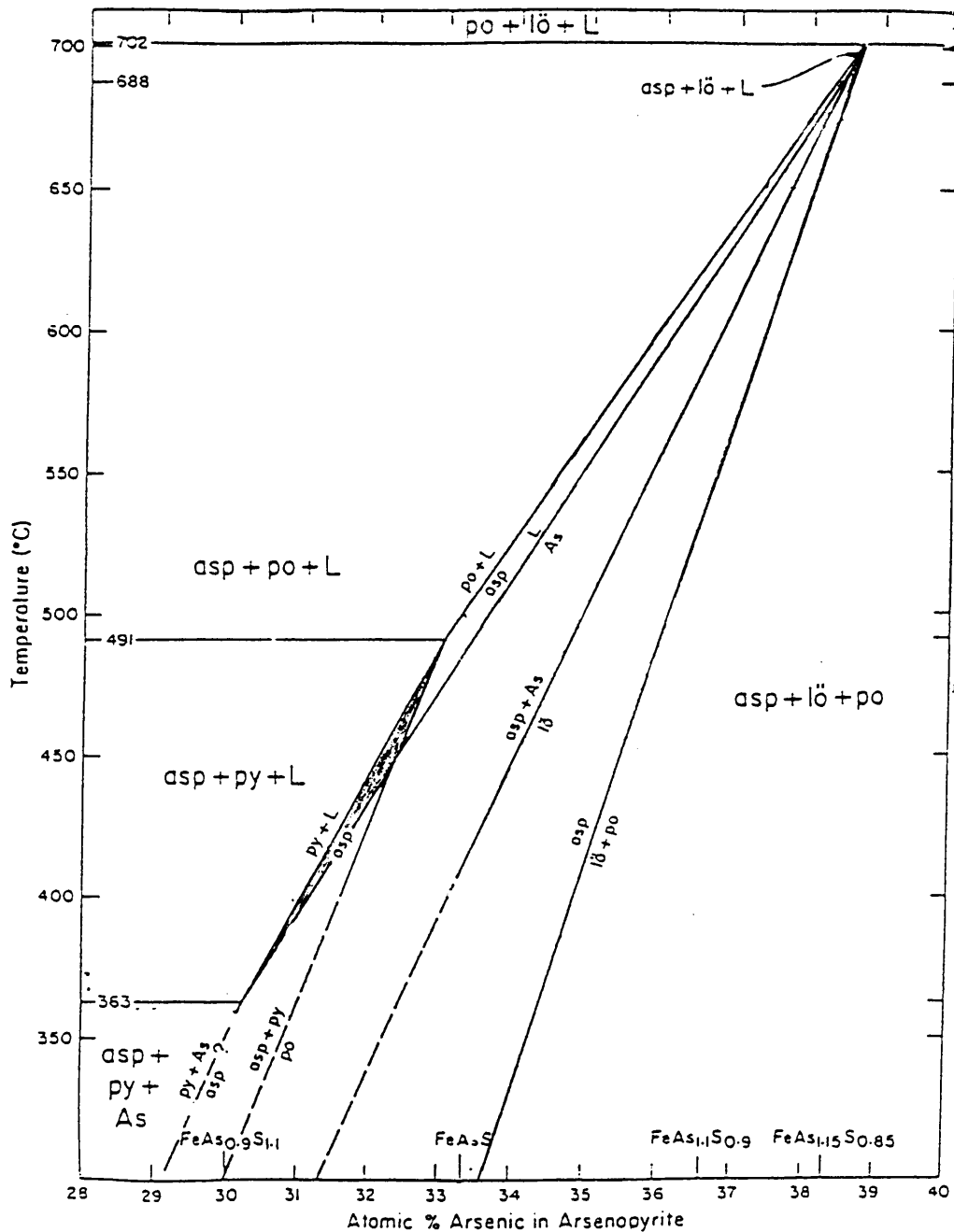
Figure 6.6: Pseudobinary T-X section along the pyrite-loellingite join showing arsenopyrite composition as a function of temperature and bulk composition, asp = arsenopyrite; py = pyrite; lö = loellingite; po = pyrrhotite; L = liquid (after Kretschmar and Scott, 1976). The shaded area indicates the field in which the arsenopyrite in the study area falls.
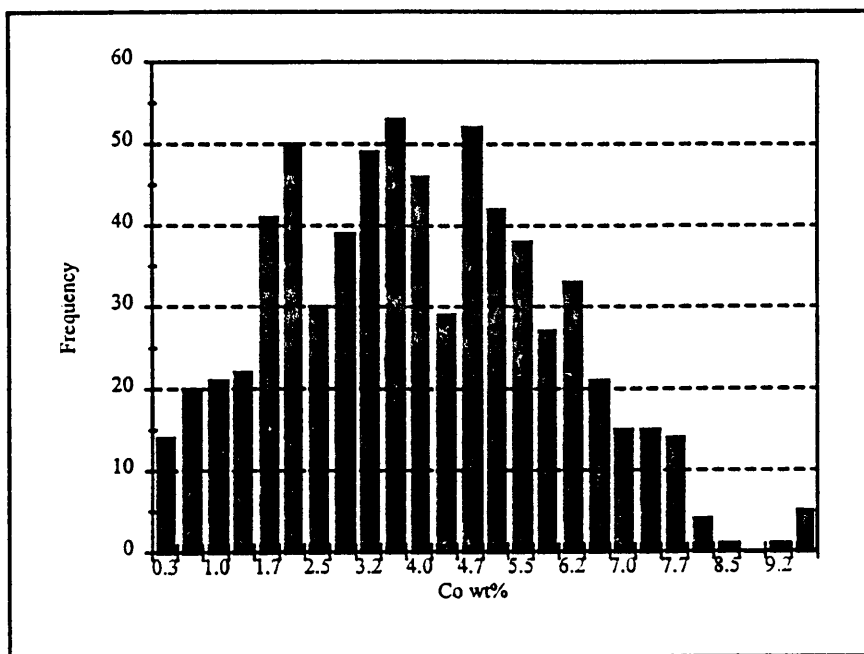
Figure 6.7: Histogram showing the distribution of Co in the arsenopyrite (The values indicate the middle point of each class).
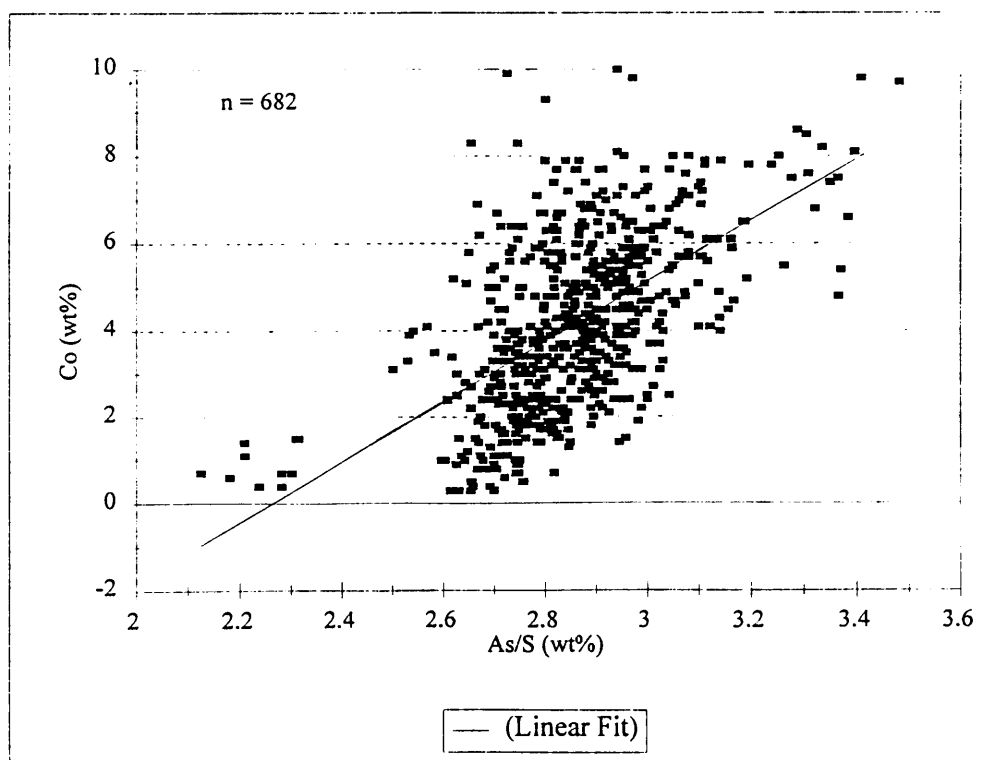
Figure 6.8: Plot of Co against the As:S ratio in arsenopyrite (Spearman rank correlation coefficient = 0.5680).

64

6.2 Bi-Pb-Cu SULPHOSALTS

6.2.1 Mode of occurrence:

This second stage sulphide mineral, described as a sulphosalt, normally occurs interstitially with respect to arsenopyrite grains (**Fig. 6.9**), but single arsenopyrite crystals may also occur in the sulphosalt (**Fig. 6.10**). In some areas the sulphosalt appears to be replaced by copper sulphides (**Fig. 6.11 and 6.12**). In polished sections it has a light greyish to green colour with a strong anisotropism, and it is clearly softer than arsenopyrite and chalcopyrite, with no distinct euhedral shape.

6.2.2 Chemical composition

6.2.2.1 Bismuthinite-aikinite:

A semi-quantitative electron microprobe study (**Appendix I**) indicated that it contains Bi, Pb, and Cu and probably belongs to the solid-solution series aikinite ($CuPbBiS_3$)-bismuthinite (Bi_2S_3) (**Fig. 6.13**). Further treatment of the data support this suggestion with the antipathetic behaviour of Bi and (Pb+Cu) (**Fig. 6.14**). From Figure 6.14 the ratio Bi:(Pb+Cu) is roughly 1:1 which indicates that the composition of this sulphosalt may plot close to krupkaite ($CuPbBi_3S_6$). However, as for the identity of the sulphosalt, no final conclusions can be drawn from the semi-quantitative analyses.

6.2.2.2 Wittichenite:

In some areas the Bi-Pb-Cu-sulphosalt is rimmed by an optically darker mineral (**Fig. 6.10**). Qualitative analyses indicate that this is a Bi containing sulphosalt high in Cu and very low in Pb. The ratio $Cu_2S:Bi_2S_3$ seems to be close to 3:1 which implies that this possibly represents wittichenite ($3Cu_2S.Bi_2S_3$) (**Fig. 6.15**). Wittichenite is a mineral in the solid solution series chalcocite-bismuthinite, and in the studied assemblages this sulphosalt is often replaced by a copper sulphide.
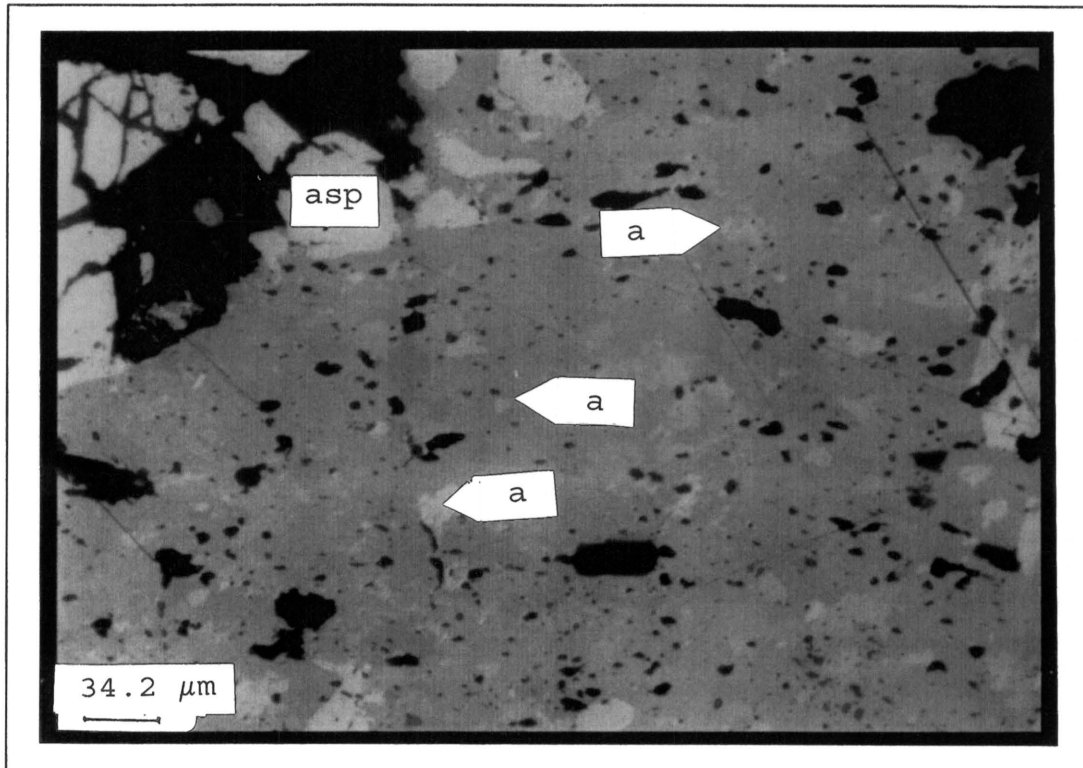
Fig. 6.9: Bi-Pb-Cu sulphosalt(a) in spaces between
arsenopyrite(asp) grains. Note the strong anisotropism with
colours changing from dark grey to light green; photograph taken
with a blue filter (GD1 at 25.50m).
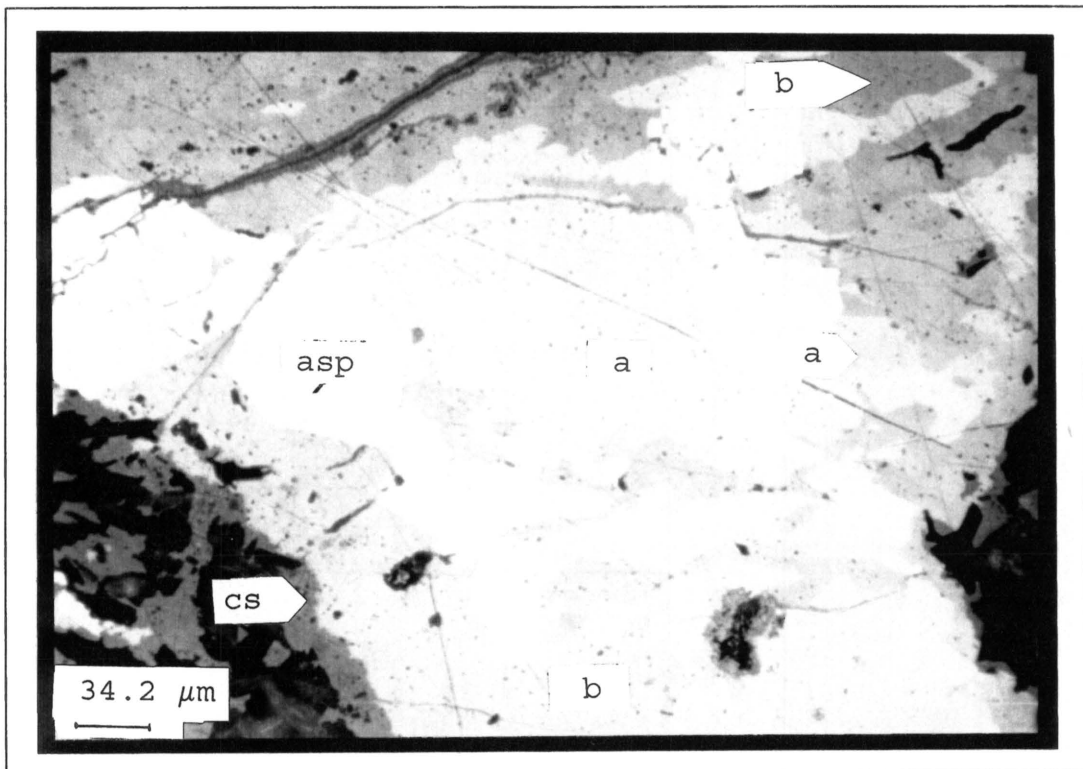
Fig. 6.10: Single arsenopyrite(asp) crystals in the Bi-Pb-Cu
sulphosalt(a). The darker mineral on the rims and along cracks
is the Cu rich (Pb poor) sulphosalt(b). On the outer rims is a
copper sulphide(cs) overgrowth; photograph taken without a blue
filter (GD2 at 15.85m).

66

Fig. 6.11: Bi-Pb-Cu sulphosalt(a) rimmed by copper-sulphides(cs). The copper-sulphides replace the chlorite(chl); oil-immersion (GD2 at 15.85m).
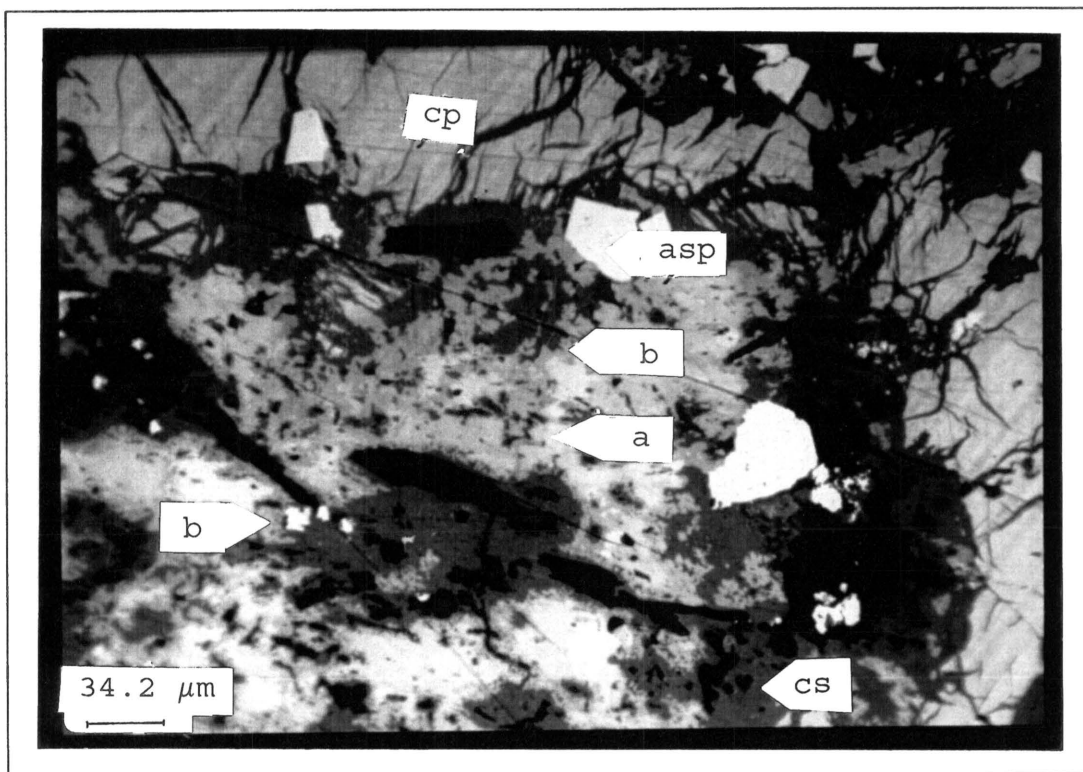
Fig. 6.12: Chalcopyrite(cp), Bi-Pb-Cu sulphosalt(a) and Bi-Cu sulphosalt(b) rimmed and replaced by a copper-sulphide(cs). The single crystals are arsenopyrite(asp); oil-immersion (GD1 at 47.20m).

67
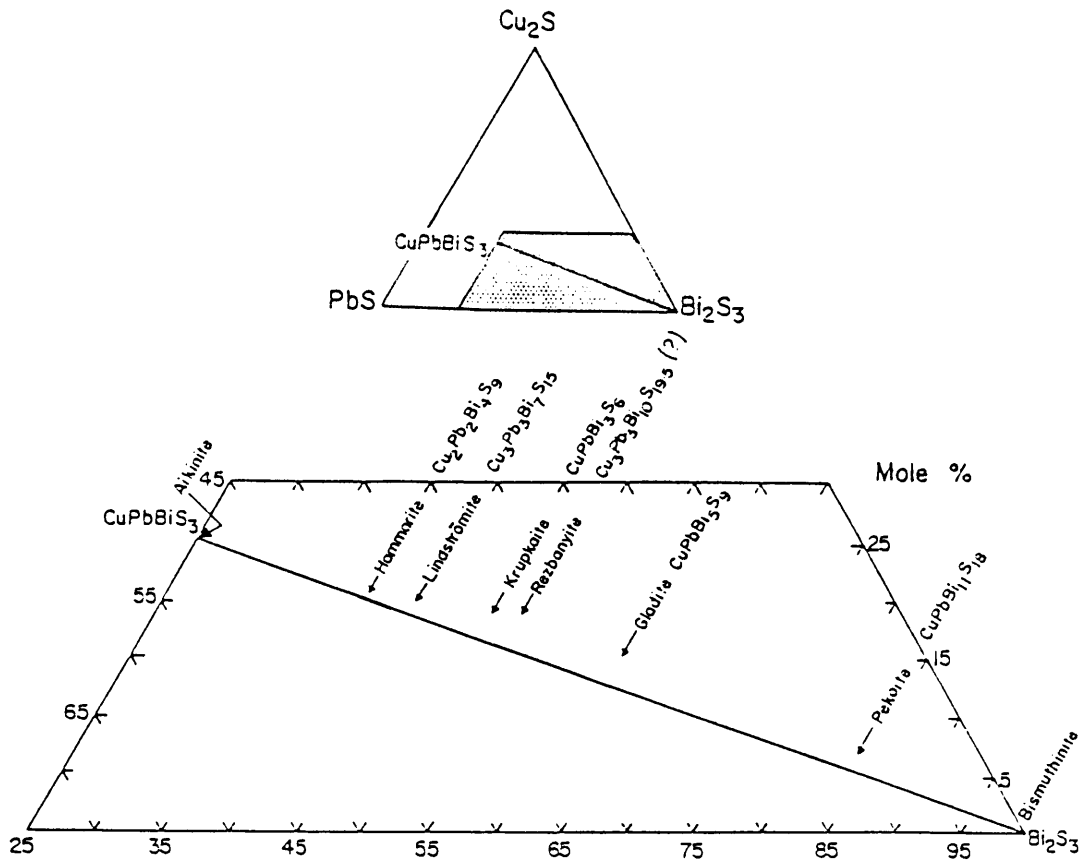
Figure 6.13: Composition of sulphosalts in the Cu_2S-PbS-Bi_2S_3 (after Harris and Chen, 1976).
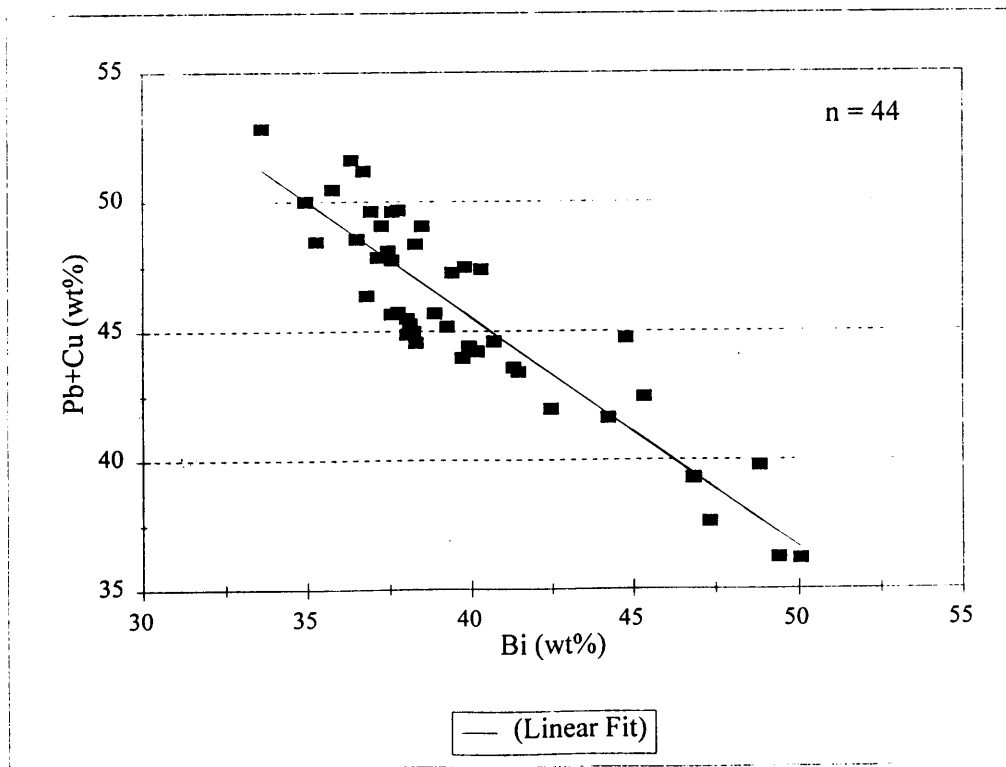
Figure 6.14: The linear relationship between Bi and (Pb+Cu) in the investigated sulphosalt.
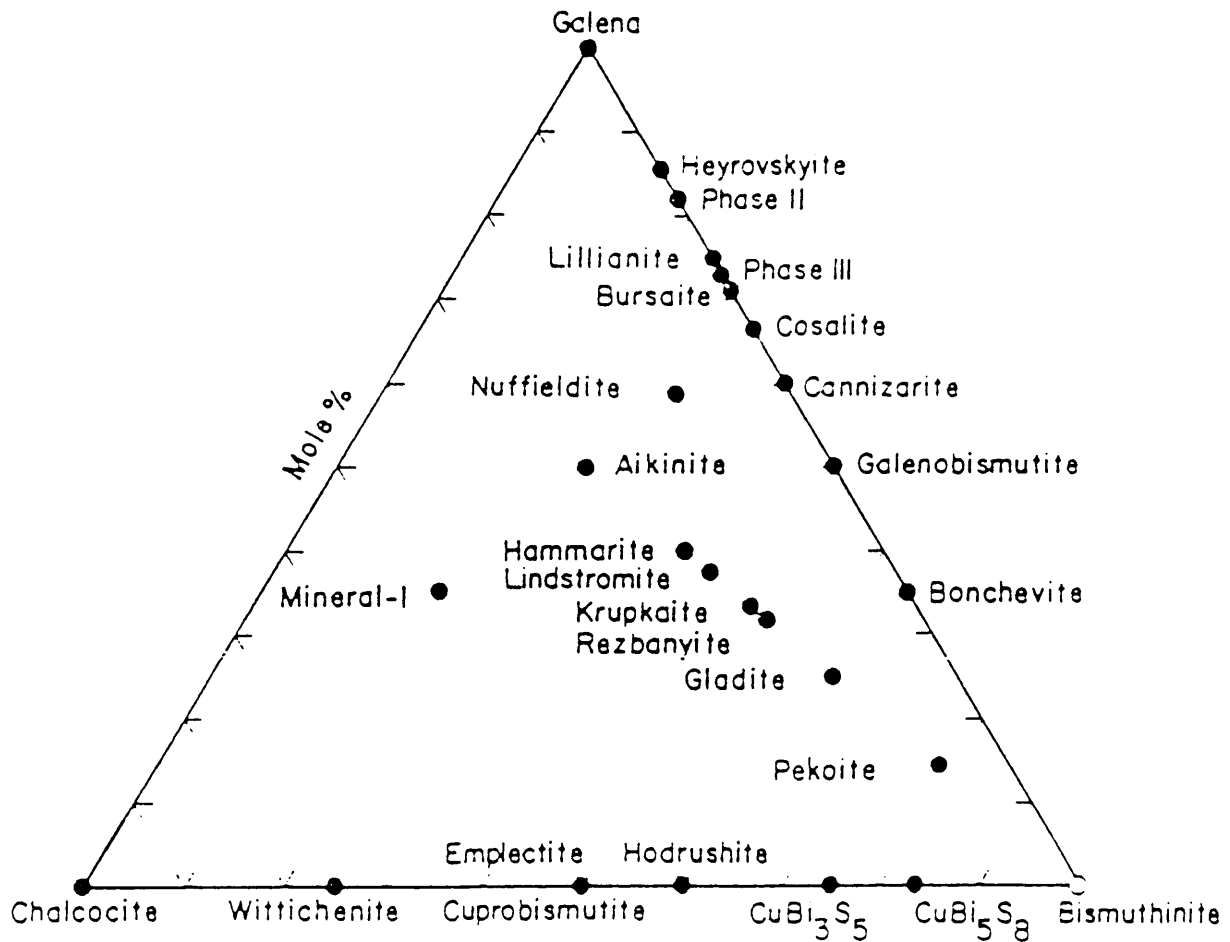
Figure 6.15: Phases reported in the system PbS-Cu$_2$S-Bi$_2$S$_3$ (from Chang and Hoda, 1977).

6.3 SPHALERITE

6.3.1 Mode of occurrence:

More or less equigranular sphalerite together with other sulphides are disseminated in the agglomerate matrix (**Fig. 6.16 and 6.17**). Small grains were sporadically observed in veins. Characteristic of all the sphalerite is "chalcopyrite-disease" (**Fig. 6.18**) (Barton, 1973; Barton, and Bethke, 1987; Bente and Doering, 1993), and white internal reflections. Sporadically, pyrite seems to be replaced by sphalerite (**Fig. 6.19**), although this texture can also be interpreted as pyrite "inclusions" in sphalerite. Galena is present in small amounts between sphalerite grains.

Figure 6.18 illustrates two possible generations of sphalerite. The areas with a larger amount of chalcopyrite inclusions might represent an older (and possibly higher temperature) phase, whereas the areas between these "grains" have less inclusions and must have formed at a later stage. The first generation

69

sphalerite seems to have been broken up in fragments and "welded" together by the second generation.

6.3.2 Chemical analyses:

Quantitative microprobe analyses (**Appendix J**) of disseminated sphalerite in the agglomerate showed that it contains only very small amounts of Fe (up to a maximum of 1.9 wt%) and Cu (maximum of 1.6 wt%) (**Fig. 6.20a & 6.20b**). The low concentration of Fe is the reason for the white internal reflections.

6.3.3 Sphalerite geothermometery:

Sphalerite coexists with pyrite, in an environment that is predominantly iron rich (e.g. Fe-rich chlorite). According to the stability diagram (**Fig. 6.21**) of Barton and Toulmin (1966) the disseminated sphalerite in the study area will fall somewhere in the sphalerite + pyrite field at a very low FeS (mol%), close to 0. Therefore, the maximum temperature of formation could have been approximately 500°C.

6.4 PYRITE

Pyrite fills veins and also occurs as disseminated grains of varying size in the matrix of the agglomerate. In some polished sections, the pyrite crystallised in strings of small euhedral grains, surrounded by either silicates or sphalerite. Occasionally, pyrite was observed as possible "remnants" replaced by sphalerite (**Fig. 6.19**) and chalcopyrite. Pyrite also appears as inclusions in sphalerite, arsenopyrite, and chalcopyrite.

In the zone of supergene alteration pyrite is often replaced by a copper-sulphide along rims or fractures in the pyrite crystal (**Fig. 6.4**). Pyrite also occurs as cataclasts in some of the chloritic veins. Smaller amounts of pyrite were found in chlorite + quartz veins (GD1 and GD2) and quartz + siderite veins (GD3) in the rhyolite.

70
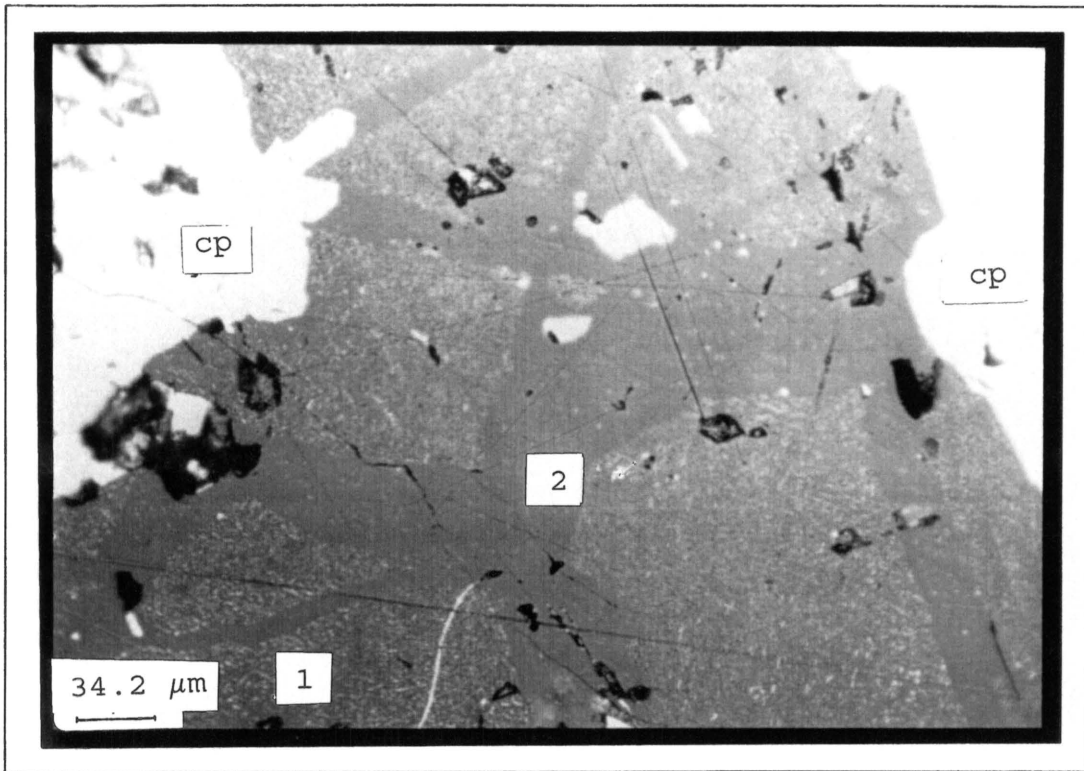
Fig. 6.16: Disseminated sphalerite(sph), chalcopyrite(cp), covellite(cv) and pyrite(py) in the matrix of the agglomerate; oil-immersion (GD2 at 20.20m).
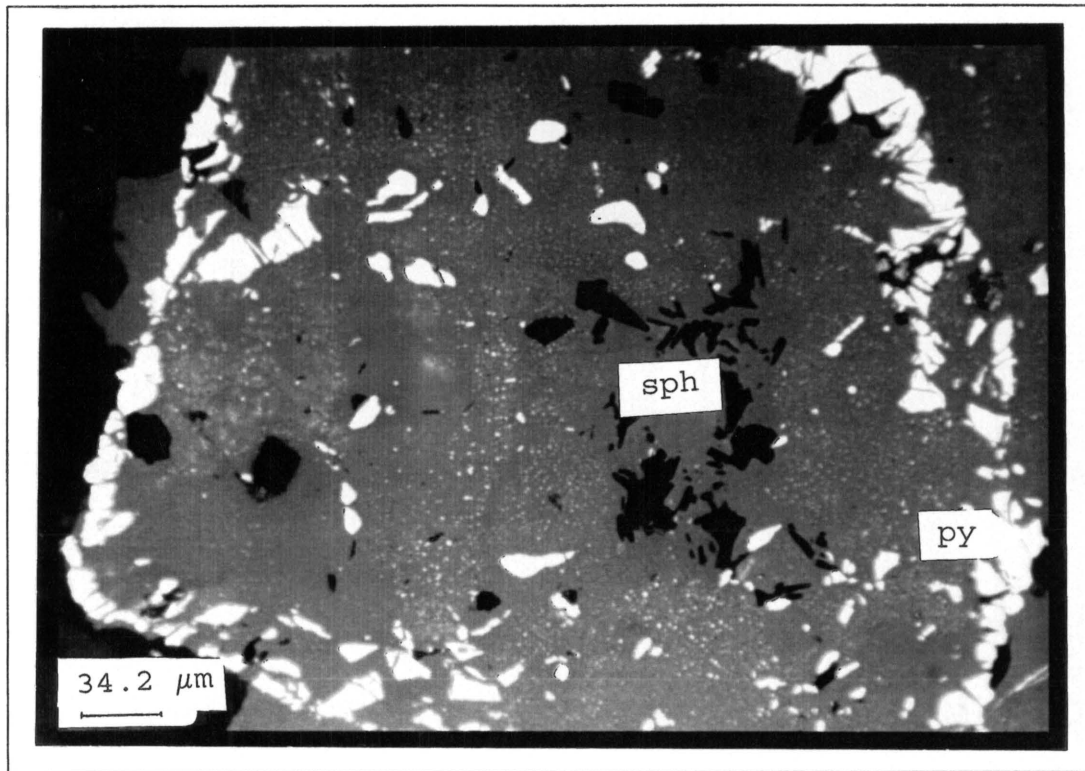
Fig. 6.17: Disseminated sphalerite(sph) with pyrite(py) and galena(ga) in the agglomerate matrix; oil-immersion (GD1 at 70.50m).

71
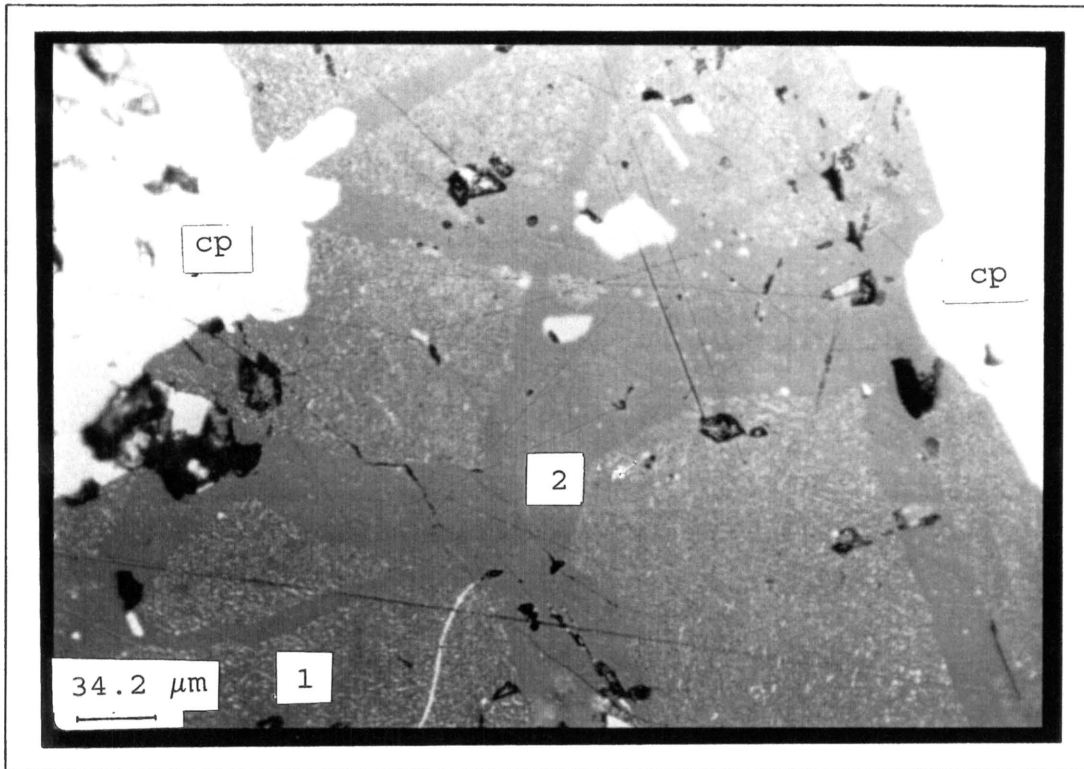
Fig. 6.18: Sphalerite with chalcopyrite(cp) inclusions ("chalcopyrite-disease"); oil-immersion. The areas with lesser inclusions may be a second(2) generation that differs from the first(1) generation sphalerite (GD2 at 75.65m).
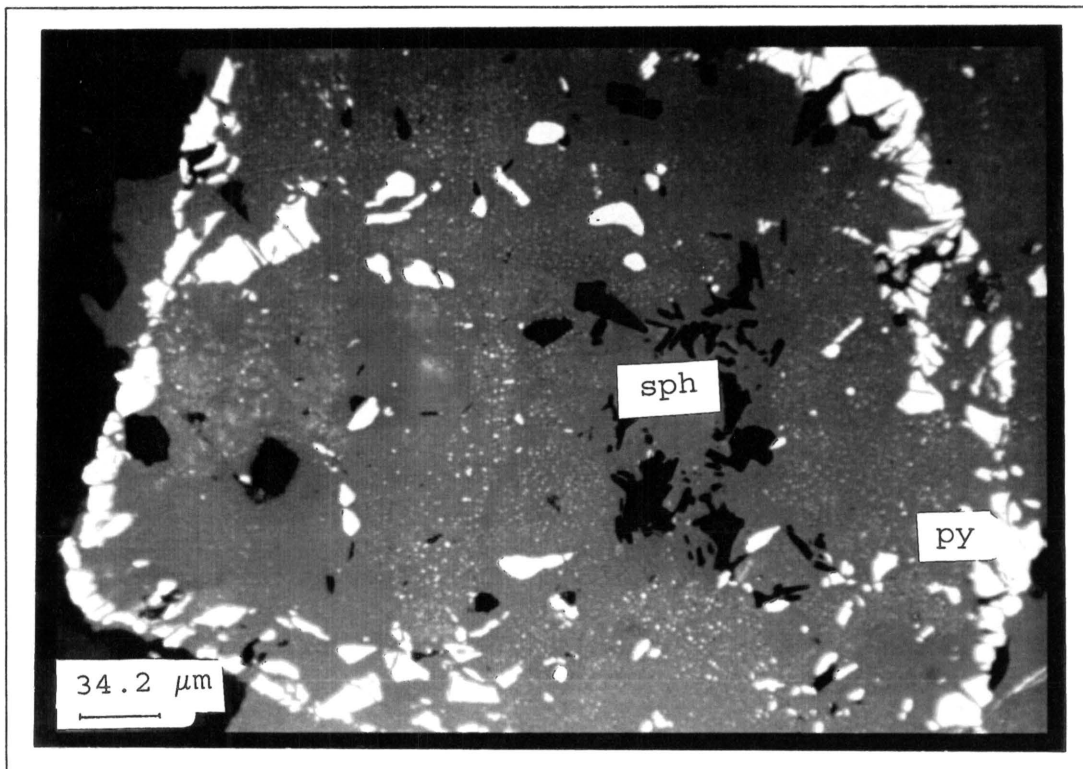
Fig. 6.19: Pyrite(py) inclusions in sphalerite(sph); oil-immersion (GD2 at 75.65m).

72
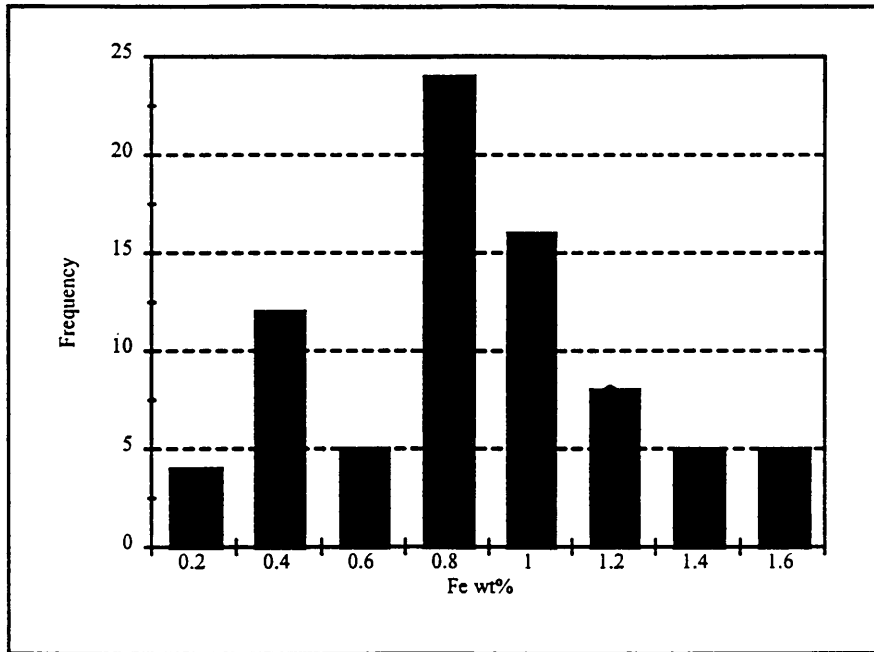
Figure 6.20a : Histogram of the Fe contents in disseminated sphalerite (n = 79) (The values indicate the middle point of each class).
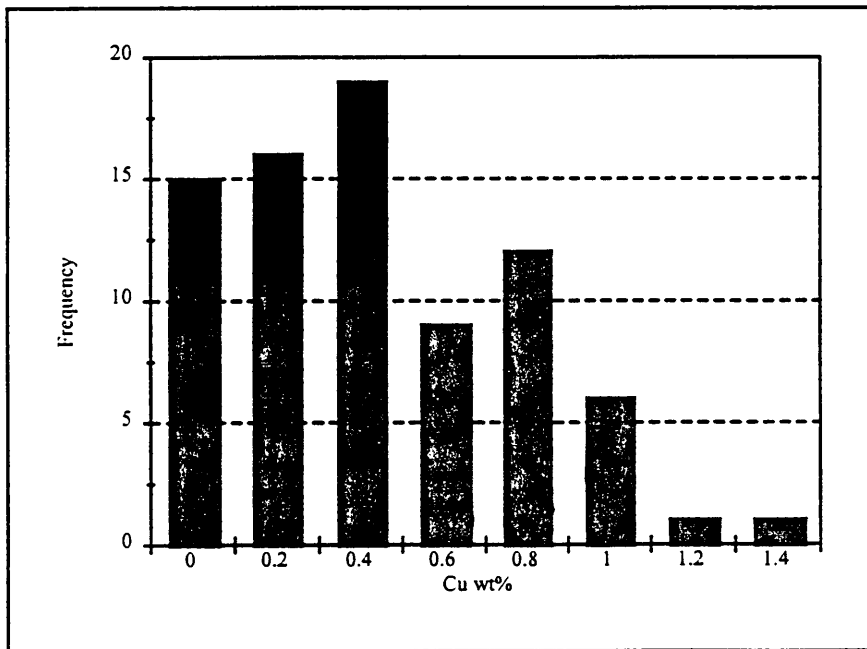
Figure 6.20b : Histogram of the Cu contents in disseminated sphalerite (n = 79) (The values indicate the middle point of each class).
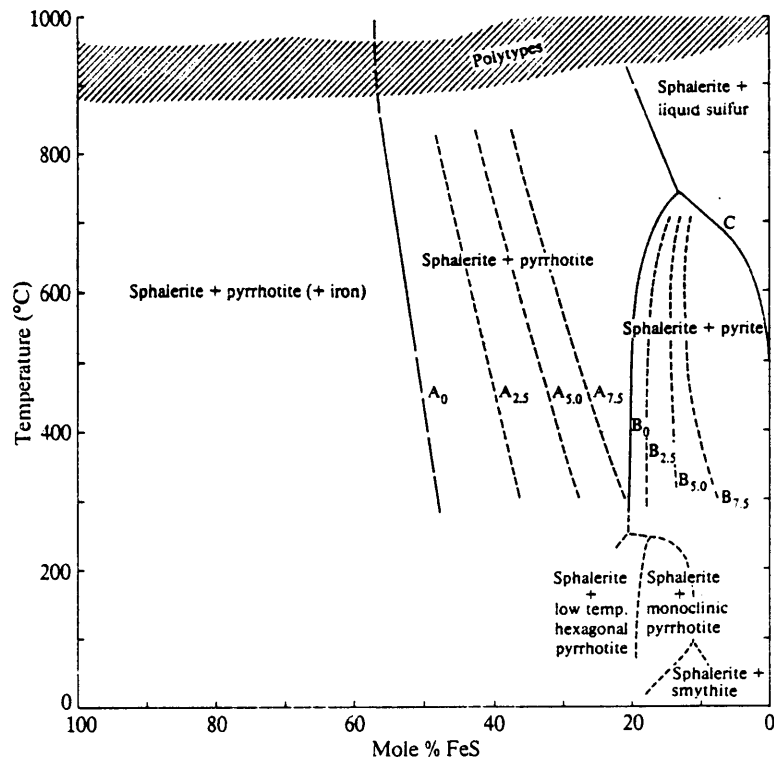
Figure 6.21: Composition of sphalerite, in the FeS-ZnS system, in equilibrium with iron sulphides (after Barton and Toulmin, 1966). The dashed lines labeled 2.5, 5.0, and 7.5 represent the compositions of sphalerite in equilibrium with iron and pyrrhotite (A series) and sphalerite in equilibrium with pyrrhotite and pyrite (B series) at 2.5,5.0, and 7.5 kbar respectively. The dotted lines represent the low-temperature relationships according to Scott and Kissin (1973).

6.5 CHALCOPYRITE

Like pyrite, chalcopyrite is very common in all the vein types as well as in the matrix of the agglomerate. Chalcopyrite is often overgrown or replaced by copper-sulphides in the zone of supergene alteration (Fig. 6.12), but unaltered chalcopyrite was also observed, with sporadic replacement of bornite along small cracks. Galena and pyrite are occasionally present as inclusions in chalcopyrite.

Chalcopyrite, along with the sulphosalts and galena, is present as fracture fillings and also as inclusions in arsenopyrite grains,

(Fig. 6.22). In sphalerite dominated areas, chalcopyrite occurs as "chalcopyrite-disease" (Fig. 6.23) (Barton, 1973; Barton, and Bethke, 1987; Bente and Doering, 1993) in the sphalerite. Assemblages with pyrite are common in quartz veins in the brecciated zone between the underlying rhyolite and agglomerate, and in quartz + siderite veins in the red rhyolites of GD3.

6.6 COPPER SULPHIDES

A variety of different copper sulphides (sometimes finely intergrown) are present in the zone of supergene alteration. By means of XRD analyses it was shown that the copper sulphides comprise digenite (Cu_7S_5), djurleite ($Cu_{49}S_{25}$), roxbyite (Cu_7S_4), and covellite (CuS) (Fig. 6.24), and possibly other intermediate compositions associated with malachite and goethite. These copper sulphides frequently rim/overgrow chalcopyrite and replace pyrite, and arsenopyrite (Fig. 6.12 and 6.25). In some areas chlorite seems to be replaced by the copper sulphide minerals (Fig. 6.11). Figure 6.26 illustrates the different phases in the Cu-S system.

6.7 GALENA

Although present in minor amounts, galena is common in veins and as disseminations in the matrix of the agglomerate. It coexists with many of the sulphides discussed, either as inclusions in arsenopyrite, chalcopyrite, and sphalerite, or as fracture fillings in arsenopyrite (Fig. 6.27). Unlike the pyrite, chalcopyrite, and arsenopyrite, galena is not affected by supergene alteration. Although widely distributed in small amounts, galena shows no preferential association with sphalerite.

6.8 NATIVE BISMUTH

Native bismuth is only present in the arsenopyrite as small inclusions (Fig. 6.28). Because no thermal expansion cracks could be observed in the arsenopyrite (Ramdohr, 1975), it can be assumed that native bismuth was included in the arsenopyrite as an already crystallised phase. It is not associated with any other sulphide mineral in the arsenopyrite, but does occur with gold.

6.9 NATIVE GOLD

Like the case with native bismuth, gold also only occurs in the arsenopyrite in very small amounts (**Fig. 6.2**).
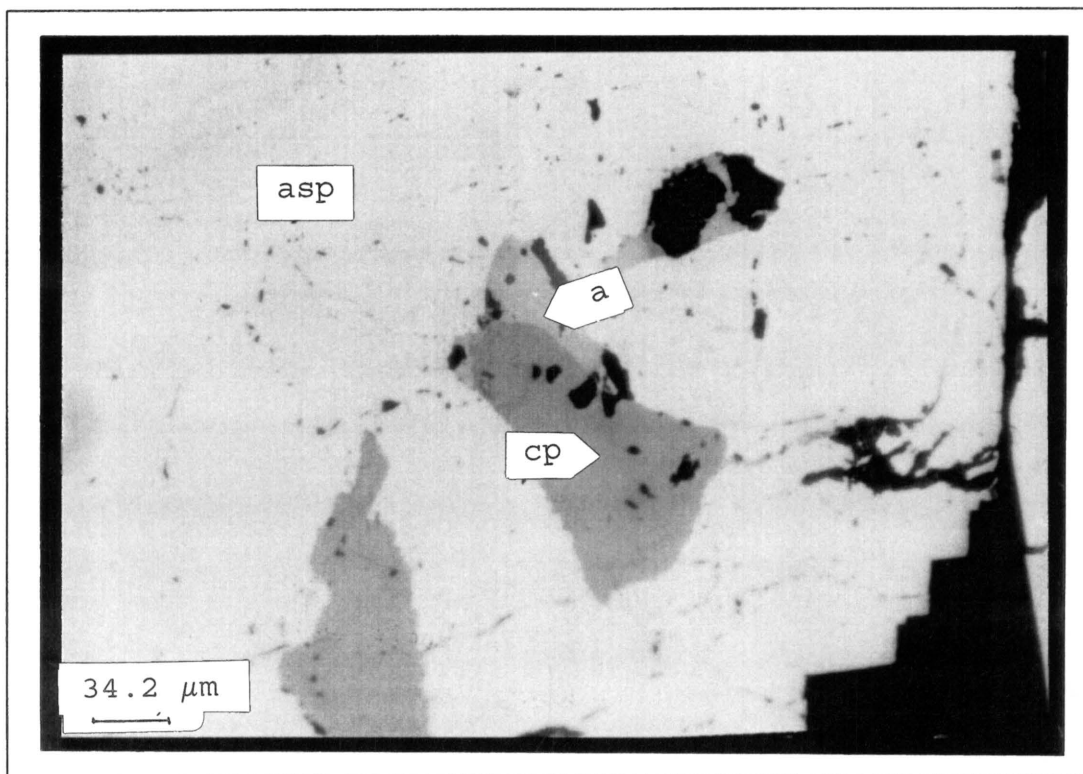
Fig. 6.22: Chalcopyrite(cp) together with the Bi-Pb-Cu sulphosalt(a) as inclusions in arsenopyrite(asp); oil-immersion (GD1 at 25.50m).
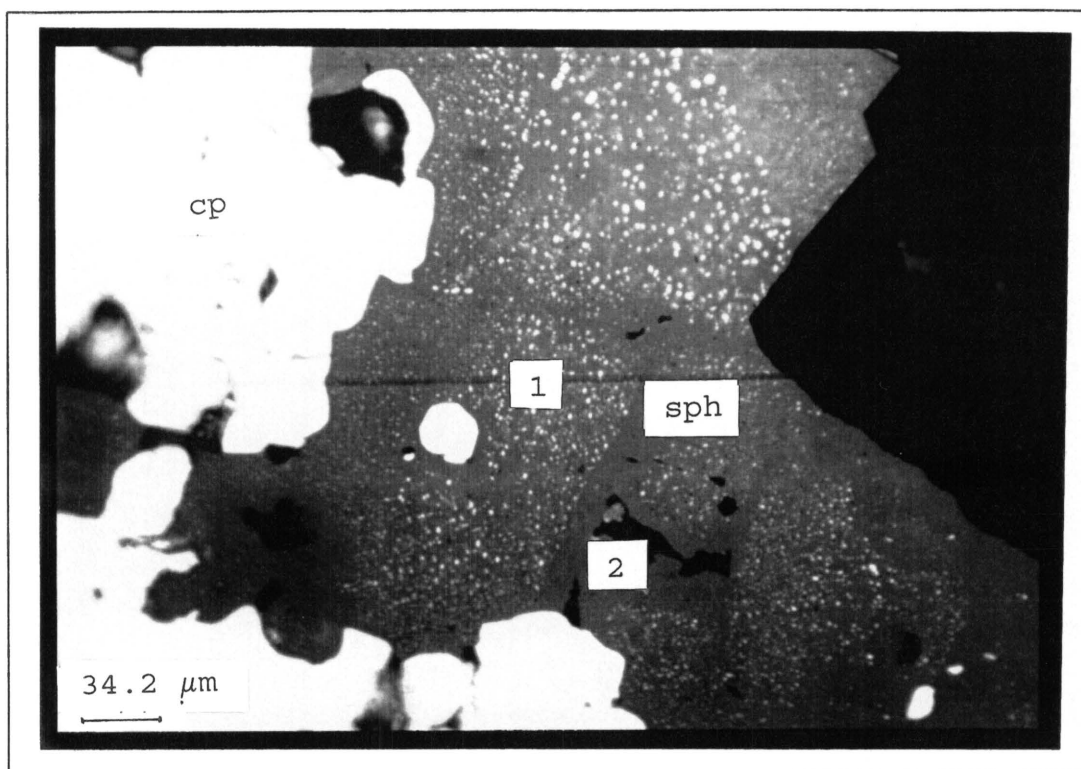
Fig. 6.23: Chalcopyrite(cp) as inclusions or "chalcopyrite-disease" in sphalerite(sph) and larger chalcopyrite grains associated with sphalerite. Two generations sphalerite can be seen (1) and (2); oil-immersion (GD2 at 75.65m).
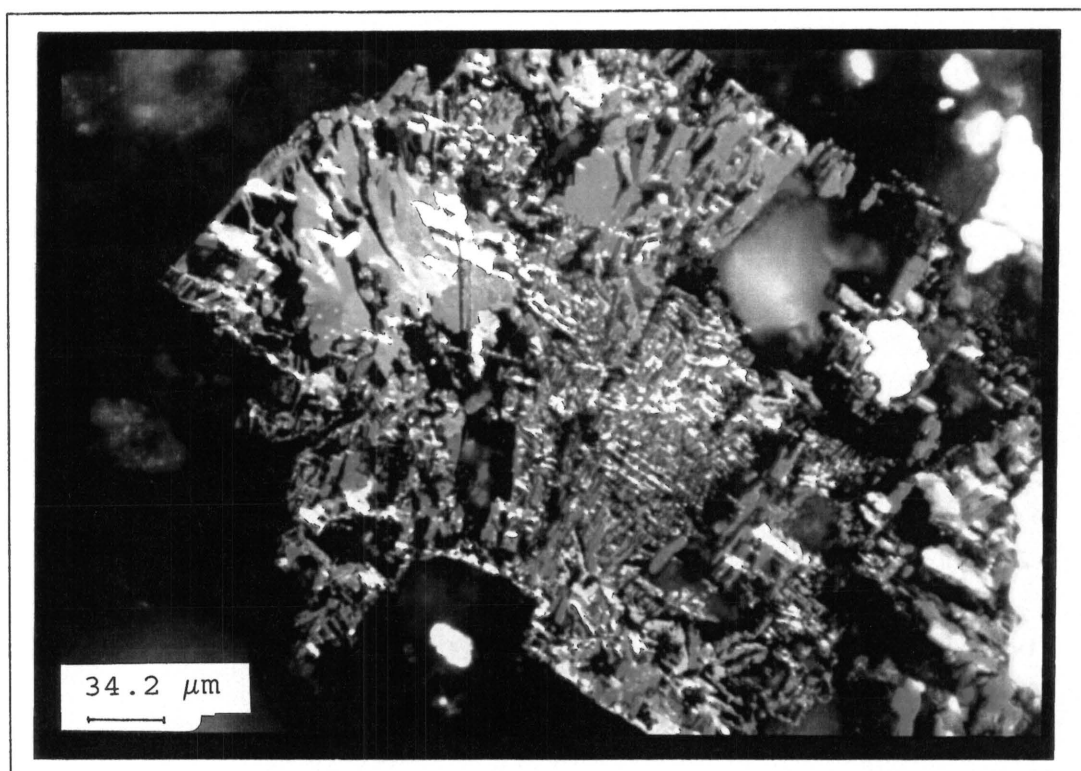
Fig. 6.24: Covellite grain, with strong anisotropism; oil-immersion (GD2 at 32.10m).
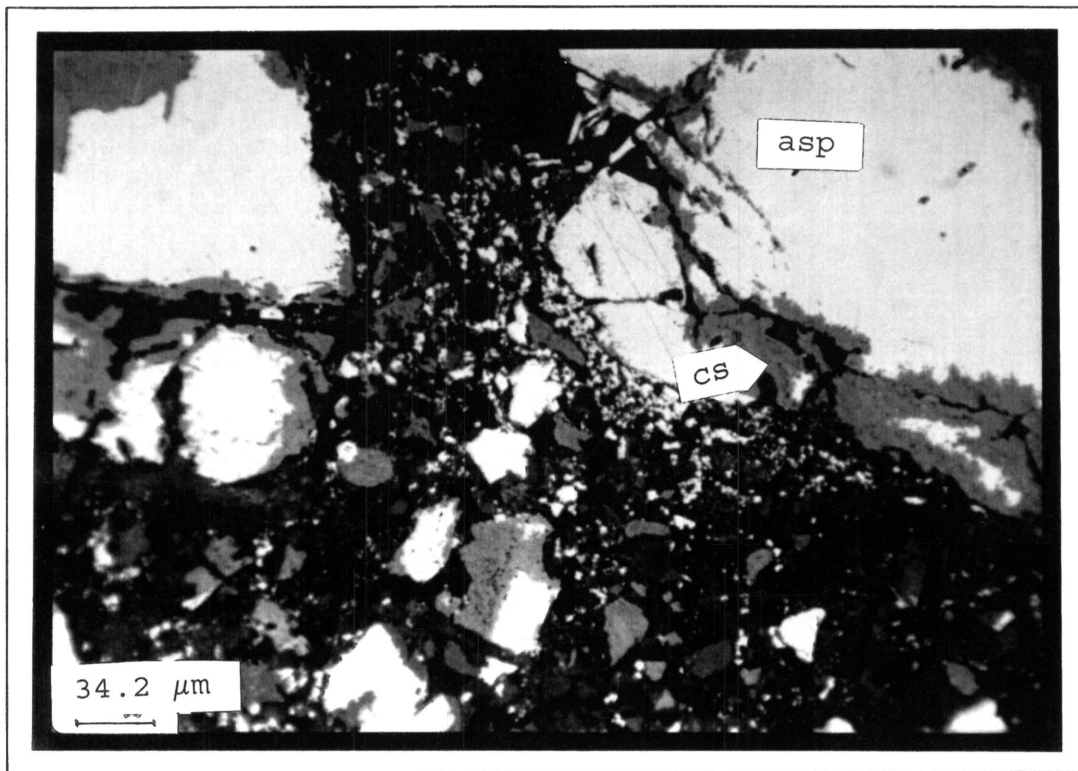
Fig. 6.25: Copper-sulphides(cs) replacing arsenopyrite(asp) along the rims and cracks; in oil (GD1 at 46.85m).
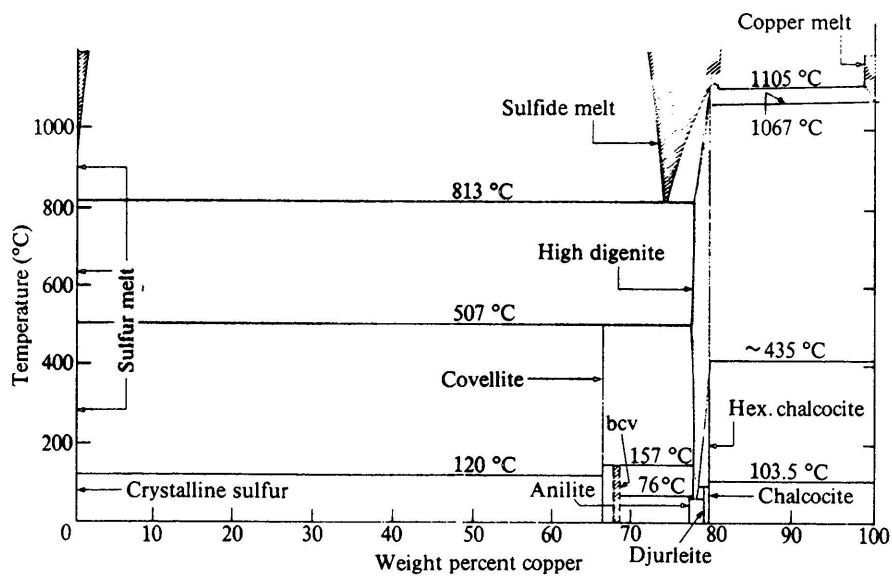
Fig.6.26: Temperature-composition diagram of condensed phases in the Cu - S system (after Roseboom, 1966).
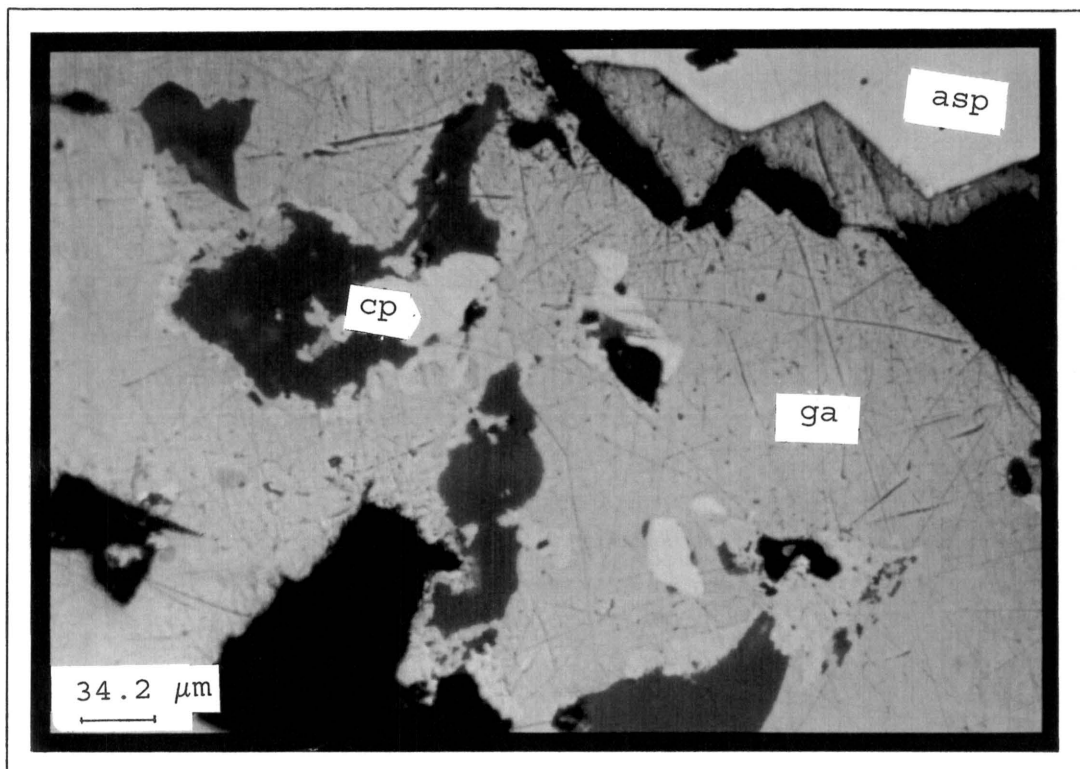
Fig. 6.27: Galena(ga) between arsenopyrite(asp) grains together with chalcopyrite(cp); oil-immersion with a blue filter (GD1 at 25.30m).
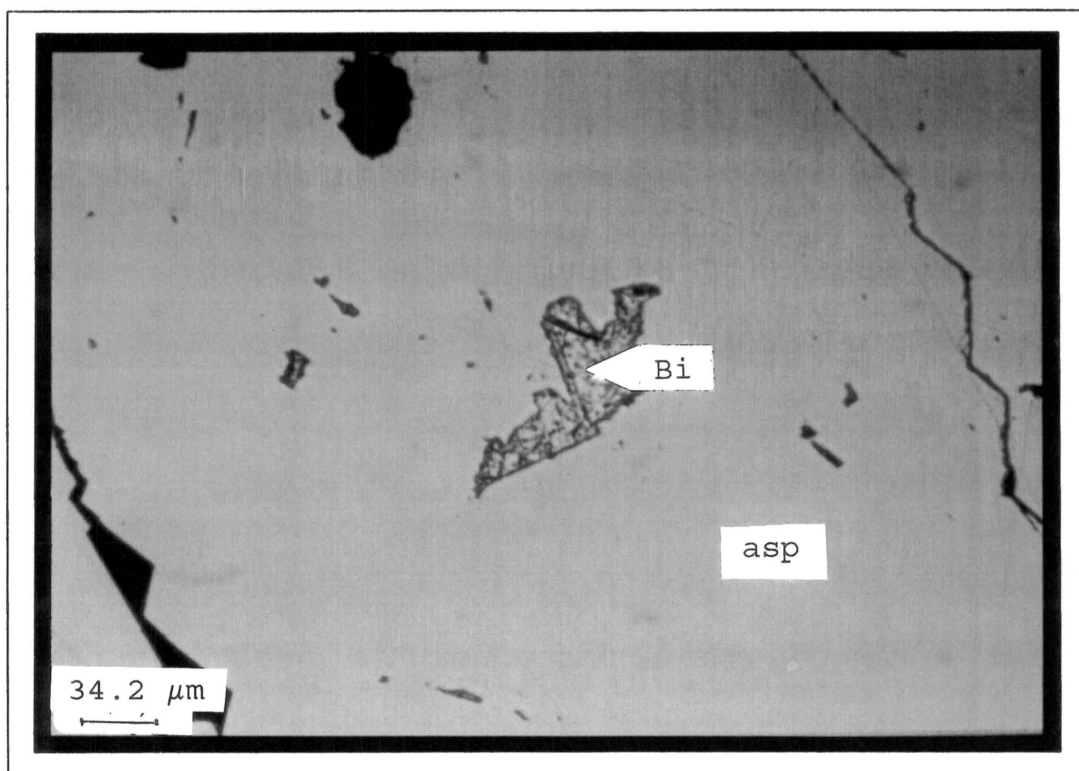
Fig. 6.28: Native bismuth(Bi) as inclusion in arsenopyrite(asp); oil-immersion with a blue filter (GD1 at 25.30m).

Chapter 7

Properties of the fluid inclusions

7.1 INTRODUCTION

Fluid inclusion studies proved to be a valuable tool in the understanding of ore transport and deposition in hydrothermal systems (Roedder, 1979; Spooner, 1981) as well as other petrogenetic processes. Minerals most favourable for observation of fluid inclusions are the transparent minerals e.g. quartz, fluorite, halite and calcite. The strong cleavage of the carbonate and halide minerals can cause leakage of the fluids during cooling; therefore quartz is more often used. Opaque minerals, like sphalerite and galena, can only be studied with the aid of a special infra-red microscope (Calas et al., 1976). For this study only fluid inclusions in quartz were investigated.

To be able to use fluid inclusions and the information derived from them, it is generally assumed that at least some of the inclusions are primary (P) and that these P-inclusions are truly representative of the fluids present during primary crystal growth. It must also be assumed that the inclusions studied behaved as closed systems since trapping (Shepherd et al., 1985), meaning that none of the contents leaked after trapping. Secondary (S) and pseudo-secondary (PS) fluid inclusions are an indication that the rock has been subjected to alteration.

Geologically, fluid inclusions (1) help to estimate the composition of the fluids present during crystallisation of minerals; (2) predict whether the determined pressure-temperature (PT) state of the fluid favours ore deposition (e.g. when and if the fluids boiled) (Shepherd et al., 1985); (3) aid to determine patterns of fluid flow, (i.e. to outline areas where fluid activity has been most pronounced); and (4) aid in mineral exploration (e.g. to "fingerprint" certain types of ore-forming fluids, to characterise particular ore mineral assemblages and to define areas where these fluids are most likely to concentrate). To answer any of these questions will already be a significant accomplishment. To assist in this

quest, different techniques can be used to determine the
composition of the inclusion fluid and the possible PT
conditions.

7.2 DETERMINATION OF CHEMICAL COMPOSITION

To estimate the general chemical composition of the inclusion is
problematic but to determine the exact composition is almost
impossible without the utilisation of highly specialised
analytical equipment. The most common quantitative technique
used is the crush-leach method, whereby the sample is crushed
under water and the resulting solution, containing the soluble
inclusion contents in diluted form, is chemically analysed
(Roedder, 1972; Poty et al., 1974). The foremost problems with
this technique are contamination during preparation and
disregard of the types of inclusions. Therefore, a technique
where individual inclusions can be measured separately will be
much more meaningful. Raman spectroscopy is such a technique,
but is restricted to polyatomic species (e.g. SO_4^{2-}, CO_2 and NaCl)
only. It will not give a quantitative indication on the
chemical composition of the inclusion, because mono-atomic ions
in aqueous solution (e.g. Na^+, Cl^-) cannot be measured.

A method, neither well known nor generally used, is the
technique of decrepitation, whereby an inclusion is heated under
vacuum until it bursts. After the contents of the inclusion
have been released it is cooled down rapidly to ensure
crystallisation of the fluid phase(s) on the surface of the
sample. While the sample is kept under vacuum, the composition
of the newly formed crystals on the surface are determined by an
electron microprobe (Haynes et al., 1988; Samson et al., 1995).
This technique is, however, unable to give a quantitative
account of all the components in the inclusion due to the fact
that certain complexes will evaporate at such high temperatures.

Therefore, with restricted time and equipment, most researchers
have to be satisfied with a mere estimation of the composition
of the inclusions. In hydrothermal systems, minerals that
formed at high temperatures are commonly characterised by two-
phase (vapour + liquid) inclusions. These tiny vapour bubbles
(which formed due to thermal contraction of fluid during
cooling) are used in estimating the salinity of the inclusion
fluid.

Double-polished sections (wafers) of a transparent mineral (e.g. quartz) are prepared and first studied microscopically to identify the areas with inclusions to be analysed. The section is then placed on a heating-freezing stage attached to an optical microscope. While watching the inclusion closely, the temperature is slowly lowered (below 0°C), until the content of the inclusion has solidified. Sometimes this temperature is indicated by the disappearance or contraction of the vapour bubble. The temperature at which the inclusion-liquid finally freezes does not provide a reliable estimate of composition. The degree of supercooling (i.e. the actual temperature of solidification below the temperature of freezing) is strongly dependent on the presence or absence of sites for the nucleation of crystals (Shepherd et al., 1985). Interestingly, nucleation is triggered during slow heating and the contents of the inclusion freeze instantaneously. On continued heating the contents melt again, until the slowly appearing vapour bubble has grown to its original size. This is an indication that melting is completed, and is recorded as the melting temperature (T_m).

Conventionally, ice melting temperatures (T_m) are reported as "weight % NaCl equivalents", but other salts (e.g. KCl, $MgCl_2$ and $CaCl_2$) are likely to contribute to the salt content as well. The higher the salt content, the lower T_m, and the closer T_m to 0°C, the lower the salt content (i.e. the purer the aqueous solution) (Shepherd et al., 1985). **Figure 7.1** shows the depression of the freezing point of pure water as a function of the wt% salt in solution.

7.3 DETERMINATION OF TEMPERATURE OF FORMATION

The potential to use inclusions as geothermometers lies in the fact that the higher the proportion of vapour, the higher the trapping temperature (T_t). The trapping temperature is defined as the temperature at which a specific host mineral formed and entrapped the present fluid phase(s).

The most commonly used method to determine the temperature at which a mineral, or mineral association, formed, is the technique of heating the inclusion. The wafer is placed on a heating-freezing stage, attached to an optical microscope. The

stage is heated and the temperature at which the vapour bubble disappears is referred to as the temperature of homogenisation (T_h). Normally this temperature is preceded by a stage where the vapour bubble starts to move around vigorously and is slowly shrinking until it completely disappears. T_h is rarely equivalent to the temperature at which the inclusion was entrapped during crystal growth (T_t). The difference between T_h and T_t is a function of pressure and density of the fluid and is generally compensated for by a "pressure correction" (Shepherd et al., 1985).
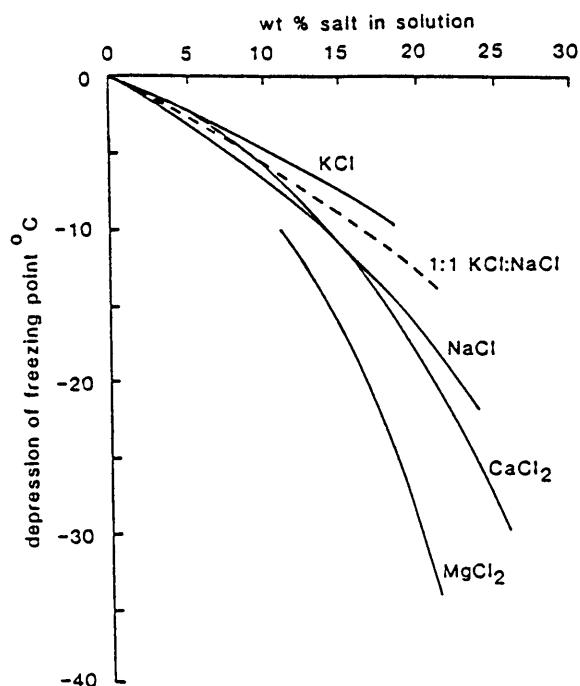
Figure 7.1: Depression of the freezing point of pure water as a function of the wt% salt in solution for NaCl, KCl, CaCl$_2$ and MgCl$_2$ (from Shepherd et al., 1985).

On a temperature-pressure diagram like **Figure 7.2**, the cooling path which individual inclusions will follow since trapping are defined by lines of constant density or "isochores" (of which the slope is a function of density). T_t is normally in the "liquid only"- field and by lowering the temperature the internal pressure will decrease and the inclusion reaches the boiling curve where a "gas" phase can coexist with a fluid. T_h is measured at the intersection of the relevant isochore and the boiling curve. The three unknowns are T_h, T_t and P: T_h is measured on the heating stage and pressure or depth is estimated using geological or geobarometer information, T_t is then read from the diagram. The "pressure correction" is, therefore, the

83

temperature difference (based on P) added to T_h to represent the true temperature of formation.
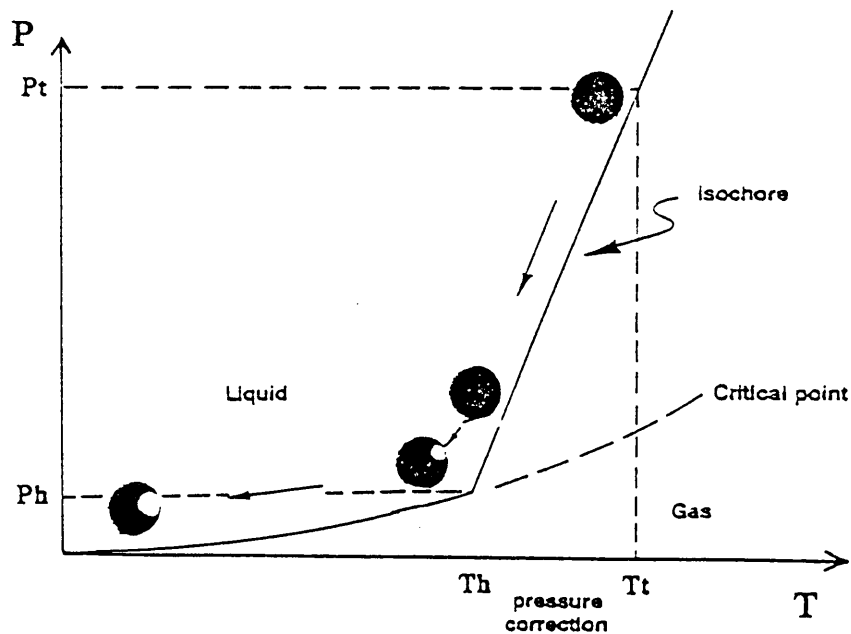
Figure 7.2: Behaviour of an initially homogeneous and closed isovolumic fluid inclusion upon cooling from trapping temperature (T_t) to room temperature. In such a system, the overall density is constant, and the internal P and T are unequivocally related. Upon reheating in the laboratory, the inclusion follows the reverse path, so that $T_h < T_t$ (after Pecher, 1984).

A third temperature that can be measured is the temperature of decrepitation (T_d). This is the temperature at which the inclusion will burst on heating. Parilov et al. (1990) showed through an experimental study that at low pressures, not only T_h, but also T_d can be used for thermometric investigations. They found that for salt concentrations of 10-80 wt%, and pressures of 20 - 60 MPa, the temperature of mineralization using the homogenisation method, is estimated at most 10-15 % too low, and the decrepitation method, the temperature determined can be at most 105°C too high or too low (Parilov et al., 1990). The method of vacuum decrepitation can be used on a broad range of minerals, including sulphides.

84

7.4 RESULTS AND DISCUSSION

Generally three groups of inclusions could be identified (**Fig. 7.3**): those with a very low T_m between $-20°$ and $-30°C$ (i.e. 18-29 eq. wt% NaCl); inclusions with T_m between $-10°$ and $-20°C$ (i.e. 6-16 eq. wt% NaCl); and the last group which have melting temperatures close to $0°$ C (i.e. 0-4 eq. wt% NaCl). Unfortunately, inclusions which appear to be primary do not fall exclusively into any particular group.
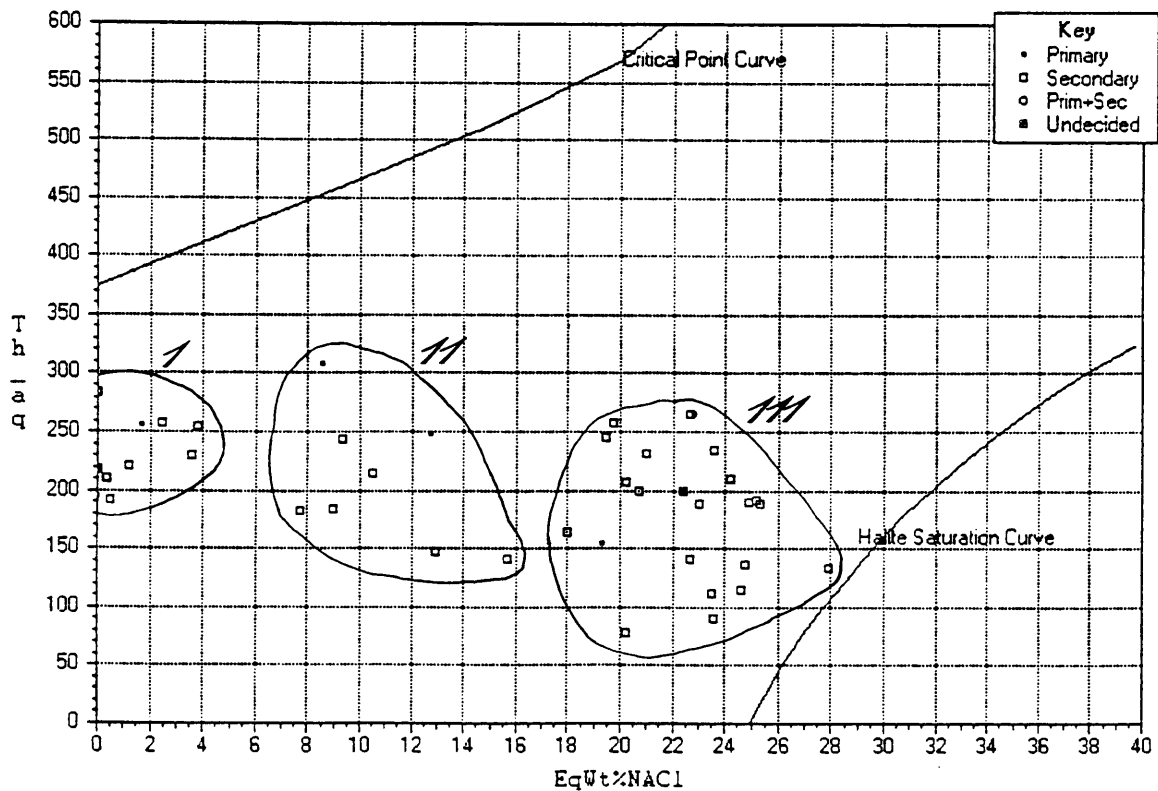
Figure 7.3: A plot of salinity (eq. wt% NaCl) and homogenisation temperature (T_h) in $°C$. Three groups of inclusions can be identified: Group I with a generally low salinity, group II of intermediate salinities and a wide range of temperatures, and group III that has a much higher average salinity and a trend towards lower temperatures.

85

If it is assumed that the group II inclusions contain the original fluid responsible for formation of the mineral assemblages in the veins, two trends can be interpreted. Group I inclusions show a direct decrease in salinity that may indicate mixing with a less saline fluid (possibly groundwater). The group III inclusions can be interpreted as the result of boiling and slight cooling (Shepherd et al., 1985) of the original fluid. The drop in temperature can be explained by adiabatic cooling during boiling, whereas physical separation of the liquid and vapour during boiling results in a liquid trend towards higher salinities. However, Shepherd et al. (1985) cautioned that this trend can only be interpreted as boiling if "it can be shown that (1) there are vapour inclusions which homogenise into the vapour state (L + V -> V) over the same temperature range as the liquid inclusions, and if (2) the inclusions were trapped simultaneously." Homogenisation of the inclusion into the vapour phase cannot always be observed, and such an inclusion can be unnoticeably small and therefore cannot being analysed.

If adiabatic boiling did indeed take place during the ascent of the hydrothermal fluid, it will have a pronounced effect on the deposition of precious (i.e. gold and silver) and base metals. The mechanisms active during transport and deposition of precious and base metals will be discussed in **Chapter 8**. At this stage it can be mentioned that the transport form, most likely to have been responsible for the mobilisation and movement of some of these metals, was HS^- complexes. During boiling, these complexes became unstable and this resulted in the deposition of mainly sulphides with lesser gold in the veins.

The salinities of the group II inclusions appear to fall within the salinity range for epithermal vein deposits containing base metal sulphides (Sillitoe, 1977; Buchanan, 1981), which have apparent fluid inclusion salinities ranging from 0.1 to over 13 eq. wt % NaCl. For inclusions from precious metal vein deposits, apparent salinities range from 0 to 3 eq. wt% NaCl and average less than 1.5 eq. wt% NaCl according to Hedenquist and Henley (1985). The experiments of Wood (1987) imply that a salinity of 3 eq. wt% NaCl is most favourable to mobilise gold from source rocks while leaving base metals behind. Therefore, it can be deduced that the fluid responsible for the transport

of metal-complexes had a salinity between 6 and 13 eq. wt% NaCl (Group II), and even after mixing with cooler, less saline ground water, was still able to transport certain metals (like gold).

On heating, temperatures of homogenisation (T_h) varied over a wide range of relatively low values (~100° - 300° C). The T_h represents only the minimum possible temperature at which an inclusion was enclosed. If a depth of roughly 1000m is assumed, the pressure correction will be between 50° - 100°C. This means that the temperature of formation (T_t) of the inclusion (and accordingly the mineral assemblages in the veins) will be generally 50° - 100°C higher than T_h (i.e. 150 - 380°C). The temperatures of homogenisation (T_h) (**Fig. 7.4**) do not fall into well defined classes. Most of the T_h's fall between 200° and 300°C and the rest are lower than 200°C. If the pressure correction is taken into account (that is estimated at 1000 bars for this layer in the Rooiberg Felsites) the temperature of trapping will be almost 50° - 100°C higher, depending on the density of the fluid (i.e. slope of the isochore). Therefore, the temperature of formation (of at least the quartz in the veins) ranges between 150° and 380°C (**Fig. 7.5**). This temperature interval overlaps with the temperatures obtained from the chlorite geothermometer (315° - 360°C). The lower (<250°C) temperatures probably represent a stage of alteration by a later, cooler fluid with different physico-chemical conditions. In the sulphide mineralogy there is clear evidence of the presence of later (cooler) fluids that circulated through the same vein system.

Therefore, although fluid inclusion studies do not unambiguously unravel the history of fluids responsible for a hydrothermal deposit, they do provide information that may be valuable in formulating a model. In this study it became clear that the original fluid most probably underwent boiling but also mixed with a cooler, less saline fluid. The temperatures at which this system operated varies between 100° and 350°C, and represents various stages of hydrothermal activity.
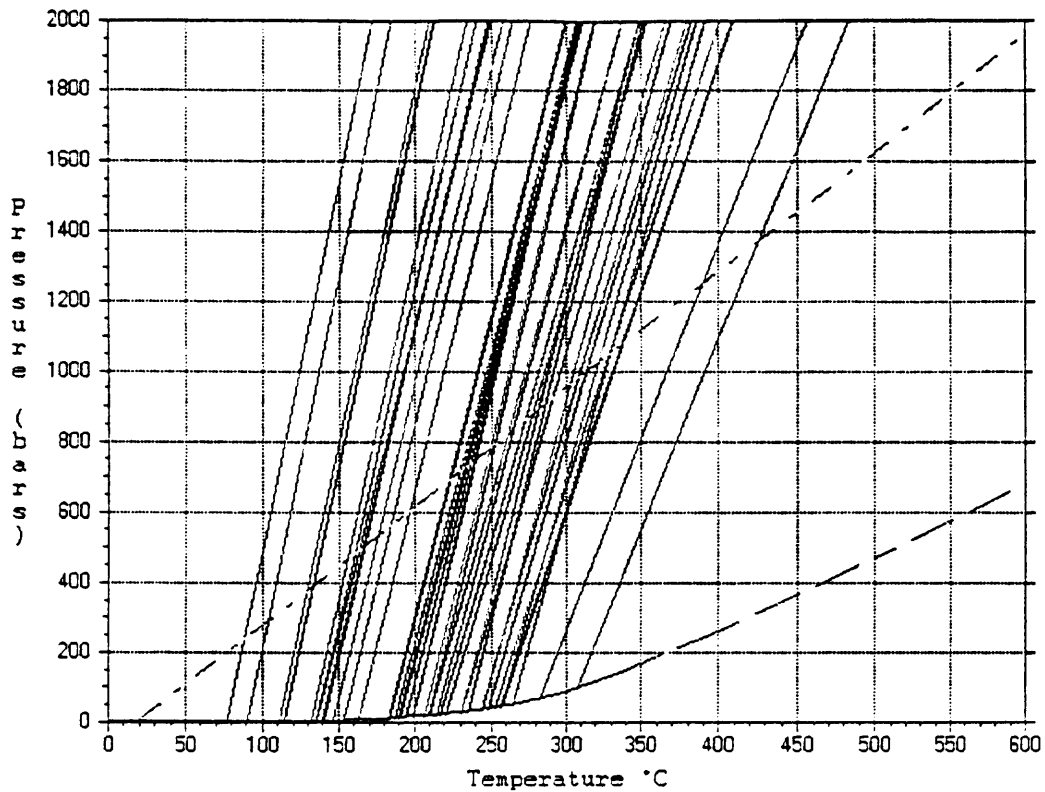
Figure 7.4: Isochore diagram showing the lines of equal density for the inclusions analysed in this study. A pressure of 1000 bars is taken as the possible pressure of formation and subsequent entrapment of fluid inclusions. This implies that the temperature of trapping (T_t) will be the temperatures where the isochore cuts the 1000 bars line. (The curved line is the liquid-vapour curve and the straight line indicates the geothermal gradient.)
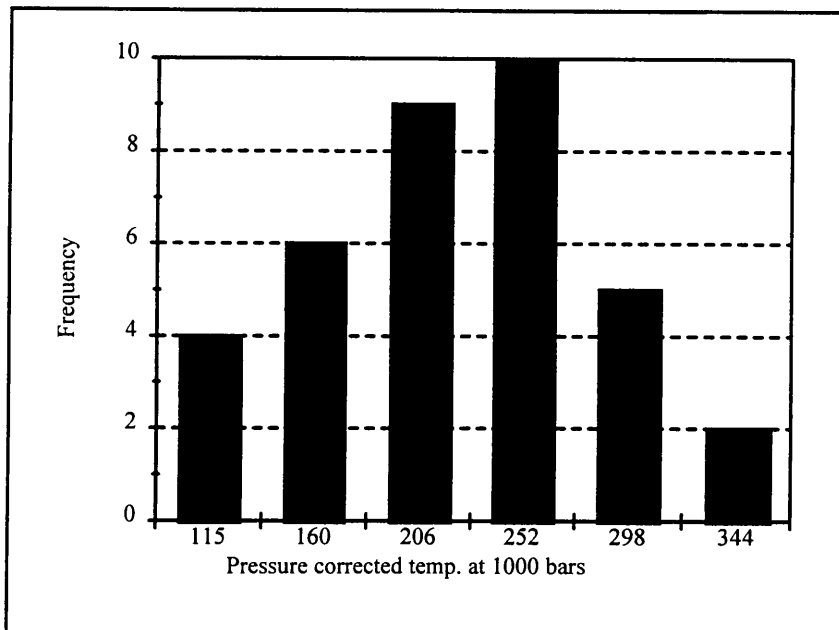
Figure 7.5: Histogram of the pressure corrected temperatures in the fluid inclusion (The values indicate the middle point of each class).

88

The hydrothermal system

8.1 ACQUISITION AND TRANSPORT OF ORE-FORMING ELEMENTS

Although a number of inter-related parameters influence the character and size of an ore deposit, two of the more important parameters are the source of the ore-forming components (i.e. metals and ligands) and the origin of the ore-forming fluid.

Hemley and Hunt (1992) classify the acquisition of ore-forming elements by a hydrothermal fluid in three groups: (a) The first is the process of acid volatile and exotic element enrichment in magma, resulting from crystal fractionation and/or other differentiation processes, followed by separation of an aqueous phase and its partitioned constituents. (b) The second process is the dissolution of minerals; and (c) thirdly the leaching of trace elements from unmineralised source- or host rocks at a late magmatic and post-solidification stage.

It is generally agreed on that metals are leached by the solution from the rocks of the hydrothermal system, but the country rocks through which this fluid migrates determine to a great extent the element concentrations and complexes in solution, as well as the leaching properties of the fluid. The source of the sulphur may be the same as that of the metals or may be derived by the organic or inorganic reduction from seawater sulphate (Franklin et al., 1981).

Sources for hydrothermal fluids include seawater or groundwater, juvenile or modified magmatic water, or metamorphic fluids evolved during the devolatalisation of buried sequences (Barnes, 1979). Through the years, careful case studies and experimental work established in a broad sense the signatures of these types of hydrothermal fluids. Skinner (1979), for example, concluded that modern near-surface ore forming fluids (e.g. groundwater and seawater) are commonly brines. Acid sulphate-chloride waters can be attributed to magmatic processes (White, 1975), whereas metamorphic rocks (Crawford, 1981; Roedder, 1984), epithermal (Henley, 1985) and Archean gold deposits (Kerrich and

Fryer, 1981) are typically CO_2-enriched. Mixing and dilution of the original ore-forming fluid is likely to have taken place during its ascent; however, with the use of light stable isotope ratios (e.g. $^2H/^1H$ and $^{18}O/^{16}O$) it can be estimated what the origin (and history) of the fluid was.

8.1.1 Gold and base metal complexing:

The complexing ability of a hydrothermal fluid strongly depends on its physical and chemical properties. For this reason it is important to know what the different "transporting agents" for precious and base metals are, and to understand under which conditions they will operate optimally.

In view of the high ionisation energy of Au and the very low stability of hydrated gold, gold-complexing ligands are necessary to transport dissolved gold in solution (Phillips and Groves, 1983). Two ionic forms (Au^+ and Au^{3+}) are common in nature, but at the relatively high temperatures and low oxygen fugacities in the geochemical environment, the solubility of Au^+ is negligible (Seward, 1976). Monovalent gold has a strong tendency to form linear, two-co-ordinated complexes (Puddephatt, 1978) and this together with its soft base character (Ahrland et al., 1958) are properties that affect its transport in solution. Ligands of potential importance in the complexing of Au^+ in natural hydrothermal fluids are listed in **Table 8.1.**

Table 8.1: Ligands of potential importance in the complexing of gold(I) in natural hydrothermal fluids (from Seward, 1991).

Increasing Stability →

Cl^-	Br^-	I^-		
HS^-	S^{2-}	Sn^{2-}	$S_2O_3^{2-}$	SnO_6^{2-}
$As_3S_6^{3-}$	$Sb_3S_6^{3-}$	Te_2^{2-}		
NH_3	OH^-			
CN^-	SCN^-			

The stability of the simple tri-atomic gold-halogen complexes (e.g. $AuCl_2^-$) increase in the sequence: $Cl^- < Br^- < I^-$. Seward (1991) calculated that the AuI_2^- complex is about ten orders of magnitude more stable than the $AuCl_2^-$ complex. However, due to the small concentration of I^- in hydrothermal systems, this type

90

of complexing will not transport ore-forming amounts of gold in solution. In saline hydrothermal systems, Cl^- will be the common transport agent for gold (and base metals) according to the reaction (Seward, 1991):

$$Au° + 2Cl^- + H^+ = AuCl_2^- + \tfrac{1}{2}H_2(g) \dots\dots\dots\dots(8.1)$$
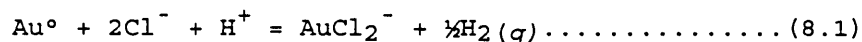
On the other hand, the ligands that play a fundamental role in the transport and deposition of gold by most hydrothermal fluids are the hydrosulphide complexes, HS^-, $(HS)_2^-$ and $(HS)_4^-$ (Seward, 1973). These are present in appreciable concentrations in ore-forming fluids as reduced sulphur, and will complex with gold according to the reaction (Seward, 1991):

$$Au° + H_2S_{(aq)} + HS^- = Au(HS)_2^- + \tfrac{1}{2}H_2(g) \dots\dots\dots(8.2)$$
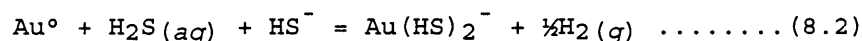
Large polarisable ligands (soft bases), such as HS^- tend to form complexes selectively with large, weakly charged cations (soft acids) of which Au^+ is one of the best examples (Ahrland et al., 1958). From their size and charge characteristics, Ag, Cu and other base metals might be expected to show weaker soft base features than Au^+ (Pearson, 1963). Crerar et al. (1985) predicted that the Cu^+ ion may prefer bisulphide complexing, whereas the Cu^{2+} ion may prefer chloride complexing. Other elements that form soft acids include As, Sb and Hg (Crerar et al., 1985).

Kerrich and Fryer (1981) found that in massive base metal sulphide deposits, Cu, Pb, Zn, Ag, and Au are all enriched by similar amounts relative to their crustal abundances, suggesting a common form of transport, probably as chloride complexes. Except at low fluid/rock ratios, at which relative metal solubilities may be important (Kerrich and Fryer, 1981), chloride (being a hard base) would be unselective in its metal complexing, and metal concentration in solution would broadly reflect source abundances.

In contrast to most metals (e.g. Fe, Pb, and Zn) which form chloride complexes, As concentration in a fluid is not

correlated with that of chloride. Aqueous As species occur predominantly in two oxidation states, As^{3+} and As^{5+}. Although As^{3+} and As^{5+} both occur in hot spring fluids, As^{3+} predominates in springs related to reservoir fluids, whereas As^{5+} dominates in acid sulphate and bicarbonate springs. The concentrations of As in geothermal fluids range from less than 0.1 to nearly 50 ppm (Ballantyne and Moore, 1988). Yokoyama and co-workers (1993) found that arsenic was mostly present as As^{3+} in geothermal waters directly discharged from geothermal wells, but the geothermal samples have be acidified to a pH of 2 immediately after sampling to prevent oxidation to As^{5+}. Therefore, a low pH will stabilise As^{3+}. Criaud and Fouillac (1989) confirmed that fluids directly related to hydrothermal systems contain mainly As^{3+}, whereas acid sulphate springs have a variable As^{3+} content. Bicarbonate waters are generally enriched in oxidised As. In their discussion on arsenic in geothermal systems, Ballantyne and Moore (1988) stated that the As content of the reservoir fluids varies inversely with P_{H2S} and directly with temperature.

Most base metals will be transported as Cl^- complexes, but it is generally accepted that gold transportation as a chlorine complex will be favoured at high temperatures (> 300°C), whereas the $Au(HS)_2^-$ complex is more common in lower temperature fluids (150°-300°C) (Large et al., 1989). These temperatures are, however, dependent on very specific pH, salinities, and f_{O2}. For example, Large and co-workers (1989) estimated that the switchover from $AuCl_2^-$ transport to $Au(HS)_2^-$ will be at 290°C for a pH of 4 (**Fig. 8.1**) but drop to 272°C for a pH of 3.5. **Figure 8.2** shows the effect of salinity on the solubility of $Au(HS)_2^-$ and $AuCl_2^-$ complexes, at a fixed temperature.

According to Pearson's rule (1963), in a competitive situation, the soft acids bind preferentially with soft bases, and hard acids with hard bases. From this it can be derived that HS^- and H_2S form strong complexes with Au, Ag and Cu and weaker complexes with Fe. On the other hand, the Cl^- base form stronger complexes with Fe, Pb and Zn. Crerar et al. (1985) argued that Pearson's rule is only valid for temperatures to at least 200° C and if there are large differences in hardness/softness. Seward (1981) pointed out that at higher temperatures, all metal-ligand interactions become harder.
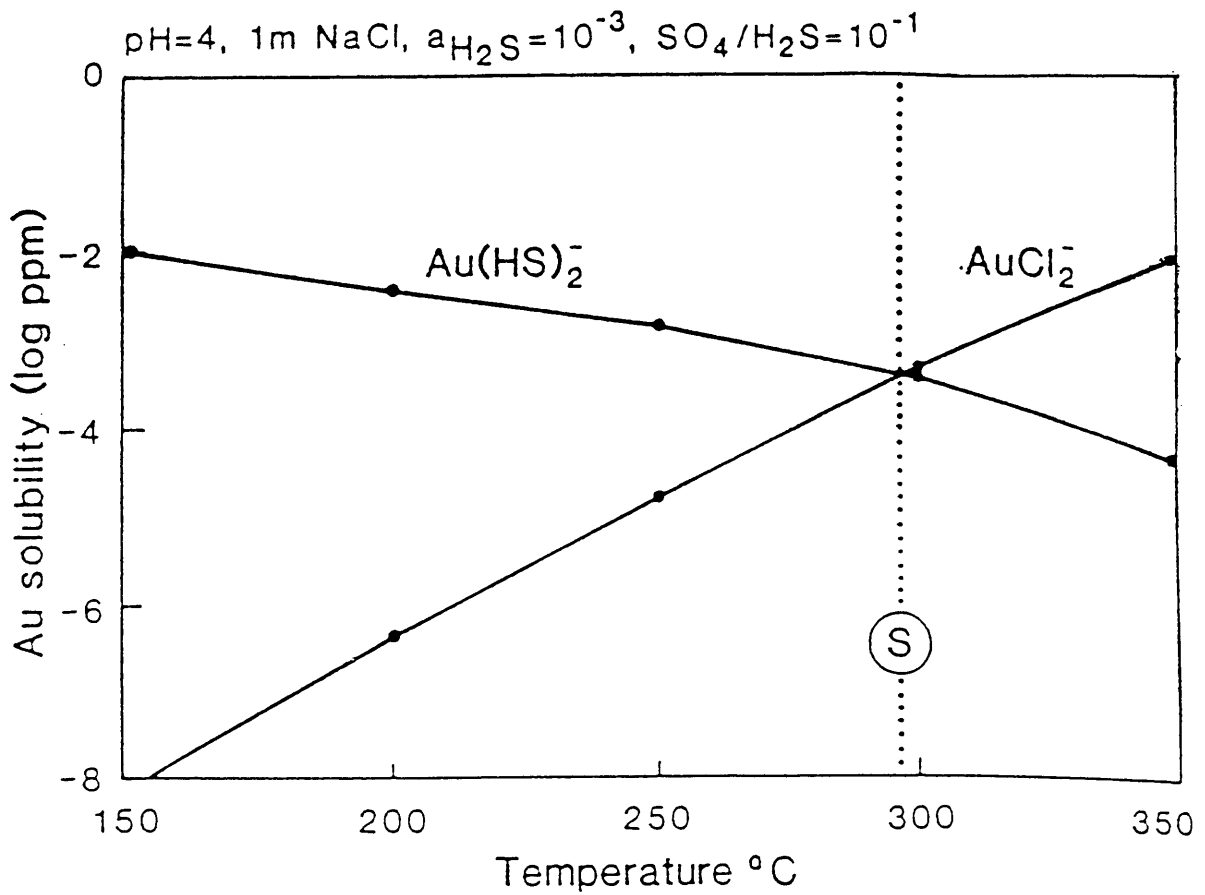
Figure 8.1: The predominant form of transport for gold: thio-complex and chloro-complex. Under these conditions the switchover line (S) is at 290°C, with the $AuCl_2^-$ complex more stable above 290°C (from Large et al., 1989).
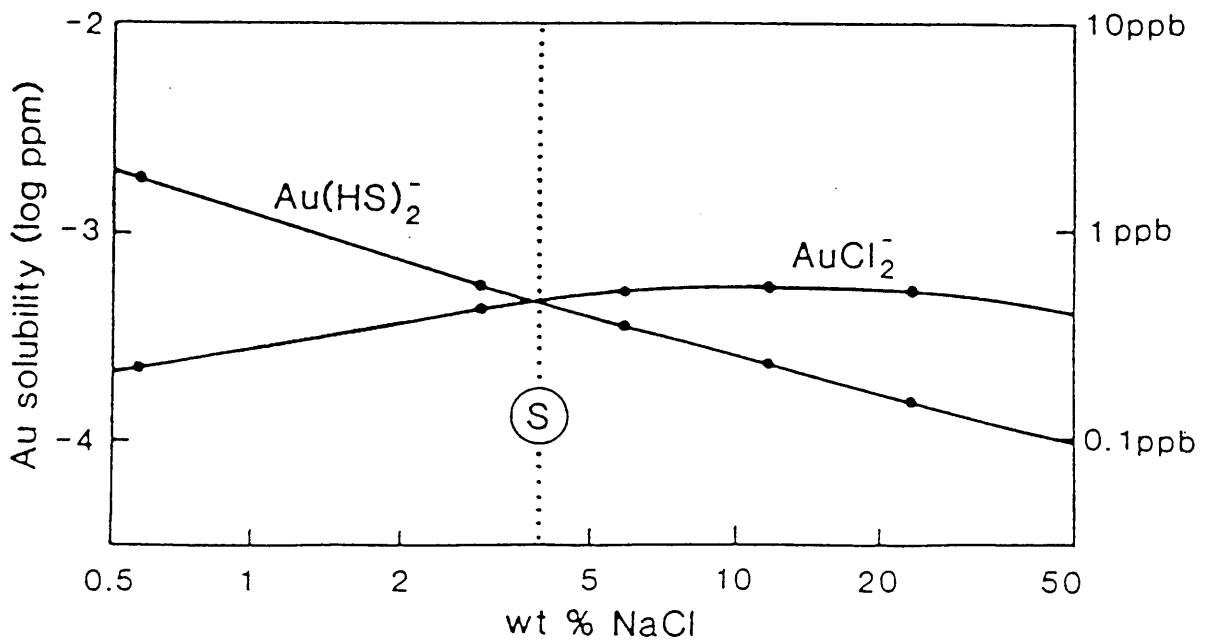
Figure 8.2: The effect of salinity on the solubility of the $Au(HS)_2^-$ and $AuCl_2^-$ complex for pH = 4, log $a(H_2S)$ = -3, and T = 300°C (from Large et al., 1989).

Therefore, the two important transporting ions of gold in hydrothermal systems are Cl⁻ and HS⁻. Generally, most of the base metals tend to form Cl⁻ complexes, although some of them may be transported as HS⁻ complexes under low salinity, sulphide-rich conditions (**Table 8.2**). The further discussion of gold and base metals in solution assumes one of these complexes to be the major transporting agent.

Table 8.2: Summary of principal dissolution reactions for metals (and metal sulphides) tabulated in decreasing order of affinity for bisulphide ligand (from Hemley, 1990)

HS^-

$Au + 2H_2S = Au(HS)_2^- + H^+ + \tfrac{1}{2}H_2$

Ag

Cu

$PbS + 2H^+ + 2Cl^- = PbCl_2 + H_2S$

Zn

Cl^-
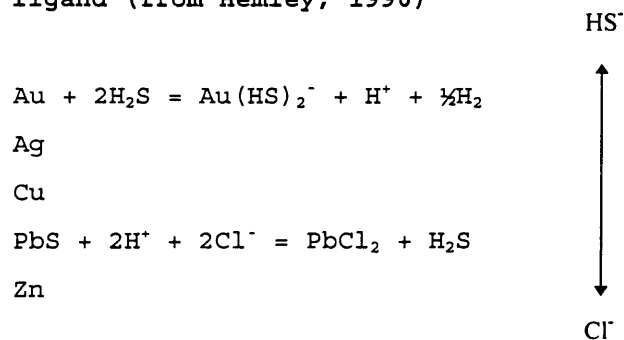
8.1.2 Fluid properties:

The physico-chemical properties at each stage during ascent of the hydrothermal fluid are of utmost importance when gold and metal complexing are discussed. Properties like temperature, pH, salinity, f_{O2}, f_{S2} and CO_2-content tend to change continuously and affect each other strongly. Many of these changes are strongly influenced by the properties of the country rocks through which the fluid migrates at that stage. When the history of migration of the fluid is studied, each change in physico-chemical property is normally characterised by the precipitation or dissolution of a specific mineral, solid solution or mineral assemblage. One of these stages might lead to the precipitation of gold and/or base metals (sometimes in ore amounts).

Two conditions are of importance in ore formation: firstly the conditions under which gold and metals will be transported by the hydrothermal fluid and secondly the conditions under which deposition from this fluid will take place.

Hemley and Hunt (1992) postulated that the transport path of a hydrothermal fluid is likely to lie somewhere between an adiabatic (no heat loss to adjacent rocks) and a geothermal (complete thermal equilibration with adjacent rock) path. In such a "quasi-adiabatic" setting, the pressure effect on rock-buffered metal solubilities is significant. This effect will allow metal transport over long distances, because the trend of decreasing metal solubility with decreasing temperature is compensated by the trend of increasing metal solubility with decreasing pressure.

Large et al. (1989) summarised a list of parameters which favour high gold grades in zinc- and copper-rich zones of volcanogenic massive sulphide deposits. These two gold associations relate to different gold transport mechanisms. Gold in zinc ores is considered to be transported as the $Au(HS)_2^-$ complex at moderate temperatures (150° - 280°C), moderate pH (4.5 - 6), high a_{S2} and moderate f_{O2}. A low FeS content in sphalerite (Zn > 10 %) is characteristic. In copper ores, gold is transported as the $Au(Cl)_2^-$ complex at high temperatures (> 300°C), low pH (< 4.5), high salinity (> 5 wt% NaCl), and moderate to high f_{O2}. In these ores, copper is generally more than 2 wt%. However, Hannington and Scott (1989) cautioned that the Cu-Au association by itself is insufficient proof for chloride complexing of gold. They found enrichment of gold in pyrite-chalcopyrite assemblages at some H_2S-rich vent sites.

Low f_{O2} solutions will not be expected to transport gold, but could derive other metals from the silicates in sediments during metasomatism (Helgeson, 1967).

Salinity is a major controlling factor in Au transport. Wood (1987) showed through experimental work that gold solubilities of 5 - 500 ppb are attained in solutions between 0 and 0.5 molal NaCl. He also stated that: "it may be that only low-salinity solutions (near 0.5 at% or lower) are capable of nearly complete extraction of gold from the source rock, yet are close enough to saturation to allow for efficient precipitation at the site of deposition".

Seward (1973) demonstrated that sulphide complexes of Au^+ were of major importance in the near-neutral region of pH. Gold

solubility increases, with the stabilisation of the $Au(HS)_2^-$ complex in response to increasing pH.

According to Henley (1991), the transportation of gold as a HS^- complex is inversely related to the CO_2 concentration of the fluid. Burnham (1967) suggested that the first hydrothermal fluids to separate from a felsic magma (at total pressures generally below 2kb) can be greatly enriched in CO_2 relative to fluids separated later.

To transport base metals, on the other hand, a much higher salinity is needed. Wood (1987) demonstrated that for the formation of an economically significant massive sulphide deposit, temperatures between 200° and 350° C, pH between 4 and 6 and solutions with NaCl concentrations above 1.0 molal (5.5 wt%) are required. Thus, to transport base metals either a higher salinity or a lower pH is necessary. Boiling of seawater or evolution from a deeper magmatic source could result in a high-salinity fluid (Wood, 1987).

Seyfried and Bischoff (1981) concluded from experimental results that to achieve high concentrations of metals in solution, temperatures must be ~300°C for high water/rock ratios, and ~400°C for low water/rock ratios (< 10:1).

It is therefore apparent that the conditions under which gold and base metals will be transported most efficiently, differ in many respects. Temperatures and salinities for Cl^- complexes are generally higher than for HS^- complexes. A low pH solution will transport base metals as Cl^- complexes but not as HS^- complexes. A synthesis of all solubility and transport data leads to the conclusion that it will be unlikely for ore amounts of gold and large amounts of base metals to be transported by the same fluid.

8.2 PRECIPITATION

Different mechanisms of deposition of gold and base metals from hydrothermal systems have been suggested by various researchers (Seward, 1989; Brown, 1989; Hemley and Hunt, 1992). Virtually all mechanisms are based on changes in the physico-chemical properties of the solution during its ascent, which affect its

metal carrying capacity. Deposition of metals in hydrothermal
systems occurs where changes such as cooling, pH increase due to
rock alteration, or fluid mixing cause the aqueous metal
concentration to exceed saturation. Relative metal
solubilities, the availability of sulphur, the disposition of
the saturation surfaces relative to each other, and the
interplay of these variables through time are the major factors
controlling the pattern of metal deposition (Hemley and Hunt,
1992). The processes most commonly responsible for physico-
chemical changes are fluid mixing and boiling. Mixing usually
involves the mixing of near surface brines with magmatically
evolved acidic-sulphate-chloride waters. Boiling occurs when
the hydrostatic pressure exceeds the equilibrium-saturated
vapour pressure (Seward, 1989). Fluids with a higher gas
content, under otherwise equal conditions, will boil at a higher
hydrostatic pressure.

Helgeson and Garrels (1968) concluded that in gold-quartz veins,
temperature and not rock alteration is the controlling factor in
gold deposition. The mass ratios of gold, pyrite, and other
sulphides to quartz prove to be important criteria for
determining the importance of temperature as the controlling
mechanism for gold deposition in such gold-quartz veins
(Helgeson and Garrels, 1968). However, Seward (1989) showed
that adiabatic cooling alone cannot be responsible for large
gold deposits. On the contrary, boiling that leads to phase
separation (H_2S and CO_2 gasses partition into the liquid phase
and H_2 and CH_4 into the vapour phase) will result in the
deposition of most of the gold in solution. For example, the
stability of $Au(HS)_2^-$ will be greatly influenced by the loss of
CO_2 which cause an increase in the pH (Seward, 1989).

Brown (1989) experimentally studied the kinetics of gold
precipitation from epithermal-hydrothermal sulphide solutions,
and reached interesting conclusions concerning the solubility of
gold as a function of changes in f_{O2}, f_{S2}, pH, and pressure. A
change in the oxidation state of the fluid caused by addition of
oxygen leads to an initial increase in concentration of $Au(HS)_2^-$
in solution (this might be the result of competing kinetics of
reaction:

$$Au^\circ + H_2S_{(aq)} + HS^- = Au(HS)_2^- + \tfrac{1}{2}H_2{}_{(g)} \quad \dots\dots\dots\dots(8.2)$$
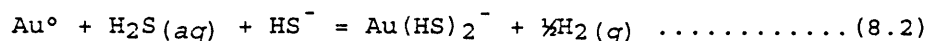
and reactions involving the oxidation of H_2S (8.3):

$$2H_2S + O_2 = 2H_2O + 2S^\circ \dots\dots\dots\dots\dots(8.3)$$
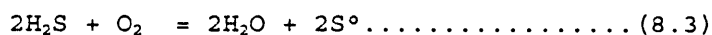
But, as H_2S is oxidised to native sulphur and sulphuric acid begins to dominate, the loss of available HS^- ligands (in combination with a pH drop) will cause gold to precipitate (Brown, 1989).

The change in the oxidation state of the fluid can be brought about by a mixing of O_2-rich surface waters with reduced geothermal waters. Boiling normally also produces more oxidising conditions by the partition of H_2 from the liquid phase into the vapour phase (Brown, 1989). Shenberger and Barnes (1989) showed that at constant pH, the maximum gold concentration is found if f_{O2} is fixed at the sulphate-sulphide equal activity boundary (**Fig. 8.3**). This coincides with the pyrite stability field and explains why gold is often found in association with pyrite.

According to Brown (1989), depressurisation is responsible for the loss of H_2 and H_2S to the vapour phase. H_2 will be volatilised more easily than H_2S and this will result in an initial rise in the gold concentration in solution. As the more soluble H_2S is slowly lost from the solution, the gold concentration falls in response to loss of the ligand (Brown, 1989). In addition to boiling, the simultaneous precipitation of metal sulphides may affect the stability of $Au(HS)_2^-$ by lowering the concentration of reduced sulphur in solution.

Generally, base metal sulphides (e.g. galena and sphalerite) will precipitate at the onset of boiling. Gold will stay in solution until the two-phase fluid encounters an environment of increased permeability which induces more extensive boiling and /or open-system gas removal (Seward, 1989). However, if the solution is transporting more base metals (implying a more saline solution), sulphide mineral precipitation accompanying boiling will accentuate the decrease in reduced sulphur concentration with a consequent deposition of small amounts of gold. In this case, gold will be associated with base metal sulphides although sulphide deposition preceded that of gold (Seward, 1989). Therefore, any processes (e.g. boiling, sulphide precipitation, dilution, sulphidisation of the wall

rocks or oxidation of sulphides) which decrease the activity of reduced sulphur in the hydrothermal ore solution will ultimately lead to gold precipitation.
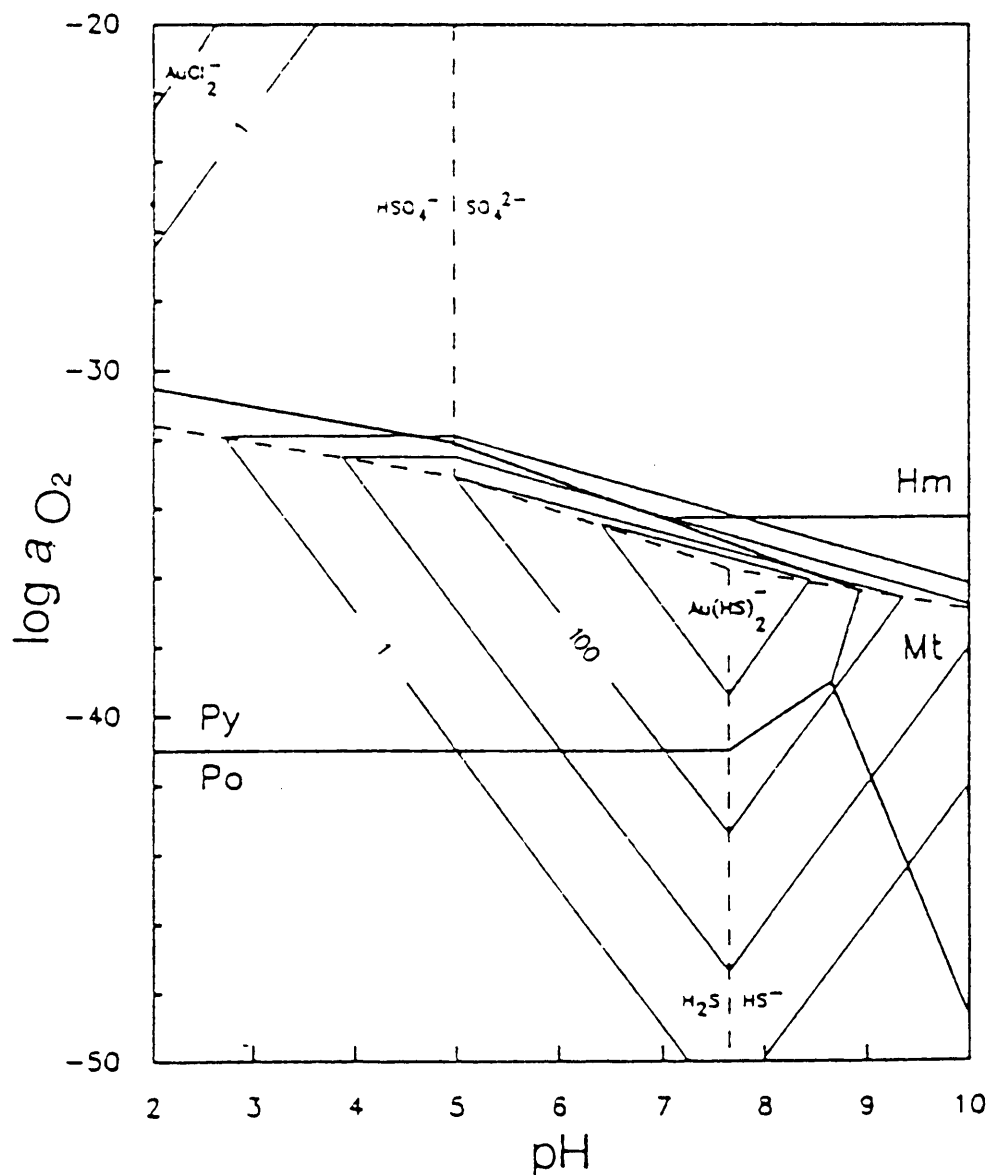
Figure 8.3: Log a_{O2} - pH diagram constructed at 250°C with total sulphur activity equal to 0.01 and total chloride activity equal to 0.1. Solubility contours for gold (light lines) are given in $\mu g/kg$ (from Shenberger and Barnes, 1989) (Py = pyrite, Po = pyrrhotite, Mt = magnetite, Hm = hematite).

An effective and fast mechanism to precipitate gold in large quantities is a rapid drop in the pH of the fluid. This can be achieved by mixing of near-surface derived acid sulphate waters and deeper derived gold-bearing geothermal waters (Brown, 1989). Paterson et al. (1989) suggested a magmatic origin for ore

forming fluids in an epithermal-mesothermal precious metal system in the Northern Black Hills (South Dakota) and argued that "the gradation in fluids from high-temperature, high-salinity to low-temperature, low-salinity suggests mixing of two end-member fluids, the former being magmatic and the latter meteoric". The mixing of a deep, hot, metal-bearing saline fluid with a shallow, cool, low-salinity fluid of meteoric origin, affected the metal-bearing ability of the fluids to transport metals. This consequently leads to the precipitation of gold.

On the other hand, Sander and Einaudi (1990) reckoned that "deposition of enough gold to form large deposits does not require an anomalous transporting fluid, such as one rich in ΣS to complex gold; the chief constraints are a sufficient volume of typical fluid and a source of gold for the fluid to dissolve". Nevertheless, at some stage in the evolution of a hydrothermal system most of these mentioned parameters will influence the circulating/ascending fluid. It will be difficult to single out any one parameter to be more important in the ore-forming process than others.

8.3 APPLICATION TO THE INVESTIGATED SYSTEM

Although a hydrothermal fluid can represent a mixture of fluids of different origins, the geological environment often allows the interpretations of one (or two) major contributors. In the case of the hydrothermal system in the Rooiberg Felsites it can be expected that ground water and magmatic water contributed to this system. The studied system occurs in the upper part of the Rooiberg succession, which implies that ground water was possibly the largest contributor to the hydrothermal fluids. A nearby granitic/acidic intrusion (e.g. Lebowa granites) could be a likely source of magmatic water. In the area of Rust de Winter a geophysical anomaly interpreted as a granite body (possibly close to the studied hydrothermal system), was found (verbal communication by Genmin exploration staff). Metamorphic fluids could account for a small proportion of the ore forming fluid, but would be difficult to identify. The possibility of seawater being present in the surrounding rocks can be ruled out, when the geological setting of the Rooiberg Group is considered.

A study of oxygen isotopes could give an indication of the relative proportions of the various fluids, but money was not available for such an investigation. The fluid inclusion study on the quartz in the veins, indicated that two types of fluids were present, a high salinity fluid as well as a very diluted fluid. These two salinities could be attributed to either two separate fluids or be the effect of boiling. The possibility of two generations of sphalerite formation, as suggested by its textural appearance, will support such an argument. A high concentration of Cl^- in the fluid (i.e. high salinity) will lead to a larger proportion of base metals to be taken in solution. On the other hand, a low salinity will enhances the formation of hydrosulphide complexes (e.g. $Au(HS)_2^-$), provided that the concentration of sulphur in the fluid or surrounding rock is sufficiently high and the pH is near neutral.

Gold is more likely to be transported as a HS^- complex, whereas most of the base metals favour Cl^- complexing. However, it has been established that gold can be transported as a chlorine complex at temperatures above $\pm$ 290°C at a specific pH (Large et al., 1989).

The pH of the fluid(s) is probably the most difficult parameter to estimate. In a broad sense, gold will be transported as the $Au(HS)_2^-$ complex under near neutral conditions, whereas the $AuCl_2^-$ complex is stable under acid conditions. Most of the base metals which will be transported as chlorine complexes will naturally also require an acidic environment. It can be expected that the pH in a hydrothermal system will not stay constant, as a result of continuous changes in the temperature and composition of the fluid. The pH is affected by the salinity and the temperature. In the fluid inclusion study an attempt was made to link the mineral type with the fluid inclusion data. Overlaps of the fluid inclusion data, temperature, and salinity will give a statistical meaningful result in separating populations, and their association with mineralisation types.

In the studied hydrothermal veins no common buffered assemblages like quartz + magnetite + fyalite or pyrite + pyrrhotite, were present. However, it can be argued that the absence of these assemblages can possibly still be used to delineate the oxygen and sulphur fugacities, although it would be strongly temperature dependent. Because pyrite is the only mineral in

the Fe-O-S system to occur in the main mineralised veins, its stability field can be used to discuss the extreme oxygen and sulphur fugacities, at temperatures indicated by microthermometry and chlorite geothermometry. The f_{S2} and f_{O2} at 200°C had to be above $1^{-13.37}$ and smaller than $1^{-34.872}$, respectively, but will change to between $1^{-6.601}$ and $1^{-2.709}$ for f_{S2} and smaller than $1^{-24.481}$ for f_{O2}, for a temperature increase to 350°C (**Fig. 8.4a & b**).

It is assumed that the precipitation of chlorite and quartz happened under the same conditions as that for the sulphide minerals. Uncertainties exist about the temperature ranges at which the system was actively precipitating base metal sulphides (and gold), because the geothermometers used in this study were applied for the silicate minerals (chlorite and quartz) in the veins. The different stages of crystallisation in the veins will be discussed in the next chapter. From the chlorite geothermometer and the microthermometery from fluid inclusions in quartz, it is implied that the temperature interval ranges from very low (~150°C) to temperatures typical for this type of mineralization (~360°C) (**Table 8.3**). Due to different complexing agents, gold can be transported at a lower temperature than the average base metal sulphide. But this does not have to indicate that the gold and base metals in the studied hydrothermal system were transported by completely different fluids at different temperatures. Gold is present in such small quantities (gold grades confidential) that it could easily have precipitated from a low concentration of $Au(HS)_2^-$ and $AuCl_2^-$ in a generally base metal dominated fluid. This argument is supported by the textural relationship of gold and arsenopyrite. Gold occurs in the arsenopyrite and therefore, implies a similar fluid and simultaneous precipitation.
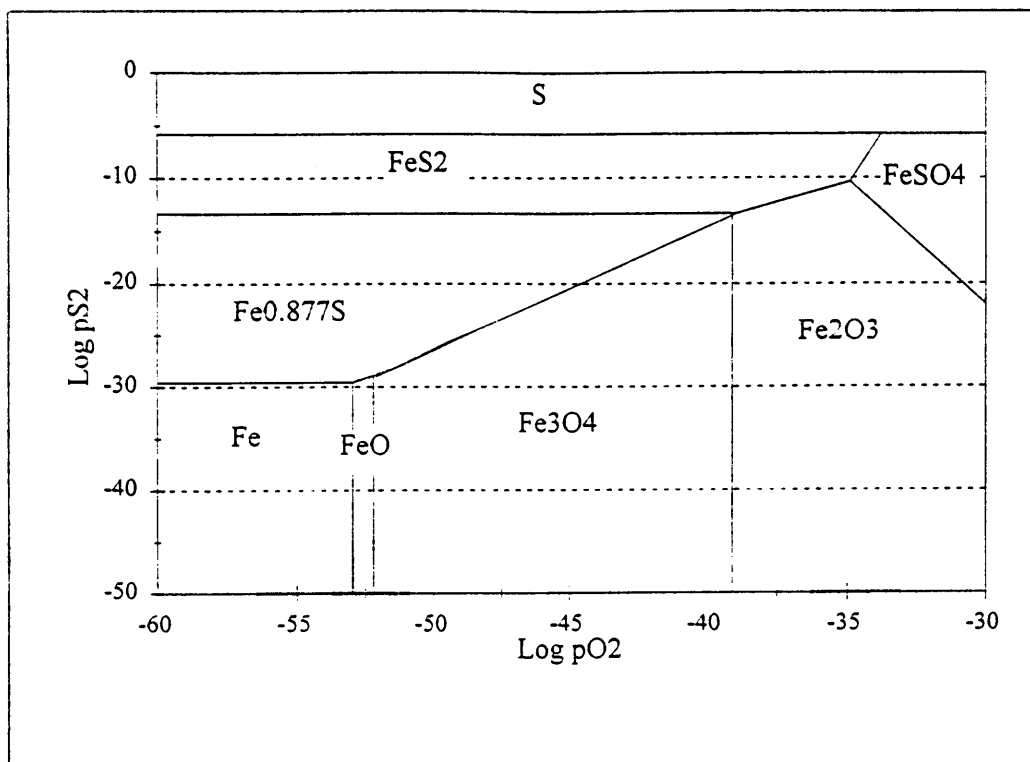
Figure 8.4a: Log $p(S_2)$-log $p(O_2)$ stability diagram for Fe at 200°C.
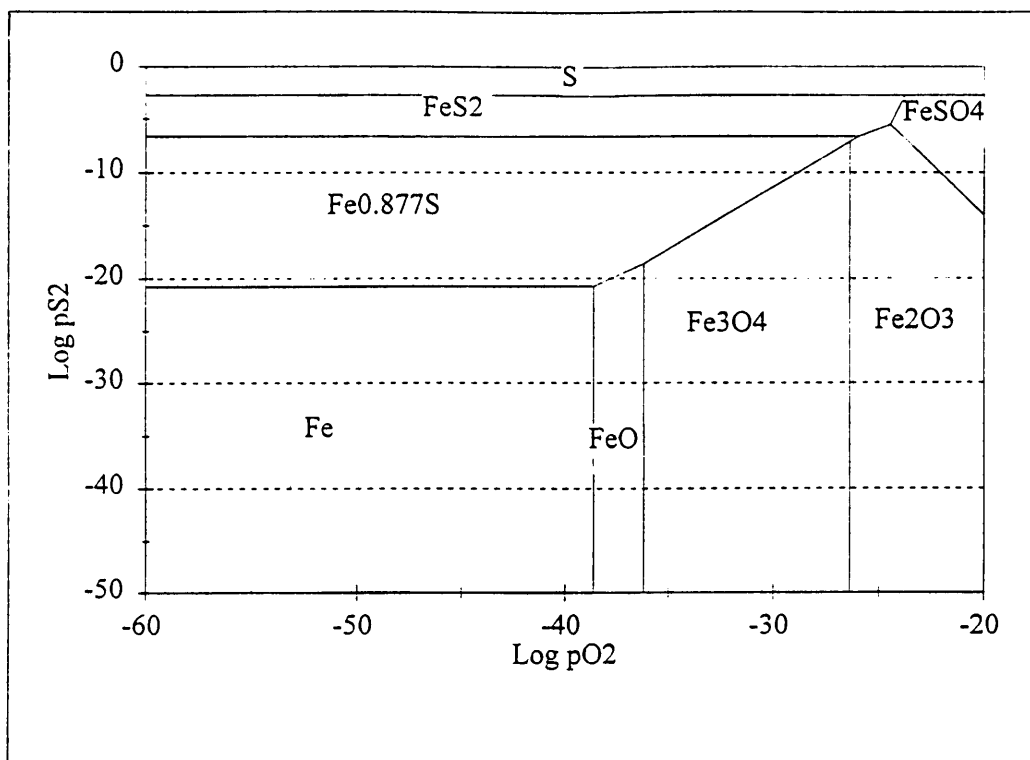
Figure 8.4b: Log $p(S_2)$-log $p(O_2$ stability diagram for Fe at 350°C.

8.4 SUMMARY OF THE TEMPERATURES CALCULATED WITH THE DIFFERENT GEOTHERMOMETERS

Table 8.3: Temperatures ranges of the different geothermometers used in this study:

Temperature (°C)

100	150	200	250	300	350	400	450	
				←——	—→			Chlorite geothermomerty
	←—	——	——	——	——	—→		Micro-thermometery
					·······	·······→		Arsenopyrite geothermometry
←—	——	——	——	——	——	——	—	Sphalerite geothermometry
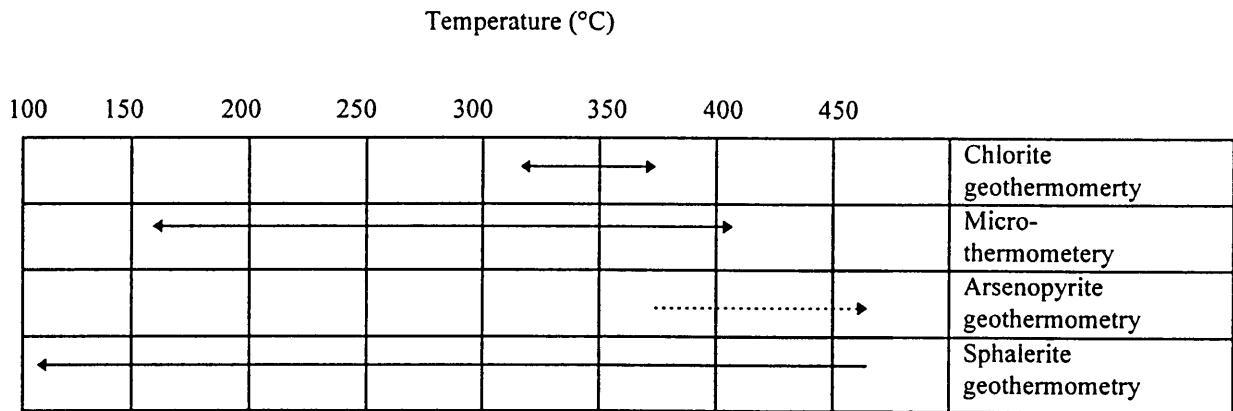
Conclusions

The hydrothermal system operated in an agglomerate layer which forms part of the "Union Tuff member" that occurs in the uppermost part of the Rooiberg Felsites. In contrast to the Sn and F deposits characteristic of this part of the Rooiberg Group, this hydrothermal system in the Rust de Winter area resulted in predominately base metals and a small amount of gold. Schweitzer et al. (1995b) claimed that base metal mineralization is largely confined to the two basal Rooiberg formations, over- and underlying the Rustenburg Layered Suite. To the author's knowledge, no similar systems, economic or sub-economic, have been found in the upper rhyolite successions.

It is believed that this hydrothermal system was either not the product of the intrusion of a granite body, as is the case with the Sn and F mineralisations at Zaaiplaats, Stavoren, Union, and Vergenoeg (Croker, 1986), or it is indeed the product of a granitic intrusion, but represents a later, cooler mineralisation stage further away from the body (**Fig. 9.1**).
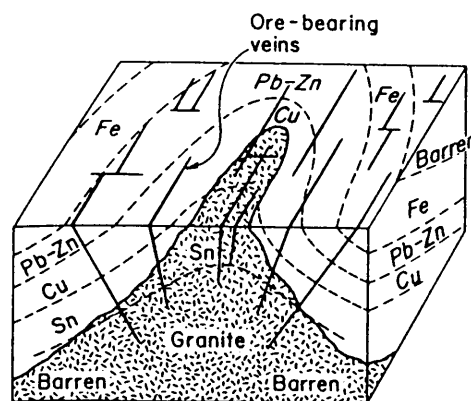
Figure 9.1: A schematic block diagram showing the arrangement of ore zones relative to a granitic body (from Hosking, 1951).

The mineralised areas in the agglomerate layer of the Rooiberg Felsites at Rust de Winter can be divided into three types, based on differences in the host rock, mineralisation style and mineral associations. The first type occurs in quartz + chlorite veins in the agglomerate and carries mainly arsenopyrite, pyrite, chalcopyrite, sulphosalts and Cu-sulphides. The second type is disseminated in the agglomerate and consists predominately of sphalerite and chalcopyrite. The third type is found at the contact between the agglomerate and the massive rhyolite in a brecciated zone and consists of quartz + chlorite + siderite veins with lesser pyrite and chalcopyrite.

The sulphide minerals of the quartz + chlorite veins suggest a history of precipitation in at least three stages. This division is based purely on the mineral associations and their relationships in the veins. The first stage includes the precipitation of the arsenopyrite, pyrite and chalcopyrite. The sulphide minerals of the second stage (Bi-Pb-Cu-sulphosalt, galena and chalcopyrite) precipitated interstitially in the first generation sulphides. The third stage includes minerals that formed due to supergene alteration by a Cu-rich fluid, for example a variety of Cu-sulphides and the Pb-poor sulphosalt. Chlorite and quartz are the dominant silicate minerals associated with the sulphides, and seem to have precipitated continuously throughout the whole sequence of sulphide mineral crystallisation.

In GD2 a zone in the agglomerate is encountered where sphalerite and chalcopyrite occur as main sulphides. Zones dominated by sphalerite alternate with zones dominated by chalcopyrite. Quartz and chlorite occur only occasionally in small veins, but no alteration by a Cu-rich fluid was detected. Because this mineralisation differs much from that of the quartz-chlorite veins it is not certain when precipitation took place and how it is related to the main mineralised veins.

An interesting aspect of the mineralogy of the hydrothermal veins is that the matrix minerals (i.e. chlorite and siderite) are extremely enriched in Fe, so much so that these minerals are classified as the iron end-members in the respective solid solution series. On the other hand, the sulphide minerals (i.e. sphalerite and sulphosalts) are generally low in Fe. Inclusions of chalcopyrite and pyrite in the sphalerite could have formed in response to the migration of Fe from the sphalerite to form Fe-rich inclusions in a now Fe-poor, sphalerite. The second generation sphalerite with the lesser

chalcopyrite inclusions must have formed from a relative iron poor fluid. Continuous leaching of Fe will eventually lead to the formation of copper-sulphides surrounding chalcopyrite.

Alternatively a Cu-saturated fluid could be responsible for the leaching of Fe from chalcopyrite, pyrite and arsenopyrite, and Pb from the Bi-Pb-Cu-sulphosalt. Simultaneously Cu-sulphides could have precipitated on the rims of some sulphide minerals (e.g. chalcopyrite) and replaced other sulphide minerals (e.g. pyrite and arsenopyrite) along cracks.

Because some of the chlorite seems to be a slightly later phase than some sulphides, it can be argued that the Fe removed from the sulphide was again captured in the chlorite. However, not all the chlorite formed during the same stage, but it always has the same characteristic very high Fe content. There could be two possible explanations, firstly that the chamosite crystallised simply because of the lack of MgO in the fluid. This is unlikely because the geochemical data indicate an enrichment of MgO in the green (chloritisised) agglomerate relative to unaltered rhyolite. Secondly, the earlier chamosite could have crystallised from an initially Fe-saturated fluid, or being the product of overprinting by a later Fe-rich fluid that replaced the Mg in the "older" chlorite.

The chlorite geothermometer indicates temperatures of formation in the range 315° - 360°C, but if it is assumed that at least some of the chlorite was overprinted by a Fe-rich fluid, one can expect that these chlorites originally formed at higher temperatures as intermediate compositions in the chamosite-amesite solid solution series. Along with these higher temperature chlorites, some of the primary sulphides (arsenopyrite, pyrite, and chalcopyrite) could have crystallised. A second stage of sulphide precipitation followed at slightly lower temperatures resulting in the formation of the Bi-Pb-Cu-sulphosalt and small amounts of galena and a second generation chalcopyrite. These two stages were succeeded by a period of "alteration" by a Cu-rich fluid, that represents the last stage of sulphide mineral precipitation.

The microthermometric investigation gives pressure corrected temperatures in the range 150° - 380°C. These temperatures clearly account for more than one stage of hydrothermal activity. However, it is not sure which sulphide phases precipitated at what temperature interval.

The salinity of the fluid(s) falls into three groups (i.e. a very high salinity, an intermediate salinity and a very low salinity), which can be explained by fluid mixing (resulting in lowering the salinity) and fluid boiling (increasing the salinity). Both of these stages in the history of the fluid could have resulted in the deposition of base and precious metals. As has been discussed, base metals will be preferentially transported by a higher salinity fluid (5.5 eq. wt% NaCl), whereas gold complexes prefer low salinities (0 - 5 eq. wt. NaCl). The possibility that this temperature range actually represents two or more different fluids cannot be ruled out.

The bulk source of the hydrothermal fluid can only be determined exactly by stable isotope analyses, but it can be expected that ground water and magmatic water were the two major contributors.

REFERENCES

Ahrland, S., Chatt, J., and Davies, N.R. (1958) The relative affinities of ligand atoms for acceptor molecules and ions. Q. Rev. Chem. Soc. **12**, 265-276.

Albee, A.L., Bingham, E., Chodos, A.A., and Maynes, A.D. (1965) Phase equilibria in three assemblages of kyanite-zone pelitic schists, Lincoln Mountain Quadrangle, Central Vermont. Journal of Petrology **6**, 246-301.

Ayora, C., Liesa, M., and Delgado, J. (1993) Low-thermal-gradient Hercynian metamorphism in the eastern Pyrenees. Journal of Metamorphic Geology **11**, 49-58.

Bailey, S.W. and Brown, B.E. (1962) Chlorite polytypism I. Regular and semi-random one-layer structures. American Mineralogist **47**, 819-850.

Ballantyne, J.M. and Moore, J.N. (1988) Arsenic geochemistry in geothermal systems. Geochimica et Cosmochimica Acta **52**, 475-483.

Bancroft, G.M. and Jean, G. (1982) Gold deposition at low temperature on sulphide minerals. Nature (London) **298**, 730-731.

Barnes, H.L. (1979) Solubilities of ore minerals. In: Barnes, H.L. (editor) Geochemistry of Hydrothermal Ore Deposits. 2nd ed. Wiley and Sons, New York, Chapter 8, 404-460.

Barton, P.B.J. (1973) Solid solutions in the system Cu-Fe-S. I. The Cu-S and CuFe-S joins. Economic Geology **68**, 455-465.

Barton, P.B.J. and Bethke, P.M. (1987) Chalcopyrite disease in sphalerite: pathology and epidemology. American Mineralogist **72**, 451-467.

Barton, P.B. and Toulmin, P. (1966) Phase relations involving sphalerite in the Fe-Zn-S system. Economic Geology, **61**, 815-849.

Bayliss, R. (1975) Nomenclature of the trioctahedral chlorites. Canadian Mineralogist **13**, 178-190.

Bente, K. and Doering, T. (1993) Solid-state diffusion in sphalerites: an experimental verification of the "chalcopyrite disease". European Journal of Mineralogy **5**, 465-478.

Boctor, N.Z. (1985) Rhodonite solubility and thermodynamic properties of aqueous $MnCl_2$ in the system $MnO-SiO_2-HCl-H_2O$. Geochimica et Cosmochimica Acta **49**, 565-575.

Bottrell, S.H. and Yardley, B.W.D. (1991) The distribution of Fe and Mn between chlorite and fluid: evidence from fluid inclusions. Geochimica et Cosmochimica Acta **55**, 241-244.

Brown, K.L. (1989) Kinetics of gold precipitation from experimental hydrothermal sulfide solutions. In: Keays, R.R., Ramsay, W.R.H. and Groves, D.I. (editors) The Geology of Gold Deposits: The Perspective in 1988. The Economic Geology Publishing Company, 320-327.

Brown, B.E. and Bailey, S.W. (1962) Chlorite polytypism: I. Regular and semi-random one layer structures. American Mineralogist **47**, 819-850.

Buchanan, L.J. (1981) Precious-metal deposits associated with volcanic environments in the southwest. In: Dickinson, W.R. and Payne, W.D. (editors) Relations of Tectonics to Ore Deposits in the South Cordillera. Arizona Geol. Soc. Dig. **14**, 237-262.

Burnham, (1967) In: Barnes, H.L. (editor) Geochemistry of Hydrothermal Ore Deposits. 2nd ed. Wiley and Sons, New York,

Calas, G., Huc, A.-Y., and Pajot, B. (1976) Utilisation de la spectromètrie infrarouge pour l'ètude des inclusions fluides des minèraux: intèrets et limites. Bulletin de la Société Francaise de Minéralogie et de Cristallographie **99**, 153-161.

Cathelineau, M. (1988) Cation site occupancy in chlorites and illite as a function of temperature. Clay Minerals **23**, 471-485.

Cathelineau, M., Boiron, M.C., Holliger, P., Marion, P., and Denis, M. (1989) Gold in arsenopyrites: Crystal chemistry, location and state, physical and chemical conditions of deposition. In: Keays, R.R., Ramsay, W.R.H. and Groves, D.I. (editors) The Geology of Gold Deposits: The Perspective in 1988. The Economic Geology Publishing Company, 328-341.

Cathelineau, M. and Nieva, D. (1985) A chlorite solid solution geothermometer. The Los Azufres (Mexico) geothermal system. Contributions to Mineralogy and Petrology **91**, 235-244.

Chang, L.L.Y. and Hoda, S.H. (1977) Phase relations in the system $PbS-Cu_2S-Bi_2S_3$ and the stability of galenobismutite. American Mineralogist **62**, 346-350.

Clarke, D.S. and Govett, G.J.S. (1988) Rock geochemistry in the exploration for Southwest Pacific epithermal gold deposits. Proceedings of Bicentennial Gold 88 Conference. Geol. Soc. Austr. 369

Clarke, D.S. and Govett, G.J.S. (1990) Southwest Pacific epithermal gold: a rock-geochemistry perspective. Journal of Geochemical Exploration **35**, 225-240.

Clubley-Armstrong, A.R. (1977) Petrochemistry of the Rooiberg Felsite Group and overlying Loskop Formation, north of Middelburg, southeast Transvaal. Annals of the Geological Survey of South Africa **14**, 11-28.

Clubley-Armstrong, A.R. (1980) Petrochemistry of the Rooiberg Felsite Group and overlying Loskop Formation, north of Middelburg, southeastern Transvaal. Annals of the Geological Survey of South Africa **14**, 11-28.

Crawford, M.L. (1981) Fluid inclusions in metamorphic rocks - low and medium grade. In: Hollister, L.S. and Crawford, M.L. (editors) Short Course in Fluid Inclusions: Applications to Petrology. Mineral. Ass. of Canada, 6, 156-181.

Crerar, D., Wood, S., Brantley, S., and Bocarsly, A. (1985) Chemical controls on solubility of ore-forming minerals in hydrothermal solutions. Canadian Mineralogist 23, 333-352.

Criaud, A. and Fouillac, C. (1989) The distribution of arsenic (III) and arsenic (V) in geothermal waters: examples from the Massif Central of France, the Island of Dominica in the Leeward Islands of the Caribbean, the Valles Caldera of New Mexico, U.S.A., and southwest Bulgaria. Chemical Geology 76, 256-269.

Crocker, I.T. (1979) Metallogenic aspects of the Bushveld granite: Fluorite, tin and associated rare metal-carbonate mineralisation. Geological Society of South Africa Special Publication, 5, 275-295.

Davies, J.F., Grant, R.W.E., and Whitehead, R.E.S. (1979) Immobile trace elements and Archean volcanic stratigraphy in the Timmins mining area, Ontario. Canadian Journal of Earth Sciences 16, 305-311.

Davies, J.F. and Whitehead, R.E.S. (1980) Further immobile element data from altered volcanic rocks, Timmins mining area, Ontario. Canadian Journal of Earth Sciences 17, 419-423.

De Bruiyn, H. (1980) The geology of the acid phase of the Bushveld complex, north of Pretoria - geochemical statistical approach. PhD thesis Univ. Orange Free State

Decaritat, P., Hutcheon, I., and Walshe, J.L. (1993) Chlorite Geothermometry - A Review. Clays and Clay Minerals 41, 219-239.

Deer, W.A., Howie, R.A., and Zussman, J. (1992) Editors: Deer, W.A., Howie, R.A., and Zussman, J. An Introduction to the Rock-Forming Minerals. 2nd ed. Longman Group Ltd. 343 p

Eriksson, P.G., Schweitzer, J.K., Bosch, P.J.A., Schreiber, U.M., Van Deventer, J.L., and Hatton, C.J. (1993) The Transvaal Sequence: An overview. Journal of African Earth Sciences 16,

Ferrow, E. and Roots, M. (1989) A preparation technique for TEM specimens; application to synthetic Mg-chlorite. European Journal of Mineralogy 1, 815-819.

Finlow-Bates, T. and Stumpfl, E.F. (1981) The behaviour of so-called immobile elements in hydrothermally altered rocks associated with volcanogenic submarine exhalative ore deposits. Mineralium Deposita 16, 319-328.

Franklin, J.M., Lydon, J.W., and Sangster, D.F. (1981) Volcanic-associated massive sulfide deposits. In: Skinner, B.J. (editor) *Economic Geology, Seventy-Fifth Anniversary Volume*. 75th Annniv. ed. The Economic Geology Publishing Company, ElPaso, Texas, 485-627.

Gieré, R. (1986) Zirconolite, allanite and hoegbomite in a marble skarn from the Bergell contact aureole; implications for mobility of Ti, Zr and REE. Contributions to Mineralogy and Petrology 93, 459-470.

Gieré, R. (1989) Hydrothermal mobility of Ti, Zr, and REE: examples from the Bergell and Adamello contact aureoles (Italy). Terra Nova 2, 60-67.

Giggenbach, W.F. (1984) Mass transfer in hydrothermal alteration systems - a conceptual approach. Geochimica et Cosmochimica Acta 48, 2693-2711.

Goodman, B.A. and Bain, D.C. (1979) Mössbauer spectra of chlorites and their decomposition products. Proc. 6th Int. Clay Conference 1978 (Oxford). Elsevier, Amsterdam, 65-74.

Grant, J.A. (1986) The isocon diagram - a simple solution to Gresens' equation for metasomatic alteration. Economic Geology 81, 1976-1982.

113

Gresens, R.L. (1967) Composition-volume relationships of metasomatism. Chemical Geology 2, 47-65.

Hannington, M.D. and Scott, S.D. (1989) Sulfidation equilibria as guides to gold mineralization in volcanogenic massive sulfides: evidence from sulfide mineralogy and the composition of sphalerite. Economic Geology **84**, 1978-1995.

Harris, D.C. and Chen, T.T. (1976) Crystal chemistry and re-examination of nomenclature of sulfosalts in the aikinite-bismuthinite series. Canadian Mineralogist **14**, 194-205.

Hayes, J.B. (1970) Polytypism of chlorite in sedimentary rocks. Clays and Clay Minerals **18**, 285-306.

Haynes, F.M., Sterner, S.M., and Bodnar, R.J. (1988) Synthetic fluid inclusions in natural quartz. IV. Chemical analyses of fluid inclusions by SEM/EDA: Evaluation of method. Geochimica et Cosmochimica Acta **52**, 969-977.

Hedenquist, J.W. and Henley, R.W. (1985) The importance of CO_2 on freezing point measurements of fluid inclusions: evidence from active geothermal systems and implications for epithermal ore deposition. Economic Geology **80**, 1379-1406.

Helgeson, H.C. (1967) Solution chemistry and metamorphism. In: Abelson, P.H. (editor) Researches in Geochemistry. John Wiley & Sons Inc. New York, **2**, 362-404.

Helgeson, H.C. and Garrels, R.M. (1968) Hydrothermal transport and deposition of gold. Economic Geology **63**, 622-635.

Hemley, J.J. and Hunt, J.P. (1992) Hydrothermal ore-forming processes in the light of studies in rock- buffered systems: II. Some general geologic applications. Economic Geology **87**, 23-43.

Henley, R.W. (1985) The geothermal framework of epithermal deposits. In: Berger, B.R. and Bethke, B.M. (editors) Reviews in Econ. Geol.: Geology and Geochemistry of Epithermal Systems. 2nd ed. Chapter 1, 1-24.

Henley, R.W. (1990) Ore transport and deposition in epithermal environments. In: Golding, H.H. and Ho, S.E. (eds) Stable Isotopes and Fluid Processes in Mineralization, Geol. Dept. and Univ. Extension, Univ. of Western Australia Publ., 23, 51-69.

Henley, R.W. (1991) Epithermal gold deposits in volcanic terranes. In: Foster, R.P. (editor) Gold Metallogeny and Exploration. Blackie & Son Ltd. Glasgow, London, 133-164.

Hosking, K.F.G. (1951) Primary ore deposits in Cornwall. Royal Geol. Soc. Cornwall Trans. 18, 309-356.

Hynes, A. (1980) Carbonatization and mobility of Ti, Y, and Zr in Ascot formation metabasalts, SE Quebec. Contributions to Mineralogy and Petrology 75, 79-87.

Jowett, E.C. (1991) Fitting iron and magnesium into the hydrothermal chlorite geothermometer. GAC-MAC Annual Meeting Abstract. 16, A62

Kavalieris, I., Walshe, J.L., Halley, S., and Harrold, B.P. (1990) Dome related gold mineralization in the Pani volcanic complex, North Sulawesi, Indonesia: a study of geologic relations, fluid inclusions, and chlorite compositions. Economic Geology 85, 1208-1225.

Kerrich, R. and Fryer, B.J. (1981) The separation of rare elements from abundant base metals in Archean lode gold deposits: implications of low water/rock source regions. Economic Geology 76, 160-166.

Kodama, H., Longworth, G., and Townsend, M.G. (1982) A Mössbauer investigation of some chlorites and their oxidation products. Canadian Mineralogist 20, 585-592.

Kranidiotis, P. and MacLean, W.M. (1987) Systematics of chlorite alteration at the Phelps Dodge massive sulfide deposit, Matagami, Quebec. Economic Geology **82**, 1898-1911.

Kretschmar, U. and Scott, S.D. (1976) Phase relations involving arsenopyrite in the system Fe-As-S and their application. Canadian Mineralogist **14**, 364-386.

Large, R.R., Huston, D.L., McGoldrick, P.J., and Ruxton, P.A. (1989) Gold distribution and genesis in Australian volcanogenic massive sulfide deposits and their significance for gold transport models. In: Keays, R.R., Ramsay, W.R.H. and Groves, D.I. (editors) The Geology of Gold Deposits: The Perspective in 1988. The Economic Geology Publishing Company, 520-536.

Lee, J.H., Peacor, D.R., Lewis, D.D., and Wintsch, R.P. (1984) Chlorite-illite/muscovite interlayered and interstratified crystals: A TEM/STEM study. Contributions to Mineralogy and Petrology **88**, 372-385.

Lesher, C.M., Goodwin, A.M., Campbell, I.H., and Gorton, M.P. (1986) Trace-element geochemistry of ore-associated and barren, felsic metavolcanic rocks in the Superior Province, Canada. Canadian Journal of Earth Sciences **23**, 222-237.

MacLean, W.H. (1990) Mass change calculations in altered rock series. Mineralium Deposita **25**, 44-49.

Mather, J.D. (1970) The biotite isograd and the lower greenschist facies in the Dalradian rocks of Scotland. Journal of Petrology **11**, 253-275.

McDowell, S.D. and Elders, W.A. (1980) Authigenic layer silicate minerals in borehole Elmore 1, Salton Sea geothermal field, California, USA. Contributions to Mineralogy and Petrology **74**, 293-310.

McLeod, R.L. and Stanton, R.L. (1984) Phyllosilicates and associated minerals in some paleozoic stratiform sulphide deposits in southeastern Australia. Economic Geology **79**, 1-22.

McPhail, D.C. (1993) The behaviour of iron in high temperature chlorine brines. Geol. Soc. Aust. ,Program Abstr. **34**, 50-51.

Mellini, M., Nieto, F., Alvarez, F., and Gomez-Pugnaire, M.T. (1991) Mica-chlorite intermixing and altered chlorite from the Nevado-Filabride micaschists, Southern Spain. European Journal of Mineralogy **3**, 27-38.

Nieto, F., Velilla, N., Peacor, D.R., and Huertas, M.O. (1994) Regional retrograde alteration of sub-greenschist facies chlorite to smectite. Contributions to Mineralogy and Petrology **115**, 243-252.

Parilov, Y.S., Mikhaleva, V.A., and Yeshkeyeva, N.T. (1990) Experimental verification of the reliability of fluid inclusion thermometry as applied to sulfide deposits. International Geology Review 1028-1034.

Paterson, C.J., Uzunlar, N., and Groff, J. (1989) A view through an epithermal-mesothermal precious metal system in the Northern Black Hills, South Dakota: A magmatic origin for the ore-forming fluids. In: Keays, R.R., Ramsay, W.R.H. and Groves, D.I. (editors) The Geology of Gold Deposits: The Perspective in 1988. The Economic Geology Publishing Company, 564-570.

Pearson, R.G. (1963) Hard and soft acids and bases. Journal of the American Chemical Society **85**, 3533-3539.

Pecher, A. (1984) Chronolgie et re-equilibrage des inclusions fluides: quelques limites à leur utilisation en microthermomètrie. In: Lagache, M. (editor) Thermomètrie et baromètrie gèologiques. 2nd ed. Soc. Franc. Minèral. Cristallogr. 463-485.

Phillips, G.N. and Groves, D.I. (1983) The nature of archaen gold-bearing fluids as deduced form gold deposits of western Australia. J. Geol. Soc. Australia **30**, 25-39.

Phillips, W.R. (1964) A numerical system of classification for chlorites and septechlorites. Mineralogical Magazine **34**, 1114-1124.

Poty, B.P., Stadler, H.A., and Weisbrod, A.M. (1974) Fluid inclusion studies in quartz from fissures of Western and Central Alps. Schweiz. Mineral. Petrogr. Mitt. **54**, 717-752.

Puddephatt, R.J. (1978) The Chemistry of Gold. Elsevier, Amsterdam-Oxford-New York.

Ramdohr, P. (1975) The Ore Minerals and Their Intergrowths. Second Edition, Pergamon Press, 410-411.

Renders, P.J. and Seward, T.M. (1989) The adsorption of thio gold (I) complexes by amorphous As_2S_3 and Sb_2S_3 at 25 C and 90 C. Geochimica et Cosmochimica Acta **53**, 255-267.

Rhodes, R.C. and Du Plessis, M.D. (1976) Notes on some stratigraphic relations in the Rooiberg Felsite. Geological Society of South Africa Transactions **79**, 183-185.

Roedder, E. (1972) Composition of fluid inclusions. U. S. Geol. Survey Prof. Pap. 440-JJ.

Roedder, E. (1979) Fluid inclusions as samples of ore fluids. In: Barnes, H.L. (editor) Geochemistry of Hydrothermal Ore Deposits. 2nd ed. Wiley-Interscience, New York, 684-737.

Roedder, E. (1984) Fluid Inclusions. Min. Soc. America, Washington, D.C.

Roobol, M.J. and Hackett, D. (1987) Paleovolcanic facies and exhalite geochemistry: Guides for selecting exploration areas in volcano-sedimentary complexes. Economic Geology **82**, 691-705.

Roseboom, E.H. (1966) An investigation of the system Cu - S and some natural copper sulfides between 25° and 700°C. Economic Geology 61, 641-672.

Rubin, J.N., Henry, C.D., and Price, J.G. (1989) Hydrothermal zircons and zircon overgrowths, Sierra Blanca Peaks, Texas. American Mineralogist 74, 865-869.

Rubin, J.N., Henry, C.D., and Price, J.G. (1993) The mobility of zirconia and other "immobile" elements during hydrothermal alteration. Chemical Geology, 110, 29-47.

Samson, I.M., Williams-Jones, A.E., and Liu, W.N. (1995) The chemistry of hydrothermal fluids in carbonatites: Evidence from leachate and SEM-decrepitate analysis of fluid inclusions from Oka, Quebec, Canada. Geochimica et Cosmochimica Acta 59, 1979-1989.

Sander, M.V. and Einaudi, M.T. (1990) Epithermal deposition of gold during transition from propylitic to potassic alteration at Round Mountain, Nevada. Economic Geology 85, 285-311.

Schweitzer, J.K., Hatton, C.J., and De Waal, S.A. (1995a) Regional lithochemical stratigraphy of the Rooiberg Group, upper Transvaal Supergroup: A proposed new subdivision. South African Journal of Geology 98, 245-255.

Schweitzer, J.K., Hatton, C.J., and De Waal, S.A. (1995b) Economic potential of the Rooiberg Group: Volcanic rocks in the floor and roof of the Bushveld Complex. Mineralium Deposita 30, 168-177.

Scott, S.P. and Kissin, S.A. (1973) Sphalerite composition in the Zn-Fe-S system below 300°C. Economic Geology, 68, 475-479.

Seward, T.M. (1973) Thiocomplexes of gold and the transport of gold in hydrothermal ore solutions. Geochimica et Cosmochimica Acta 37, 379-399.

Seward, T.M. (1976) The stability of chloride complexes of silver in hydrothermal solutions up to 350 C. Geochimica et Cosmochimica Acta **40**, 1329-1341.

Seward, T.M. (1981) Metal complex formation in aqueous solutions at elevated temperatures and pressures. 13-14 ed. Phys. Chem. Earth, Nobel Symposium on the Chemistry and Geochemistry of Solutions at High Temperatures and Pressures, 113-132.

Seward, T.M. (1989) The hydrothermal chemistry of gold and its implications for ore formation: Boiling and conductive cooling as examples. In: Keays, R.R., Ramsay, W.R.H. and Groves, D.I. (editors) The Geology of Gold Deposits: The Perspective in 1988. The Economic Geology Publishing Company, 398-404.

Seward, T.M. (1991) The hydrothermal geochemistry of gold. In: Foster, R.P. (editor) Gold Metallogeny and Exploration. Blackie & Son Ltd. Glasgow, London, 37-62.

Seyfried, W.E.J. and Bischoff, J.L. (1981) Experimental seawater-basalt interaction at 300 C, 500 bars, chemical exchange, secondary mineral formation and implications for the transport of heavy metals. Geochimica et Cosmochimica Acta **45**, 135-147.

Sharp, Z.D., Essene, E.J., and Kelly, W.C. (1985) A re-examination of the arsenopyrite geothermometer: pressure considerations and applications to natural assemblages. Canadian Mineralogist **23**, 517-534.

Shenberger, D.M. and Barnes, H.L. (1989) Solubility of gold in aqueous sulfide solutions from 150 to 350 C. Geochimica et Cosmochimica Acta **53**, 269-278.

Shepherd, T.J., Rankin, A.H., and Alderton, D.H.M. (1985) A Practical Guide to Fluid Inclusion Studies. Blackie, Glasgow, London.

Shikazono, N. and Kawahata, H. (1987) Compositional differences in chlorite from hydrothermally altered rocks and hydrothermal ore bodies. Canadian Mineralogist **25**, 465-474.

Sillitoe, R.H. (1977) Metallic mineralization affiliated to subaerial volcanism: a review. Volcanic Processes in Ore Genesis. Inst. Mining and Metallurgy - Geol. Soc. London, **7**, 99-116.

Skinner, B.J. (1979) The many origins of hydrothermal mineral deposits. In: Barnes, H.L. (editor) Geochemistry of Hydrothermal Ore Deposits. 2nd ed. Wiley, New York, 1-21.

Smith. B. (1993) A geological investigation of the Rooiberg volcanic successions at Melkhoutfontein 183JR. Honours Project, Univ. Pretoria.

South African Committee for Stratigraphy (SACS) (1980) Editor: Kent, L.E. Lithostratigraphy of the Republic of South Africa, South West Africa/Namibia and the Republics of Bophuthatswana, Transkei and Venda. Goverment Printer, Pretoria,

Spooner, E.T.C. (1981) Fluid inclusion studies of hydrothermal ore deposits. In: Hollister, L.S. and Crawford, M.L. (editors) Short Course in Fluid Inclusions: Applications to Petrology. Mineral. Ass. of Canada, **6**, 209-240.

Stear, W.M. (1977) The stratigraphy and sedimentation of the Pretoria Group at Rooiberg, Transvaal. Geological Society of South Africa Transactions **80**,

Stoessel, R.K. (1984) Regular solution site-mixing model for chlorites. Clays and Clay Minerals **32**, 205-212.

Townsend, M.G., Longworth, G., and Kodama, H. (1986) Magnetic interaction at low temperature in chlorite and its products of oxidation: a Mössbauer investigation. Canadian Mineralogist **24**, 105-115.

121

Twist, D. (1983) An economic evaluation of the Rooiberg Felsite. Inst. Geol. Res. Bushveld Complex, Res. Rep. **41**, 1-25.

Twist, D. (1985) Geochemical evolution of the Rooiberg silicic lavas in the Loskop Dam area, Southeastern Bushveld. Economic Geology **80**, 1153-1165.

Veblen, D.R. (1983) Microstructures and mixed layering in intergrown wonesite, chlorite, talc, biotite, and kaolinite. American Mineralogist **68**, 566-580.

Walshe, J.L. (1986) A six-component chlorite solid-solution model and the conditions of chlorite formation in hydrothermal and geothermal systems. Economic Geology **81**, 681-703.

Watts, K.J. and Hassemer, J.R. (1989) Geochemical signatures of possible deep-seated ore deposits in Tertiary volcanic centres, Arizona and New Mexico, U.S.A. Journal of Geochemical Exploration **32**, 413-414.

White, D.E. (1975) Thermal waters of volcanic origin. Geological Society of America Bulletin **68**, 1637-1658.

Williams, P.J. (1994) Iron Mobility During Synmetamorphic Alteration in the Selwyn Range Area, NW Queensland - Implications for the Origin of Ironstone-Hosted Au-Cu Deposits. Mineralium Deposita **29**, 250-260.

Wood, S.A. (1987) Application of a multiphase ore mineral solubility experiment to the separation of base metal and gold mineralization in Archean greenstone terrains. Economic Geology **82**, 1044-1048.

Yokoyama, T., Takahashi, Y., and Tarutani, T. (1993) Simultaneous determination of arsenic and arsenious acids in geothermal water. Chemical Geology **103**, 103-111.

Appendix A

Drill core logs of GD1, GD2, and GD3:

Drill core logs of GD1, GD2, and GD3:

GD 1

0,0 - 6,16 : Weathered oxidised agglomerate
              Red coloured

6,16 - 7,0 : Red coloured
              Strongly weathered

7,0 - 7,33 : Green colour
              Matrix -> Green
              Clasts -> Big red clasts
                        Small green clasts
                        White clasts
                        Deformed red clasts (varies in size)

7,33 - 7,44 : Red zone

7,44 - 7,87 : Green colour
               Matrix -> green
               Clasts -> small green
                         big red
                         Huge red (10 * 10 cm)
               Sulphides in fracture at 7,57m, maybe Asp.
               Sulph. in matrix too

7,87 - 7,97 : Red zone
               Horizontal fractures

7,97 - 8,10 : Green coloured zone

8,10 - 8,30 : Oxidation along unorientated fract.
               Red on outer rim and yellow directly along
               fract.
               Oxidation along fract. a few mm up to 5cm in
               width.

8,30 - 8,88 : Green zone with fine fract.
               Oxidation along fract. rare to absent
               Fract. no specific orientation
               Amount of fract. :   7

8,88 - 9,03 : Red Zone
               Big red clast at 8,9m

9,03 - 9,45 : Green zone
               Fairly massive
               Clasts the same
               2-3 unoxidised fract.
               Sulph. (Cp ?) at 9,35m, disseminated

9,45 - 9,67 :   2 Red zones along hor. and diag. fract., with
               unoxidised green zone in middle (2-5 cm wide).
               In immediate area of fract. oxidation is yellow
               and change then to red.

9,67 - 9,87 : Green zone
               Few small unoxidised fract.

9,87 - 10,0 : Red zone

10,0 - 10,30 : Green zone

10,30 - 11,60 : Red zone

11,60 - 11,65 : Green zone
                 Oxidised fract. (hor. & diag.), 5mm wide

11,65 - 11,75 : Massive dark green zone (chlorite ?)

11,75 - 12,33 : Green zone
                 At 12,16m there is a white clast (Q) with a
                    golden sulph. included.
                 NOTE : The huge red clasts are all
                    characterized by small greenish
                    inclusions as well as the deformed
                    red clasts.

12,33 - 12,36 : Open fract. zone of which the oxidation
                    grades over to dark green (chlorite) zone.

12,36 - 12,63 : Red zone
                 Fract. nearly horizontal

12,63 - 13,0 : Massive green zone (=> no fract.)

13,0 - 13,15 : Red zone

13,15 - 13,40 : Massive green zone
                 Cp in small white clast

13,40 - 13,50 : Red zone

13,50 - 13,90 : Massive green zone

13,90 - 13,95 : Red zone

13,95 - 14,20 : Green zone with 2-3 minor unoxidised fract.

14,20 - 14,45 : Red zone with hor. fract.

14,45 - 14,57 : Pinkish zone (=> matrix is red)
                 Seems to be more weathered/altered

14,57 - 15,03 : Red zone
                 Fract. is hor. to slightly dipping

15,03 - 15,50 : Massive green zone

15,50 - 15,66 : 2 Red zones divide by a 5cm green zone

15,66 - 15,77 : Green zone

15,77 - 15,88 : Red zone
                 Fract. is dipping at 45°

15,88 - 16,95 :   Massive green zone
                  At 16,60m Cp in a red deformed clast
                  Cp still in white clasts
                  Cp appears in small green clasts in larger
                      amounts than those in white clasts (at
                      15,58-16,20m).
                  Cp in red clasts seems to be associated with
                      dark green spots.

16,95 - 17,10 :   Red zone

17,10 - 17,84 :   Pink zone grading over to a green zone
                  One diag. oxidised fract. at 17,34m
                  Cp still associated with small green spots

17,84 - 17,87 :   Red zone with one hor. fract.

17,87 - 18,00 :   Pink zone grading over to a green zone
                  At 18,0m a silvery sulphide (Asp) appears as
                      single xtals ("flaky").

18,0 - 18,70 :   Green zone
                  Asp seems to form either single xtals or
                      clusters of x'tals, associated with the
                      dark green min. (chlorite)
                  Cp is still in the green grains and spot in
                      red clasts
                  Cp appears also in a thin Q-vein at 18,60m
                  Q-vein seems to be continues and vertical

18,70 - 18,96 :   Pinkish altered/weathered zone
                  Directly above this zone there is a yellow
                      mineral which seems to be alteration
                      product of chlorite

18,96 - 20,40 :   Green-pink coloured zone
                  Almost vertical Q-veins carrying Cp at 19,0m,
                      Cp-mineralizing in these vein becomes more
                      prominent
                  Fract. dipping 30° not very wide and no
                      sulph.
                  Cp still ass. with green grains
                  Bornite-like sulph. starts to appear in Q-
                      veins at 19,55m
                  At 19,80m Q-veins become wider with more Cp
                  Between 19,84 - 19,90m there is a dark green
                      zone with a silvery sulph.
                  Asp reappears at 20,0m as single " flaky"
                      xtals, but doesn't seem to be ass. with
                      chlorite (not sure)
                  The chlorite zone seems to appear more often
                  At 20,35m a large Cp cluster is appearing
                      together with a silvery sulph. (Asp)
                      although not directly in contact with the
                      Q-vein nearby, it may be ass.
                  This Q-vein is not vert. but almost hor.

```
20,40  -20,60 :    Dark green  broken zone  with several Q-veins
                   cutting     across     with     no     specific
                   orientation

20,60 - 20,80 :    Massive Asp cutting into the Chl-zone
                   Sulph.-rich  fluid  seems  to  have drop  into
                      the Chl-zone
                   A yellow groundmass  is present with the Asp
                      (on  the  boundaries between  the  chlorite
                      and sulph.)
                   Q-veins seem to be broken up  and "invaded" by
                      the massive Asp clusters

20,80 - 21,0 :   Sulph. content decrease
                 Texture the same as the above zone, that is:
                      ->large open holes
                      ->no definite direction of movement  by the
                         Asp
                      ->broken Q-veins
                      ->chlorite breccia

21,0  - 21,10  :   Chl-zone intruded  by wide  Q-veins with Cu-
                      sulph.
                 Have not seen any Asp

21,10 - 21,50 :   Highly brecciated
                  It seems  as if the  Chl-zone was intruded  by
                     Q-veins  and then the whole system had been
                     broken in intruded by a  second Chl-bearing
                     fluid
                  At 21,40m a few  Asp xtals have been seen in a
                     yellow (oxidised)  groundmass next  to the
                     Chl-zone
                  At  21,50m a 50   dipping fract. is carrying Q
                     and Asp (no sign of Cp)

21,50 - 21,68 :   Green zone with a Chl-zone cutting through
                  There is a Q-vein but no sign of any sulph.
                  No big red clasts only small green clasts
                  (This might  not be typical  of this zone  but
                     purely accidently)

21,68 - 22,15 :   Chl-zone
                  Q-veins cutting  across in all directions  but
                     no visible sulph.

22,15 - 22,40 :   Asp reappear
                  First   as  small  single  xtals but  further
                     downwards  as a  massive  sulph. mass that
                     seems  to  have "drop"  into  the  Chlorite
                     surrounding
                  Asp xtals form clusters in the sulph. mass

22,40 - 23,35 :   Green zone with large red clasts
                  Red clasts have Cp as inclusions
                  Cp is also ass. with small green clasts
                  Cp and  Bn appear with and  without Q in  fine
                     fract.  that  sometimes  cut  through   the
```

clasts (no specific orientation?)
From 23,0m downwards there is a disseminated
dark sulph. (Bn or Sph1) xtallized in fine
fract. with no specific orientation

23,35 - 23,50 :   Chl-zone
Cu-sulph. still in fine fract.

23,50 - 23,85 :   Chl-zone with Asp mass

23,85 - 24,70 :   Chl-zone
Sulph.- bearing fract. cuts through a huge
red clast (sulph.= Cp,Bn,Asp)
Cp and Bn are also in fine fract.
Asp is also xtall. as single clusters in the
Chlorite
A Cu-sulph.- bearing-Q-veins are cutting
through the Chlorite in all
directions

24,70 - 25,50 :   Chl-zone with Asp mass
Asp also ass. with Cp and Bn
Have not seen any fract. or veins cutting
through the massive sulph.

25,50 - 25,90 :   Green-pink coloured zone
Asp appears in fract. as single xtals and not
as a mass
The ass. fluid in the fract. with the sulph.
seems to be chlorite-bearing
At 25,90m it seems as if the fluid used the
same channel ways as that of the Q-veins
but was a later intrusion

25,90 - 26,40 :   Pink zone (=> matrix = red)
70° dipping fract. filled with Q (no sulph.
seen)
Cp appears in the green spots (grains) in the
red matrix
Cp also in very fine fract. in the host rock,
again ass. with possibly chlorite

26,40 - 26,50 :   Red zone
In the break a dark blue mineral xtallize
(hematite)

26,50 - 27,26 :   Green zone
Sulph. ass. with dark green mineral
(chlorite) where ever it occurs as
inclusions in the red clasts or where
there is small grains in the matrix
Occasionally very fine fract. are filled with
Cu-sulph.
NOTE: In every Green zone the clasts are very
similar:
-> small green clasts
-> small white clasts sometimes with Cp
included

```
                        -> big to huge red clasts
                        -> deformed red clasts
                           both of which have dark green spots
                           or zones in which Cp is
                           sometimes present

27,26 - 27,30 :  Chl-zone
                 Cu-sulph. disseminated

27,30 - 27,60 :  Green zone
                 A 80° dipping fract. (3mm wide) is filled
                    with 2 sulphides:
                  -> probably bornite and pyrite
                 Cp and Bn appear diss. as previously seen

27,60 - 27,85 :  Pink zone => red matrix
                 Sulph. are diss., and consist of a Bn- or
                    sphalerite-like dark mineral, less Cp
                 This darker sulph. sometimes surrounds the
                    smaller red clasts

27,85 - 28,16 :  Cp content increases
                 No fract. the sulph. are only diss.
                 NOTE: the golden sulph. might also be Py

28,85 - 28,40 :  Bn/Sphal is increasing and the Cp is
                    decreasing
                 Host rock is more pinkish

28,40 - 28,55 :  The dark and the golden sulph. are occurring
                    together, and are still diss.
                 No major fract.

28,55 - 29,00 :  Golden sulph. content is increasing and are
                    still diss.
                 Dark sulph. is visible but only in small
                    amounts and seems to concentrate where the
                    golden sulph. are absent

19,00 - 29,30 :  Content of the golden sulph. are decreasing
                    and seem to concentrate around grain and
                    clast boundaries
                 Matrix is red and the clasts are red, green
                    and white

29,30 - 29,75 :  Matrix change to greenish but the clasts do
                    not change
                 Sulph. contents decrease
                 Golden sulph. (Cp) appears in fine vert.
                    fract.
                 Small amounts sulph. still diss.
                 No dark sulph.

29,75 - 29,80 :  Red zone

29,80 - 30,00 :  Green zone with Cp diss. and around small
                    clasts
```

30,00 - 30,10 :   Red zone

30,10 - 32,66 :   Green zone
                  Diss. Cp in varying amounts
                  Fine vert. fract. filled with Bn and Cp
                  At 31,65m a 60° dipping fract. filled with Cp
                      and Q
                  Golden sulph. still appear as inclusions in
                      white clasts as well as in deformed red
                      clasts
                  No major fract. , fairly massive

32,66 - 32,82 :   Red zone
                  60° dipping fract.

32,82 - 33,44 :   Massive Green zone
                  Cp in some of the clasts
                  Broken fract. at 33,20m is filled with Q and
                      Cp and dips 70°

33,44 - 46,00 :   Green massive zone
                  Only sulph. are found in clasts like Q and
                      some deformed red calsts or clasts with
                      green spots
                  Occasionally there is also a golden sulph. in
                      fine fract.
                  Red zones (oxidised) cuts occasionally through
                      the agglomerate
                  The colour of the matrix may change from
                      greenish to a bit more pinkish from time
                      to time but no unusual mineralization
                      occurs with that
                  Clasts stay throughout the same

46,00 - 46,41 :   Green zone
                  Asp appears again in clusters in the Chl.
                  Some fract. are cutting through but seem to
                      postdate the sulph. deposit and are no
                      mineralized
                  At 46,30m there is a 40° dipping fract. which
                      has Asp mineralized
                  There are nearly hor. Q-veins with no sulph.

46,41 - 46,43 :   Chl. zone with As-pew clusters and single
                      xtals

46,43 - 46,85 :   Fractured Green zone
                  Most of the open unmin. fract. are not
                      orientated in any specific direction
                  Asp appears in fine more or less vert. fract.
                      (this direction are not fixed)
                  Bigger fract. with Asp min. appear in ass.
                      with more chl.-rich zones

46,85 - 47,36 :   Asp is becoming more prominent and still
                      seems to have invaded the chl. zones
                  Chl. zones show signs of weathering effects
                  More short open fract. appear

At 47,0m a long fract. cuts vertically
through the host rock and is filled with
Asp
Q-rich zones appear in the Chl. zone and are
broken up fract. filled with chl. and
later invaded by sulph. too
At 47,17m Cu-sulph. appear together with Asp
in these fract.

46,36 — 47,73 :   Weathering more prominent
Nearly vert. fract. filled with Asp in the
middle (together with a yellow groundmass)
and chl. on the rim
At one side of the mineralized fract. the
host rock is also fract. but not altered
or mineralized
The other side is strongly weathered to a soft
brittle green min. (malachite)

47,73 — 48,13 :   Green zone with less fract.
Cu-sulph. in fine fract. which are not very
long and cut through clasts
Sometimes also ass. with nearly hor. Q-veins
Unmineralized chl. fractured zone at 47,83m,
dipping 50°

48,13 — 48,60 :   Green zone
At 48,13m a fract. dipping 60° is filled with
chl. and Asp
At 48,20m a dark green zone (8cm wide) have
no sulph. mineralized
Golden sulph. appear still in clasts and with
green spots
At 48,50m there are 2 fract. one filled with
Q only (dipping 70°) and the other one
filled with chl. and Cp. (dipping 50)

48,60 — 48,68 :   Weathered zone
Yellow colour
Big clasts with yellow spots and rims, Asp
veins are cutting through these clasts
These big red clasts are also surrounded by
Asp and Cp.
The yellow spots are probably an alteration
product of chl.
This zone is bounded by 2 fract. dipping 50°

48,68 — 49,00 :   Green-yellow zone
Certain min. seem to have been subjected to
alteration => yellow min. and holes
Rest of zone is fract. free
Only Cp. is diss. in matrix (no Asp)

49,00 — 50,50 :   Red matrix with a lot of yellow spots
Fract. are abundant — some are open and in
other areas it looks as if something was
removed
Other fract. are mineralized with

- Asp (at 49,15m)
- Q at 50,0m, dipping 80°
- Malachite
- Black mineral (sometimes ass. with malachite)

The fract. varies in length and size

50,50 - 54,10 : Strongly altered/weathered zone (VROT)
                 Minerals - Light green (Malachite)
                          - Yellow (altered chl./FeO)
                          - Dark green (Chl.)
                          - Charcoal (Hematite)
                          - Blue (Azurite)
                 No sulph. visible

54,10 - 54,45 : Massive Asp zone
                 Host rock still altered
                 Golden sulph. ass. with Asp

54,45 - 55,00 : Pink zone (=> red matrix)
                 Clasts are red and green, and the red clasts
                     have yellow spots and holes in places
                 Cp. appears only in the clasts

55,00 - 55,25 : Green zone
                 A few fract. dipping 60°
                 No sulph.

55,25 - 56,00 : Red zone
                 Oxidation along fract. dipping 70°
                 Cp. and Malachite in fract. that are coloured
                     yellow and red
                 Cp. and Asp are also present in finer fract.
                     (with no specific orientation) ass. with
                     chl.
                 Matrix in between fract. are red

56,00 - 56,45 : Pink zone
                 Holes in matrix where minerals were taken
                     away
                 Some fract. were filled with chl. and Cp.,
                     but the chl. is starting to erode and only
                     Cp. is left
                 At 56,0m there seems to be either a huge red
                     clast or the matrix had been silicified.
                     It is broken up by Cp-chl bearing fluids
                 Cp appears in big units (1*1cm)
                 At 56,30m there are red clasts with white
                     clasts included => reworked?

56,45 - 56,66 : Mixture of green and red matrix

56,66 - 56,84 : Red and green zone showing deformation
                 No sulph. ass.

56,84 - 58,00 : Matrix change 2 times from red to green
                 2 Major red oxidised zones along fract.

dipping 60 -70°
No sulph. in fract. red zones
In the massive zone in between fract., there
is only minor Cp in clasts

58,00 - 58,15 :   Fract. dipping 60° which are filled with
Chl.,py and Asp
No other sulph. except in red clasts

58,15 - 59,70 :   Matrix again is changing colour gradually and
3 major red oxidised zones cut through
At 59,30m some black spots appear which maybe
an alteration product (it is spread over
and area of 7cm)
At 59,40m there are some strange alteration
(?) grading over into a chl. rich zone (no
sulph.)
Very fine fract. with Cp start to appear at
59,40m (vert.)

59,70 - 59,85 :   Chl. rich zone carrying Cu-sulph. in veins
through the chl.

59,85 - 50,45 :   Green zone intruded by chl.- Cu-sulph. fluids
in nearly vert. fract.
Also Asp xtals starts to appear in these
fract.
At 60,20m Q appears with chl. and Cp in
fract.
Cp is increasing in the matrix

50,45 - 61,85 :   Cu-sulph. content increase diss. in matrix
Cu-sulph. appear also in fine fract. at
60,80m
Matrix is basically red
At 61,10m a 60° dipping fract. is carrying
Cu-sulph.
Minor single Asp xtals appear in the matrix

61,85 - 62,15 :   Large Q-vein dipping 60° - 1-3cm wide
- carrying Cu-sulph.

- no Asp
- Chl. seems to have
eroded in some
places
Cp also appears diss. in the host rock where
it tend to concentrate around Q-grains
Yellow spots are still present in matrix

62,15 - 63,00 :   Pink zone
Fairly massive
Py and Cp in matrix (around Q-grains)
No Asp visible
Red clasts still with Cp inclusions
Small very fine fract. seem to be channel
ways for a sulph.-rich fluid to reach
grains and the grain boundaries

Dark blue sulph. appears in matrix (Bn or Sphal.)

63,00 - 63,03 : Chl. zone
Cp is the only sulph. present

63,03 - 64,35 : Massive Green zone
Sulph. content increase in matrix concentrating around grains
Asp only as rare single xtals

64,35 - 64,90 : Pink zone
Sulph. content decreases rapidly

64,90 - 65,10 : Chl. zone
Red rim around the zone
Py and Cp are ass.
Asp in fract.

65,10 - 67,00 : Pink zone
Fairly massive
Only sulph. that can be seen are in the clasts

67,00 - 68,00 : Green zone
Cp content increases, and concentrates in green grains and along fine fract. ass. with chl.
Sometimes Bn is also in the fine fract. Lower down there is more open fract.

68,00 - 69,00 : Green matrix and huge red clasts Bn,Cp and Py concentrate in the matrix in large amounts around grains and ass. with green grains (=> inside)
Sulph. concentration increases downwards
At 69,0m Bn appears in large amounts and Cp and Py are almost massive

69,00 - 69,14 : Chl. zone
High concentrations of Cp and Bn
No Asp visible

69,14 - 69,55 : Cp,Py and Bn still diss. in matrix and clasts
A silvery sulph. appears in the matrix and clasts ass. with golden sulph.
Large red clasts are broken up and intruded by veins of golden sulph.
At 69,46m 2 fract. are filled with Cp and Py

69,55 - 69,79 : Red zone of deformed material
The material seems to be banded (green and red)
Green bands have sometimes Cp,Py and the silvery sulph. xtallized
The red bands have only the silvery sulph.
This zone is cut by a chl.-Cp-Bn-Py bearing fract. dipping 40°

69,79 - 70,16 : Green zone
                 Very fine hor. fract. filled with Cp
                 Other veins are filled with a dark green min.
                    and not so often Cp
                 The silvery sulph. is still present in the
                    matrix and small green clasts

70,16 - 70,29 : Deformed red and green banded zone with the
                    same mineralization as higher up
                 No fract.

70,29 - 70,40 : Chl. zone
                 Fine hor. veins of Cp and Py

70,40 - 70,87 : Green zone
                 Strongly sulph. mineralized
                 At 70,70m there is a 70° dipping fract.
                    filled with a brick red min. which seems
                    to older than the sulph.

70,84 - 71,00 : Chl. zone
                 Lots of fract. and holes
                 No sulph. except one spot of Bn
                 The brick red min.·is present (K-Feldsp.?)

71,00 - 72,55 : Green zone
                 60° dipping fract. filled with the brick red
                    min.
                 Cp,Py and Bn are present in the matrix
                 Sulph. concentrations increases downwards
                  becoming more massive
                 There is one fract. filled with Bn
                 The silvery sulph. is not visible any more
                 At 72,28m there is again a fract. filled with
                    the brick red min. and Bn

72,55 - 72,70 : Chl. zone
                 Vert. fract. filled with Cu-sulph. and Py
                 Cp present in matrix as well

72,70 - 73,65 : Green zone
                 Fract. filled with golden sulph. and chl.
                    dipping 70° at 73,50m
                 Sulph. concentration decreases downwards

73,65 - 73,85 : Chl. zone
                 Py in centre

73,85 - 73,87 : Pink zone
                 Sulph. scares
                 Large clasts of porphyric lavas from 74,25m
                    downwards
                 Lava-clasts have very fine sulph. veins
                  cutting through
                 Before the lavas is met the sulph. min. stops

74,87 - 100,00 : Porphyric lavas

15,00 - 15,64 : Red zone
                 Holes in matrix where something was   removed

                 At 15,17m flakes of sulph. appear
                 The sulph. -> Silvery sulph. (Asp)
                           -> Dark sulph. (Sphl/ Bn)
                 Asp mostly in matrix but also included
                   in red clasts (15,18)
                 At 15,28m there is a dark min. which
                   might be Hematite
                 From 15,28m downwards the matrix seems to be
                 silicified but no sulph.

15,64 - 15,95 : Green-whitish zone
                 Strongly silicified
                 Fract. are common in any orientation
                   filled with both a red and green
                   min./fluid
                 At 15,80m a zone appears which is
                   less silicified and darker
                   -> a dark silvery -blue sulph.
                      is present in veins through
                      this zone
                   -> Ass. with this sulph. is a
                      yellow (oxidised) min. which
                      is also present in the fract.
                      dipping 60°

15,95 - 16,00 : Red zone
                 Characterized by small brick-red grains

16,00 -16,50 :   Green zone
                 Areas near the red zone are also
                   charact. by the small red spots
                   included in grains and matrix
                 At 16,32m there is a golden sulph.
                   which appears to be in ass. with
                   a small green grain
                 At 16,32m there is a large green clast
                   with red inclusions
                 Fract. in this area are open and not
                   mineralized with no similar orientation
                   but mostly hor.

16,50 - 16,70 : Pink zone
                 Sulph. at 16,55m
                   -> Silvery sulph. (Asp) as flakes
                      in matrix, no chl. in surrounding
                      like in GD1 deposits
                   -> A dark sulph. (sphl/Bn) seems to
                      be sometimes near Cp at 16,59m

16,70 - 17,34 : Green zone
                 Cp in small green grains
                 At 17,29m there is a Q-clast with
                  Cp included
                 From 17,14 - 17,34m the matrix is
                  charac.by small eroded holes (seems
                  to be the green grains which had been
                  altered and taken away
                 No major fract.

17,34 - 19,00 : Pink zone with darker red oxidation
                 areas
                 It seems to be subjected to weathering
                  bec. there are holes in the matrix
                  and also that yellow min. (alteration
                  prod. of chl.?)
                 There is a dark min. which might be
                  sphl present as small grains in the
                  matrix (not in clasts?)
                 At 17,44m there is a red clast with
                  a dark rim
                 At times some of the red clasts seem
                  to have been reworked
                 The small green grains seem to have
                  eroded and what is left inside is a
                  sulph.(Cp/Py/Sphl)
                 At 18,70m there is a dark grey-black
                  min. along a hor. fract. (hematite)
                 Fract. in this zone are less common
                  and mostly hor.,but no mineralization
                  in them except for oxidation along
                  some of them
                 Typical then is alteration of chl.
                  which creates holes in both the matrix
                  and the clasts. Ass. with these areas
                  are sometimes fine xtallized sulph.
                  (Cp/Sphl)

19,00 - 19,67 : Green zone
                 At 19,03m there is a silvery sulph.
                  ass. with the small green grains
                 Other sulph. present are Cp/Py and
                  sphl as described previously
                 At 19,15m the green matrix grade
                  over to a red matrix
                 At 19,38m there is a red clast with
                 an inclusion of a dark min. (sphl)
                 At 19,60m the silvery sulph. reappear
                 as small single xtals in the surrounding
                 of a strongly deformed red clast with
                 green bands which seems to have sulph.
                 ass. with it

19,67 - 19,90 : Matrix is very red
                 Fract. cutting   through   in   different
                 directions but are not min. (open)
                 Sulph. visible are only sphl which is now

increasing and a golden sulph. is (Py)
sometimes ass. with sphl.
The matrix seems to be altered to a yellow
green min. (as previously seen)

19,90 - 21,10 : Pink zone
Sphl concentration increases
At 20,00m there is a 60° dipping
Q-vein which doesn't seem to be
sulph. min.
Other fract. with no specific orient.
are carrying a yellow-green min. and
cut through clasts
Sphl doesn't seem to be ass. with
any fract. or passing through fluids

20,10 - 20,20 : Dark green zone which seems to be
weathered in the centre and fluids
carrying a silvery sulph. are cutting
through in a 40° dipping fract.
Under this chl. zone there is a red
zone with 50° dipping fine fract.
carrying chl. (?)
In this zone (which may be a huge red
reworked clast) the silvery sulph. and
sphl are both present

20,20 - 21,75 : Pink zone with large amounts of sphl.
xtall. (spotty appearance)
Fine fract. cutting in any direction
carrying the yellow-green min. and
in places the sphl seems to concentrate
next to these fract. (see 20,84m)
At 21,15m the Cp/Py seems to be included
by sphl (sits in the middle of a sphl
xtal/grain)
The sphl content increase downwards and
almost becomes massive between 21,60 -
21,70m
In this area the amount of fract. with
the yellow-green min. are also increasing
Other sulph. are rarely visible

21,75 - 22,56 : Pink zone
Sphl content a lot less massive
Other Golden sulph. seem to be more
prominent but still ass. with the sphl
At 22,10m there is a 70° dipping fract.
which doesn't seem to be min. but acted
as an oxidation path for the fluids
This zone is otherwise rather massive
(=> few fract.)
Golden sulph. content increases downwards

22,56 - 23,00 : Chl. zone dipping 60°
Eroded in the middle where it looks as if
a fluid carrying a white min. (Q) and
others, had been responsible for a com-

position change which was subjected to
faster weathering and erosion
Downwards as 22,80m sphl seems to reappear
as very fine xtals

23,00 - 23,52 : Pink zone
                Sphl again more prominent
                At 23,22m there is a fault dipping 70°
                which seems to have sulph. xtall.
                Sphl and golden sulph. appear mostly
                diss. in the matrix
              Cp and Py is also xtall. in fine fract.
                at 23,30m dipping 65°

23,52 - 23,57 : Green zone
                Small single xtals of a silvery sulph.
                appear diss.
                2 Hor. fract. are cutting through

23,57 - 23,62 : Red zone
                Seems to be deformed in the middle
                No sulph.

23,62 - 23,80 : Pink zone
                Fine fract. of which some of them have
                sphl xtall. next to it
                There is a 40° dipping fract. carrying
                sulph. (Cp/Py)
                The silvery sulph. seems to be present
                in very fine xtals in the matrix around
                grain boundaries (not sure)
                There is again a sphl xtal with Cp
                included at 23,71m

23,80 - 24,37 : Pink zone
                Sphl dominates along fine fract. (with
                no specific orient.) and along grain
                boundaries
                In places Cp/Py is ass. with sphl
                The silvery sulph. seems to be ass.
                with the sphl too but still very
                fine (not sure whether there is any
                difference between it and sphl)

24,37 - 25,23 : Py zone
                At 24,37m there are a few fine fract.
                with Py xtall. ,again no orient.
                The golden sulph. increase and the sphl
                decrease
              Py >> Cp > Sphl
                The sulph. appear both diss. and as
                fillings in fract.
                At 24,64m there is a 50° dipping fract.
                filled with Py and Q
                At 24,63m there is a fault (3mm) dipping
                75° carrying large amounts of Py and
                less Q

In this area the Py content increase
drastically and it looks as if this
fault was the main path way for the
sulph. bearing fluids which also
intruded the surrounding area through
minor fine fract. and around grain
boundaries
At 25,05m there is a hor. fract. (partly
open) which carries Py and Cp and I
think chl. as well but it had eroded

25,23 - 25,72 :   Sphl zone
Py decreases and Sphl increase
Sphl appears diss.
Ass. with sphl is again the fine silvery
sulph.
At 25,51m there is a fract. carrying both
Cp and a silvery sulph. (not sure if it
is the same as that ass. with the sphl)

NOTE   the whole rock stays basically red, with the variety
of clasts. The whole rock is not weathered much and
a sphl. rich fluid sometimes filled the fract. and
faults

25,72 - 26,05 : Py zone
At 25,72m there is a fract. filled with a
chl. looking min.
--> to the one side of the fract. the host
    rock seems to be more altered bec. it is
    darker than the other side which looks
    more fresh (red)
--> in the fresh rock there is Q-grains
    surrounded by a golden sulph.
--> near to the fract. there is a few single
    xtals of possibly Asp
--> other sulph. like Cp and Py are also
    present near this zone
Both sphl. and the ass. silvery sulph. are
still present in the matrix
Cp also appears in small fine fract.
There are a few single visible Asp looking
xtals but they don't seem to be ass. with
major chl. areas, although it seems as if it
might origin from fluids passing through
fract.

26,05 - 27,16 :   Sphl. zone
At 26,05m the sphl. concentration increase
and there is also a 65° dipping Q and Cp
fine fract.
From 25,80m the sphl becomes more prominent
The hor. fract. are mostly uneven and seem
to be filled with a chl. type of min.
At 26,88m there is a 5cm red oxidised zone
which is more fract.
In the area of 27,00m the silvery sulph. is
again more prominent and diss.

27,16 - 27,28 :   Py zone
                  Py is present in both the matrix and as
                  inclusions in the red clasts
                  At 27,20m there is a fine fract. bearing
                    possibly sphl which cuts through a red clast

27,28 - 27,90 :   At 27,82m there is a fault dipping 50°
                    carrying the silvery sulph. Cp and
                    possibly chl.
                  The silvery sulph. sometimes appears to
                    be included in the red clasts (27,80)
                  Cp and Py still are present in some of
                    the clasts and diss. in matrix

27,90 - 28,41 :   Py and Cp zone (sphl decrease)
                  The matrix appears to be more green
                    which might have something to do with
                    the nearby chl. filled fract.
                  At 28,10m the matrix turns red again
                  Py and less Cp appears both diss. and
                    in a 40° dipping fine fract.
                  Py xtall. around grain boundaries too
                    and in green zones in deformed red
                    clasts
                  At 28,23m there is a fault dipping 50°
                    but with no min. (it looks as if it
                    predated the major sulph. bearing
                    fract.
                  Sphl is still present but in very small
                    amounts
                  The whole rock is fairly fresh

28,41 - 28,49 :   Matrix is less red and more weathered
                    (chloritized)
                  Py still appears is fract. but seems to
                    be chloritized as well
                  Py and Cp are diss. in matrix and also
                    in red clasts
                  NOTE: Occasionally through the rock there
                        are black and brown spots which
                        are possibly due to weathering

28,49 - 28,72 :   Pink zone with Py mineralized as seen
                    above (also small amounts sphl)

28,72 - 28,89 :   Pink zone
                  Py decrease and sphl increase
                  The sphl = dark and silvery sulph.
                  At 28,80m there is an oxidised Py bearing
                    fract. dipping 75°
                  Py is also present along grain boundaries
                    and included in clasts

28,89 - 28,94 :   Red oxidised zone with sphl and Py xtals

28,94 - 29,23 :   Matrix is a mixture of green and red
                  Almost vert. oxidised fract. bears Py
                  and Cp and is continues, nearly massive

Q is also present with the golden sulph.
Diss. Py and Cp appear in the matrix but
  larger amounts of the silvery sulph.
Py and Cp are more concentrated in fine
  fract. than in matrix
The sphl like sulph. are still the more
  dominant diss. sulph.

29,23 - 29,78 : Matrix still mixture of red and green
                 Py increases and sphl decreases
                 Py is present diss. and in fract.
                 At 29,??m there is a hor. fract. filled
                   possibly chl. and Q, and not sulph.

29,78 - 30,54 : Matrix sill the same
                 Sphl increases and less Py
                 The silvery sphl(?) appears diss as well
                   as in deformed red clasts
                 Small Cp xtals are also present in matrix
                   and Q clasts and red clasts
                 The sphl concentration seems to increase
                   downwards

30,54 - 30,95 : The matrix is grading over from red to
                   green at 30,60m
                 Major sulph. are Py with less Sphl and
                   diss. Cp in small amounts
                 At 30,62m there is a 30° dipping fract.
                   bearing Py surrounded by this green zone
                 At 30,77m there is as area with almost
                   massive very fine xtallized golden sulph.
                 The matrix seems to change from time to
                   time from red to green but there don't
                   seem to be any difference in sulph. be-
                   tween these areas

30,95 - 31,30 : " The return of the Silvery Sulph."
                 At 31,26m there is an open fract. dipping
                   50° with no visible min.
                 Matrix is rather red

31,30 - 31,58 : Green zone
                 Py increases with decrease of sphl
                 The Py concentration is fairly massive
                   is in the fine fract. zones which is
                   more or less hor.

31,58 - 31,77 : Pink zone
                 Diss. sphl,Cp and Py with sphl increasing
                   downwards
                 In this zone the sphl content is not as
                   high a it was higher up

31,77 - 32,20 : Again the matrix is not constant in
                   colour
                 The whole rock is fresh
                 Py content increases, diss. and
                   along fine fract.

Between 32,00 and 32,20m there seems
to be a chl. rich zone to the one side
of the core. To the other side the
rock is rather green and along the
boundary there has been oxidation
which affected the green zone more
than the chl.zone
Ass. with this oxidation Py xtall. took
place in greater concentrations than
the diss. sulph.

32,20 - 32,26 : Red zone with hor. open fract. of which
of the fract. have Py xtallized

32,36 - 32,60 : Green zone
The sulph. min. is low and mainly diss.
Sulph. = Py,Cp and sphl
At 32,35m there is a 70° dipping fract.
with Py xtallized
At 32,33m there is a vert. oxidised
fract. bearing Py
This continues downwards and the Py
min. is strongly ass. with red oxidised
areas in the rock
At 32,45m there are 2 open unmin. fract.
dipping $60-70^{\circ}$ that seem to postdate
the sulph. min.
Chl. rich zones don't seem to have higher
concentrations of sulph. ass. with it -
in fact only a few small diss. sulph.
can be seen

32,60 - 32,88 : Red stained zone
In the hor. fract. there is Py
At 32,87m there is a fault dipping
75° with no sulph. min., only fluids
carrying a FeO intruded (hematite)

32,88 - 33,30 : Green zone
Vert. and hor. fract. are strongly
oxidised but with a lot less Py
Some oxidised fract. don't even have
any sulph. xtall.
The sulph. min. in the green host
rock are very small
At 33,15-33,30m the Py content in the
red zone increases again

33,30 - 34,49 : Massive green zone
Only diss. Cp and Py and possibly
sphl in small amounts
The whole rock is fresh except for
holes where a min./grain had been
taken away
No fract.
At 34,31m there is a chl. rich area
but no sulph. ass. with it

34,49 - 36,68 : Green zone
                 Fract. are not sulph. min. but carried
                   fluids for oxidation processes (dip-
                   ping in different directions)
                 Sulph. are diss. in the matrix
                 At 34,83m there is a fine fract. dipping
                   75° which carries a sulph. (Py) and
                   is ass. with a red oxidation rim
                 NOTE: It seems as if the oxidation
                         process responsible for the sulph.
                         xtall. was different for the later
                         oxidation processes, bec. the
                         sulph. bearing fract. have red rims
                         or stains and the open fract. or
                         those with no sulph. have a yellow
                         oxidation min.
                 The whole rock is not strongly weathered
                   but is characterized by small holes and
                   the yellow alteration prod. of chl.

36,68 - 36,74 : Green-yellow zone rimmed by a red zone
                 No sulph.

36,74 - 36,87 : Green zone
                 Cp and Py min. are stronger and appear diss.
                 in matrix

36,87 - 36,95 : Red zone
                 Hor. fract. with yellow coloured zone
                   next to fract. and a red rim
                 No sulph. min. ass. with fract.
                 Only golden sulph. diss. in matrix

36,95 - 37,46 : Pink zone with holes
                   Cp and Py ass. with green clasts
                 Slightly higher concentrations than
                   in above green zone
                 No sulph. in fract.
                 Sphl seems to be absent (not sure)

37,46 - 37,79 : Green Chl. effected zone
                 Q-veins (3-5mm) are cutting through
                   carrying Cp
                 Small diss. Cp appears also in this
                   zone

37,79 - 39,15 : Green zone grading over to the more dominant
                     Pink zone
                 At 38,27m there is a red zone with a small
                     amount of golden sulph.
                 After this red stained zone a yellow
                     alteration (?) min. appears in the matrix
                 Sulph. are very rare and appear only
                     occasionally in the matrix and some
                     clasts

39,15 - 43,80 : At 39,20m there is a 65° dipping Q-vein which
                     seems to be intruded by oxidised fluids

which precipitated also golden sulph.
From 39,30 - 39,85m there is a 80° dipping
    fract along which oxidation took place
    and the ass. sulph. precip.
    -> golden sulph.
    -> black sulph.
The golden, black, and silvery sulph. appear
    also diss. in the matrix
From 40,22 - 40,38m there is a chl. rich zone
    but no difference in sulph. min.
Up till 41,80m the whole rock is fairly fresh
    with a few fine open unmin. fract. and 3
    red stained zones
From 41,80 - 42,43m the matrix has in places
    holes but the sulph. content remains the
    same
The dominant sulph. are Cp and Py in the
    green clasts

43,80 - 45,70 : At 43.90m there is a red area/clast which has
    a few single xtals of a silvery sulph.
    This sulph. is not found downwards. The
    rest of the zone is not different from the
    previous zone
From   44,50m   downwards   the   matrix   is
    chloritized strongly with a large amount
    of fract. cutting through (54,0 - 54,25)
    carrying golden sulph. rich fluids. There
     is also a darker min. in these veins. The
    sulph. content does not decrease much, if
    at all

45,70 - 47,80 : Weathered zone
Asp appearing in a small interval (45,70 -
    45,80m) but fairly massive
Beneath the Asp   zone there is a   dark-
    silvery min. probably chalcocite
Other min.   are   malachite   and a   yellow
    oxidition prod. (limonite)
At 46,0m there is a broken up Q-area
    ass. with possibly limonite. These
    oxidised fluids seem to have been
    responsible for this texture
At 46,80m Asp xtals appear again but not
    ass. with any chl. zones rather with the
    oxidised fluids

46,80 - 47,30 : This zone has a strange looking texture :
    Chl. grains seem to be dominant with a
    whitish matrix
Where   a   fract.   cuts   through   the   zone
    oxidation took place along the fract. and
    invaded the matrix too
No sulph.

47,30 - 75,03 : At 47,30m there is a brecciated Q-vein (30°)
    with no sulph.
Sulph. appear in very fine fract. at 47,90m

The overall sulph. content is very low
At 49,0m there is again a golden sulph. in a
    red stained chl. zone
At 49,35m there is a huge oxidised fract.
    dipping 70° (partly open) but with no
    sulph.
At 49,65m there is a red stained zone which
    have fine veins filled with sulph.

NOTE: Since 45,50m the matrix is mainly green

Typical is a low Sulph. (Cp & Py) content
    but occasionally a whole green grain/
    clast has been replaced by sulph. and
    not all the red stained zones have sulph.
    ass. with it
At 54.30m there is 2 60° dipping fract.
    filled with Cp
At 54,50m the silvery sulph. appears in a red
    clast
At 56,20m the Cp content increases, it
    appears in grains and around grains
At 56,25m there is a chl. zone with sulph. in
    a 70° dipping fract. There is also a
    silvery sulph. not in veins but as small
    clusters of xtals
At 68,30m the silvery sulph. appears again in
    a red clast and the surroundings
From 70,0m downwards the silvery sulph.
    (Asp?) appears as more abundant diss.
    xtals in the matrix
From 70,80m the general sulph. content is
    increasing
At 71,10m there is a 60° dipping fract with
    strongly precip. golden sulph.
At 72,10m Bn is also present in the matrix
The whole rock is rather fresh

75,03 - 76,00 : Matrix turns red
                 Sulph. content increases
                 Sulph. ass. with Q-veins are Cp/Py/Bn/Asp

76,00 - 100,0 : Porphyric lavas
                 Q rich hydrothermal fluids occasionally brake
                     up the lavas and are usually sulph. min.
                 At 80,0m there is a similar round texture
                     which has been seen in GD1 (looked then
                     as an alteration prod.)
                 At 83,0m and 95,84m there are chl. zones with
                     that strong golden sulph. precip. along
                     some of the fract.

1,00 - 60,00 : Agglomerate
Sulph. min. as seen in GD1 and GD2
No major sulph. precip. though

60,00 - 60,20 : Pink zone
At 60,05m there is an altered yellow clast
consisting of both golden sulph. and a
silvery sulph.
The yellow min. is probably an alteration
prod. of chl. as seen previously

60,20 - 147,0 : Entering the brecciated zone between the
aggl. and the lavas
In the felsite there is dark spots which have
also ass. with it very fine (small) xtals
of sulph.
Another yellow min. appears also in the Q-
veins which are responsible for the brake
up of the felsite (siderite?)
Occasionally there is a zone of chl. but no
sulph. ass. with that
This zone is typified by Q-veins through the
felsite which is also filled by siderite
and some golden sulph.
In some of these veins there is also the
brick red min. appearing as small xtals
K-feldspar?)
At 65,85m there is a Q-vein with sulph.
precip. in the centre
The Q in these veins doesn't look as milky
as the Q-veins in the aggl.
At 76,73m there is a silvery sulph. appearing
together with the normal golden sulph.
From 77,0 - 77,30m there is a chl. zone with
strong Cp min. in fract. zones
At 79,85 -80,0m there is a strange brecciated
zone which is filled with a dark min.
(sulph.?) which seems to xtall. in needles
between the clasts
From 78,0 -147,0m the felsites are less
brecciated => less to no sulph. The colour
might change from grey to red but no other
changes ass. with that Occasionally a chl
rich zone appears but no sulph. ass. with
that either The felsites are rather fresh
and massive with almost no oxidised fract.
only fine fract. fills with Q and some
times sulph.

147,0 149,0 : Strongly sulph. min. zone
Felsites are red with fract. dipping
60° filled with sulph. cutting through
sulph. = Cp ,Py
Silvery sulph. at 148,30m
These veins are also filled with chl. and

minor Q
                   At 149,0m the silvery is again present (Asp?)

149,0 - 152,30 :   Felsite turns to grey again with only
                   occasionally min. in veins

152,30 - 152,50 : Red Felsite
                   At 152,40m   there is massive Cp and Py
                   with diss. Asp

152,50 - 154,00 : Grey Felsite
                   At 153,73m there is Cp and Py   fairly
                   massive with an Asp xtal too in the
                   fract.

154,00 - 155,60 : Red Felsite
                   More brecciated with accordingly more
                   sulph. precip.
                   Siderite appears again in veins
                   At 154,25m open fract. have Q xtals growing
                   in them
                   At 154,90m a good sample

155,00 - 157,70 : Felsite less red' (not really grey)
                   The siderite content in the veins/fract.
                   is increasing
                   The golden sulph. content stays constant
                   The silvery sulph. content is very low to
                   zero
                   Fract. are vert. to very steep orientated
                   Some black min. is sometimes ass. with the
                   siderite as 158,33m

162,70 - 163,50 : Grey Felsite

163,50 - 165,90 : Red Felsite
                   Siderite >> Golden sulph. > Silvery sulph.
                   Good sample at 164,0m
                   At   165,30m   there is   vert. fine fract.
                   filled with   a dark min. that seems to
                   postdate the   sulph. and siderite bearing
                   fract.

165,90 - 167,40 : The less red felsite is grading over to a
                   more red felsite
                   Less sulph. but they do appear in fine hor.
                   fract. sometimes ass. with a dark min. in
                   the fract.

167,40 - 171,85 : Red felsite with more hor. fract. filled
                   with the dark min. (chl?) and sulph.
                   At 168,30m there is some strange yellow-
                   white alteration along a certain fract.
                   At 168,50m Cp, Py and Asp appear in a
                   fract. that seem to be filled with a chl.-
                   sulph. bearing fluid in a small chl. zone
                   The same feature is appearing again lower
                   down

171,95 - 200,00 :   Grey felsite
                    Fairly massive
                    No sulph.
                    Dark   spots   in   the   felsite   sometimes
                     replaced by a green-yellow min. (chl.?)

                    FIN.....

Appendix B

Major and trace element data for the red and green agglomerate:

Major element data for red agglomerate:

Sample	SiO$_2$	TiO$_2$	Al$_2$O$_3$	FeO(Total)	MnO	MgO	CaO	Na$_2$O	K$_2$O	P$_2$O$_5$
5-25.8	74.38	0.29	10.24	4.98	0.26	0.23	0.06	0.00	6.17	0.05
5-49.25	70.75	0.32	11.30	8.02	0.20	0.26	0.05	0.00	6.19	0.05
5-50.0	67.16	0.40	12.68	8.96	0.19	0.33	0.33	0.00	6.26	0.04
5-55.00	73.65	0.27	9.56	7.21	0.23	0.23	0.08	0.00	5.59	0.05
1-16.00	71.17	0.30	11.33	8.44	0.07	0.48	0.00	0.00	5.50	0.05
1-28.3	70.58	0.34	11.37	3.82	0.01	0.11	0.00	0.00	6.22	0.05
1-64.60	69.11	0.31	10.93	7.83	0.00	0.29	0.06	0.00	6.35	0.04
2-42.75	72.65	0.34	10.98	7.44	0.06	0.56	0.02	0.01	5.49	0.02
2-71.50	68.71	0.26	10.23	7.24	0.07	0.45	0.01	0.17	5.67	0.03
3-27.0	69.69	0.33	11.66	7.24	0.16	0.28	0.04	0.00	6.80	0.05
3-39.4	70.06	0.32	10.59	7.97	0.18	0.14	0.05	0.02	6.79	0.04
Average	70.72	0.32	10.99	7.20	0.14	0.30	0.06	0.02	6.09	0.04
Std. Dev.	2.06	0.04	0.80	1.44	0.08	0.13	0.09	0.05	0.45	0.01
Max	74.38	0.40	12.68	8.96	0.26	0.56	0.33	0.17	6.80	0.05
Min	67.16	0.26	9.56	3.82	0.01	0.11	0.00	0.00	5.49	0.02

Major element data for green agglomerate:

Sample	SiO$_2$	TiO$_2$	Al$_2$O$_3$	FeO(Total)	MnO	MgO	CaO	Na$_2$O	K$_2$O	P$_2$O$_5$
5-28.0	71.86	0.32	12.23	8.17	0.01	0.33	0.03	0.00	5.39	0.03
5-37.45	73.17	0.32	10.69	8.26	0.09	0.27	0.02	0.00	4.99	0.06
5-46.00	67.11	0.34	11.48	14.51	0.06	0.43	0.04	0.00	3.97	0.04
5-66.0	69.12	0.32	11.58	11.36	0.01	0.31	0.00	0.00	4.91	0.06
5-104.0	70.08	0.32	11.16	11.80	0.05	0.45	0.02	0.00	3.83	0.04
5 115.6	70.34	0.29	11.23	11.81	0.14	0.46	0.02	0.00	2.99	0.04
5 126.1	72.67	0.30	11.49	8.91	0.07	0.31	0.04	0.00	4.38	0.08
5-127.0	71.09	0.29	11.42	11.08	0.08	0.48	0.03	0.00	3.33	0.04
1-13.50	69.82	0.32	11.50	9.33	0.08	0.48	0.01	0.00	5.31	0.04
1-31.0	66.56	0.30	11.85	12.71	0.10	0.61	0.00	0.00	4.38	0.04
1-47.85	70.17	0.29	10.06	13.05	0.11	0.74	0.00	0.00	2.63	0.04
1-58.50	67.85	0.31	11.32	13.53	0.12	0.79	0.00	0.00	2.37	0.01
2-16.8	67.39	0.31	10.97	12.73	0.09	0.66	0.00	0.02	3.23	0.00
2-34.0	70.76	0.29	11.06	8.89	0.05	0.53	0.00	0.01	4.76	0.01
2-42.2	66.14	0.29	10.06	16.52	0.13	0.92	0.00	0.00	2.08	0.00
2-42.80	72.00	0.29	10.17	9.90	0.08	0.59	0.00	0.00	3.83	0.02
2-57.8	71.03	0.32	11.14	9.19	0.11	0.51	0.03	0.00	4.67	0.06
3-29.5	69.83	0.31	10.98	9.67	0.17	0.29	0.03	0.07	5.16	0.04
Average	69.83	0.31	11.13	11.19	0.09	0.51	0.01	0.01	4.01	0.04
Std. Dev.	2.03	0.01	0.57	2.28	0.04	0.18	0.01	0.02	1.01	0.02
Max	73.17	0.34	12.23	16.52	0.17	0.92	0.04	0.07	5.39	0.08
Min	66.14	0.29	10.06	8.17	0.01	0.27	0.00	0.00	2.08	0.00

Sample	Zn	Cu	Ni	Ga	Mo	Nb	Zr	Y	Sr	Rb	U	Th	Pb	Ba	Sc
5-25.8	28.0	43.0	5.0	18.0	9.0	15.0	340.0	45.0	11.0	338.0	6.0	16.0	4.0	524.0	10.0
5-49.25	46.0	37.0	4.0	15.0	7.0	19.0	378.0	57.0	11.0	296.0	10.0	15.0	13.0	703.0	10.0
5-50.0	51.0	35.0	5.0	27.0	2.0	21.0	461.0	83.0	14.0	364.0	4.0	23.0	9.0	695.0	13.0
5-55.00	46.0	33.5	4.0	16.5	8.5	17.5	319.0	44.5	7.0	268.5	5.5	11.5	7.0	495.5	8.0
1-16.00	324.0	1,005.0	3.0	15.0	4.0	24.0	370.0	57.0	8.0	272.0	5.0	25.0	77.0	445.0	5.0
1-28.3	118.0	22,000.0	3.0	9.0	3.0	19.0	404.0	90.0	30.0	271.0	5.0	33.0	402.0	907.0	5.0
1-64.60	479.0	1,993.5	3.0	18.5	3.0	19.0	376.0	59.5	14.5	352.0	6.5	20.0	66.5	626.0	6.0
2-42.75	3,179.5	2,704.0	3.0	18.5	2.5	23.5	382.0	76.5	9.5	310.5	8.0	24.0	437.5	472.5	5.0
2-71.50	30,000.0	5,515.0	3.0	3.0	6.5	17.0	348.5	74.0	9.5	248.5	6.5	31.0	1,140.5	883.5	5.0
3-27.0	60.0	339.0	4.0	16.0	2.0	15.0	375.0	59.0	26.0	352.0	5.0	14.0	5.0	1,252.0	15.0
3-39.4	50.0	48.0	7.0	19.0	3.0	21.0	363.0	44.0	27.0	356.0	9.0	11.0	4.0	909.0	6.0
Average	3,125.5	3,068.4	4.0	15.9	4.5	19.1	374.2	62.6	15.2	311.6	6.4	20.3	196.8	719.3	8.0
Std. Dev.	8,961.0	6,505.8	1.2	6.0	2.6	3.0	36.7	16.0	8.3	42.4	1.8	7.5	351.8	248.1	3.5
Max	30,000.0	22,000.0	7.0	27.0	9.0	24.0	461.0	90.0	30.0	364.0	10.0	33.0	1,140.5	1,252.0	15.0
Min	28.0	33.5	3.0	3.0	2.0	15.0	319.0	44.0	7.0	248.5	4.0	11.0	4.0	445.0	5.0

Trace element data for Green agglomerate:

Sample	Zn	Cu	Ni	Ga	Mo	Nb	Zr	Y	Sr	Rb	U	Th	Pb	Ba	Sc
5-28.0	91.0	55.0	8.0	23.0	3.0	22.0	402.0	50.0	8.0	311.0	6.0	18.0	4.0	447.0	7.0
5-37.45	73.0	60.0	3.0	18.0	2.0	20.0	379.0	60.0	7.0	251.0	5.0	23.0	4.0	412.0	8.0
5-46.00	110.5	39.0	7.0	21.0	3.0	20.0	385.0	58.5	6.0	249.0	4.0	17.0	10.5	8.0	8.0
5-66.0	88.0	40.0	5.0	23.0	7.0	20.0	377.0	52.0	7.0	265.0	10.0	14.0	4.0	439.0	9.0
5-104.0	131.5	41.0	7.0	22.0	3.5	19.5	387.0	51.5	6.5	325.0	4.5	18.0	4.0	314.5	10.0
5-115.6	158.0	45.0	7.0	27.0	2.0	17.0	366.0	51.0	5.0	356.0	10.0	15.0	4.0	178.0	6.0
5-126.1	107.0	32.0	7.0	20.0	8.0	18.0	375.0	64.0	10.0	279.0	4.0	16.0	4.0	344.0	4.0
5-127.0	139.5	38.0	5.0	21.5	2.5	17.0	370.5	57.5	4.5	266.0	8.0	12.5	5.5	239.5	8.0
1-13.50	348.5	179.0	3.0	13.5	3.5	18.0	385.0	95.5	10.0	270.5	6.0	14.5	45.0	576.5	8.5
1-31.0	434.0	2,072.0	3.0	21.0	2.0	20.0	389.0	55.0	15.0	223.0	7.0	23.0	321.0	523.0	10.0
1-47.85	598.0	1,545.0	4.0	33.0	2.0	17.0	345.0	109.0	3.0	158.0	7.0	23.0	434.0	205.0	5.0
1-58.50	613.5	2,036.0	3.0	27.0	2.0	19.5	390.5	62.5	6.5	247.0	8.0	18.0	160.0	158.5	8.0
2-16.8	2,045.0	1,524.0	3.0	11.0	4.0	20.0	379.0	64.0	10.0	227.0	7.0	44.0	2,136.0	262.0	6.0
2-34.0	1,846.0	1,672.0	3.0	22.0	4.0	19.0	372.0	61.0	7.0	257.0	5.0	18.0	127.0	531.0	60.0
2-42.2	1,877.0	1,772.0	3.0	20.0	4.0	20.0	365.0	83.0	9.0	106.0	4.0	24.0	382.0	242.0	5.0
2-42.80	780.5	1,440.0	3.0	18.5	2.0	20.0	355.5	93.5	8.0	206.5	7.0	18.5	136.0	395.5	5.5
2-57.8	281.0	431.0	3.0	17.0	3.0	21.0	368.0	67.0	8.0	258.0	6.0	21.0	68.0	662.0	5.0
3-29.5	84.0	58.0	5.0	23.0	6.0	20.0	367.0	79.0	13.0	272.0	6.0	21.0	6.0	560.0	9.0
Average	544.7	726.6	4.5	21.1	3.5	19.3	375.4	67.4	7.9	251.5	6.3	19.9	214.1	360.9	10.1
Std. Dev.	669.3	836.3	1.8	4.9	1.7	1.4	13.6	17.3	2.9	57.0	1.8	6.9	499.4	173.8	12.5
Max	2,045.0	2,072.0	8.0	33.0	8.0	22.0	402.0	109.0	15.0	356.0	10.0	44.0	2,136.0	662.0	60.0
Min	73.0	32.0	3.0	11.0	2.0	17.0	345.0	50.0	3.0	106.0	4.0	12.5	4.0	8.0	4.0

Appendix C

X-ray diffraction pattern of a vein chlorite in GD2:

```
DIFFRACTION SCAN FOR    : CHLORITE- (RKW1)
FILE NAME               : RKW1
SCANNED FROM            : 5.00 TO 75.00
REPORT FROM             : 5.00 TO 75.00
STEP SIZE               : 0.05
LAMDA                   : 1.54
```

PEAK	2 THETA	D VALUE	INTENSITY	RELATIVE INTENSITY
1	6.20	14.241	11.00	15.28 ✓
2	12.60	7.018	72.00	100.00 ✓
3	15.40	5.748	3.00	4.17
4	18.85	4.703	10.00	13.89 ✓
5	19.70	4.502	3.00	4.17
6	20.90	4.246	4.00	5.56 ✓
7	25.25	3.523	55.00	76.39 ✓
8	26.60	3.348	6.00	8.33 ✓
9	29.15	3.060	2.00	2.78
10	30.20	2.956	1.00	1.39
11	31.60	2.828	7.00	9.72 ✓
12	33.40	2.680	13.00	18.06 ✓
13	35.65	2.516	7.00	9.72 ✓
14	36.85	2.437	16.00	22.22
15	42.50	2.125	4.00	5.56 ✓
16	45.00	2.012	3.00	4.17 ✓
17	50.05	1.821	16.00	22.22
18	51.80	1.763	3.00	4.17 ✓
19	54.00	1.696	2.00	2.78
20	54.90	1.671	2.00	2.78
21	56.25	1.634	4.00	5.56
22	56.95	1.615	3.00	4.17
23	59.25	1.558	5.00	6.94 ✓
24	60.90	1.520	2.00	2.78 ✓
25	63.05	1.473	2.00	2.78 ✓
26	65.10	1.431	2.00	2.78 ✓
27	66.15	1.411	4.00	5.56 ✓
28	69.80	1.346	3.00	4.17 ✓
29	71.05	1.325	2.00	2.78 ✓
30	72.15	1.308	2.00	2.78 ✓
31	73.10	1.293	2.00	2.78 ✓

CHLORITE- (RKW1)

125
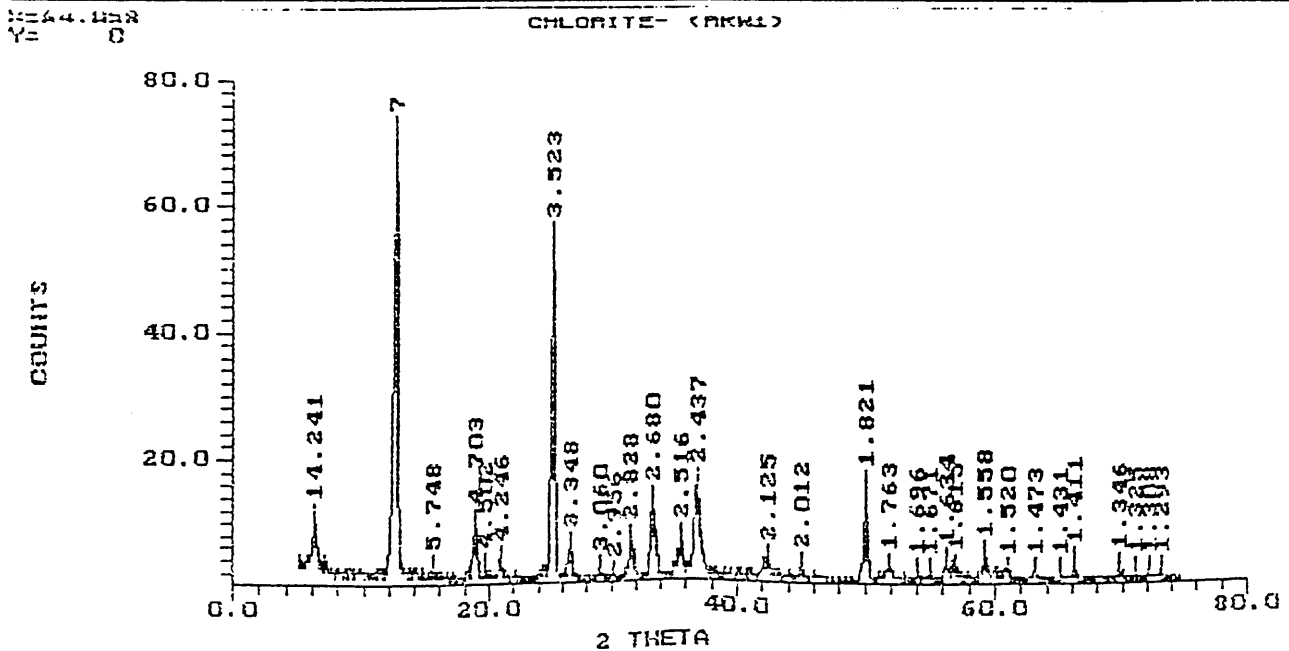
X-ray diffraction pattern of the vein chlorite in GD2 after treatment with an ethylene glycol solution to test for the presence of a swelling clay. If a swelling clay is present, the position of the 14.127Å line would shift to the left of the diagram (i.e. lower 2 θ values).

126

Appendix D

X-ray diffraction pattern of copper sulphides (and other alteration minerals) in a vein in GD2:

```
DIFFRACTION SCAN FOR  : CUSULPHIDES- (WVDB71)
FILE NAME             : WVDB71
SCANNED FROM          : 5.00 TO 75.00
REPORT FROM           : 5.00 TO 75.00
STEP SIZE             : 0.05
LAMDA                 : 1.54
```

PEAK	2 THETA	D_VALUE	INTENSITY	RELATIVE INTENSITY
1	14.75	6.001	9.72	18.40 •
2	17.50	5.063	14.64	27.72(0) •
3	21.15	4.197	21.54	40.78 o
4	24.00	3.705	14.46	27.37 •
5	24.70	3.601	4.44	8.40 .
6	26.25	3.392	17.39	32.93(o) X
7	26.60	3.348	12.38	23.44 ✓ ->
8	27.90	3.195	13.35	25.27 ✓ x
9	28.65	3.113	7.32	13.87 x
10	29.30	3.046	17.31	32.76(•) x
11	30.25	2.952	6.28	11.89 x
12	31.20	2.864	22.25	42.13 • x
13	32.15	2.782	18.22	34.50 ✓ • ,
14	33.10	2.704	15.20	28.77 o x
15	33.60	2.665	10.18	19.28 X
16	35.53	2.523	26.13	49.46 • ⁄
17	36.60	2.453	25.10	47.51 o x
18	37.60	2.390	39.07	73.97 % x
19	41.20	2.189	10.96	20.76 o •
20	42.35	2.132	8.93	16.91 ✓
21	43.60	2.074	7.90	14.95 .
22	46.30	1.959	52.82	100.00 ✓ •
23	48.60	1.872	45.75	86.62 X
24	51.70	1.767	7.66	14.51
25	53.10	1.723	9.62	18.22 C
26	54.05	1.695	19.60	37.10(•) x
27	54.55	1.681	14.58	27.61 ✓
28	58.75	1.570	7.46	14.13 o
29	68.75	1.364	6.18	11.7 c

CUSULPHIDES- (WVDB71)

X=82.919
Y= 11

COUNTS vs 2 THETA
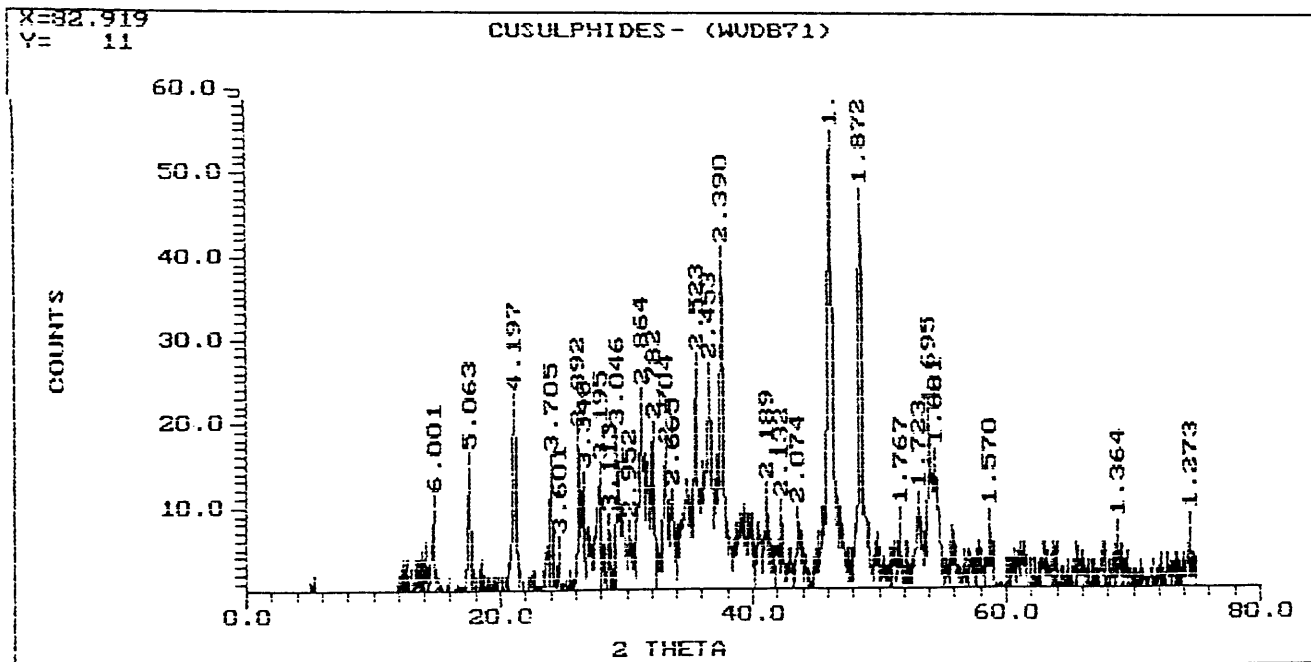
Appendix E

Analytical conditions for minerals analysed with the electron microprobe:

Chlorite:

Accelerating potential:	20 kV
Probe current:	20 nA
Lines analysed:	K α
Standard:	chlorite
Reproducibility:	FeO:1.81, MgO:0.57, Al$_2$O$_3$:1.25, SiO$_2$:1.20

Arsenopyrite:

Accelerating potential:	20 kV
Probe current:	20 nA
Lines analysed:	K α
Standard:	arsenopyrite and CoS$_2$
Reproducibility:	Fe:0.797, As:0.65, Co:0.765, S:0.629

Bi-Pb-Cu-Sulfosalt:

Accelerating potential:	20 kV
Probe current:	20 nA
Lines analysed:	K α (Bi,S and Cu) and L α (Pb)
Standards:	Bismuthinite, cuprite, and PbTe.

Sphalerite:

Accelerating potential:	20 kV
Probe current:	20 nA
Lines analysed:	K α
Standard:	sphalerite, troilite and chalcopyrite.

Siderite:

Accelerating potential:	20 kV
Probe current:	20 nA
Lines analysed:	K α
Standard:	FeO, MnO, MgO and CaO.

Chlorite microprobe analyses (with calculated temperatures according to Walshe's thermometer):

Name	1-20.8	1-25.9				1-61.9	1-62			2-54			
No.	7	3	7	6	9	10	5	2	6	9	3	4	7	8
Na_2O	0.59	0.54	0.92			0.48	0.06	0.12					1.2	0.05
FeO (total)	41.52	46.05	42.9	42.75	45	42.78	41.53	42.44	42.28	42.59	42.15	44.71	44.48	44.28
MnO	0.49	0.1	0.38	0.34	0.07	0.34	0.46	0.41	0.36	0.36	0.52	0.12	0.18	0.26
SiO_2	21.26	20.58	21.44	21	20.2	20.61	20.45	20.56	20.51	20.51	21.32	20.28	20.56	19.83
Al_2O_3	21.38	19.38	19.93	19.52	18.76	21.04	19.6	20.11	19.28	19.59	20.2	20.08	19.51	19.28
MgO	1.62		1.49	1.79		1.45	0.89	1.97	0.65	2.2	1.64		0.18	0.17
TiO_2	0.04				0.03		0.01				0.04	0.06		
CaO		0.04	0.02			0.01	0.03			0.01				0.07
K_2O		0.05		0.03			0.02				0.04		0.01	0.01
NiO			0.08	0.04	0.05	0.05		0.01		0.02	0.02		0	0.24
Cr_2O_3		0.01							0.02		0.03		0.02	0.01
ZnO		0.31	0.15	0.02	0.01	0.01	0.44	0.16	0.26				0.17	0.19
Total	86.9	87.06	87.31	85.59	84.12	86.77	83.49	85.78	83.36	85.28	85.96	85.25	86.31	84.39
Na^+	0.28	0.28	0.28	0.28	0.28	0.28	0.28	0.28	0.28	0.28	0.28	0.28	0.28	0.28
Fe^{2+}	8.2	8.2	8.2	8.2	8.2	8.2	8.2	8.2	8.2	8.2	8.2	8.2	8.2	8.2
Mn^{2+}	0.1	0.1	0.1	0.1	0.1	0.1	0.1	0.1	0.1	0.1	0.1	0.1	0.1	0.1
$Si^{4+}(T)$	5.02	5.02	5.02	5.02	5.02	5.02	5.02	5.02	5.02	5.02	5.02	5.02	5.02	5.02
$Al^{3+}(T)$	2.98	2.98	2.98	2.98	2.98	2.98	2.98	2.98	2.98	2.98	2.98	2.98	2.98	2.98
$Al^{3+}(O)$	2.98	2.98	2.98	2.98	2.98	2.98	2.98	2.98	2.98	2.98	2.98	2.98	2.98	2.98
Mg^{2+}	0.58	0.58	0.58	0.58	0.58	0.58	0.58	0.58	0.58	0.58	0.58	0.58	0.58	0.58
Ti^{4+}	0	0	0	0	0	0	0	0	0	0	0	0	0	0
Ca^{2+}	0	0	0	0	0	0	0	0	0	0	0	0	0	0
K^+	0	0	0	0	0	0	0	0	0	0	0	0	0	0
Ni^{2+}	0	0	0	0	0	0	0	0	0	0	0	0	0	0
Cr^{3+}	0	0	0	0	0	0	0	0	0	0	0	0	0	0
Zn^{2+}	0	0	0	0	0	0	0	0	0	0	0	0	0	0
cations	20.12	20.12	20.12	20.12	20.12	20.12	20.12	20.12	20.12	20.12	20.12	20.12	20.12	20.12
Fe/(Fe+Mg)	0.935	1	0.969	0.931	1	0.963	0.925	0.973	0.916	0.935	1	0.993	0.993	0.912
Temp.	339.5	340	322.4	333.2	331.9	323.7	329.1	319	329.8	324.8	353.2	330	338.8	332.5

Name	2-79.63A			2-79.63A			2-90.4	3-152.4			5-154.65		5-73.4				
No.	3	6	10	3	6	10	1	2	4	9	4	10	2	4	5	9	10
Na_2O								0.55		0.16					0.46		
FeO (total)	41.99	42.25	44.93	41.99	42.25	44.93	42.65	39.58	41.44	41.18	41.4	42.15	43.59	42.74	44.07	43.69	43.8
MnO	0.43	0.4	0.24	0.43	0.4	0.24	0.6	0.34	0.28	0.62	0.65	0.75	0.12	0.2	0.16	0.17	0.18
SiO_2	21.02	21.46	20.87	21.02	21.46	20.87	20.88	21.22	21.27	21.91	20.76	20.67	20.31	20.48	20.06	20.56	20.8
Al_2O_3	19.55	20.17	19.73	19.55	20.17	19.73	19.39	19.66	19.84	19.54	18.69	18.72	18.52	19.23	19.6	19.65	19.67
MgO	1.54	2.36	0.3	1.54	2.36	0.3	1.69	0.18	0.16	2.18	2.02	1.11	0.64	0.51		0.6	0.69
TiO_2	0.04			0.04			0.05		0.01						0.09	0.01	0.06
CaO		0.04			0.04		0.05	0.01			0.01	0.08		0.05			0.05
K_2O	0.01		0.02	0.01		0.02	0.07	0.18					0.01		0.05		0.03
NiO			0.02			0.02									0.2		
Cr_2O_3							0.01		0.01								
ZnO	0.34	0.05	0.15	0.34	0.05	0.15		0.35	0.11	0.04	0.02		0.26			0.2	
Total	84.92	86.73	86.26	84.92	86.73	86.26	85.39	82.07	83.12	85.63	83.55	83.48	83.45	83.21	84.69	84.88	85.28
Na^+	0.28	0.28	0.28	0.28	0.28	0.28	0.28	0.28	0.28	0.28	0.28	0.28	0.28	0.28	0.28	0.28	0.28
Fe^{2+}	8.2	8.2	8.2	8.2	8.2	8.2	8.2	8.2	8.2	8.2	8.2	8.2	8.2	8.2	8.2	8.2	8.2
Mn^{2+}	0.1	0.1	0.1	0.1	0.1	0.1	0.1	0.1	0.1	0.1	0.1	0.1	0.1	0.1	0.1	0.1	0.1
$Si^{4+}(T)$	5.02	5.02	5.02	5.02	5.02	5.02	5.02	5.02	5.02	5.02	5.02	5.02	5.02	5.02	5.02	5.02	5.02
$Al^{3+}(T)$	2.98	2.98	2.98	2.98	2.98	2.98	2.98	2.98	2.98	2.98	2.98	2.98	2.98	2.98	2.98	2.98	2.98
$Al^{3+}(O)$	2.98	2.98	2.98	2.98	2.98	2.98	2.98	2.98	2.98	2.98	2.98	2.98	2.98	2.98	2.98	2.98	2.98
Mg^{2+}	0.58	0.58	0.58	0.58	0.58	0.58	0.58	0.58	0.58	0.58	0.58	0.58	0.58	0.58	0.58	0.58	0.58
Ti^{4+}	0	0	0	0	0	0	0	0	0	0	0	0	0	0	0	0	0
Ca^{2+}	0	0	0	0	0	0	0	0	0	0	0	0	0	0	0	0	0
K^+	0	0	0	0	0	0	0	0	0	0	0	0	0	0	0	0	0
Ni^{2+}	0	0	0	0	0	0	0	0	0	0	0	0	0	0	0	0	0
Cr^{3+}	0	0	0	0	0	0	0	0	0	0	0	0	0	0	0	0	0
Zn^{2+}	0	0	0	0	0	0	0	0	0	0	0	0	0	0	0	0	0
cations	20.12	20.12	20.12	20.12	20.12	20.12	20.12	20.12	20.12	20.12	20.12	20.12	20.12	20.12	20.12	20.12	20.12
Fe/(Fe+Mg)	0.909	0.988	0.934	0.909	0.988	0.934	0.953	0.956	0.984	0.92	0.955	0.975	0.979	1	0.976	0.973	0.941
Temp.	332	329.6	334.4	332	329.6	334.4	360.6	323.9	360.5	321.8	317	323.3	319.4	345.5	332.9	326.5	333.6

129

Appendix G

Microprobe analyses of siderite (wt%) in the brecciation zone between the agglomerate and the rhyolite:

FeO	MnO	MgO	CaO	Total
55.7	2.7	0.4	0.75	59.54
54.6	2.8	0.6	0.93	58.95
55.6	2.6	0.4	1.31	59.94
56.5	2.8	0.4	0.58	60.31
53.7	3.4	1.4	0.60	59.19
56.4	2.0	0.3	0.61	59.30
55.7	3.8	0.7	0.53	60.73
55.8	2.5	0.8	0.37	59.50
55.4	2.8	0.8	0.29	59.26
55.6	2.9	0.6	0.68	59.76
55.0	2.8	0.9	0.83	59.59
53.5	3.9	0.7	0.57	58.70
56.1	2.3	0.7	0.31	59.47
58.8	0.5	0.6	0.08	60.07
58.6	0.9	0.9	0.00	60.41
58.8	0.6	0.6	0.21	60.25
58.7	0.9	0.6	0.00	60.17
57.0	2.3	0.6	0.09	59.93
59.1	0.6	0.8	0.00	60.50
57.3	1.4	0.8	0.31	59.75
58.2	0.4	0.8	0.43	59.80
57.0	2.1	0.7	0.14	59.92
56.4	1.9	0.9	0.20	59.43
58.4	1.8	0.5	0.17	60.95
55.8	2.5	0.9	0.43	59.62
59.0	0.6	0.6	0.33	60.45
55.4	3.0	0.7	0.46	59.52
55.7	2.4	0.7	0.30	59.11
54.6	2.7	0.5	0.73	58.59
54.1	3.8	0.5	0.79	59.21
54.5	3.1	0.7	0.69	59.01
56.6	2.5	0.5	0.33	59.86
55.7	3.0	0.4	0.58	59.76
55.3	2.9	0.9	0.51	59.56
55.0	2.7	0.7	0.84	59.18
55.7	2.8	0.5	0.35	59.39
55.6	2.6	0.8	0.57	59.59
55.7	2.7	0.9	0.34	59.66
56.4	2.7	0.5	0.62	60.18
56.0	2.4	0.4	0.54	59.29
56.8	2.5	0.4	0.22	59.89
55.1	3.0	0.8	0.62	59.51
55.6	2.4	0.9	0.75	59.58
56.5	2.3	0.5	0.57	59.88
57.4	1.8	0.3	0.15	59.73
57.0	2.1	0.5	0.13	59.73
53.8	3.3	1.2	0.70	59.07

FeO	MnO	MgO	CaO	Total
56.1	2.8	0.8	0.30	60.02
57.9	2.2	0.6	0.19	60.82
56.6	2.2	0.6	0.16	59.53
56.8	2.2	0.5	0.11	59.65
57.8	1.3	0.6	0.17	59.90
45.6	6.7	5.3	0.13	57.70
57.2	1.8	0.5	0.17	59.64
56.1	2.4	0.9	0.52	59.91
57.0	2.3	0.3	0.17	59.79
56.0	2.3	0.6	0.30	59.30
54.9	2.5	0.6	0.95	58.88
57.3	1.7	0.0	0.20	59.24
56.1	2.4	0.7	0.42	Average
1.95	1.0	0.7	0.28	Std. Dev.
59.1	6.7	5.3	1.31	Max
45.6	0.4	0.0	0.00	Min

Appendix H

Microprobe analysis of arsenopyrite (wt%) in the hydrothermal veins.

Fe	As	S	Co	Total	As/S
27.2	49.4	17.7	6.7	101.08	2.79
31.8	48.4	17.5	1.9	99.92	2.77
31.7	49.7	17.2	1.8	100.3	2.89
31.9	48.3	18.1	1.9	100.33	2.67
32	48.1	18	2	100.59	2.67
30	49.3	17.9	3.8	101.24	2.75
29.7	48.3	17.6	3.7	99.61	2.74
31.2	48.1	18.2	2.8	100.66	2.64
30.8	47.8	18.2	3	100.24	2.63
29.6	49.4	17.2	4	100.34	2.87
30	49.1	17.3	3.7	100.33	2.84
30.7	49.5	17.7	3.1	101.07	2.80
30.6	48.6	17.5	3.2	100.21	2.78
30.5	48.6	17.6	3.1	99.86	2.76
30.1	49.2	17.8	3.4	100.61	2.76
30	49.6	17.3	3.7	100.94	2.87
29.6	49.8	17.2	3.5	100.32	2.90
30.2	48.6	17.7	3.4	100.25	2.75
29.8	48.2	17.7	3.8	100.35	2.72
30	49.3	17.2	3.1	100.71	2.87
30	49	17.2	3.2	100.62	2.85
29.8	49.7	16.9	3.9	101.21	2.94
29.3	49.2	16.7	3.9	99.23	2.95
28.4	48.2	17.9	5.4	99.95	2.69
28	48.6	17.8	5.6	100.25	2.73
31.1	49.6	17.4	2.4	100.69	2.85
30.7	48.1	17.5	2.4	99.11	2.75
30.8	48.3	17.9	2.7	100.71	2.70
30.5	47.8	17.9	3	99.43	2.67
32.3	48.5	17.8	1.4	101.54	2.72
32	48.7	17.9	1.6	100.88	2.72
30.7	48.8	18	3	100.77	2.71
30.6	48.1	17.8	3	99.74	2.70
32.9	48.3	17.9	0.9	100.06	2.70
32.6	48	18	0.8	99.66	2.67
29.9	49	17.4	3.6	100.54	2.82
30.2	47.3	17.4	3.6	98.61	2.72
31.6	48.8	17.5	2.2	100.29	2.79
31.4	49.5	17.8	2.2	102.03	2.78
28.6	49.5	17	4.5	99.88	2.91
28.8	49.7	16.9	4.5	100.15	2.94
29.4	48.5	17.5	4.1	100.92	2.77
29.3	47.3	17.6	4.2	98.82	2.69
29.4	49.8	17.3	4.4	101.23	2.88
30.4	48.9	17.4	3.9	100.89	2.81
29.9	48.5	17.4	4	100.52	2.79
27.3	48.9	17.1	6	99.85	2.86
27.2	48.8	16.8	6.2	99.93	2.90
28.7	49.5	17.4	4.8	100.78	2.84
28.4	48.5	17	4.9	99	2.85
25.8	49.5	17	7.7	100.2	2.91
25.7	49.1	16.9	7.7	100.25	2.91
25.7	49.4	17.4	7.9	100.65	2.84

Fe	As	S	Co	Total	As/S
25.9	48.8	17.3	7.7	100.06	2.82
25.9	42.9	14.4	6.8	89.98	2.98
25.8	42.6	14.5	6.7	89.96	2.94
27.6	49.9	16.3	5.7	99.76	3.06
27.5	50.8	16.3	5.6	100.6	3.12
31.9	48.9	17.4	1.8	100.16	2.81
31.4	48.4	17.4	2	99.22	2.78
31.7	48.8	17.3	1.9	100.57	2.82
30.1	48.6	16.8	3.1	98.92	2.89
30.5	49.1	17.8	3	100.55	2.76
30.6	48	17.5	3	99.88	2.74
31.7	48.4	17.7	2	100.12	2.73
31.5	47.9	17.5	1.9	99.21	2.74
28.1	48.7	17.4	5.6	100.33	2.80
28.2	48.3	17.5	5.6	99.83	2.76
30.4	49	17.5	3.4	100.41	2.80
30.4	48.4	17.6	3.2	100.91	2.75
33	49.5	18	1	101.74	2.75
32.6	48.9	17.8	0.9	101.3	2.75
28.8	49.6	17.6	4.8	101.19	2.82
28.6	49.3	17.5	5	100.61	2.82
32.6	48.5	17.6	0.5	99.6	2.76
33.2	48	17.5	0.7	99.47	2.74
33.1	48.1	18.1	0.4	99.78	2.66
33	47.3	18.1	0.3	98.72	2.61
31.7	48.8	17.5	1.7	100.09	2.79
31.6	48.6	17.6	1.5	99.36	2.76
30.7	50.2	16.8	2.2	101.7	2.99
30.6	48.8	16.8	2.3	98.73	2.90
31.3	47.2	18.1	2.4	98.92	2.61
30.9	47.8	18.2	2.5	100.73	2.63
31.5	48.8	17.4	1.9	99.78	2.80
31.6	49	17.3	2	100.56	2.83
31.2	49.1	17.6	2.8	100.78	2.79
30.8	49.9	17.3	2.7	100.86	2.88
27.2	49.2	16.8	6.4	101.24	2.93
27.4	49.2	17.1	6.4	100.61	2.88
27.7	50	16.7	5.9	101.01	2.99
27.6	49.7	16.8	5.9	100.86	2.96
28	50.1	17	5.6	101.5	2.95
28.2	50	17	5.4	100.84	2.94
28.1	49.5	16.9	5.3	100.23	2.93
28	50.8	16.7	5.4	101.14	3.04
27.4	49.6	16.6	5.3	99.44	2.99
28.3	49.3	16.8	5.1	99.9	2.93
28.2	48.7	16.8	4.9	99.54	2.90
28	48.7	16.9	5	98.62	2.88
28.2	49.4	16.8	5.2	99.73	2.94
27.9	49.6	16.9	5.4	100.14	2.93
27.9	48.3	16.7	5.5	99.45	2.89
28.1	48.9	17.1	4.9	99.17	2.86
28.1	48.5	17	5	98.75	2.85
29.7	48.1	17.5	3.7	99.31	2.75
29.7	47.3	17.4	3.5	98.03	2.72
30.1	48.7	16.8	3	98.65	2.90
30.4	49.9	16.8	3.1	100.31	2.97
28.2	50.1	17	5.2	100.52	2.95

Fe	As	S	Co	Total	As/S
27.9	49.8	16.9	5.1	99.97	2.95
26.2	47.7	16.5	6.8	98.6	2.89
25.7	48.7	17	7.9	99.41	2.86
25.8	48.7	17.4	7.9	100.31	2.80
28.4	48.6	17	5.1	100.49	2.86
28.2	49.1	17.3	5.1	100.59	2.84
26.7	49.7	16.5	6.1	99.86	3.01
27.1	49.1	16.4	6.3	99.87	2.99
28.4	49.4	16.7	5.1	99.87	2.96
28.1	49.8	16.7	4.9	100.03	2.98
29.6	49.1	17	4	100.01	2.89
29	50.6	17	4	101.49	2.98
29.5	49.6	17.1	4	100.35	2.90
29.1	49.3	16.9	4.2	100.08	2.92
30	47	18.5	4	99.61	2.54
29.5	47.5	18.5	4.1	100.12	2.57
32	48.5	17.6	1.9	100.63	2.76
31.5	48.2	17.6	1.9	100.33	2.74
32.2	49.3	17.7	1.4	100.8	2.79
32.1	47.9	17.8	1.3	99.06	2.69
27.7	47.6	17.6	6.7	99.77	2.70
27	48.4	17.7	6.4	99.8	2.73
30.3	49.3	16.8	2.8	99.74	2.93
30.4	49.8	17.1	2.6	99.99	2.91
29.2	48.6	16.9	4.1	99.37	2.88
29	48.6	16.9	3.9	98.86	2.88
32.6	48	17.5	0.9	99.02	2.74
32.2	48.5	17.7	1	99.53	2.74
27.7	49.1	17	5.9	99.95	2.89
27.3	48.6	16.8	6	99.12	2.89
31.2	47.9	17.7	2.4	99.46	2.71
30.8	47.5	17.9	2.2	99.42	2.65
29.8	49.1	17	4	99.98	2.89
29.2	49.5	17.1	3.9	100.18	2.89
29.2	49.5	16.8	4	100.64	2.95
29.1	48.9	16.8	4.1	101.3	2.91
29.5	50.1	17.1	3.7	101.19	2.93
29.7	50.2	16.9	3.9	101.63	2.97
28.8	49.5	17.1	4.8	101.33	2.89
28.6	49	16.9	4.5	100.02	2.90
30	49.4	17.4	3.6	100.6	2.84
29.8	49.1	17.6	3.9	100.91	2.79
29.8	49.6	17	3.8	100.38	2.92
30	49.1	17.1	3.8	101.6	2.87
32.6	48.1	18	1.1	100	2.67
32.2	47.8	18.1	1	99.35	2.64
31	47.8	17.6	2.5	99.38	2.72
31.2	48.3	17.6	2.4	100.28	2.74
25.7	50.8	15.1	7.5	101.43	3.36
25.2	50.9	15.2	7.4	99.9	3.35
27.9	49.3	16.8	5.7	100.66	2.93
27.5	50.1	16.7	5.6	100.91	3.00
31.7	50.3	17.2	2.1	102.1	2.92
31.4	47.8	17.1	2.1	98.96	2.80
26.5	49.8	16.6	7.3	101.83	3.00
26.9	49.3	17	7.1	101.33	2.90
26.7	50.2	16.4	7	101.38	3.06

Fe	As	S	Co	Total	As/S
26.6	50.1	16.4	6.9	100.13	3.05
28.8	49.1	17	4.8	99.9	2.89
28.3	49.1	16.8	5	100.58	2.92
28	50	16.9	5.5	100.59	2.96
27.9	49.2	17	5.6	100.38	2.89
30.3	49.4	17.2	3.3	100.92	2.87
30.4	49.2	17	3.1	99.99	2.89
29.9	50.2	16.8	3.1	100.41	2.99
29.5	49	16.7	3.2	98.6	2.93
30.8	49.1	17.1	2.6	99.91	2.87
30.9	48.7	17.3	2.4	100.36	2.82
30.5	47.8	17.5	3.6	99.99	2.73
30.3	47.9	17.7	3.6	99.74	2.71
26.8	50.8	16.6	7	101.39	3.06
26.7	50.6	16.5	7.1	101.21	3.07
30.8	49.3	17.3	2.8	100.23	2.85
28.9	51.5	16.4	4.3	101.2	3.14
29	49.9	16.1	4.1	100.86	3.10
29.2	50.1	16.4	4.6	101.36	3.05
28.7	49.9	16.9	4.6	100.15	2.95
28.8	49.4	16.8	4.5	99.83	2.94
28.8	49.5	16.4	4.1	99.97	3.02
28.9	50.6	16.7	4	101.25	3.03
31.2	50.4	16.9	1.9	101.81	2.98
31.8	49.5	17.1	2	100.67	2.89
30.8	49.4	17.7	2.8	100.99	2.79
30.7	48.7	17.6	2.8	100.3	2.77
29.6	49.8	16.9	3.4	99.75	2.95
31.3	49.5	17	2.2	100.22	2.91
31.7	49.4	17.1	2.2	100.81	2.89
30	50	16.5	3.3	100.03	3.03
29.9	50.2	16.6	3.1	100.44	3.02
27.9	48.7	17	6	99.7	2.86
27.7	49.6	17.2	5.8	100.35	2.88
27.6	50.5	16.9	5.9	101.69	2.99
27.7	49.9	16.8	5.9	100.69	2.97
33.4	47.9	18.4	1	101.39	2.60
33.1	47.5	18.3	1	100.24	2.60
27.9	49.8	16.8	5.6	100.34	2.96
28.3	49.8	16.8	5.5	100.47	2.96
30	50.1	17	3.2	101.47	2.95
30.5	50.3	17.2	3.3	102.19	2.92
28.3	49.9	16.9	5.6	101.32	2.95
28.4	49.6	16.8	5.3	100.57	2.95
30.3	49.7	17.2	3.2	100.58	2.89
30.3	49.4	17.1	3.3	100.7	2.89
31.3	48.7	17.9	2.3	100.32	2.72
31.4	49	17.5	2.4	101.15	2.80
31.4	49.7	17.8	2.3	101.9	2.79
31.6	48.6	17.5	2.4	100.27	2.78
30.4	48.5	17.7	3.1	100.84	2.74
30.7	49.3	17.8	3	100.93	2.77
32.2	48	17.5	1.6	99.41	2.74
32.1	49.2	17.5	1.6	100.86	2.81
30.7	48.2	17.8	3.3	100.07	2.71
30.1	48	17.9	3.1	99.48	2.68
31	49.9	17.1	2.8	101.27	2.92

Fe	As	S	Co	Total	As/S
30.8	48.4	17.1	2.6	99.34	2.83
30.2	50.2	17.2	3.4	101.77	2.92
30.2	50.2	17.2	3.4	101.97	2.92
31	50.8	17.2	2.4	102.23	2.95
30.9	50.4	17	2.4	101.66	2.96
31.1	49.5	17.5	2.1	100.56	2.83
31	49.6	17.5	2.2	100.98	2.83
26.9	50	16.9	6.5	100.47	2.96
27.3	49.6	16.7	6.5	101.3	2.97
27.2	50.5	16.8	6.3	101.56	3.01
26.8	49.1	16.6	6.4	99.94	2.96
25.6	51.1	15.6	7.5	101.28	3.28
25.5	50.6	15.3	7.6	101.47	3.31
25.7	51.8	16	7.8	101.4	3.24
25.6	50.8	15.9	7.8	100.42	3.19
23.4	52.9	15.2	9.7	102.68	3.48
23.7	51.8	15.2	9.8	100.67	3.41
29.5	50	16.8	4.5	101.52	2.98
29	50.1	16.7	4.5	101.48	3.00
28.5	49.7	16.8	5.1	100.13	2.96
28.6	50.1	16.9	5	100.96	2.96
29.8	49.8	17.2	4.3	101.1	2.90
29.5	49.6	17.1	4.3	100.81	2.90
26.6	51	16	6.5	101.54	3.19
26.7	50.3	15.8	6.5	101.12	3.18
26.1	50.2	16.5	7.7	100.85	3.04
31.9	48.2	18.1	1.5	99.83	2.66
31.9	48.6	17.9	1.6	100.1	2.72
31.9	49.2	17.7	2	100.94	2.78
31.7	48.7	17.8	2.2	101.02	2.74
32.2	49.2	17.8	1.8	101.26	2.76
32.1	49.5	17.6	1.8	101.05	2.81
29.1	49	17.2	4.9	100.53	2.85
31.5	49.1	17.8	2.4	101.1	2.76
31.2	49.4	17.8	2.5	100.87	2.78
30.9	48.6	18	2.9	101.44	2.70
30.7	48.3	17.8	2.7	99.62	2.71
29	49.4	17.1	4.4	101.15	2.89
29	49.8	17.2	4.8	100.68	2.90
29.5	49.5	17.7	4.5	101.16	2.80
29.5	49.6	17.4	4.2	100.89	2.85
27.9	46.6	18.4	3.9	97.58	2.53
29	48.4	17.8	5.2	101.12	2.72
29.5	49.4	17.4	4.4	100.79	2.84
30.6	49.4	17.4	3.7	101.68	2.84
30.2	50	17.5	3.4	101.46	2.86
29.4	49.4	16.8	4.1	100.56	2.94
31.6	49.2	17.8	2.2	100.79	2.76
29	49.9	17.3	4.6	101.45	2.88
28.1	51.5	15.3	4.8	100.51	3.37
27.5	51.9	15.4	5.4	101.2	3.37
26.6	50.9	16.4	6.9	101.64	3.10
29.4	48.3	17.8	4.2	99.78	2.71
29.3	49.4	16.7	4.1	100.29	2.96
29.6	50	17	4	101	2.94
29.1	50.7	16.6	4.7	101.25	3.05
30.5	48.6	17.4	3.1	100.2	2.79

Fe	As	S	Co	Total	As/S
30.5	48.8	17.6	3	100.09	2.77
30.5	50.2	16.9	3.1	101.01	2.97
30.3	49.5	17.2	3.1	100.07	2.88
27.8	50.4	16.8	5.6	101.78	3.00
27.5	49.8	16.7	5.9	100.91	2.98
29.7	49.7	17.2	3.8	100.66	2.89
29.9	49.5	17.2	3.7	100.36	2.88
27.9	50.5	16.5	6.3	101.52	3.06
27.3	51.1	16.4	6.1	101.03	3.12
32.2	49.4	17.7	1.4	101.03	2.79
32.2	49.4	17.5	1.5	101.11	2.82
29.7	50.8	16.8	4.2	101.8	3.02
29.1	50.9	16.8	4.4	101.45	3.03
26	49.7	16.9	8.1	101.54	2.94
25.9	49.9	16.9	8	101.94	2.95
29.1	49.2	17.7	4.8	101.1	2.78
30	47.8	17.4	3.5	98.76	2.75
29.6	48.6	17.1	3.6	99.21	2.84
27.5	49.1	17.5	5.8	100.47	2.81
27.6	48.5	17.4	5.9	100.53	2.79
25.7	50.4	15.5	8	100.3	3.25
27.8	49.3	16.9	5.2	99.87	2.92
27.9	48.4	16.8	5.4	98.56	2.88
27.3	49.2	16.6	5.5	98.97	2.96
27.2	49.5	16.6	5.5	100.77	2.98
28	49.6	16.6	5.7	100.6	2.99
30.3	50	16.9	3.5	100.95	2.96
30	49.6	17.3	3.5	100.59	2.87
29.9	50	17.3	3.6	101.12	2.89
30.6	50.5	17	3.1	101.65	2.97
30.2	50.9	16.9	2.7	101.41	3.01
29.5	50.4	17.3	3.9	101.34	2.91
29.8	50.4	17.2	3.7	101.66	2.93
29.9	49.9	17.3	4	101.42	2.88
29.6	49.6	17.1	3.9	101.13	2.90
29.2	50	16.8	4	100.13	2.98
28.7	49.5	17.3	5	100.87	2.86
29.5	49.1	17	4	99.8	2.89
29.5	49.5	17.1	4.2	100.49	2.89
29.4	51.2	16.3	4	100.97	3.14
29.2	51.2	16.4	4.1	101.35	3.12
25	51.6	15.7	8.6	101.67	3.29
25	52	15.6	8.2	101.48	3.33
32.6	49	18.2	1.3	101.5	2.69
32.8	48.3	18.1	1.4	100.75	2.67
30	48.9	17.9	4	100.92	2.73
30.1	48.3	17.7	4	100.36	2.73
26.6	50	16.6	6.4	99.63	3.01
26.5	50.1	16.5	6.5	100.04	3.04
29.4	48.9	17	3.6	99.4	2.88
29.5	48.5	17.4	3.6	99.63	2.79
32.1	48.2	17.8	1.7	99.91	2.71
32	48.1	17.8	1.8	100.64	2.70
26.1	52.1	15.4	6.6	101.13	3.38
26.1	50.8	15.3	6.8	99.06	3.32
29.6	49.2	17.2	4.3	100.91	2.86
29.6	48.5	17.2	4	100.09	2.82

Fe	As	S	Co	Total	As/S
24.2	51.6	15.2	8.1	99.3	3.39
24.3	51.2	15.5	8.5	99.77	3.30
27.2	49.9	16.8	5.8	100.76	2.97
26.9	49.3	16.7	5.9	98.91	2.95
27.2	49	17.1	6.4	100.24	2.87
27.2	49.3	17.2	6.3	100.24	2.87
27.1	49.2	17.3	7.2	101.1	2.84
26.8	49	17.4	7.4	100.99	2.82
27.2	49.1	17.1	6.5	100.27	2.87
27	50.1	17	6.6	100.73	2.95
27.4	49.1	17.4	6.3	100.79	2.82
31.1	48	17.2	2.5	99.01	2.79
31	48.5	17.2	2.4	99.28	2.82
26.6	49.8	17.1	7.2	100.9	2.91
26.5	49.7	16.9	7.1	100.51	2.94
31.6	48.7	17.1	1.4	98.89	2.85
31.9	49.8	17.5	1.3	100.74	2.85
30.9	48.7	17.5	2.7	99.9	2.78
30.7	48.8	17.7	3	100.62	2.76
32.3	48.6	17.9	1.4	100.53	2.72
32.4	48.6	17.7	1.4	100.19	2.75
28.3	49.3	17.5	5.5	100.82	2.82
28.4	49.4	17.5	5.4	100.85	2.82
28.6	48.4	17.6	4.8	100.75	2.75
28.3	48.5	17.6	5	99.93	2.76
25.8	49.7	16.6	7.7	100.37	2.99
27.2	50.2	17.3	6.5	101.64	2.90
27.6	49.1	17.4	6.6	101.48	2.82
26.7	50	17.2	6.7	100.79	2.91
26.8	50.5	17	6.5	101.26	2.97
30.2	48.6	17.5	3.7	100.14	2.78
30	48.6	17.5	3.8	100.9	2.78
28.7	49	17.4	5.2	100.65	2.82
28.6	50.1	17.4	5.1	102.09	2.88
27.7	49.5	17.5	5.8	101.01	2.83
27.2	48.7	17.2	5.6	99.46	2.83
27.2	50.3	16.6	6.4	101.2	3.03
27.3	50.6	16.9	6.3	101.18	2.99
30.2	49.6	17.5	3.1	100.52	2.83
30.5	48.7	17.3	3.3	100.14	2.82
27.5	48.9	17.5	6	99.99	2.79
27.9	48.8	17.3	6.1	100.54	2.82
25.6	49.7	16.3	8	99.8	3.05
25.6	50.8	16.5	8	100.9	3.08
30.3	48.4	17.9	3.3	100	2.70
30.3	48.8	18	3.3	100.51	2.71
26.2	50.8	16.4	7.3	100.91	3.10
25.9	50.3	16.4	7.2	99.84	3.07
29	49.6	16.5	4.7	100.69	3.01
28.5	50	16.7	4.7	100.04	2.99
30.2	48.9	17.3	3.4	101.5	2.83
30.2	49.6	17.1	3.3	102.04	2.90
30.5	49	17.6	3.1	100.52	2.78
30.2	48.6	17.7	3.2	99.73	2.75
31.7	48.8	17.5	1.7	99.94	2.79
31.1	48.7	17.3	1.9	99.02	2.82
28.4	51.7	16.2	5.2	102.15	3.19

Fe	As	S	Co	Total	As/S
28.6	50.2	16.2	5.1	100.87	3.10
28.4	49.8	17.1	5.3	100.7	2.91
28.5	49.3	16.9	5.1	100.02	2.92
25.7	50.7	16.3	7.8	100.84	3.11
25.5	50.9	16.2	7.9	101.44	3.14
32.2	49.1	17.7	2.1	101.51	2.77
32	49.3	17.8	2	101.71	2.77
32.9	49.2	18.2	0.8	101.97	2.70
32.7	47	17.9	0.9	98.45	2.63
29.5	48.3	17.9	3.9	100.3	2.70
29.2	47.5	17.8	4.1	99.17	2.67
27.4	50.4	16.9	6.3	101.69	2.98
26.5	49.3	16.8	6.7	100.75	2.93
26.3	48	17	6.7	98.21	2.82
29.8	49	17.4	3.2	99.89	2.82
30.1	47.8	17.5	3.3	98.66	2.73
28.5	48.4	17.6	5	99.7	2.75
28.8	47.4	17.6	4.7	99.16	2.69
31.6	49.1	17.9	1.8	100.48	2.74
31.7	48.6	17.7	2	100.18	2.75
30.7	46.5	18.6	3.1	99.18	2.50
30.4	46.3	18.3	3.3	99	2.53
29.5	48.5	17.3	4.1	100.56	2.80
29.4	47.5	17.3	4	99.04	2.75
29.7	49.4	17.2	4.1	101.42	2.87
29.7	47.6	17.1	3.7	98.93	2.78
31.4	48.8	18	2.8	101.26	2.71
31.1	47.6	17.7	2.6	99.57	2.69
28.2	48.9	17.4	5.5	100.82	2.81
27.5	48.5	17.6	6.4	100.19	2.76
27.8	48.2	17.4	5.7	99.79	2.77
27.5	48.4	17.1	5.7	98.89	2.83
26.7	49.9	17.4	6.9	101.33	2.87
26.7	48.6	17.2	6.7	100.89	2.83
28.8	48.2	18.4	5.2	100.75	2.62
28.8	48.4	17.9	5	100.3	2.70
30.2	50.6	17.1	3.2	101.49	2.96
30.3	48.9	16.9	2.9	99.03	2.89
28	49	16.6	5.4	100.15	2.95
27.4	49.5	16.9	5.3	99.16	2.93
27.4	48.3	17.6	6.4	100.92	2.74
27.1	47.5	17.3	6.1	98.55	2.75
26.1	50.2	16.3	7.1	100.37	3.08
26.1	49	16.6	7.3	99.16	2.95
31.1	49.6	16.9	2.4	100.58	2.93
30.6	50.7	16.9	2.4	101.05	3.00
33.2	44.2	20	1.1	99.21	2.21
33	44.4	20.1	1.4	99.59	2.21
27.5	50.9	16.4	5.7	102.19	3.10
28.3	49.9	16.8	4.9	100.06	2.97
25.5	50.7	16.3	7.9	100.6	3.11
25.2	50.1	16.3	7.6	99.28	3.07
27.6	50.8	16.5	5.8	101.8	3.08
27.3	50	16.4	5.5	99.85	3.05
33.8	43.6	20	0.6	101.63	2.18
33.4	42.7	20.1	0.7	100.85	2.12
26.8	49.5	17.2	7.4	100.86	2.88

Fe	As	S	Co	Total	As/S
27.1	48.7	17.5	7.1	100.51	2.78
27.9	49.2	16.8	5.8	100.74	2.93
28	49.5	17	5.5	100.15	2.91
27.7	49.8	16.8	5.7	101.2	2.96
27.7	49.8	16.7	5.8	100.49	2.98
30.3	48.5	17.6	3.2	100.33	2.76
30.6	49.1	17.6	2.8	100.95	2.79
30.7	49.3	17.6	2.9	102.33	2.80
29.4	48.9	17.2	4.1	100.71	2.84
29.7	49.1	17.3	4.1	100.25	2.84
28.8	49.7	16.7	4.2	99.66	2.98
28.6	49.3	16.6	4.2	99.46	2.97
26.7	49.1	17	6.9	100.2	2.89
25.8	48.7	16.8	7.1	99.83	2.90
28.4	49.5	16.9	5.1	100.15	2.93
28.4	49	16.6	4.9	99.24	2.95
28.5	48.7	16.8	4.8	99.12	2.90
28.4	48.5	17.1	4.6	98.76	2.84
31	49.4	17.3	2.4	100.15	2.86
30.9	48.8	17.5	2.4	99.77	2.79
33.1	45.6	19.7	1.5	100.3	2.31
32.7	45.5	19.7	1.5	100.41	2.31
28.1	48.8	16.6	4.8	99.63	2.94
28.2	50.4	16.6	4.9	100.93	3.04
29.3	49.1	17.2	4.5	100.46	2.85
28.4	50.5	16.7	4.8	100.52	3.02
30.2	49.3	17.7	3.4	101.39	2.79
30.2	48	17.8	3.3	100.24	2.70
27.7	51	16.1	4.7	100.51	3.17
28	49.6	15.8	4.9	99.09	3.14
28.9	49.6	16.6	4.7	100.48	2.99
28.6	50.5	16	4.5	99.68	3.16
28.8	51.3	16.2	4.7	101.22	3.17
29.1	48.7	17.2	4.3	100.39	2.83
29.3	48.4	17.3	4.6	100.85	2.80
28.2	50.2	17.2	5.6	102.22	2.92
27.9	50.6	17.3	5.4	101.94	2.92
28.8	48.9	17.1	5	99.99	2.86
28.3	49.3	17.2	4.9	99.81	2.87
29.2	48.4	17.8	4.5	100.43	2.72
29	47.4	17.5	4.5	99.75	2.71
29.3	49.1	17.3	4.1	100.24	2.84
29.3	50	17.5	4.2	101.42	2.86
27.3	51.1	16.3	6.1	101.72	3.13
27	50.2	16.3	6.2	101.03	3.08
27.2	50.9	16.1	6.1	100.88	3.16
27.1	50.3	15.9	5.9	100.07	3.16
28.6	49.4	16.9	5.1	101.26	2.92
28.8	48.3	16.9	4.6	98.95	2.86
27.5	50.1	17.1	6.3	101.65	2.93
27.3	47.8	17	6.3	99.83	2.81
27.9	48.3	17.7	5.8	100.24	2.73
27.7	49.2	17.7	5.9	101.16	2.78
32.7	49.6	18.2	1.1	101.97	2.73
32.7	48.9	18	1.1	100.85	2.72
32.9	49	18.3	1	101.28	2.68
32.5	49.6	18.3	1.1	101.66	2.71

Fe	As	S	Co	Total	As/S
29.9	48.5	17.7	3.9	100.43	2.74
29.4	49.8	17.4	3.7	100.59	2.86
28.5	50.7	16.5	4.9	100.73	3.07
28.4	50	16.4	4.7	99.51	3.05
28.4	50	16.9	5.2	102.04	2.96
28.1	49.7	17.1	5.2	100.39	2.91
27.5	48.6	17.3	6.3	100.78	2.81
27.5	49.3	17.6	6.3	100.68	2.80
29.6	49.4	17.3	4.1	101.3	2.86
29.4	49.4	17.1	4.4	101.8	2.89
24.5	49.4	16.8	10	100.95	2.94
23.9	49.9	16.8	9.8	100.93	2.97
28.1	48.6	17	5.7	100.03	2.86
27.9	49	16.7	5.6	100.14	2.93
32.6	48.3	17.9	0.3	99.96	2.70
32.8	48.4	17.8	0.6	100.3	2.72
32	49.9	17.6	2	101.63	2.84
31.7	49.4	17.4	2	100.94	2.84
28.4	50.1	16.9	4.6	100	2.96
28.4	49.1	16.6	4.5	98.69	2.96
28.1	50.2	17	5.2	102.02	2.95
28	49.8	17	5.4	100.47	2.93
33.8	45.8	19.9	0.7	101.64	2.30
33.7	45.4	19.9	0.7	100.68	2.28
33.1	47.6	18.1	0.3	100.75	2.63
33.3	47.8	18	0.5	101.17	2.66
30.5	48.5	17.8	3.3	100.56	2.72
30.3	48.8	17.7	3.4	100.49	2.76
28.3	48.7	17.2	5.7	100.18	2.83
28	49.1	17.4	5.8	100.66	2.82
26.8	49.6	17	7	100.87	2.92
26.7	48.6	16.9	6.8	99.28	2.88
33.6	44.3	19.8	0.4	99.22	2.24
33.4	45.4	19.9	0.4	99.86	2.28
28	48	16.7	4.2	97.93	2.87
28.2	47.5	16.6	4.1	98.03	2.86
26.9	49.3	16.5	5.8	99.74	2.99
26.7	48.6	16.4	6.1	97.93	2.96
27.7	49.4	16.5	5.1	99.95	2.99
27.8	48.8	16.5	5.1	98.79	2.96
30.6	48.4	17.2	2.2	98.97	2.81
30.8	47.1	17.2	2.3	98.19	2.74
29	48.6	16.7	4.2	99.42	2.91
28.5	48.5	16.8	4.3	98.17	2.89
31.2	48.8	16.5	1.5	99.26	2.96
31.3	48.6	16.5	1.4	99.29	2.95
32.3	49.1	17.5	1.7	102.1	2.81
32.3	48.9	17.8	1.7	101.57	2.75
30.3	50.3	17.3	3.5	102.1	2.91
30.5	48.8	17.8	3.5	100.56	2.74
29.1	48.8	17.4	4.8	101.1	2.80
29	49.4	17.3	4.3	100.09	2.86
28.3	49.8	17	5.1	101.08	2.93
28.4	49.2	17	5	100.6	2.89
32.7	48.6	18	1.1	100.59	2.70
32.7	48.9	18.1	1.1	101.4	2.70
28	48.9	16.8	5.5	99.31	2.91

Fe	As	S	Co	Total	As/S
27.6	49.5	17.1	5.3	100.25	2.89
30.5	49.2	17.5	3.2	100.61	2.81
29.9	48.5	17.3	3.4	99.64	2.80
28.8	50	17.5	4.7	101.48	2.86
28.9	49.1	17.2	4.9	100.68	2.85
28.3	50.2	17	5.4	102.03	2.95
28.4	49.3	16.7	5.3	101.09	2.95
26.2	51.2	16.5	7.4	101.75	3.10
25.8	50	16.1	7.2	100.08	3.11
33.6	48.3	18.2	0.3	100.38	2.65
33.3	48.3	18.2	0.5	101.32	2.65
31.4	50.1	17.3	2.5	102	2.90
29.5	49.2	17.3	4.2	101.38	2.84
30.2	49	17.5	4.2	101	2.80
28.4	50.7	16.8	5.8	102.17	3.02
28.2	50.4	16.9	5.9	101.76	2.98
26.5	50.2	16.5	6.8	100.47	3.04
26.6	49	16.3	6.8	99.65	3.01
27.5	49.7	16	5.7	100.08	3.11
27.2	50.2	16.3	5.7	99.49	3.08
31.4	49.8	17.2	2.5	101.41	2.90
30.8	49.3	17.2	2.4	99.92	2.87
29.2	49.4	16.8	3.6	99.97	2.94
29.6	49.6	16.8	3.9	100.66	2.95
27.2	49.7	16.7	5.7	100.28	2.98
27.3	49.2	16.8	5.6	99.48	2.93
30.3	49.3	17.8	3.4	101.29	2.77
30.1	48.2	17.3	3.3	99.86	2.79
30.5	49.9	17.5	2.9	102.19	2.85
31	48.7	17.4	2.9	100.07	2.80
26.6	48.7	17.3	6.4	100.03	2.82
26.7	49	17.1	6.2	99.54	2.87
28.9	49.8	16.7	4.4	102.34	2.98
29.1	47.8	16.8	4.4	98.09	2.85
32.2	49.1	17.6	1.8	101.12	2.79
32.4	48.1	17.5	1.8	100.24	2.75
30	48.5	17.1	3.6	99.64	2.84
29.8	49.2	17.4	3.7	101.13	2.83
33.5	47.9	17.8	0.4	99.7	2.69
33.3	48.8	17.7	0.5	102.15	2.76
31.3	48	17.5	2.5	99.88	2.74
31	48.8	17.7	2.3	101.01	2.76
27.4	49.2	17	5.4	100.81	2.89
27.6	48.9	16.9	5.5	99.47	2.89
28.2	48.6	18	5.5	100.43	2.70
28	47.7	18	5.8	99.8	2.65
32.3	48.3	17.8	1.7	100.41	2.71
31.8	48	17.9	1.8	99.92	2.68
31.6	49	18.2	2.7	101.53	2.69
31.4	48.4	18	2.4	100.17	2.69
33.2	48.9	17.8	0.7	100.68	2.75
32.8	49.3	17.5	0.7	100.85	2.82
31.4	49.9	18.1	2.3	102.47	2.76
31.5	48.7	18.2	2.4	101.56	2.68
32.9	49.3	18.2	1.7	102.3	2.71
32.7	47.6	18.1	1.5	100.23	2.63
33.1	48.6	18.2	0.8	101.37	2.67

Fe	As	S	Co	Total	As/S
33.1	48.9	18.2	0.8	101.31	2.69
32.9	48.7	18.4	1.2	101.43	2.65
32.8	47.7	18.1	1.1	100.19	2.64
27.9	49.5	18.1	5.9	101.38	2.73
27.9	47.8	17.9	6.2	100.22	2.67
27.5	49.1	18.1	6.4	102.51	2.71
27.3	48	18	6.9	100.8	2.67
31.3	49.3	18	2.7	102.08	2.74
31.3	48.3	18.2	2.7	100.64	2.65
31.8	49.9	17.6	1.9	101.22	2.84
31.5	49.1	17.3	1.9	100.32	2.84
31.1	50.1	16.7	2.5	100.66	3.00
30.8	50.5	16.6	2.5	101.28	3.04
31.4	49.2	17.3	2.1	100.03	2.84
31.3	48.5	17.2	2.2	99.24	2.82
27	49.5	17.7	6.7	102.16	2.80
27.1	50.1	17.7	6.7	102.11	2.83
32.4	49	17.4	1.7	101.15	2.82
32.1	48.9	17.3	1.5	100.01	2.83
26.2	49.4	18	8.3	101.91	2.74
26.5	48.3	18.2	8.3	101.43	2.65
31.4	49.7	17.7	2.4	101.62	2.81
31.5	48.8	17.9	2.3	101.67	2.73
27.9	52.2	16	5.5	102.3	3.26
29.4	50.2	17.2	4.5	101.84	2.92
29.5	47	18.2	3.5	99.56	2.58
29.5	47.1	18	3.4	98.62	2.62
24.3	49	17.5	9.3	100.42	2.80
24.3	47.4	17.4	9.9	99.57	2.72
29.8	50.5	16.7	3.7	101.09	3.02
29.6	50.2	16.7	3.7	100.57	3.01
30.6	50.4	17.3	2.9	101.67	2.91
30.4	49.7	17	3	100.17	2.92
31.1	50	17.3	2.6	101.92	2.89
31.1	49.4	17	2.6	101.22	2.91
28.4	50.4	16.4	4.8	99.98	3.07
30.6	49.8	17.3	2.8	102.04	2.88
29.9	50.2	17	3.6	102.38	2.95
29.8	49.3	17	3.5	100.69	2.90
26.7	49.7	16.7	7.1	100.36	2.98
26.7	50.6	16.9	7.2	101.91	2.99
29.1	48.4	18	5	100.71	2.69
29	48.4	18.3	5.1	101.22	2.64
31.5	49.3	17.6	2.3	101.56	2.80
31.1	48.2	17.6	2.3	99.32	2.74
26.1	50	17.5	7.7	102.15	2.86
26.3	49.5	17.3	7.7	101.23	2.86
31.7	49.5	17.4	1.7	100.35	2.84
32	49.4	17.5	1.6	100.72	2.82
32.4	48.9	17.8	2	101.23	2.75
32.1	49.6	17.5	2	101.09	2.83
32	49.5	17.9	1.8	101.72	2.77
31.7	49.2	17.7	1.8	100.88	2.78
32.1	48.7	17.6	1.8	100.27	2.77
31.7	48.4	17.7	2	99.79	2.73
29.8	48.9	17.5	3.8	100.05	2.79
29.6	49.5	17.2	4	100.87	2.88

Fe	As	S	Co	Total	As/S
30.4	48.6	17.8	3.3	100.23	2.73
30.7	48.2	17.8	2.3	100.45	2.71
28.4	49.1	17.4	4.3	99.36	2.82
27.7	48.1	16.9	4.3	98.07	2.85
29.36	49.15	17.23	4.16	Avg Wt%	
2.06	1.13	0.69	1.97	Std. Dev.	
29.37	36.65	30.03	3.95	At%	

Appendix I:

Microprobe analysis of the Bi-Pb-Cu sulfosalt (wt%) in the hydrothermal veins:

Bi	Pb	Cu	S
39	35	10	14
37	37	11	15
35	40	10	14
38	37	10	15
37	38	11	15
35	38	10	14
34	43	10	14
38	35	11	15
38	38	10	15
36	42	10	14
37	40	10	15
38	39	10	14
39	37	10	15
37	38	10	14
38	35	10	15
37	36	10	15
38	33	12	15
38	34	11	15
38	35	10	15
40	34	10	14
38	36	10	14
40	34	10	14
41	34	10	14
40	37	10	14
40	34	10	14
38	40	10	14
49	32	8	13
39	36	10	14
38	39	10	14
40	38	10	14
50	29	7	12
47	32	7	13
42	32	10	13
41	33	10	14
41	34	10	14
45	37	8	11
49	29	8	13
44	33	9	14
47	29	8	13
37	41	10	14
36	40	10	14
37	39	10	14
38	35	10	14
45	34	9	12

	Bi	Pb	Cu	S
Average	40	36	10	14
Std Dev	4	3	1	1
Max	50	43	12	15
Min	34	29	7	11

Appendix J

Microprobe analysis of disseminated sphalerite (wt%):

Zn	S	Fe	Cu	Total
66.3	33.7	1.2	0.2	101.72
65.5	33.8	1.8	0.7	101.76
66.4	33.7	1	0	101.47
65.5	33.9	0.8	0.8	101.38
65.3	33.8	1.2	0.6	100.91
65.5	33.8	1.3	0.4	100.95
66.1	33.9	1.1	0.2	101.7
66.1	33.8	1.1	0.2	101.25
65	33.6	1.4	0.7	100.67
64	32.9	0.8	0.4	98.13
65.6	33.9	0.6	0.6	100.66
64.2	33.9	1	0.9	99.94
64.5	34.3	0.7	0.6	100.19
65.1	33.7	0.8	0.5	100.12
64.1	33.4	1	0.9	99.44
65.3	33.6	1.3	0.7	101.13
66.5	33.8	0.6	0	101.16
67.2	33.8	0.6	0	101.56
63.8	32.5	0.9	1	98.14
65.9	33.4	0.6	0.5	100.71
65.2	33.7	0.9	0.9	101.01
64.9	33.5	0.9	0.9	100.37
65.3	33.8	0.8	0	99.86
65	33.6	0.8	0.3	100.09
65.2	33.1	0.4	0.4	99.38
65.7	33	0.3	0.3	99.33
64.6	32.3	1	0.9	98.88
66.3	33.9	0.8	0.6	101.76
64.6	33	0.8	1	99.4
65.6	33.6	0.9	0.9	100.95
63.9	33.8	1.5	1.6	101.06
64.9	33.3	1.5	0.9	100.53
65.5	33.9	0.4	0.4	100.47
64.2	33.7	1.6	1.1	100.92
65.4	33.7	0.6	0.7	100.64
64.7	33.8	0.4	0.4	99.37
65.2	33.5	0.8	0.3	100.12
65.2	33	0.8	0.7	100.04
66.2	33.8	0.8	0.4	101.1
64.2	33.8	1.1	1.1	100.09
66.7	33.7	0.9	0	101.25
65.6	33.6	0.9	0.8	101.12
66.2	34	0.7	0.5	101.39
65.7	33.9	0.7	0.9	101.22
64.9	33.8	1	1	100.77
64.5	33.4	0.9	0.8	99.91
66.5	33.7	0.6	0.7	101.66
64.3	33.3	0.7	0.3	98.66
64.4	33.5	0.8	0.7	99.75
67.3	33.5	0.2	0.2	101.6
65.5	33.7	1.6	0.3	101.23
66.7	33.9	0.8	0.2	101.68

Zn	S	Fe	Cu	Total
65	33.3	0.7	0.7	100
66.1	33.9	0.8	0	100.79
66	34	0.9	0.4	101.59
64.2	33	0.6	0.3	98.08
65.5	33.4	1.1	0.6	100.69
65.5	33.7	1.1	0.6	100.82
66.5	33.8	0.2	0	101.11
64.9	33.5	0.9	0.9	100.24
66.5	33.8	0.2	0	100.8
64.8	33.3	0.4	0.3	98.96
66.4	33.6	1.2	0	101.47
66.9	33.8	1.1	0	102.03
66	33.6	1.2	0	100.95
63.7	33.5	1.8	0.7	99.65
66.4	34.1	1.4	0	101.92
65.2	33.7	1.6	0.3	100.83
66.6	33.9	1	0	101.51
65.8	33.2	0.8	0.2	100
66.4	34	1	0	101.45
64.7	33.3	1	0	98.94
63.8	33.7	1.1	1.1	99.63
64.8	33.7	1	0.6	100.32
64.3	32.7	1.2	0.3	98.59
65.6	33.5	1.4	0.4	101.19
66.1	33.5	0.9	0.3	101.02
64.8	33.8	1.3	1.3	101.19
66.8	34	0.4	0.4	101.91
65.41	33.60	0.92	0.5	**Average**
0.88	0.35	0.36	0.37	**Std. Dev.**
63.7	32.3	0.2	0	**Min**
67.3	34.3	1.8	1.6	**Max**

Appendix K

List of abbreviations:

P-inclusion	:	Primary inclusion
S-inclusion	:	Secondary inclusion
PS-inclusion	:	Pseudo-secondary inclusion
PT	:	Pressure-temperature
Tm	:	Melting temperature
Th	:	Homogenisation temperature
Tt	:	Trapping temperature
Td	:	Decrepitation temperature
eq. wt% NaCl	:	Equivalent weight percentage NaCl
FI	:	Fluid inclusion
V	:	Vapour
L	:	Liquid
Std. Dev.	:	Standard deviation
Max	:	Maximum
Min	:	Minimum
Avg.	:	Average
At%	:	Atomic percent
Wt%	:	Weight percent

148